CHARACTERISATION OF SAMHD1'S ANCESTRAL FUNCTION



Tamara Sylviane Andréa Davenne

Radcliffe Department of Medicine

Merton College

University of Oxford

Supervisor: Jan Rehwinkel

Thesis submitted for the degree of Doctor of Philosophy in

Infection, Immunology and Translational Medicine

September 2018

Acknowledgements

I am extremely grateful to Jan Rehwinkel for having opened the door of his lab to me. His trust, support and mentorship during my D.Phil have been fantastic. It has been a real pleasure to learn under his supervision, to develop as a scientist in his lab and to accomplish this exciting project together. I feel privileged to have had such an opportunity.

A special thank you goes to Alice Mayer, whose kindness initially showed me the path to the WIMM and who has inspired me to help others. Jonathan Maelfait played a special role during my time in the lab, allowing a Belgian majority that we have since lost. Rachel Rigby has always been there for scientific support, and as a good friend, who taught me British manners. My early morning companion Anne Bridgeman has always been helpful. I want to thank all members of the Rehwinkel lab (and Adel) who somehow contributed to this work and made the lab a friendly place. I also thank C.Cursi for generating the *Samhd1*$^{-/-}$ B16F10 cells as well as A.Schuh and J.Klintman for the clinical samples.

My gratitude goes to Persephone Borrow for being my co-supervisor, her enthusiasm was priceless, and to Vincenzo Cerundolo for his precious time and advice.

I am lucky to have met Theodore Sanders who became my husband. I found a purpose other than riding a bike, and I managed to squeeze in experiments between our adventures. Thank you Theo for making everything so easy, life has never been so sweet.

I am most grateful to my parents, for their love, their education and their constant support. I want to thank the rest of my family who has always been so supportive at each stage of this journey.

Thanks to Oxford University Sports for their support. I learned to train, to compete and to thrive with Oxford University Cycling Club. These years at the top of the sport taught me a lot and will always remind me of a great time.

I dedicate this thesis to my dad Philippe Davenne, who was diagnosed with cancer when I started this work, and who passed away during this journey. His strength was inspirational and his life has defined my values and ambitions, which I have developed during this work.

Abstract

Deoxynucleoside triphosphates (dNTPs) are the building blocks of DNA. DNA synthesis requires dNTPs for replication and subsequent cell division. Therefore, nucleotide metabolism in cells is tightly regulated and failure of this regulation results in damage, toxicity and cell death. SAMHD1 is a highly conserved protein that degrades dNTPs and restricts HIV-1 through dNTP starvation. *SAMHD1* is mutated in Aicardi-Goutières syndrome, a disease characterised by the chronic production of type I interferon. SAMHD1 is also involved in DNA repair and is mutated in cancer. SAMHD1 evolved before lentiviruses, suggesting that SAMHD1's main function is not to restrict viruses. This project aimed to identify and characterise SAMHD1's ancestral function. I show that addition of deoxynucleosides (dNs) to the culture medium resulted in the death of SAMHD1-deficient cells but not of WT cells. dNs were taken up by the cells and converted into dNTPs through the nucleotide salvage pathway. Cell death was most pronounced upon feeding with deoxyguanosine (dG) alone, suggesting that dGTP overload is particularly toxic to cells. In this model SAMHD1 tunes dNTP levels and protects cells against apoptosis triggered by dNTP overload or imbalances in the dNTP pools. Characterisation of this mechanism shed light on the mechanism of action of forodesine, an anti-cancer agent that inhibits purine nucleoside phosphorylase. Forodesine induces the accumulation of dGTP and subsequent cell death. Nevertheless, forodesine showed efficacy only in a minority of leukaemic patients, for unknown reasons. PBMCs from CLL patients with *SAMHD1* loss-of-function mutations showed a significant reduction of CLL B-cells upon treatment with forodesine and dG compared with the control group. Therefore, I propose a model where SAMHD1 limits the efficacy of the PNP inhibitor forodesine which predict that patients with *SAMHD1* mutations respond well to forodesine treatment. Forodesine could be used as a precision medicine. This new important role of SAMHD1 in dealing with dNTP overload and unbalances may be SAMHD1's ancestral function. This mechanism can be exploited physiologically where dNTP accumulation is required for toxicity, such as forodesine treatment.

Table of contents

CHAPTER 1. INTRODUCTION 14

1.1 Overview 14

1.2 Nucleotide biosynthesis 15

1.2.1 Purine metabolism 16
1.2.2 Pyrimidine metabolism 19
1.2.3 Ribonucleotide reductase 20
1.2.4 Nucleotide salvage pathway 21
1.2.5 Purine nucleoside phosphorylase 22

1.3 Cell death pathways 29

1.3.1 Apoptosis 29
1.3.2 Necrosis 34
1.3.3 Autophagic cell death 38

1.4 Sterile alpha motif histidine aspartate domain 1 (SAMHD1) protein 40

1.4.1 SAMHD1 in Aicardi-Goutières syndrome 41
1.4.2 SAMHD1 is a virus restriction factor 43
1.4.3 SAMHD1 is involved in DNA repair 45
1.4.4 *SAMHD1* mutations in cancer 46
1.4.5 SAMHD1 and nucleoside analogues 48
1.4.6 Regulation of SAMHD1 49

1.5 Interferons 51

1.5.1 Interferon production 52
1.5.2 Interferon-stimulated genes 55
1.5.3 Restrictions factors 55

1.6 Chronic lymphocytic leukaemia 56

1.6.1 Causes of chronic lymphocytic leukaemia 57
1.6.2 Clinical presentation and diagnosis 59
1.6.3 Management and treatment 60

1.7 Summary 63

CHAPTER 2. MATERIALS & METHODS 65

2.1 Mice 65

2.2 Cells 65

2.2.1 Generation of *Samhd1*$^{-/-}$ B16F10 cells 66

2.2.2 Patients' samples 67

2.3 Plasmids 67

2.4 Western blots 68

2.5 Viability measurements 68

2.6 Apoptosis assays 69

2.7 Cell cycle analysis 69

2.8 Retroviral vectors 70

2.9 Reverse transcription and qPCR 71

2.10 Micro array 72

2.11 dNTP measurements 72

2.12 Mass cytometry analysis of patient samples 73

2.13 Quantification and statistical analysis 74

2.14 Reagents 75

CHAPTER 3. SAMHD1 DEFICIENCY PREDISPOSES CELLS TO DEOXYNUCLEOSIDE-TRIGGERED APOPTOSIS 77

3.1 *Samhd1*$^{-/-}$ cells die upon exposure to deoxynucleosides 77

3.2 Deoxyguanosine is the most toxic deoxyribonucleoside to *Samhd1*$^{-/-}$ cells 80

3.3 dG treatment induces an increase in dGTP in *Samhd1*$^{-/-}$ cells 82

3.4 dG toxicity is independent of genomic DNA replication 83

3.5 dGTP overload triggers apoptosis in *Samhd1*$^{-/-}$ cells 86

3.6 Discussion 89

3.7 Conclusion 97

CHAPTER 4. DEOXYGUANOSINE INDUCES A TLR7-DEPENDENT CYTOKINE RESPONSE 98

4.1 BMDMs produce cytokines upon dG treatment 98

4.2 TNFα production upon dG treatment is not caused by endotoxins 100

4.3 TNFα is induced by dG treatment independently of TLR4 102

4.4 dG induces a pro-inflammatory response through MyD88 104

4.4.1 Microarray 104

4.4.2 Gene clustering and pathway analysis 106

4.5 dG-induced cytokine production is TLR7-dependent 110

4.6 Cytokine production and dG-induced apoptosis are independent events 112

4.7 Discussion 115

4.8 Conclusion 120

CHAPTER 5. DEOXYGUANOSINE KILLS SAMHD1-DEFICIENT CANCER CELLS... 121

5.1 SAMHD1-depleted cancer cell lines are sensitive to dG 121

5.2 Jurkat cells are highly sensitive to dG treatment 124

5.3 *Samhd1*$^{-/-}$ B16F10 cells die upon dG treatment 125

5.3.1 Choosing a cancer model 125

5.3.2 Validation of *Samhd1*$^{-/-}$ B16F10 cells 126

5.4 *Samhd1*$^{-/-}$ melanoma cancer model *in vivo* 127

5.4.1 *Samhd1*$^{-/-}$ melanoma grow slower than WT melanoma 127

5.4.2 dG treatment had no effect on WT B16F10 tumours 129

5.4.3 dG treatment had no effect on *Samhd1*$^{-/-}$ melanoma 131

5.5 Discussion 132

5.6 Conclusion 138

CHAPTER 6. SAMHD1 MUTATED CELLS ARE KILLED BY FORODESINE AND DEOXYGUANOSINE 139

6.1 *Samhd1*$^{-/-}$ BMDMs are more sensitive to forodesine than WT cells 140

6.2 Jurkat cells are sensitive to dG and forodesine treatment 143

6.3 Vpx-treated PBMCs showed limited sensitivity to forodesine and dG 145

6.3.1 Low efficiency of Vpx-mediated degradation of SAMHD1 in PBMCs 145

6.3.2 CyTOF optimization on human PBMCs 147

6.4 CLL patients with *SAMHD1* mutations are more sensitive to forodesine and dG treatment 153

6.4.1 Viability assessed by CellTiter-Glo..... 154

6.4.2 Viability assessed by western blot 158

6.4.3 Assessment of forodesine and dG toxicity with CyTOF..... 159

6.5 Discussion 165

6.6 Conclusion 172

CHAPTER 7. CONCLUSIONS AND FUTURE WORK..... 173

List of figures

Chapter 1. Introduction

Figure 1.1 Structure of purines and pyrimidines 16

Figure 1.2 Purine metabolism 18

Figure 1.3 Pyrimidine metabolism 19

Figure 1.4 Regulation of ribonucleotide reductase 20

Figure 1.5 Nucleotide salvage pathway 22

Figure 1.6 Purine nucleoside phosphorylase 23

Figure 1.7 BCL-2 proteins and their BH domains 30

Figure 1.8 Mechanisms of intrinsic and extrinsic apoptosis 32

Figure 1.9 Necroptosis cascade 35

Figure 1.10 NLRP3 inflammasome 37

Figure 1.11 Model of gasdermin pore formation 37

Figure 1.12 Membrane dynamics of autophagy in yeast and mammals 38

Figure 1.13 Reaction catalysed by the dNTPase SAMHD1 40

Figure 1.14 Sequence alignments of SAMHD1 in indicated species 45

Figure 1.15 Structure of SAMHD1 49

Figure 1.16 Model of SAMHD1 regulation. 50

Figure 1.17 Pattern recognition receptors. 52

Figure 1.18 Toll-like receptors signalling pathways and characteristics 53

Figure 1.19 Age of CLL patients. Adapted from 56

Figure 1.20 Frequencies of chromosomal deletions in CLL 57

Figure 1.21 Somatic mutations in chronic lymphocytic leukaemia 59

Chapter 2. Materials & Methods

Figure 2.1 SAMHD1 CRISPR/Cas9 strategy in B16F10 cells 67

Chapter 3. SAMHD1 deficiency predisposes cells to deoxynucleosides-triggered apoptosis

Figure 3.1 Deoxynucleosides are toxic to cells lacking SAMHD1 78

Figure 3.2 dN treatment induces death of *Samhd1*$^{-/-}$ cells 79

Figure 3.3 SAMHD1 reconstitution protects *Samhd1*$^{-/-}$ BMDMs 80

Figure 3.4 dG is the most toxic dN 81

Figure 3.5 dG treatment induces an increase of dGTP in *Samhd1*$^{-/-}$ cells. 83

Figure 3.6 dG toxicity is independent of genome replication 85

Figure 3.7 *Samhd1*$^{-/-}$ BMDMs die by apoptosis upon dG treatment. 86

Figure 3.8 *Samhd1*$^{-/-}$ cells become Annexin^{+}PI^{+} post-dG treatment 87

Figure 3.9 *Samhd1*$^{-/-}$ BMDMs die through caspase-dependent cell death 88

Figure 3.10 Synthesis of dGTP pool 91

Figure 3.11 Models of dGTP toxicity in PNP-deficient cells 94

Figure 3.12 SAMHD1 protects cells against dNTP overload 97

Chapter 4. Deoxyguanosine induces a TLR7-dependent cytokine response

Figure 4.1 z-VAD induces death of dG treated cells 99

Figure 4.2 dG-induced TNFα production in WT and *Samhd1*$^{-/-}$ BMDMs 100

Figure 4.3 dG from Medchem is endotoxin free. 101

Figure 4.4 dG-induced TNFα production is TRIF and TLR4 independent 102

Figure 4.5 dG-induced cytokine production is MyD88 dependent 103

Figure 4.6 dG treatment induces upregulation of pro-inflammatory genes 105

Figure 4.7 Pathway analysis of the gene set 109

Figure 4.8 dG signals through TLR7 to induce cytokine production 111

Figure 4.9 Cytokines do not contribute to dG-induced apoptosis 113

Figure 4.10 *Samhd1*$^{-/-}$*Tlr7*$^{-/-}$ BMDMs die by apoptosis upon dG treatment 114

Chapter 5. Deoxyguanosine kills SAMHD1-deficient cancer cells

Figure 5.1 Vpx-targeted cells are sensitive to dNs and dG treatment 122

Figure 5.2 SAMHD1-depleted MDA-MB231 cells die upon dG treatment 123

Figure 5.3 Jurkat cells are hypersensitive to dG treatment 124

Figure 5.4 *Samhd1*$^{-/-}$ B16F10 cells die upon dG treatment 126

Figure 5.5 *Samhd1*$^{-/-}$ B16F10 tumours grow slower than *Samhd1*$^{+/+}$ and *Samhd1*$^{+/-}$ in *C57Bl6* mice 128

Figure 5.6. dG treatment has no effect on tumour growth 130

Figure 5.7 SAMHD1 regulation 133

Chapter 6. SAMHD1 mutated cells are killed by forodesine and deoxyguanosine

Figure 6.1 *Samhd1*$^{-/-}$ BMDMs die upon treatment with forodesine and dG. 141

Figure 6.2 Forodesine and dG treatment induces apoptosis in *Samhd1*$^{-/-}$ BMDMs 143

Figure 6.3 Jurkat cells are sensitive to forodesine and dG treatment 144

Figure 6.4 VLP_{vpx} infected PBMCs showed limited sensitivity to forodesine and dG treatment. 146

Figure 6.5 Mass cytometry detects SAMHD1 and pSAMHD1 in PBMCs 149

Figure 6.6 Vpx degrades SAMHD1 only in monocytes 151

Figure 6.7 VLP_{vpx} degrade SAMHD1 in monocytes 152

Figure 6.8 SAMHD1 mutated CLL cells are sensitive to forodesine and dG treatment.. 155

Figure 6.9 Forodesine and dG treatment kills SAMHD1 mutated cells 157

Figure 6.10 Detection of cleaved-PARP and cleaved-caspase 3 upon forodesine and dG treatment 158

Figure 6.11 SAMHD1 mutated cells do not express SAMHD1 159

Figure 6.12 Loss of $CD5^{+}CD19^{+}$ cells in SAMHD1 mutated cells upon forodesine and dG treatment 161

Figure 6.13 CLL B cells with SAMHD1 mutations die upon forodesine and dG treatment 162

Figure 6.14 CLL B cells are active or inactive 164

Figure 6.15 Model of forodesine toxicity in SAMHD1-deficient cells. 172

Chapter 7. Conclusions and future work

Figure 7.1 Model of SAMHD1's mechanism of protection against dGTP. 174

List of Tables

Chapter 1. Introduction

Table 1.1 Clinical trials involving forodesine 27

Table 1.2 Caspases classification and specificities 31

Table 1.3 Summary of death receptors and their ligands 33

Table 1.4 Chronic lymphocytic leukaemia classification 60

Chapter 2. Materials & Methods

Table 2.1. Concentrations of plasmids transfected per 15 mm dish to generate VLP_{vpx} (SIV3+) and VLP_{ctrl} (SIV4+) 70

Table 2.2 Concentrations of plasmids transfected 71

Table 2.3 List of mouse taqman probes 71

Table 2.4 List of CyTOF antibodies 74

Table 2.5. List of reagents 75

Chapter 4. Deoxyguanosine induces a TLR7-dependent cytokine response

Table 4.1 Differently expressed genes in WT and *Samhd1*$^{-/-}$ upon dG treatment 106

Table 4.2 Functional annotation clustering of the gene set 108

Chapter 6. SAMHD1 mutated cells are killed by forodesine and dG

Table 6.1 CyTOF panel for PBMCs 148

Table 6.2 Genetic characteristics of CLL patients 153

Table 6.3 SAMHD1 mutations of CLL patients 154

Abbreviations

ADAR1: adenosine deaminase acting on RNA

AGS: Aicardi-Goutières syndrome

ALR: AIM2-like receptor

AML: Acute myeloid leukaemia

APAF1: apoptotic protease-activating factor 1

ASC: apoptosis-associated speck-like protein

BMDMs: bone marrow derived macrophages

BrdU: Bromodeoxyuridine

CARD: caspase recruitment domain

CDR: cytosolic DNA receptor

CyTOF: cytometry by time of flight

dA: 2’ deoxyadenosine

DAMPs: danger-associated molecular patterns

dC: 2’ deoxycytidine

dCK: deoxycytidine kinase

DCs: dendritic cells

DED: death effector domain

dG: 2’ deoxyguanosine

dGK: deoxyguanosine kinase

DMEM: Dulbecco’s modified Eagle medium

DMSO: dimethyl sulfoxide

dN: deoxyribonucleoside

dNTP: deoxynucleoside triphosphate

DR: death receptor

dT: 2’ deoxythymidine, also called thymidine

FADD: FAS-associated death domain protein

FCS: foetal calf serum

FDA: Food and drug administration

GSDMD: gasdermin D

HIV-1: human immunodeficiency virus 1

HR: homologous recombination

IFIH1: IFN-induced helicase C domain containing protein 1 (also called MDA5)

IFN: interferon

LINE: Long Interspersed elements

MDA5: melanoma differentiation-associated gene 5

MLKL: mixed lineage kinase domain-like protein

MOMP: mitochondrial outer membrane permeabilisation

mtDNA: mitochondrial DNA

ORN: oligoribonucleosides

P/S: penicillin and streptomycin

PAMP: pathogen associated molecular pattern

PBS: phosphate buffered saline

PCD: programmed cell death

PFD: pore forming domain

PMB: Polymyxin B

pMLKL: phosphorylated MLKL

PNP: purine nucleoside phosphorylase

poly U: Polyuridylic acid

PRR: pathogen recognitions receptor

pSAMHD1: phosphorylated SAMHD1

RIP: receptor-interacting protein kinase

RLR: RIG-I like receptor

RNaseH2: ribonuclease complex H2

RPMI: Roswell Park Memorial Institute media

SAMHD1: sterile alpha motif histidine aspartate domain 1

SLE: systemic lupus erythematosus

snRNP: small nuclear ribonuclear proteins

ssDNA: single strand DNA

ssRNA: single strand RNA

TBS: Tris buffered saline

TCL1: The proto-oncogene T-cell leukaemia 1

TIR: Toll-interleukin-1 receptor domain

TLR: toll-like receptor

TNF: tumour necrosis factor

T-PLL: T cell prolymphocytic leukaemia

TRAIL: TNF-related apoptosis induced ligand

TREX1: DNA repair 3’ exonuclease 1

TRIF: TIR-domain containing adaptor inducing IFN-β

VLPs: virus like particles

Chapter 1. INTRODUCTION

1.1 Overview

Cells require deoxyribonucleoside triphosphates (dNTPs) for DNA synthesis, to replicate their genome and divide. Generation of the dNTP pool in the cell occurs through the *de novo* pathway and the salvage pathway, both requiring numerous enzymes for dNTP synthesis (Reichard, 1988). These pathways are critical to control the dNTP pools and to maintain genome integrity. Abnormally high or low dNTP levels at the wrong time can lead to DNA damage, increased mutation rates, defective DNA repair and possibly lead to cell death (Kumar et al., 2011a; Poli et al., 2012).

The most characterised caspase-dependent form of cell death is apoptosis, but there are other forms of programmed cell death. Research on cell death over the last two decades has led to a better characterisation of new types of programmed cell death such as pyroptosis and necroptosis. Crosstalk exists between these distinct cell death pathways and often blocking one pathway results in the engagement of an alternative death pathway. When abnormalities are detected in cells and a point of no return is reached, cell death can be initiated through one of these pathways.

SAMHD1 is a deoxyribonucleoside triphosphohydrolase (dNTPase) and therefore is an important enzyme involved in regulating dNTP pools (Goldstone et al., 2011; Laguette et al., 2011; Powell et al., 2011). Its roles in virus restriction and autoimmunity have been extensively studied over the last few years. Indeed, tuning of dNTP availability is a defence mechanism that prevents replication of retroviruses, DNA viruses and perhaps the expression of endogenous retroelements. Failure to control viruses or endogenous retroelements results in sensing of their nucleic acids and induction of type I interferon (IFN). Type I IFN are molecules that signal through the IFN receptor and induce an anti-viral state, through the induction of interferon stimulated genes (ISGs). This allows the cell to fight back against the invader, to either eliminate it or to engage the cell death process when the damage cannot be repaired. SAMHD1 is an ISG and plays an essential role in restricting viruses. Mutations in the *SAMHD1* gene cause Aicardi-Goutières syndrome, a disease

characterised by the chronic production of type I IFN (Rice et al., 2009). The mechanism by which SAMHD1 prevents the production of type I IFN is not entirely clear although evidence suggest that SAMHD1 modulates the expression LINE1 retrotransposons (Herrmann et al., 2018; Hu et al., 2015; Zhao et al., 2013).

The *SAMHD1* gene is recurrently mutated in chronic lymphocytic leukaemia (CLL), T cell prolymphocytic leukaemia (T-PLL) and colon cancer (Clifford et al., 2014; Guieze et al., 2015; Johansson et al., 2018). *SAMHD1* mutations lead to higher dNTP pools, which may increase mutation rates, or simply give cancer cells a growth advantage. Since SAMHD1 has also been shown to be involved in DNA repair and/or replication, it is not entirely clear why *SAMHD1* mutations are selected in cancer cells (Coquel et al., 2018; Daddacha et al., 2017).

SAMHD1 is a conserved protein that evolved before the lentiviruses that it restricts, suggesting that restricting viruses is not its primary function. The aim of the work described in this thesis was to explore the role of SAMHD1 in metabolism in order to characterise its ancestral function.

1.2 Nucleotide biosynthesis

Cells undergo division in a process called mitosis, in which a parent cell creates two daughter cells that are genetically identical. Mitosis requires DNA synthesis to replicate the genome of the parent cell. DNA is composed of nucleotides which are made up of a phosphate group, a deoxyribose sugar and a nitrogenous base. Availability of dNTPs, which are DNA precursors, is finely controlled by a multitude of enzymes. Controlling dNTP pools is critical to maintain genome integrity and DNA replication fidelity (Kumar et al., 2011a; Kunz et al., 1994; Mathews, 2006). Drugs targeting enzymes involved in nucleoside metabolism have therefore been used for several decades as anti-cancer agents (Mathews, 2015).

Nucleotides are not only required for DNA synthesis but are important in other processes. For example, adenine nucleotide triphosphate (ATP) is the molecule used as energy currency in the cell. The guanine nucleotide GTP is also used as energy molecule for

specific processes. Concentration of NTPs in the cell are relatively constant compared with dNTPs, of which the concentration varies throughout the cell cycle.

Synthesis of nucleotides and dNTPs can be achieved *de novo*, starting from a simple molecule, or through the salvage pathway, which recycles intermediates of the nucleotide pathway. Nucleotides are made of nitrogenous nucleotide bases that are called purines or pyrimidines. Purines are heterocyclic aromatic organic compounds containing 4 nitrogen atoms (**Figure 1.1**). They contain two carbon rings, and is made of a pyrimidine ring fused to an imidazole ring (**Figure 1.1**). Pyrimidines are heterocyclic aromatic organic compound containing 2 nitrogen atoms. They contain only one carbon ring. Adenine and guanine are purine whilst cytidine, thymidine and uracil are pyrimidines. In the cell both purines and pyrimidines are nucleobases required for nucleotide production and therefore DNA and RNA synthesis. The salvage pathway uses nucleosides or deoxynucleosides as starting molecules and the recycling of these molecules allows the cell to limit its energy expenditure. *De novo* and salvage nucleotide pathways differ for purines and pyrimidines bases.

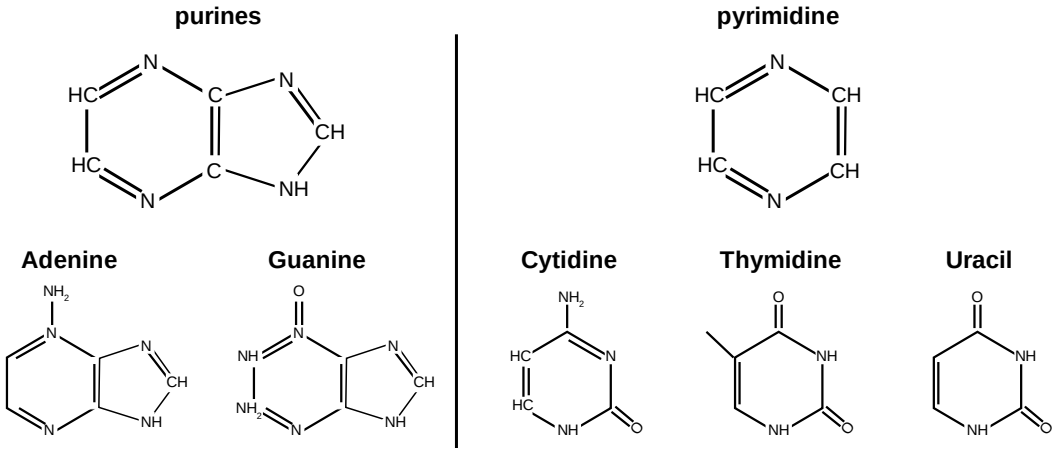


Figure 1.1 Structure of purines and pyrimidines

1.2.1 Purine metabolism

Purines are synthesised *de novo* as nucleotides bound to a ribose 5-phosphate. Inosine monophosphate (IMP) is the molecule that will be modified to form adenine and guanine (represented in red box in **Figure 1.2**). Production of IMP is a complex multistep process that involves several enzymes and intermediate products, as illustrated in **Figure 1.2**.

Purines can also be synthesised through the recycling process of the nucleotide salvage pathway. Adenine phosphoribosyltransferase salvages adenine whilst hypoxanthine-guanine phosphoribosyltransferase (HGPRT) salvages guanine and hypoxanthine. Both AMP and GMP will further be modified to form dATP and dGTP.

Rather than being recycled, guanine, inosine and their deoxy derivatives can be catabolised by purine nucleoside phosphorylase (PNP), allowing the recycling of the nucleobases. PNP is an important enzyme in the salvage pathway, with PNP-deficiency causing a severe disease as detailed in section **1.2.5.**

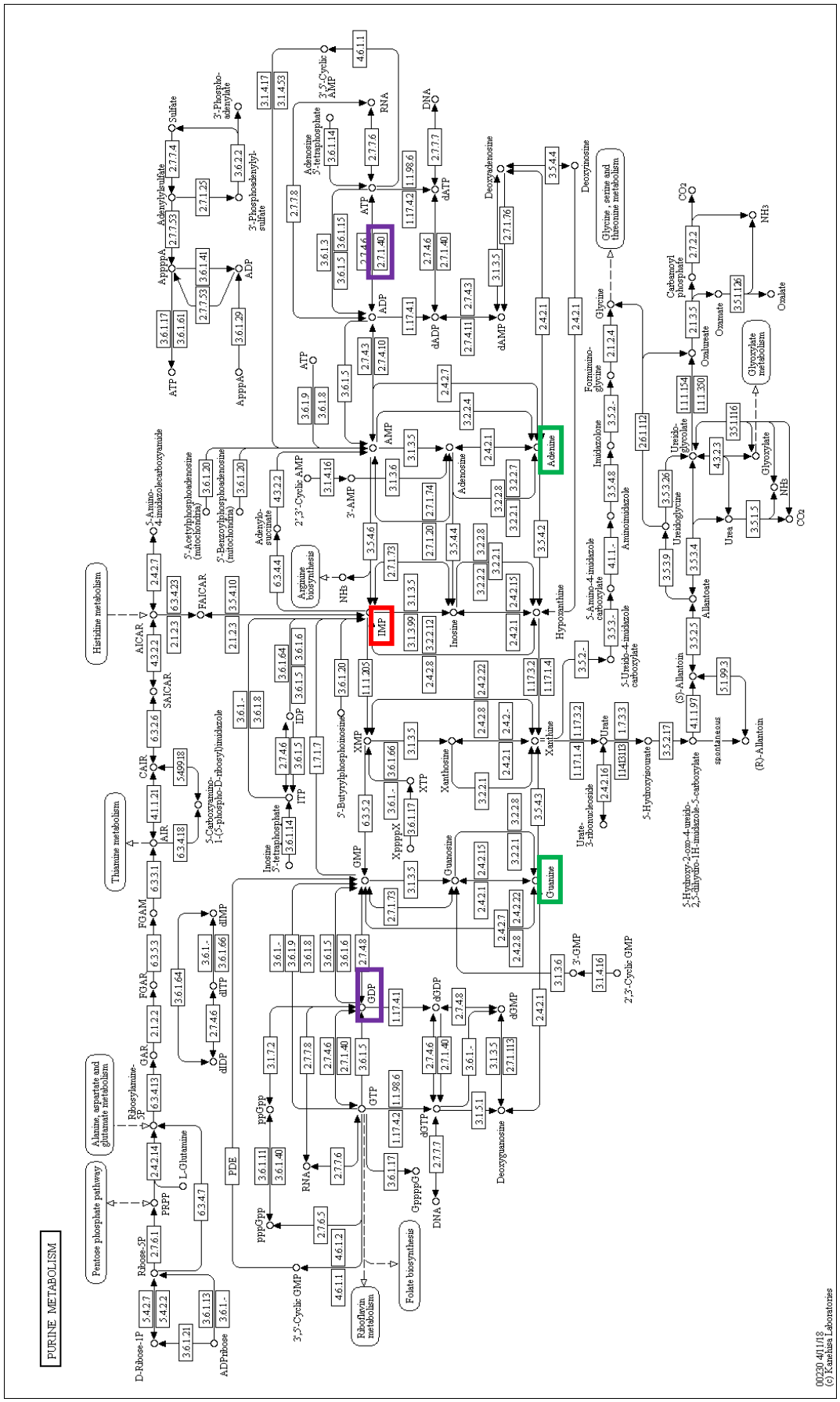


Figure 1.2 Purine metabolism (from www.genome.jp)

1.2.2 Pyrimidine metabolism

Pyrimidine metabolism uses UMP (red box in **Figure 1.3**) as a starting molecule to synthesise cytidine and uridine (green boxes in **Figure 1.3**). Through the salvage pathway, cytidine can be converted into uridine and further degraded into UMP.

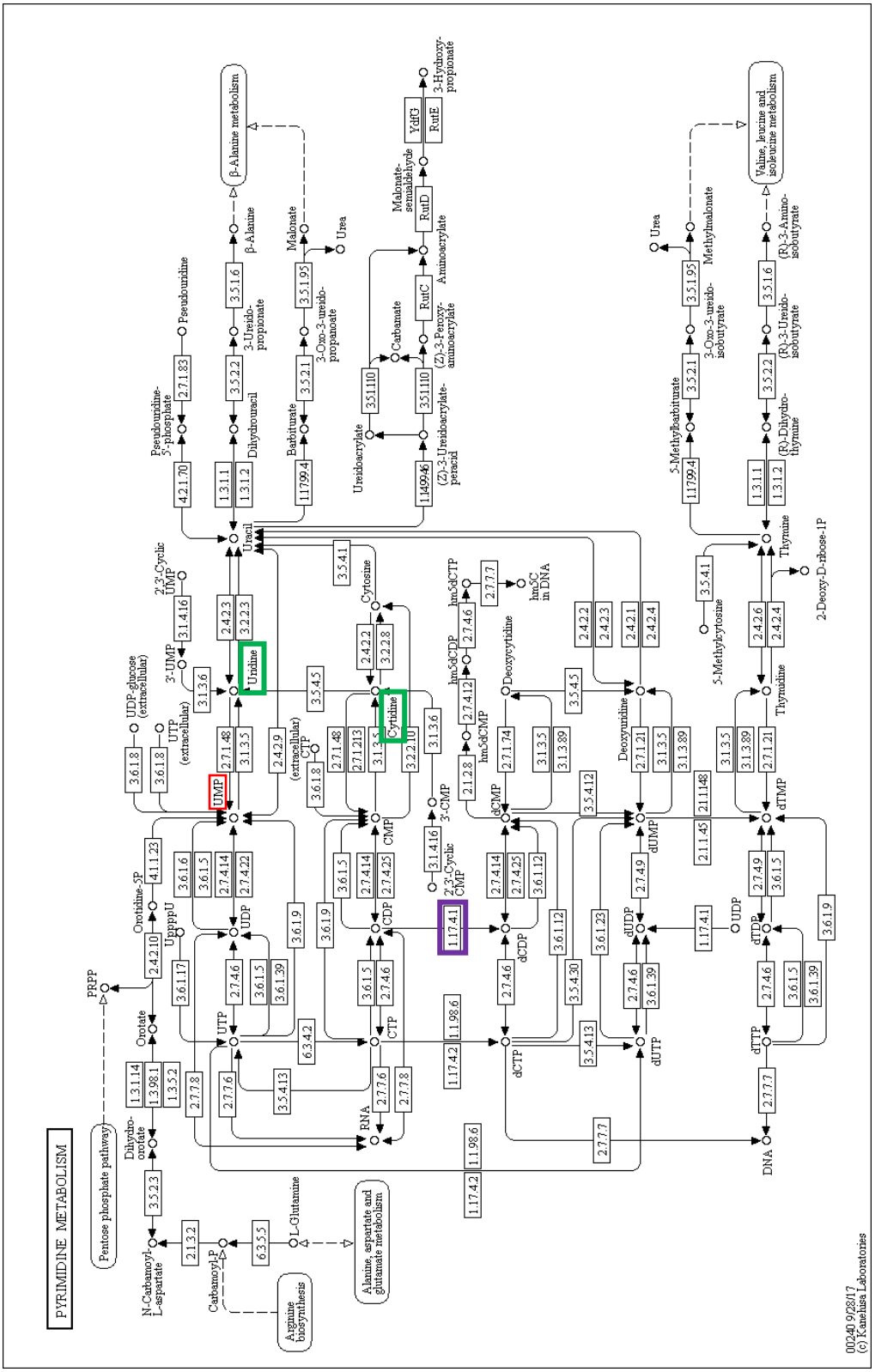


Figure 1.3 Pyrimidine metabolism (from www.genome.jp)

1.2.3 Ribonucleotide reductase

dNTPs required for DNA synthesis can be synthesised *de novo*. Once purine and pyrimidine have been phosphorylated to form nucleotide diphosphates (NDPs), they require ribonucleotide reductase (RNR) to be modified. RNR is a key enzyme required for dNTP synthesis *de novo*. It reduces all four NDPs to dNDPs with specificity regulated by the binding of an effector to a distal allosteric site, as shown in **Figure 1.4** (Zimanyi et al., 2016). RNR enzymes from different species can be divided into 3 classes based on their structure, regulation and specificity. Human RNR is a class I enzyme composed of two subunits, four large α subunits forming the R1 protein and two small β subunits forming the R2 protein (Mathews, 2015). RNR is tightly regulated through its allosteric sites, present on R1.

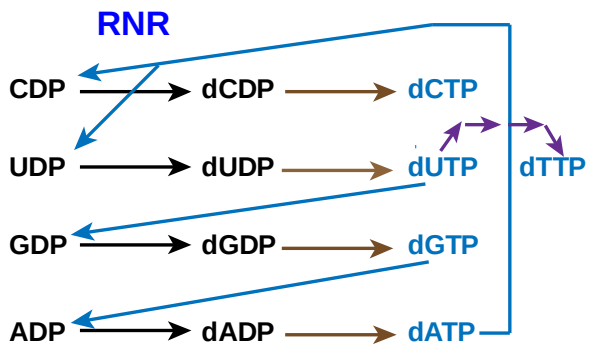


Figure 1.4 Regulation of ribonucleotide reductase. *RNR catalyses the conversion of all four NDPs into dNDPs (black arrows). dNDPs are further converted into dNTPs. UTP allosterically stimulates the conversion of GDP, dGTP stimulates the conversion of ADP, and dATP stimulates the conversion of CDP and UDP. This allows the maintenance of relative ratios of dNTPs. Brown arrows represent reactions catalysed by nucleoside-diphosphate kinases. Purple arrow represent intermediate reactions to convert dUTP into dTTP. Adapted from (Zimanyi et al., 2016).*

Once adenine, cytidine, guanine and uridine are phosphorylated twice into ADP, CDP, GDP or UDP, RNR catalyses the removal of the 2'-hydroxyl group of the ribose ring of the nucleotide diphosphate. The conversion of NDPs into dNDPs by RNR is the enzymatic reaction 1.17.4.1 highlighted in purple boxes in **Figure 1.2** and **Figure 1.3**. dNDPs are phosphorylated once more to form deoxynucleoside triphosphates (dNTPs) that can then be used for DNA synthesis.

Binding of ATP or dATP to R1 allosteric sites triggers upregulation or downregulation of the enzyme activity, respectively (Brown and Reichard, 1969). There is a second mechanism of allosteric regulation to maintain ratios of dNTPs in the cell. Whereas high levels of dATP inhibit RNR, at lower levels dATP promotes CDP or UDP reduction, TTP promotes GDP reduction and dGTP promotes ADP reduction (**Figure 1.4**). This leads to dATP synthesis

which eventually negatively regulates the enzyme. RNR is present in all organisms and requires metal co-factors to function (Cotruvo and Stubbe, 2011).

Availability of dNTPs in correct amounts is critical to maintain genome integrity and failure to control these levels can cause mitochondrial disorders, increased susceptibility to infection and cancer (Aye et al., 2015; Kunz and Kohalmi, 1991; Mathews, 2006). RNR is a rate-limiting enzyme that is therefore a key regulator of dNTP pools. Cancer cells require *de novo* dNTP synthesis and higher RNR activity is a common feature in cancer. Therefore, blocking RNR is a common strategy to inhibit proliferation of cancer cells (Zhou et al., 2013a).

1.2.4 Nucleotide salvage pathway

Nucleotides are not only be generated *de novo*, since nucleotide intermediates can also be recycled through the salvage pathway (**Figure 1.5**). Often presented as a secondary pathway, the salvage pathway is nevertheless important in the cell. Indeed, mutations in the salvage enzymes such as deoxyguanosine kinase (dGK), deoxycytidine kinase (dCK), deoxythymidine kinase (dTK), HPGRT and adenine phosphoribosyltransferase cause mitochondrial DNA depletion syndromes (MDSs). MDSs are a group of autosomal recessive disorders that can be divided into three well-established forms: myopathic, encephalomyopathic and hepatocerebral (Spinazzola et al., 2009). Indeed, nucleotide salvage deficiencies cause DNA damage and neurodegeneration (Fasullo and Endres, 2015). The nervous system, which has high ATP demand, is particularly susceptible to dNTP imbalances causing oxidative stress and DNA damage. The mitochondrial genome is susceptible to damage caused by the incorporation of 8-oxo-dGTP (Leon et al., 2016). Accumulation of 8-oxo-G in the mitochondrial DNA of neurons causes neuronal loss (Sheng et al., 2012). This illustrates the importance of the nucleotide salvage pathway in the cell, especially in the mitochondria. The mitochondrial genome (mtDNA) encodes 37 genes, including 13 proteins, 22tRNAs and 2rRNAs (Bailey and Doherty, 2017). In mammals, mtDNA is organised in nucleoid structures and contains a short triple stranded region; the third DNA strand is called 7S DNA. Unlike genomic DNA which is synthesised only during

S-phase, mtDNA is synthesised throughout the cell cycle (Antes et al., 2010). This suggests that the nucleotide salvage pathway plays an important role in generating dNTPs, since RNR synthesises dNTPs *de novo* only in S-phase. Interestingly, the synthesis of mitochondrial 7S DNA does seem to fluctuate with the cell cycle, suggesting that mtDNA does seem to fluctuate with the cell cycle (Antes et al., 2010).

1.2.5 Purine nucleoside phosphorylase

The nucleotide salvage pathway is important in the cell since mutations in the enzymes regulating it cause mitochondrial depletion syndrome. Purine nucleoside phosphorylase (PNP) is an important enzyme of the salvage pathway. PNP catalyses the cleavage of the glycosidic bond of ribo- and deoxyribonucleosides, in the presence of inorganic orthophosphate as a second substrate, to generate the purine base and ribose (deoxyribose)-1-phosphate (**Figure 1.6A**). Purine bases can then be recycled through the nucleotide salvage pathway.

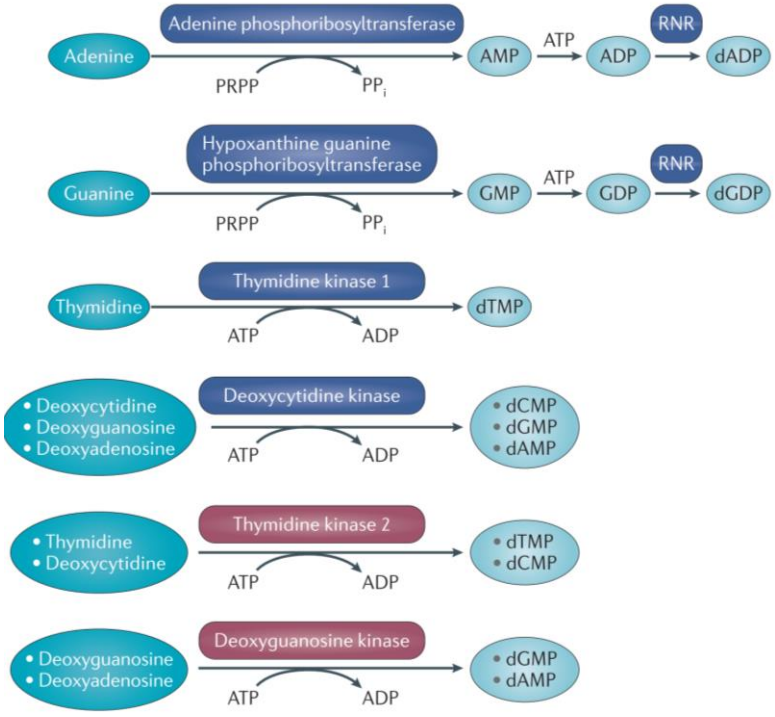


Figure 1.5 Nucleotide salvage pathway. *Thymidine kinase 2 (TK2) and deoxyguanosine kinase (dGK) are localised in the mitochondria. The other enzymes are primarily located in the cytosol. PRPP, 5-phosphoribosyl-1-pyrophosphate; RNR, ribonucleotide reductase. Illustration from (Mathews, 2015).*

PNP is ubiquitously expressed and is responsible for the degradation of inosine and guanosine as well as their deoxy derivatives. In humans, the highest PNP activities are found in the kidneys, peripheral lymphocytes and granulocytes (Bzowska et al., 2000).

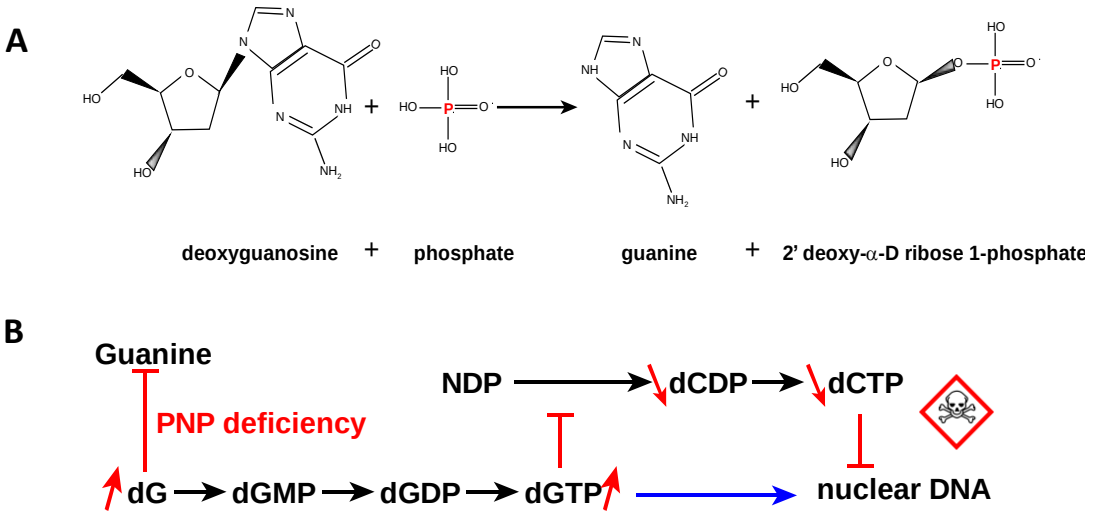


Figure 1.6 Purine Nucleoside phosphorylase*(A) Degradation of deoxyguanosine (dG) by purine nucleoside phosphorylase (adapted from BRENDA, EC 2.4.2.1). (B) Mechanism of PNP deficiency. PNP deficiency leads to accumulation of dG and dGTP. Increased dGTP inhibits RNR, leading to a decrease of the dCTP pool that will starve cells and lead to toxicity.*

1.2.5.1 PNP deficiency

Patients with a non-functional PNP suffer from a disease called PNP deficiency, characterised by T cell lymphopenia (Bzowska et al., 2000). PNP deficiency is a rare disorder that was first described more than 50 years ago and represents ~4% of all cases of severe-combined immunodeficiency (Castro et al., 2014; Giblett et al., 1975). Moreover, it is associated with a fatal lymphoproliferative disorder (Watson et al., 1981). Typically, patients display elevated levels of inosine, guanosine, deoxyinosine and deoxyguanosine (dG), and abnormally low levels of uric acid (the final product of their degradation) in urine (Castro et al., 2014). In addition, guanosine, deoxyinosine and dG can also be detected at high levels in the plasma. PNP deficiency leads to the accumulation of dG and its phosphorylated forms including dGTP (**Figure 1.6B**). dG was shown to be the most toxic purine in T cells (Chan, 1978). To explain the toxicity, a model suggested that elevated levels of dG, and therefore dGTP, inhibit RNR through a feedback loop (**Figure 1.6B**). RNR inhibition by dGTP leads to a decrease in dCTP pools and prevents DNA synthesis due to

lack of availability of dNTPs, resulting in impaired T cell proliferation and function (Cohen et al., 1978).

High levels of deoxycytidine kinase (dCK) and deoxyguanosine kinase (dGK) were reported in the spleen and the thymus (Durham and Ives, 1969). Therefore, Cohen et al suggested that high dCK and dGK expression in T cells could explain why T cells but not B cells were susceptible to the accumulation of dGTP and subsequent toxicity (Cohen et al., 1978). However, several publications later showed that RNR's inhibition by dGTP is not the cause of dGTP toxicity (Duan et al., 1990). Using cells expressing a mutant RNR partially resistant to dGTP feedback inhibition, they showed that cells which spent less time in G1 were more resistant to dGTP toxicity, since dGTP could otherwise be used for DNA synthesis. The authors suggested RNA synthesis as a possible mechanism of dG toxicity. Another paper suggested a mechanism of action of PNP inhibitors on T cell proliferation which was independent of dG and IL-2 reversible (Boehncke et al., 1994). The authors observed that PNP inhibitors interrupted the cells in S-phase of the cell cycle, and suggested the involvement of an unknown protein involved in DNA synthesis. Since they could not enhance the effect of PNP inhibitors by adding dG, Boehncke et al. concluded that dG toxicity does not act through RNR. Both dG-dependent and dG-independent mechanisms of toxicity were proposed to explain lymphopenia and toxicity in PNP deficiency.

Generation of PNP deficient mice by Snyder et al. allowed the mechanisms of dGTP toxicity to be studied further (Snyder et al., 1994). Surprisingly, the accumulation of dG was not observed in the T cells of these mice, neither in thymocytes nor splenocytes. Furthermore, no changes in purine and pyrimidine ribonucleotide pools were observed, suggesting there was no effect on RNR. Interestingly, the authors noticed that these mice also had lower levels of dG kinase (dGK), the enzyme responsible for dG phosphorylation. This explained why there was no accumulation of dG, but it was not clear whether low expression of dGK was a consequence of the absence of PNP (Snyder et al., 1994). Two studies from the same group observed, in addition to an increase in dGTP, depletion of GTP and NAD^+ in PNP deficient patients, and suggested that GTP depletion may be the cause of central

nervous system dysfunction (Simmonds et al., 1987; Simmonds et al., 1982). In contrast, patients with Lesch-Nyan syndrome (HGPRT deficiency), a condition also inducing a decrease of GTP pools, showed no effects on immune function, suggesting that low GTP was not the cause of toxicity (Sidi et al., 1989).

Later, PNP deficient mice were generated with a different method (homologous recombination), by another group. The study of these *Pnp*$^{-/-}$ mice showed elevated levels of all four PNP substrates in urine, and *Pnp*$^{-/-}$ cells had 8 time more dGTP than WT cells (Arpaia et al., 2000). These mice displayed an immunodeficiency phenotype affecting mainly T cells. Arpaia et al. who generated these mice, were the first and only group to suggest a novel mechanism for dGTP toxicity in the mitochondria. Higher levels of dGTP were detected in the mitochondria, the same location as dGK. In addition, they observed that *Pnp*$^{-/-}$ thymocytes and splenocytes had more apoptotic cells upon gamma irradiation compared with WT, suggesting that they were more sensitive to mitochondrial DNA damage. Intracellular dGTP accumulation was modest compared with urine levels in *Pnp*$^{-/-}$ mice, which reached ~ 5 mM. In these animals, a secondary loss of dGK activity was observed in all tissues examined, in line with the previous mouse model (Snyder et al., 1994). Taken together, the authors established a model in which in PNP deficient T cells, dGTP accumulates in the mitochondria (where dGK is located) and initiates apoptosis by interfering with the repair of mitochondrial DNA damage.

1.2.5.2 PNP inhibitors

PNP has been well characterised through the study of PNP deficiency, and it was clear that PNP-deficiency was particularly toxic in T cells. This observation initiated the development of PNP inhibitors to use against T cell malignancies. Targeting enzymes involved in the nucleotide pathway became a common strategy to kill cancer cells. Lymphopenia in patients and in mouse models suggested that PNP would be an ideal drug target (Montgomery John, 1993). Non-cleavable analogues of PNP substrates were developed, including transition state molecules that bind to the enzyme tighter than its substrate (Evans et al., 2000; Miles et al., 1998). Mammalian transition state analogue PNP inhibitors are called Immucilins. So

far, four generations of PNP inhibitors have been developed for use against leukaemia, autoimmunity and gout (a disease in which defective metabolism of uric acid causes arthritis) (Ho et al., 2010).

Interestingly, one of the first PNP inhibitors, BCX-34, showed inhibitory effects in the presence of dG on human T cells but not of rat or mouse T cells (Bantia et al., 1996). An increase of dGTP and decrease of GTP was observed in human but not in mouse T cells. Another study reported an inhibitory effect of BCX-34 on stimulated T cells but had no effect on resting PBMCs. Interestingly, the IC_{50} of BCX-34 increased between 4-15 fold (depending on the stimuli) when PBMCs were treated with IL-2. IC_{50} was low on T-cells and IL-2 had no effect (Conry et al., 1998). This was in line with previous findings showing that cycling cells are less sensitive to dGTP toxicity because dGTP can be used for DNA synthesis (Duan et al., 1990).

The same group reported forodesine (also called immucilin H or BCX-1777), a novel potent and orally active immunosuppressive agent (Bantia et al., 2001). Forodesine is a nucleoside analogue that was described as being 10 to 100 times more potent than BCX-34. It was the first immucilin to induce T cell lymphopenia in a mouse model, with an increase of dG detected in sera after treatment with a single dose. *In vitro*, forodesine was used in combination with low doses of dG to cause toxicity in T cells. Combination of forodesine and dG has been used *in vitro* as a model to mimic the increase of dG observed in sera after treatment with forodesine. Forodesine showed promising results *in vitro* and *in vivo* and entered phase I and II clinical trials against B cell and T cell malignancies (Alonso et al., 2009; Balakrishnan et al., 2010a; Balakrishnan et al., 2006; Balakrishnan et al., 2010b; Gandhi and Balakrishnan, 2007; Gandhi et al., 2005).

More recently, a novel immucilin compound called BCX-4208 (also called DADMe-Immucilin-H) was tested. BCX-4208 induced an increase of dGTP and subsequent cell death in T cells, B cells and NK cells when used in combination with dG (Bantia et al., 2010). BCX-4208 binding mechanism has recently been revealed and it was tested in phase II clinical trial for psoriasis (Decherchi et al., 2015). The main difference between forodesine

and BCX-4208 is that the latter is not a nucleoside analogue and therefore may have different pharmacokinetics.

Taken together, targeting PNP to induce cell death by the accumulation of dG and dGTP is a logical strategy. T cells are particularly susceptible to dGTP-induced cell death and therefore PNP inhibitors have been used against leukaemia. At the time of these studies, the deoxynucleoside triphosphate triphosphohydrolase (dNTPase) SAMHD1 was unknown (detailed in section 1.4). Now, SAMHD1 is well characterised as an enzyme that can degrade dNTPs, including dGTP. Therefore, it may be important to consider its impact on the mechanism of toxicity of PNP inhibitors, which require the accumulation of dGTP.

1.2.5.3 Forodesine efficacy in trials

Forodesine is a PNP inhibitor that showed promising efficacy *in vitro* (Alonso et al., 2009; Balakrishnan et al., 2006; Gandhi and Balakrishnan, 2007). It was evaluated in clinical trials against chronic lymphocytic leukaemia (CLL), lymphomas, B cell acute lymphoblastic

Table 1.1 Clinical trials involving forodesine (adapted from https://clinicaltrials.gov)

status	Study title	Condition
terminated	Trial of Forodesine in Patients With Relapsed B-cell Chronic Lymphocytic Leukemia	B-cell Chronic Lymphocytic Leukemia
terminated	Pharmacokinetic Study of Forodesine in Children With Relapsed or Refractory T-cell or B-cell Precursor Acute Lymphoblastic Leukaemia or T-cell Non- Hodgkin's Lymphoma.	Relapsed or Refractory T-cell Acute Lymphoblastic Leukaemia B-cell Precursor Acute Lymphoblastic Leukaemia T-cell Non-Hodgkin's Lymphoma
completed	Forodesine in the Treatment of Cutaneous T-Cell Lymphoma	Cutaneous T-cell Lymphoma (CTCL),
completed	Study of Forodesine Hydrochloride in Patients With Advanced, Fludarabine-refractory Chronic Lymphocytic Leukemia (CLL)	Leukemia, Lymphocytic, Chronic
completed	Repeat-Dose of Forodesine Hydrochloride (BCX-1777) Infusion in Patients With Advanced T-Cell Leukemia	Leukemia, T-Cell
completed	Phase I/II Clinical Study of Forodesine in Japanese Recurrent/Refractory Peripheral T-cell Lymphoma Patients	Recurrent or Refractory PTCL
completed	Oral Forodesine Hydrochloride (BCX-1777) in Patients With Recurrent or Refractory T/NK-cell Malignancies	Recurrent or Refractory T/NK-cell Malignancies
completed	Phase II Study of Forodesine in Subjects With Chronic Lymphocytic Leukemia (CLL)	Chronic Lymphocytic Leukemia (CLL)
completed	Forodesine (BCX-1777) in Treating Patients With Refractory Stage IIA, Stage IIB, Stage III, Stage IVA, or Stage IVB Cutaneous T-Cell Lymphoma	Lymphoma
terminated	Study of Forodesine Hydrochloride in Patients With Relapsed/Refractory Precursor T-Lymphoblastic Leukemia/Lymphoma Who Have Failed Two or More Prior Treatment Regimens	Leukemia
		Lymphoma
completed	Forodesine Hydrochloride (BCX-1777) for B-Cell Acute Lymphoblastic Leukemia	B-cell Acute Lymphoblastic Leukemia
completed	BCX-1777 in Treating Patients With Refractory Cancer	Cancer
completed	BCX-1777 in Treating Patients With Refractory Cutaneous T-Cell Lymphoma	Lymphoma
completed	Study of Intravenous BCX-1777 in Relapsed or Refractory Aggressive T-Cell Leukemias or Lymphomas	Leukemia, Lymphocytic Lymphoma

leukaemia, peripheral T-cell lymphoma, T-cell lymphomas and refractory cancer (**Table 1.1**). Some of these trials were terminated due to low enrolment and although most of them were completed, limited results are available.

From these 11 completed trials, 5 have published results. The first study used forodesine in CLL patients and reported 4 out of 5 patients with increased levels of dG in the plasma and increased levels of intracellular dGTP upon treatment with forodesine, but none reached an objective response (Gandhi et al., 2005). Another trial in refractory CLL observed a transient decrease in lymphocytes in 2 out of 5 patients. Despite the accumulation of dG and dGTP in the serum, the concentrations observed were much lower than those observed *in vitro* in CLL B cells (Balakrishnan et al., 2010b). Forodesine was also tested against refractory peripheral T/natural killer-cell malignancies in a trial that enrolled 13 people. The authors reported a complete response in one patient, a partial response in two and claimed that disease control was achieved in approximately half of the cohort (Ogura et al., 2012). Another trial used forodesine against B cell acute lymphoblastic leukaemia and showed promising results *in vitro* but did not observe a complete response despite a few weeks of disease control in 2 patients. The authors suggested that forodesine should be infused with dG or combined with chemotherapeutic agents based on the mechanistic rationale to have clinically meaningful activity in B-ALL (Balakrishnan et al., 2013). Finally, the latest published trial results reported a phase II trial that enrolled 144 patients with cutaneous T-cell lymphomas that failed at least 3 therapies. The authors reported that 11% achieved partial remission and 50% had stable disease (Dummer et al., 2014).

Despite promising results *in vitro*, forodesine showed limited efficacy and poor remission rates in patients. It is clear that cell toxicity is caused by dG and dGTP accumulation upon forodesine treatment. However, the known mechanism of action of forodesine seems to be missing a piece of the puzzle to explain and predict its efficacy. The dNTPase SAMHD1 can degrade dGTP and has been shown to be mutated in chronic lymphocytic leukaemia as well as T-cell prolymphocytic leukaemia (Clifford et al., 2014; Johansson et al., 2018).

Therefore, it is reasonable to speculate that mutations in *SAMHD1* could have an impact on the efficacy of PNP inhibitors, which induce cell death by dGTP accumulation.

1.3 Cell death pathways

Nucleotide metabolism is highly regulated and any disruption in this process can cause toxicity and cell death. For example, in PNP deficiency, the alteration of the salvage pathway leads to the accumulation of dG with the subsequent increase of dGTP, which triggers cell death. Cell death is an important mechanism involved in several biological processes from embryogenesis to immunity. Programmed cell death (PCD) is typically divided into 3 main types: apoptosis, programmed necrosis, and autophagic cell death. Apoptosis is the most studied type of cell death and it remained the only known form of PCD for a long time. Autophagy is a catabolic process that digests cellular contents within lysosomes and can accompany and promote cell death. In addition, programmed necrosis is an inflammatory type of cell death very distinct from apoptosis that occurs upon specific signals such as cell damage. Subtypes of programmed necrosis have been described and include necroptosis and pyroptosis. These types of cell death can be engaged when cells fail to trigger apoptosis but also have their own signalling pathways and can get activated in response to specific stimuli. Accumulation of nucleotides, for example dGTP, can trigger cell death. This part of the introduction aims to summarise the types of programmed cell death currently described in the literature.

1.3.1 Apoptosis

Apoptosis is a type of programmed cell death used by multicellular organisms to dispose of an unwanted cell in a way that does not alarm the immune system (Taylor et al., 2008). The apoptotic cell is recognised by phagocytes, which normally only phagocytose entities recognised as non-self. The apoptotic process is a multistep cascade, characterised by:

- rounded cells that detach from their neighbouring cells
- condensation of the nucleus and fragmentation of DNA
- fragmentation of mitochondria and release of its content
- plasma membrane blebbing forming small vesicles called apoptotic bodies

Apoptosis can be initiated in the mitochondria, called intrinsic apoptosis or by the binding of an extracellular ligand to a death receptor (DR), called extrinsic apoptosis. Although intrinsic and extrinsic apoptosis are distinct processes, both require the action of BCL-2 proteins and caspases.

1.3.1.1 BCL-2 proteins

The apoptotic process is highly regulated by several proteins of the BCL-2 family. Early studies reported the proliferative effect of BCL-2 proteins on B cell precursors and showed that BCL-2 proteins provide survival signals and may contribute to neoplasia (uncontrolled growth of cells) (Vaux et al., 1988). Extensive research demonstrated how BCL-2 proteins tightly regulate apoptosis. The apoptotic threshold is regulated by 3 subgroups of the BCL-2 family:

- **BH3-only proteins** (initiators): BIM, PUMA, BAD, NOXA, BIK, HRK, BMF, BID and tBID
- **Pro-survival proteins** (guardians): BCL-2, BCL-XL, BCL-W, MCL1, A1, and BCL-B
- **Pro-apoptotic proteins** (effectors): BAX, BAK and BOX

Proteins of the BCL-2 family contain BH domains, and most of them also contain a transmembrane domain (**Figure 1.7**). Both pro-survival and pro-apoptotic family members contain four distinct BH domains. These domains allow the formation of helical structures that can interact with BH3 domains, and therefore allow interactions with other proteins from the BCL-2 family. These interactions mostly happen on intracellular membranes, especially on the outer mitochondrial membrane (Czabotar et al., 2014).

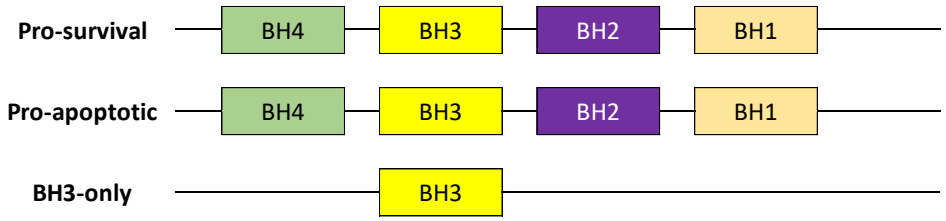


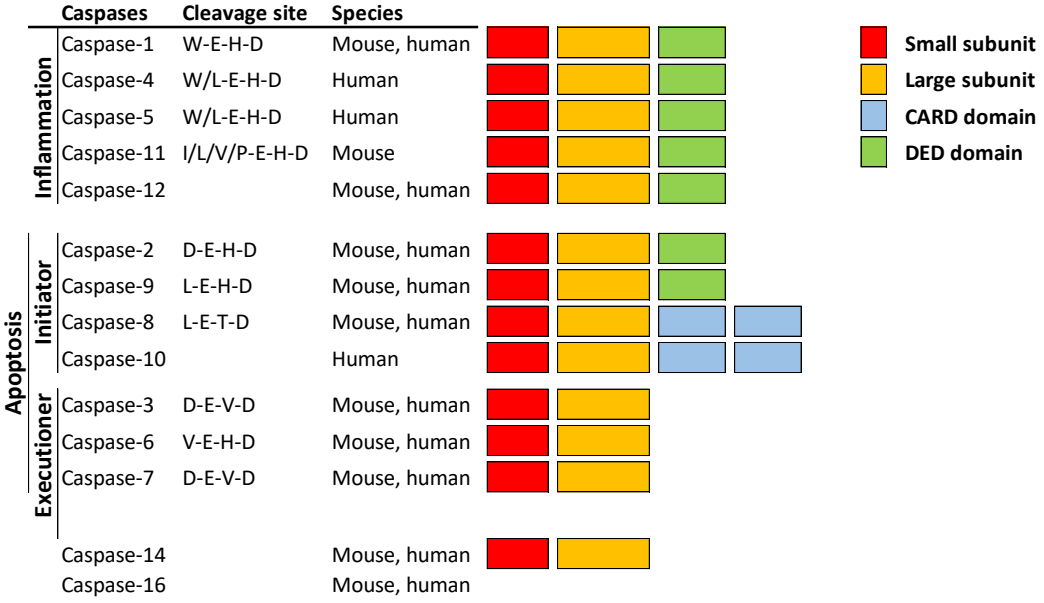
Figure 1.7 BCL-2 proteins and their BH domains. *Adapted from (Czabotar et al., 2014)*

1.3.1.2 Caspases

The execution of the apoptotic process requires key cysteine-aspartic proteases called caspases (Li and Yuan, 2008). Caspases are endoproteases important in maintaining homeostasis and involved in cell death and inflammation. In humans, the caspase family comprises 12 members while there are 11 in the mouse (Shalini et al., 2015). These caspases can be divided into apoptotic caspases, including initiators and executioners, and inflammatory caspases (**Table 1.2**).

Table 1.2 Caspases classification and specificities. *Adapted from (Shalini et al., 2015) and (Degterev et al., 2003)*

	Caspases	Cleavage site	Species
Inflammation	Caspase-1	W-E-H-D	Mouse, human
	Caspase-4	W/L-E-H-D	Human
	Caspase-5	W/L-E-H-D	Human
	Caspase-11	I/L/V/P-E-H-D	Mouse
	Caspase-12		Mouse, human
Apoptosis – Initiator	Caspase-2	D-E-H-D	Mouse, human
	Caspase-9	L-E-H-D	Mouse, human
	Caspase-8	L-E-T-D	Mouse, human
	Caspase-10		Human
Apoptosis – Executioner	Caspase-3	D-E-V-D	Mouse, human
	Caspase-6	V-E-H-D	Mouse, human
	Caspase-7	D-E-V-D	Mouse, human
	Caspase-14		Mouse, human
	Caspase-16		Mouse, human



Caspases are synthesised as inactive procaspases, containing a small and a large subunit (**Table 1.2**). They can contain a death effector domain (DED) or a caspase-recruitment domain (CARD) which can mediate their dimerisation or the recruitment of other proteins to form larger complexes. Pro caspases become active upon cleavage and can then cleave their substrates triggering the apoptotic cascade of events. Active caspases always cleave after an aspartic acid (Asp) residue but recognise and cleave a different sites depending on their specificity (**Table 1.2**). It has become clear that caspases are not only involved in cell death but also play other important roles. For example, caspase 8 is involved in homeostasis of T cells and caspase 3 in differentiation and regeneration and neural

development. Evidence suggests that caspases may also be involved in promoting tumorigenesis (Degterev et al., 2003; Shalini et al., 2015).

1.3.1.3 Intrinsic apoptosis

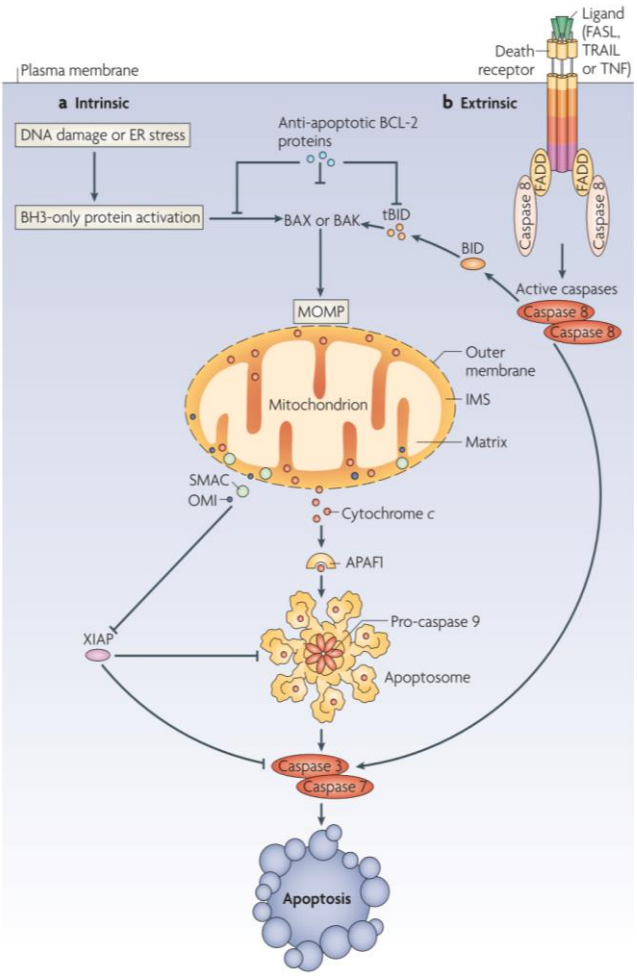


***Figure 1.8 Mechanisms of intrinsic (a) and extrinsic (b) apoptosis**. Illustration from (Tait and Green, 2010).*

Intrinsic apoptosis (also called the mitochondrial pathway) is activated within the cell by danger signals such as DNA damage or ER stress. Danger signals activate BH3-only proteins, activating BAX or BAK which can form pores into the mitochondrial membrane and trigger mitochondrial outer membrane permeabilisation (MOMP) (**Figure 1.8**). This induces the leakage of pro-apoptotic proteins, including the release of cytochrome C from the mitochondria, a key event of intrinsic apoptosis. Cytochrome C binds apoptotic protease-activating factor 1 (APAF1), inducing its oligomerisation into a platform called the apoptosome. The apoptosome recruits and activates the initiator caspase 9, which cleaves and activates executioner caspases 3 and 7, leading to apoptosis. Mitochondrial release of second mitochondria-derived activator of caspase (SMAC; also known as DIABLO) and OMI (also known as HTRA2) neutralises the caspase inhibitory function of X-linked inhibitor of apoptosis protein (XIAP) (Tait and Green, 2010).

In response to cytotoxic stress signals, BH3-only proteins can neutralise BCL-2 pro-survival proteins or directly activate BCL-2 pro-apoptotic proteins. Although it is clear that BAX and BAK oligomerisation are required to induce pore formation, several models have been

proposed for the regulation of the apoptotic switch. In the direct activation model, BH3-only proteins can directly activate BAX. In contrast, in the indirect activation model, BAX can be activated through the inhibition of BCL-2 pro apoptotic proteins by BH3-only proteins. Alternatively, both events could happen together, which is a combination of the direct and indirect model. MOMP induction leads to the release of cytochrome C and SMAC/Diablo into the cytoplasm (Tait and Green, 2008).

1.3.1.4 Extrinsic apoptosis

Extrinsic apoptosis is also called death by receptor ligand, or death receptor (DR) induced cell death. Binding of the ligand to the DR induces the recruitment of FAS-associated death domain protein (FADD) that binds, dimerises and activates the initiator caspase 8. What happens downstream of active caspase 8 depends on the cell type. In so-called type I cells, caspase 8 initiates apoptosis directly by cleaving and activating executioner caspases 3 and 7. In type II cells, caspase 8 must first activate the intrinsic apoptotic pathway by activating BID, generating tBID that can induce BAX and BAK oligomerisation and trigger MOMP (**Figure 1.8**). These two types of cells differ by the presence of intracellular inhibitor of apoptosis proteins (IAPs), which block executioner caspase function unless suppressed by proteins released from the mitochondria (McIlwain et al., 2013).

Death receptors (DRs) are transmembrane proteins expressed at the cell surface; there are 6 different human DRs (**Table 1.3**). They trigger apoptosis upon binding to their ligands: FAS ligand (FasL), TNF-related apoptosis-inducing ligand (TRAIL), TL1A, N-APP or TNF. Crosstalk between the extrinsic and intrinsic pathways occur through caspase 8 cleavage and activation of BID, which results in tBID interaction with BAX and BAK (Tait and Green, 2010). Extrinsic apoptosis is an important mechanism required for the immune system and homeostasis.

Table 1.3 Summary of death receptors and their ligands

Death receptor	Other name	Ligand
TNF-R1		TNF
CD95	Fas/APO-1	CD95L (FasL)
DR3	TRAMP/APO-3	Tl1A
DR4	TRAIL-R1	TRAIL
DR5	TRAIL-R2/APO-2/TRICK/KILLER	TRAIL
DR6		N-APP

1.3.2 Necrosis

Necrosis is a passive mode of cell death caused by cellular damage, distinct from apoptosis. It is characterised by the loss of membrane integrity and the release of intracellular content. The cellular content contains danger-associated molecular patterns (DAMPs) that alarm neighbouring cells and trigger inflammation. Therefore, unlike apoptosis, necrosis is an inflammatory form of cell death (Nikoletopoulou et al., 2013).

However, necrosis is not always a passive process. A form of PCD called necroptosis, with necrotic and autophagic features was described more than a decade ago (Degterev et al., 2005). In addition, other types of specific programmed necrosis exist such as parthanaptos, ferroptosis or oxytosis, mitochondrial permeability transition-dependent necrosis, pyronecrosis, pyroptosis, and cell death associated with the release of extra cellular traps (NETs) by neutrophils (NETosis). Pyroptosis and necroptosis are now well characterised and will therefore be detailed in the following sections.

1.3.2.1 Regulated necrosis: necroptosis

An early report showed the activation of a receptor-interacting protein kinase (RIP)-dependent necrotic-like cell death when pan caspase inhibitor zVAD was used with FasL, TNF or TRAIL (Holler et al., 2000). At the time, it was observed that caspase inhibitors were not able to block DR-induced cell death and triggered instead cell death with necrosis-like features. Necroptosis was described shortly after, as a common non-apoptotic death pathway characterised by necrotic cell death morphology and activation of autophagy (Degterev et al., 2005). The authors also identified necrostatin-1, a specific inhibitor of the necroptosis pathway. Further studies showed that necroptosis can be triggered by DRs, IFNs, toll-like receptors, intracellular RNA and DNA sensors and may other mediators (Pasparakis and Vandenabeele, 2015). Upon virus infection, the kinase RIP3 interacts and phosphorylates RIP1, forming a stable RIP3-pRIP1 complex (Cho et al., 2009). Mixed lineage kinase domain-like (MLKL) protein was later shown to also be phosphorylated by RIP3, making pMLKL a key mediator of the necroptosis cascade (Sun et al., 2012). Once phosphorylated, pMLKL polymerises to form tetramers and disrupts the plasma membrane

by a mechanism that is not entirely clear (**Figure 1.9**). One model suggested that MLKL requires BAX and BAK oligomerisation to form the mitochondrial permeability transition pore, and then triggers cell death by necroptosis (Karch et al., 2015). Alternatively, pMLKL polymers may form pores directly in the plasma membrane (Shan et al., 2018).

Mutant mice lacking RIP1, RIP3 or MLKL showed normal development, suggesting that necroptosis is not involved in maintaining homeostasis but only important in inflammatory settings (Shan et al., 2018). Better understanding of necroptosis will help to develop inhibitors against specific targets of that pathway. Necrostatin-1 is a RIP1 inhibitor shown to limit tissues injury in animal models of ischemic brain, kidney and heart injuries, multiple sclerosis and Alzheimer's disease (Shan et al., 2018). This shows that necroptosis is an important mechanism in cell death and inflammation.

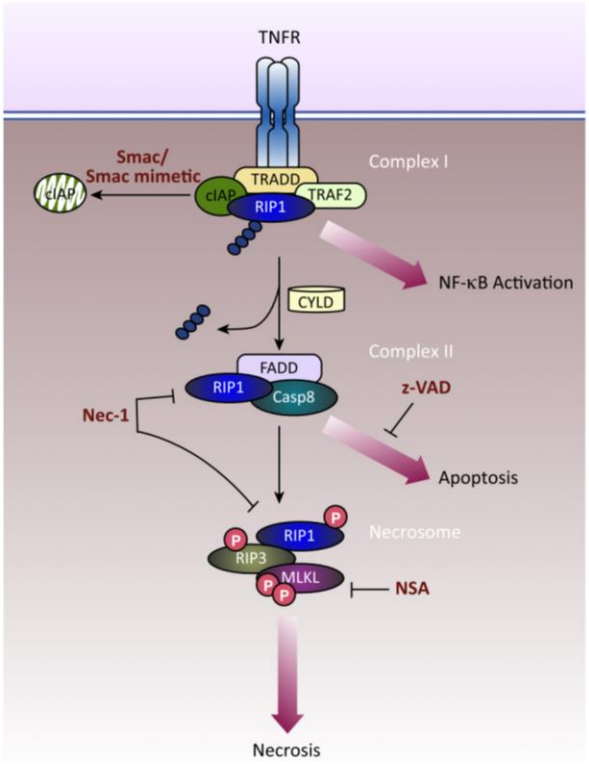


Figure 1.9 Necroptosis cascade. *Binding of TNFα to its receptor (TNFR) activates NF-κB signalling pathway. This can trigger apoptosis through recruitment of caspase 8, which can be blocked by zVAD. Engagement of TNFR and apoptosis blockage by zVAD trigger phosphorylation of RIP1, RIP3 and MLKL. pRIP1, pRIP3 and pMLKL interact together to form pores and disrupt membrane integrity. Necrostatin-1 (nec-1) prevent RIP1 phosphorylation while necrosulfonamide (NSA) blocks MLKL's N terminal coil–coil domain function. Both are specific inhibitors of necroptosis. Illustration from (Sun and Wang, 2014).*

1.3.2.2 Regulated necrosis: pyroptosis

Pyroptosis, also called caspase 1-dependent cell death, is another form of inflammatory programmed cell death triggered upon various stimuli. It can be triggered by strokes, heart attack or cancer and it is critical to control infections by various pathogens (Bergsbaken et al., 2009). Intracellular bacteria trigger caspase 1 induced pyroptosis and pyroptosis-

mediated bacteria release leads to clearing of pathogens by neutrophils *in vivo* (Miao et al., 2010). Pyroptosis allows recruitment of neutrophils through the release of cytokines. Apoptosis-associated speck-like protein (ASC) assemble to induce the formation of the inflammasome (also called pyroptosome), a large supramolecular complex, that induces the cleavage of procaspase 1 (Fernandes-Alnemri et al., 2007). Uncontrolled activation of pyroptosis can lead to tissue damage, organ failure and lethal septic shock (Aglietti and Dueber, 2017).

Pyroptosis is characterised by the rupture of the plasma membrane and the release of pro-inflammatory cellular content. This is triggered by an influx of water and ions that cause the cell to swell and lyse (Fink and Cookson, 2006). Pyroptosis is distinct from apoptosis and does not show activation of caspase 3, 6 and 8, or PARP cleavage and release of cytochrome C from the mitochondria. Instead, it is dependent on inflammatory caspases 1 or on caspase 11 (mice)/4/5 (human). Caspase 1 is activated by the ligands of the inflammasome while caspases 11/4/5 can directly recognise bacterial LPS. Caspase 1 is also able to cleave and activate the inflammatory cytokines IL-1β and IL-18, meaning that the intracellular content released contains mature forms of IL-1β and IL-18 (Cookson and Brennan, 2001).

Procaspase 1 is recruited and activated by cytosolic protein complexes called inflammasomes. Inflammasomes are large cytosolic, multimeric complexes formed upon activation of a distinct subset of nod-like receptors (NLRs) and AIM2 like receptors (ALRs). There are different mechanisms of inflammasome activation depending on the sensing proteins (the NLRP3 inflammasome is illustrated in **Figure 1.10**). Although the initiation cascade may differ, formation of the inflammasome always require the recruitment of ASC proteins and procaspase 1. The activation of the inflammasome by caspase 1 is called canonical inflammasome, in contrast to the non-canonical inflammasome activated by caspase 11 (Lamkanfi and Dixit, 2014). Inflammasome activation leads to the secretion of the proinflammatory cytokines IL-1β and IL-18 as well as the induction of pyroptosis. The

activation of the inflammasome complex aims to destroy the infected cell and expose the pathogen to circulating phagocytes by pyroptosis.

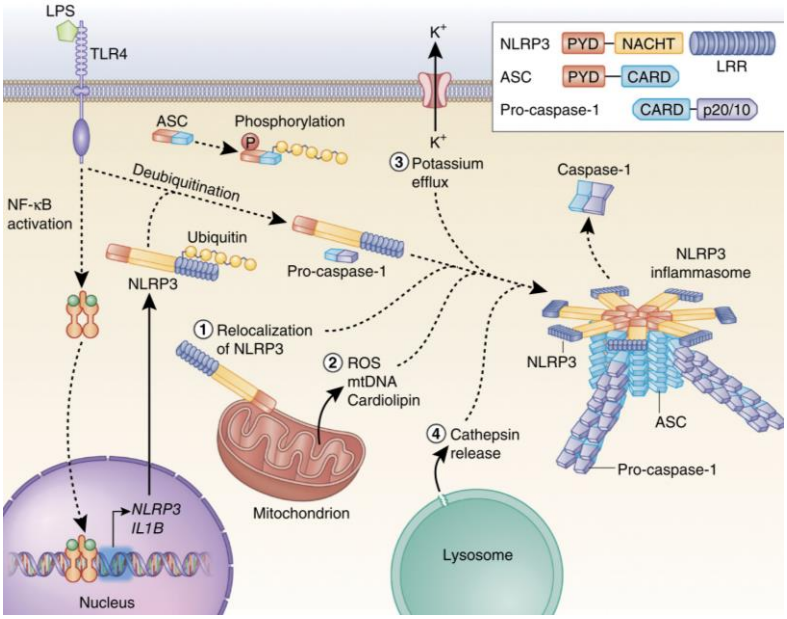


Figure 1.10 NLRP3 inflammasome. *Activation of NLRP3 triggers the assembly of the multimeric complex composed of procaspase 1, ASC proteins and NLRP3. The assembly of the inflammasome triggers the cleavage of procaspase 1. Figure from (Guo et al., 2015).*

The pyroptosis effectors were only revealed in 2015, when gasdermin D (GSDMD) was discovered by two independent groups (Kayagaki et al., 2015; Shi et al., 2015). GSDMD-deficient cells were shown to be resistant to pyroptosis induced by LPS or canonical inflammasome ligands. GSDMD is composed of a pore forming domain (PFD) and a repressor domain. GSDMD can be cleaved by caspase 1 or caspase 11/4/5, releasing the repressor domain of the protein, thereby activating the PFD (**Figure 1.11**). The PFD

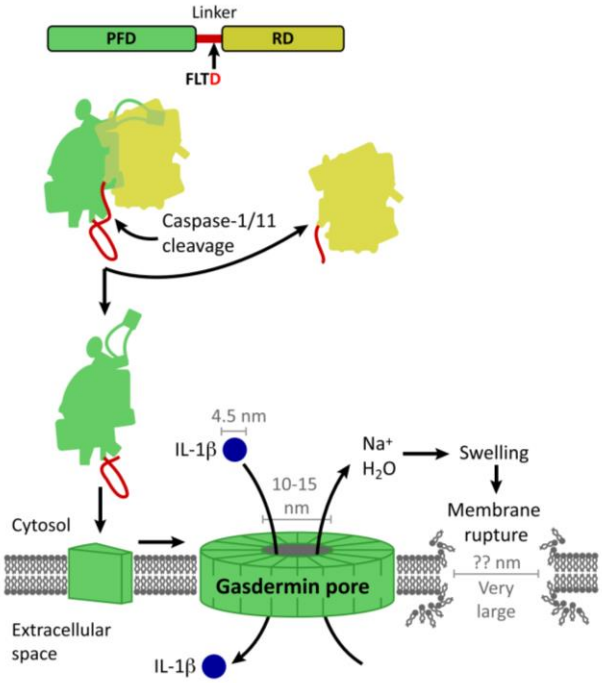


Figure 1.11 Model of gasdermin pore formation. *Caspase 1/11 or 4/5 cleave pro-IL-1b, pro-IL-18, and gasdermin D. Gasdermin D is composed of an amino-terminal PFD (green), a linker (red), and a carboxy-terminal RD. The gasdermin pore is formed by oligomerisation of gasdermin oligomers. This allows Na^+ to enter the cell, bringing with it water that causes increase of the cell volume and eventually membrane rupture. Consequently, the cytosolic contents is released rapidly. FLTD, the amino acid sequence within the gasdermin D linker that is cleaved by caspase 1/11; IL, interleukin; PFD, pore-forming domain; RD, repressor domain. Illustration from (Kovacs and Miao, 2017).*

oligomerises to form large pores in the plasma membrane that cause swelling of the cell and rupture of the cell membrane. Although there are several members in the gasdermin family (6 in humans, 10 in mice), gasdermin D is the only one activated by inflammatory caspases. Another gasdermin protein, gasdermin E is cleaved and activated by caspase 3, an effector caspase involved in apoptosis (Kovacs and Miao, 2017).

1.3.3 Autophagic cell death

In addition to apoptosis and necrosis, autophagy can be involved in the induction of cell death. Autophagy is a catabolic process by which cellular content is degraded and recycled within lysosomes. It is an important mechanism that maintains homeostasis by degrading excess or damaged cellular constituents. Cellular stressors such as nutrient starvation, DNA damage, or organelle damage, increase its activity (Shimizu et al., 2014). The autophagosome, a double membrane that isolates a fraction of the cytoplasm, constitutes a hallmark of autophagy. During autophagy, the autophagosome matures and fuses with lysosomes, leading to the degradation of its content by lysosomal enzymes (Mizushima et al., 2011). This process is called canonical macroautophagy (**Figure 1.12**). In contrast,

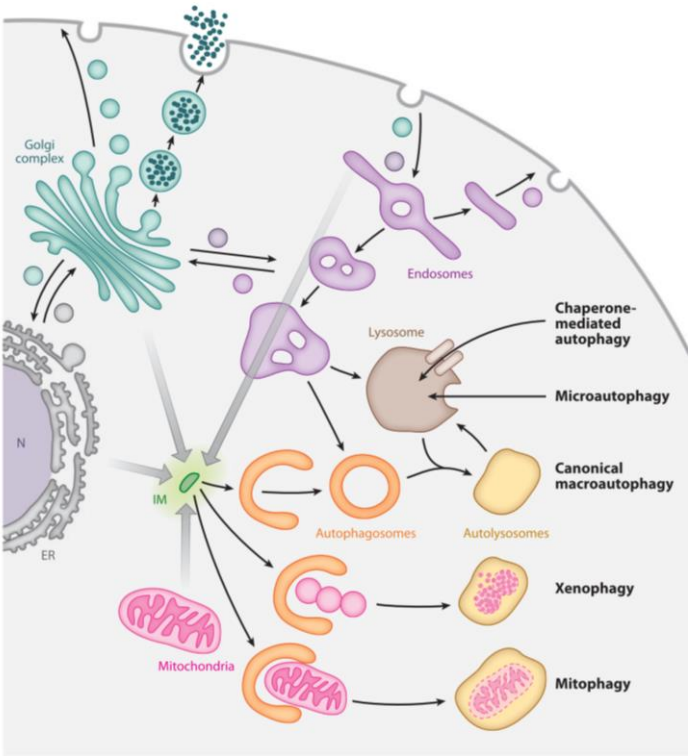


Figure 1.12 Membrane dynamics of autophagy in yeast and mammals. *Macroautophagy is mediated by the autophagosome, which contain a portion of the cytoplasm. The outer membrane of the autophagosome fuses with the lysosome, allowing lysosomal enzymes to degrade sequestered cytoplasmic materials in autolysosomes. Macroautophagy can be specific against organelles such as mitochondria (mitophagy) and against intracellular bacteria (xenophagy). In chaperone-mediated autophagy, substrate proteins are recognised specifically by cytosolic chaperones and directly transported across the lysosomal membrane to the lumen. Microautophagy occurs by invagination of the lysosomal membrane itself into the lumen. Abbreviations: ER, endoplasmic reticulum; IM, isolation membrane; N, nucleus. Figure from (Mizushima et al., 2011)*

other types of autophagy targeting to mitochondria (mitophagy), peroxisomes (pexophagy) or intracellular bacteria (xenophagy) also exist (**Figure 1.12**).

Autophagic cell death is a specific term that needs to be used with caution. The process of autophagy can be observed when cells are dying through a specific mechanism. Although autophagy happens in cells in the presence of stressors, it does not always results in autophagic cell death. Therefore, the proposed definition of "autophagic cell death" refers to a type of cell death mediated by autophagy that can be blocked by a chemical inhibitor of autophagy or by the genetic ablation of autophagy genes (Shimizu et al., 2014). BAX/BAK deficient cells die with hallmarks of autophagy upon apoptotic stimuli (Shimizu et al., 2004). The same group showed that phosphorylation of Jun N-terminal kinase (JNK) generates death signals that induce autophagic cell death (Shimizu et al., 2010). It is believed that autophagy is an important mechanism in cancer cells, since they do not undergo autophagy due to low JNK activation while healthy cells do (Shimizu et al., 2014). Autophagic cell death is a relatively newly describe type of cell death which has not been extensively studied.

In summary, cell death is an important process that includes many different types of cell death with specific mechanisms of activation. Therefore, it is important to characterise cell death when observed experimentally. Each type of cell death presents specific hallmarks that can be identified with appropriates techniques. I have mentioned earlier the importance of nucleotide metabolism in maintaining genome integrity. PNP deficiency is an example of disease where a mutation in an enzyme of the salvage pathway leads to cell death (section 1.2.5). In this condition, the accumulation of dGTP causes toxicity and triggers cell death by mechanisms that are not fully understood. The detailed characterisation of various types of PCD may provide new clues in understanding how dGTP accumulation triggers cell death.

1.4 Sterile alpha motif histidine aspartate domain 1 (SAMHD1) protein

First described as a an interferon-γ-induced protein, sterile alpha motif histidine aspartate domain 1 (SAMHD1) was identified as the mouse homologue of the interferon-γ (IFN-γ) induced protein MG11 in dendritic cells (DCs) (Li et al., 2000). SAMHD1 was shown to be upregulated in human fibroblasts upon stimulation with TNF-α (Liao et al., 2008). Mutations in the *SAMHD1* gene were shown to influence the innate immune response in Aicardi-Goutières syndrome (AGS), an inflammatory encephalopathy characterised by the chronic production of type I interferon (Rice et al., 2009). The authors showed that SAMHD1 was upregulated upon IFN-β treatment in an interferon (IFN) receptor-dependent manner and independently of MyD88 in mouse BMDMs. Later, SAMHD1 was identified as a host-restriction factor to HIV-1 in myeloid cells and its dNTPase function was revealed (Goldstone et al., 2011; Laguette et al., 2011; Powell et al., 2011). dNTPases are enzymes that catalyse the degradation of dNTPs into deoxynucleosides and phosphate (**Figure 1.13**). Therefore, SAMHD1 is an important enzyme in regulating dNTP pools in the cells (Franzolin et al., 2013; Kim et al., 2012).

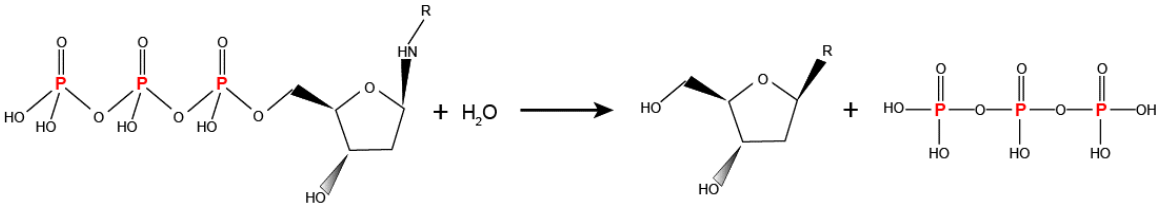


Figure 1.13 Reaction catalysed by the dNTPase SAMHD1. *dNTPs are degraded in the presence of water into deoxynucleoside and triphosphates. Adapted from BRENDA (The comprehensive enzyme information system), EC 3.1.5.B1.*

SAMHD1 contains a sterile alpha motif (SAM) domain and a HD domain. SAM domains were described as protein-protein interaction domains that can act as kinase docking sites, polymerisation sites or RNA-binding domains (Qiao and Bowie, 2005). HD domains are characterised by a motif with a doublet of divalent-cation-coordinating histidine and aspartic acid residues, found in a diverse superfamily of enzymes with a known phosphohydrolase activity and is highly conserved among eukaryotes (Aravind and Koonin, 1998). Indeed, the dNTPase EF1143 of *Enterococcus faecalis* was the first to be crystallised and showed that

dNTPs act as substrates and modulators (Vorontsov et al., 2011; Vorontsov et al., 2014). The active enzyme EF1143 is a tetramer that contains a primary and a secondary allosteric site that binds with highest affinity to dGTP. Interestingly, EF1143 hydrolyses all four dNTPs in the presence of Mn^{2+} but requires dGTP as an effector in the presence of Mg^{2+}. When SAMHD1's catalytic domain was crystallised, it showed striking similarities with bacterial dNTPase EF1143, showing the importance of dNTPase activity across species. SAMHD1 appeared to be a dimeric protein in which dNTPase activity was stimulated by dGTP (Goldstone et al., 2011; Powell et al., 2011). In addition to being required for dNTP hydrolysis, dGTP seemed to be the preferred substrate of the enzyme. Since its characterisation 7 years ago, numerous publications reported the involvement of SAMHD1 in different mechanisms suggesting that the protein has several independent functions. This part of the introduction aims to detail these roles of SAMHD1.

1.4.1 SAMHD1 in Aicardi-Goutières syndrome

Mutations in *SAMHD1* were first identified and linked to Aicardi-Goutières syndrome (AGS), a genetically determined encephalopathy characterised by increased production of type I IFN. AGS is a rare Mendelian disease that can be misdiagnosed as a congenital infection due to the inappropriate response of the immune system (Crow and Livingston, 2008). It is an heterogeneous disease that can be caused by mutations in any of these genes: DNA repair 3' exonuclease 1 (***TREX1***) endonuclease, any subunit from the ribonuclease H2 complex (***RNase H2A, B, C***), the dNTPase SAMHD1, adenosine deaminase acting on RNA (***ADAR1***) or the cytosolic sensor IFN-induced helicase C domain containing protein 1 (***IFIH1***, also called melanoma differentiation-associated gene 5 or MDA5) (Crow Yanick et al., 2015; Crow and Manel, 2015).

TREX1 is a 3'-5' DNA exonuclease and *Trex1*$^{-/-}$ mice display an inflammatory phenotype (Crow et al., 2006a; Morita et al., 2004). TREX1 was initially shown to be a negative regulator of cytosolic DNA sensing and it was suggested that autoimmunity could be triggered by an unanticipated contribution of endogenous retroelements (Stetson et al., 2008). A recent publication showed that TREX1 prevented the accumulation of single

strand RNAs (ssRNAs) from long interspersed nuclear element (LINE1) endogenous retroelements in astrocytes (Thomas et al., 2017). LINE1 are transposable elements in DNA that comprise 17% of the human genome; most LINE1 elements are inactive although some retain the ability to retrotranspose (Ostertag and Kazazian Jr, 2001).

Ribonuclease H2 (**RNase H2**) is a major nuclear enzyme involved in the degradation of RNA/DNA hybrids (Stein and Hausen, 1969). The RNase H2 complex is composed of three proteins encoded by *RNASEH2A*, *RNASEH2B* and *RNASE2C*. Mutations in *RNASEH2B*, were identified in AGS (Crow et al., 2006b). Later, mutations in *RNASEH2A* and *RNASE2C,* which prevent the formation of the RNase H2 complex were also reported (Reijns et al., 2011). RNase H2 is a key enzyme that prevents genome instability and p53-dependent DNA damage response (Reijns et al., 2012). RNase H2 knock in mice displayed an interferon signature dependent on the cGAS-STING pathway (Pokatayev et al., 2016). RNase H2 was recently shown to control LINE1 retrotransposition, adding it the list of known LINE1 repressors, which includes TREX1, SAMHD1 and ADAR1 (Benitez-Guijarro et al., 2018).

ADAR1 catalyses the deamination of adenosine to inosine in double-stranded RNA. It was shown to prevent translational shutdown during type I IFN stimulation; it binds to dsRNA to prevent PKR activation and its absence triggers type I IFN through MDA5 (Chung et al., 2018). On the other hand, the ***IFIH1*** gene encodes MDA5 protein which is a sensor for dsRNA (Kato et al., 2006). A recent paper showed that *IFIH1* mutations causing constitutive activation of MDA5 can trigger the production of type I IFN caused by the loss of tolerance to endogenous Alu retroelements transcripts (Ahmad et al., 2018). Alu elements are a short DNA sequences encoding the most abundant transposable elements of the human genome (>10^6 copies) (Szmulewicz et al., 1998). In addition, LINE1 retrotransposons may contribute to autoimmunity through ADAR1-mediated sensing of RNA by MDA5 (Zhao et al., 2018). Together, research carried out in the last decade led to some insight into the mechanisms by which TREX1, RNaseH, ADAR1 and MDA5 contribute to the chronic production of type I IFN in AGS.

Despite numerous investigations of SAMHD1's role in AGS, the mechanism that triggers the production of type I IFN production remains unclear. Mutations in *SAMHD1* initially suggested its implication as a negative regulator of the innate immune response (Rice et al., 2009). Moreover, *SAMHD1* mutations were shown to cause intracerebral large artery disease caused by inflammation (Ramesh et al., 2010) and were also associated with chronic arthropathy and contractures (Dale et al., 2010). In addition, altered cytokine expression was observed (Thiele et al., 2010) and may also be associated with mtDNA deletions (Leshinsky-Silver et al., 2011). It was later shown that SAMHD1 can modulate LINE1 and Alu/SVA retro transposition (Zhao et al., 2013). This suggests that SAMHD1, like TREX1, is a potent LINE1 suppressor. More recently it was revealed that SAMHD1-mediated block of LINE1 is dependent upon its phosphorylation (Herrmann et al., 2018). Surprisingly, generation of *Samhd1*$^{-/-}$ mice showed that these mice did not develop an autoimmune disease despite elevated levels of type I IFN in several organs (Behrendt et al., 2013; Rehwinkel et al., 2013). The IFN signature in *Samhd1*$^{-/-}$ mice was later shown to be cGAS and STING-dependent (Maelfait et al., 2016). Another group showed that SAMHD1 deficiencies lead to genome instability (Kretschmer et al., 2015). The authors were the first to suggest that high dNTP unbalances trigger DNA damage causing intrinsic production of type I IFN. Since then, several publications reported the involvement of SAMHD1 in DNA repair (detailed in section 1.4.3). Finally, a recent paper suggested that SAMHD1 abolishes sensing of RNA through PI3K/AKT/IRF3 (Oh et al., 2018). Altogether, numerous studies have shown that *SAMHD1* mutations lead to the production of type I IFN in AGS, but it is not exactly clear by which mechanism SAMHD1 deficiency triggers the disease.

1.4.2 SAMHD1 is a virus restriction factor

In 2011, SAMHD1 was identified as human immune deficiency virus 1 (HIV-1) restriction factor expressed in myeloid cells, counteracted by the virally-encoded protein Vpx (Hrecka et al., 2011; Laguette et al., 2011). SAMHD1's function as a HIV-1 host restriction factor has been intensively studied with numerous publications in the last 7 years. SAMHD1 is a

dNTPase that can be counteracted by Vpx, a protein expressed by HIV-2 (Goldstone et al., 2011; Hrecka et al., 2011). Interestingly, HIV-1 fails to transduce dendritic cells (DCs) while HIV-2 transduces myeloid cells efficiently, requiring one of its accessory proteins, Vpx. Vpx was shown to rescue the inhibition of lentiviral infection by targeting SAMHD1 for proteosomal degradation through recruitment of an E3 ubiquitin ligase (Ahn et al., 2012; Hofmann et al., 2012). SAMHD1 restricts HIV-1 through its dGTP-regulated dNTPase activity. By degrading intracellular pools of dNTPs, SAMHD1 is a major regulator of DNA precursor pools in mammalian cells (Franzolin et al., 2013; Lahouassa et al., 2012; Powell et al., 2011). Maintaining low dNTPs reduces their availability for HIV-1 that requires dNTPs to reverse transcribe its genome. The restriction activity of SAMHD1 is not only confined to myeloid cells, but was also observed in quiescent CD4 T cells (Baldauf et al., 2012; Descours et al., 2012). In mice, SAMHD1 reduced the induction of virus-specific T cells upon infection, showing that its virus restriction function limits the magnitude of the innate and adaptive immune response (Maelfait et al., 2016).

SAMHD1 was also suggested to have nuclease activity required for HIV-1 restriction (Beloglazova et al., 2013; Ryoo et al., 2014). Another group claimed that SAMHD1 specifically restricts retroviruses through its RNase activity. However, SAMHD1's nuclease function is controversial as another paper reported the binding of SAMHD1 to ssRNA but did not observe nuclease activity (Seamon et al., 2015). In addition, an independent lab generated the mutants SAMHD1$_{D137N}$ and SAMHD1$_{Q548A}$ used by Ryoo et al (Antonucci et al., 2016).Antonucci et al. could not observe HIV-1 restriction in cycling cells by WT SAMHD1 or SAMHD1 T592A (phopspho ablative mutant) nor by SAMHD1$_{D137N}$ and SAMHD1$_{Q548A}$. These two mutants SAMHD1$_{D137N}$ and SAMHD1$_{Q548A}$ significantly reduced HIV-1 reverse transcription at late stages of infection, which correlated with lower dNTP levels. Therefore the field is divided between those who postulate that SAMHD1 also has a nuclease function and those who consider these findings as artefacts.

SAMHD1's restriction function is not limited to HIV-1 and it was shown to also prevent replication of DNA viruses in non-cycling cells. SAMHD1 blocks replication by herpes

simplex virus-1 (HSV-1), human T-cell leukaemia virus type 1, vaccinia virus, murine leukaemia virus (MLV) and hepatitis B virus (Chen et al., 2014; Hollenbaugh et al., 2013; Kim et al., 2013; Sze et al., 2013; Wang et al., 2015). HSV-1 infection was shown to be blocked by CDK6 inhibitors, suggesting that preventing SAMHD1 phosphorylation through CDK6 renders SAMHD1 active and therefore restricts HSV-1 (Badia et al., 2016). This is in line with another publication showing that SAMHD1 restricts DNA viruses in non-dividing myeloid cells, where it is not phosphorylated and therefore active (Hollenbaugh et al., 2013).

SAMHD1's function as a restriction factor has been extensively studied and is well described. These studies suggest that SAMHD1 evolved to counteract infection by viruses but its nucleotide sequence suggests otherwise. SAMHD1 is an extremely conserved protein and sequence alignments showed that SAMHD1's catalytic domain, the HD domain, is conserved and is not only present in mammals but also in other species such as *Xenopus* and *Hydra* (**Figure 1.14**). Lentiviruses, a group of retroviruses (family *Retroviridae*), are modern viruses that infect mammals (Gifford, 2012). There are 7 lineages of lentivirus described in mammals (agomorph, equine, small ruminant, bovine, feline, prosimian and simian). SAMHD1 presence in *Xenopus* and *Hydra* suggests that the dNTPase did not evolve to counteract lentiviruses. Instead, we think that SAMHD1's ancestral function is not to restrict viruses, but is involved in a more ancestral cellular function related to dNTPs.

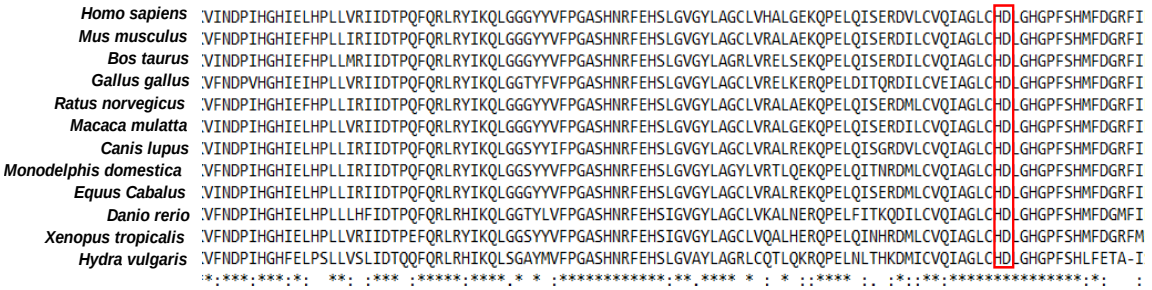


Figure 1.14 Sequence alignments of SAMHD1 in indicated species.

1.4.3 SAMHD1 is involved in DNA repair

The first publication to report *SAMHD1* mutations in CLL also reported SAMHD1 localisation at DNA repair sites (Clifford et al., 2014). SAMHD1 co-localised with 53BP1 foci, a marker of DNA damage, upon treatment with the DNA damaging agent camptothecin (CPT). In

contrast, another paper claimed that the DNA damage response does not trigger redistribution of SAMHD1 to nuclear foci (Medeiros et al., 2018). These authors demonstrated a non-specific localisation of SAMHD1 to nuclear foci upon treatment with CPT. This was observed when a monoclonal antibody was used but no co-localisation was observed with polyclonal antibodies against the N-terminus of hSAMHD1, suggesting that it is an artefact. This highlights the importance of validating reagents to confirm findings.

Nonetheless, two major publications recently demonstrated the involvement of SAMHD1 in DNA repair. The first one showed that SAMHD1 promotes DNA end restriction to facilitate DNA repair by homologous recombination (Daddacha et al., 2017). In this study, SAMHD1 promoted homologous recombination (HR) and DNA end resection independently of its dNTPase activity. A second publication demonstrated that SAMHD1 promotes the degradation of nascent DNA at stalled replication forks (Coquel et al., 2018). This work in human cell lines showed that SAMHD1 stimulates MRE11 activity, whilst in its absence nascent DNA accumulates and triggers the production of type I IFN through the cGAS-STING pathway. These two papers report a novel function of SAMHD1 in DNA repair. These mechanisms in DNA repair may explain how SAMHD1 mutations promote tumorigenesis (Coquel et al., 2018; Daddacha et al., 2017).

1.4.4 *SAMHD1* mutations in cancer

SAMHD1's dNTPase function is important to regulate dNTP pools and fine tuning of these pools is critical to maintain genome integrity (Kumar et al., 2011a). *Samhd1*$^{-/-}$ mice have elevated dNTP pools due to the accumulation of dNTPs that can no longer be degraded by SAMHD1. dNTP pools are a limiting factor in quiescent cells and genomic DNA can only be synthesised if dNTPs are available. Therefore highly proliferative cells such as cancer cells require high dNTP levels. Over the last few years, several independent groups have identified mutations in *SAMHD1* in different types of cancer cells, suggesting that transformed cells benefit from high dNTP levels.

SAMHD1 mutations were first identified in chronic lymphocytic leukaemia (CLL). A whole genome sequencing study observed that *SAMHD1* was recurrently mutated in CLL patients,

suggesting that *SAMHD1* mutations may be a founding event (Schuh et al., 2012). Schuh's group observed acquired *SAMHD1* mutations in 11% of relapsed CLL patients and these were associated with high allele variant frequency and low SAMHD1 expression (Clifford et al., 2014). Clifford et al. showed that SAMHD1 localises to sites of DNA damage, suggesting it could play a role in DNA repair. Moreover, *SAMHD1* ranked 6th as the most recurrently mutated gene in CLL (behind *TP53*, *ATM*, *SF3B1*, *NOTCH1* and *XP01*). These recurrent mutations are associated with poor outcome with *TP53*, *ATM* and *SF3B1* conferring short survival (Guieze et al., 2015). In addition, CLL can be characterised by the abundance of somatic hypermutation (SHM) in the Ig variable heavy chain locus (IgHV). Coding mutations in *SAMHD1* were identified in IgVH (Burns et al., 2017). Interestingly, one group reported that SAMHD1 enhances immunoglobulin hypermutation by promoting transversion mutations through dNTP starvation (Thientosapol et al., 2018). The authors observed that SAMHD1 inactivation triggered an increase in transition mutations at C:G base pairs and a substantial decrease in transversion mutations at A:T and C:G base pairs in both strands.

Mutations in *SAMHD1* were also observed in colon cancer, where it is frequently mutated (Rentoft et al., 2016). The authors showed that mutations in *SAMHD1* had a negative impact on its activity and that they were often associated with a defect of the mismatch repair machinery. Combination of high dNTP pools and mismatch repair deficiency may lead to an increased mutation rate. *SAMHD1* mutations in one allele was sufficient to increase dNTP pools. Another study observed lower mRNA levels of SAMHD1 in colorectal cancer tissues. The authors suggested that SAMHD1 (with cGAS, RNase H2B and RNase H2C) could be used as prognostic marker of colorectal cancer (Yang et al., 2017).

Finally, a most recent study identified *SAMHD1* as a new gene recurrently mutated in T cell prolymphocytic leukaemia (T-PLL). *SAMHD1* mutations were found in ~20% of T-PLL with a destructive mutation in 18% of cases (Johansson et al., 2018).

The advances in new technology combined with the reduction in price render technology such as whole exon sequencing more affordable. Scientists can now screen more genes, faster and cheaper. This is allowing the identification of new important genes in cancer

progression, such as *SAMHD1*. Although it is clear that *SAMHD1* is recurrently mutated in CLL and T-ALL, it is less clear whether this confers an advantage through high dNTP pools or through its function in DNA repair.

1.4.5 SAMHD1 and nucleoside analogues

SAMHD1 degrades dNTPs and was also reported to degrade nucleoside analogues. Nucleoside analogues are small molecules that can be incorporated into DNA strands and act as chain terminators. They can also block enzymes required for cell replication. They are used as anti-viral or as chemotherapeutic drugs to treat cancer. Nucleoside analogues are particularly toxic to highly dividing cancer cells but also healthy dividing cells, often resulting in side effects (Galmarini et al., 2002).

SAMHD1 is a biomarker for cytarabine efficiency (Herold et al., 2017b; Schneider et al., 2016). Cytarabine is a nucleoside analogue used as a chemotherapeutic drug. Once in the cell, it is phosphorylated and converted into ara-CTP, which incorporated into DNA, induces non-repairable DNA breaks and triggers apoptosis in proliferating cells. The authors demonstrated that SAMHD1 degrades Ara-C, reducing cytarabine treatment efficacy in acute myeloid leukaemia (AML). SAMHD1 is a biomarker for cytarabine efficacy and therefore the authors suggest patient stratification accordingly. Moreover, primary AML patients cells treated with Vpx to degrade SAMHD1 sensitised the cells to ara-C treatment (Herold et al., 2017a). Cytarabine was not the only nucleoside analogue degraded by SAMHD1, since *Samhd1*$^{-/-}$ THP1 cells lacking functional SAMHD1 are sensitised to treatment with the antimetabolites nelarabine, fludarabine, decitabine, vidarabine, clofarabine, and trifluridine (Herold et al., 2017b). These findings were strengthened by another study that identified and associated SAMHD1 single nucleotide polymorphisms (SNPs) with response or survival in AML patients (Zhu et al., 2018). This illustrates the importance of considering SAMHD1's dNTPase function in cancer when using nucleoside analogues.

1.4.6 Regulation of SAMHD1

SAMHD1's crystal structure revealed a dimeric catalytic core that binds to dGTP to form a tetramer which becomes catalytically active, and degrades dNTPs into corresponding deoxynucleosides and inorganic phosphate (Goldstone et al., 2011; Hansen et al., 2014; Ji et al., 2014; Ji et al., 2013). Each dimer contains one catalytic site and two allosteric sites that can bind dGTP or GTP (**Figure 1.15**). The first report claimed that only binding of dGTP and subsequent formation of dGTP-Mg^{2+}-dGTP interactions are responsible for tetramer formations (Ji et al., 2013). The second paper suggests that the binding of dGTP or GTP to the allosteric sites, in combination with any dNTPs, induces the formation of catalytically active tetramers (Ji et al., 2014). The tetramer has therefore 8 allosteric sites and 4 catalytic sites. The primary allosteric site was shown to bind exclusively to dGTP and GTP whilst the secondary allosteric site has similar affinities for all four dNTPs. Allosteric site 1 has slightly higher affinity for GTP rather than dGTP, and physiological concentrations of GTP in a cell are 1000 fold higher than dGTP.

Both allosteric sites have to be occupied to induce the formation of an active stable tetramer (**Figure 1.16**). Mutations in key residues lead to altered dGTP-induced tetramerisation and therefore lower dNTPase activity (Ji et al., 2013).

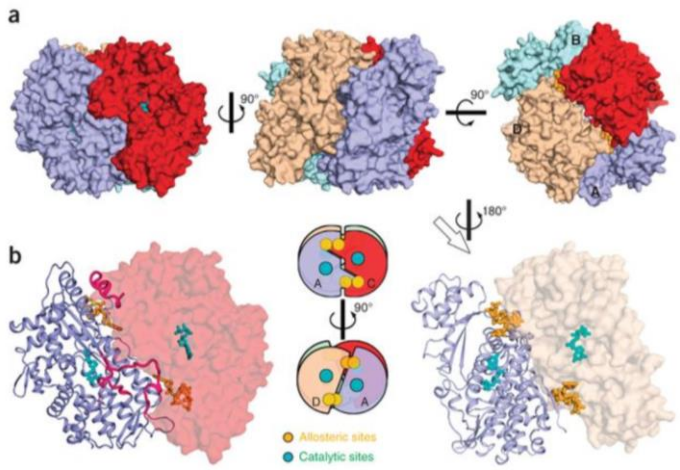


Figure 1.15 Structure of SAMHD1. *(a) SAMHD1 tetramer in three orthogonal views, with each subunit represented in a different colour. (b) Left, the dimer-2 interface between subunits A (ribbon) and C (transparent surface). Disordered regions are highlighted in magenta. A schematic cartoon of the tetramer is shown in the middle, with matching colours. Right, the previously observed dimer-1 interface between subunits A (ribbon) and D (transparent surface). Catalytic-site dGTPs are represented in cyan and the allosteric-site dGTPs in orange. Figure and legend from (Ji et al., 2013)*

Importantly, crystallisation studies showed the 592-TPQK-595 motif, which is formed upon phosphorylation, is unlikely to affect the active conformation of the enzyme (Ji et al., 2013). This supports another report that shows that SAMHD1's dNTPase activity is not regulated by phosphorylation (White et al., 2013). In addition, a recent report supported that view demonstrating that the dNTPase remained active in S-phase despite being phosphorylated on T592 (Tramentozzi et al., 2018). The phosphatase PP2A-B55α has been identified to target SAMHD1's phosphorylation on T592 during mitotic exit (M/G1). The control of SAMHD1 phosphorylation by the phosphatase regulated its antiviral activity towards HIV-1 infection (Schott et al., 2018). The current model of SAMHD1 activation through the cell cycle is detailed in **Figure 1.16**. Importantly, this model suggests that inactive tetramers are present in G0/G1 phase and therefore that GTP binds allosteric sites to allow the formation of the tetramer.

Although crystal structures of SAMHD1 shed light on its binding sites and helped us to better understand its regulation, functional reports are not always clear. SAMHD1 tetramers are required for its biological activity and HIV-1 restriction function (Yan et al., 2013). Its

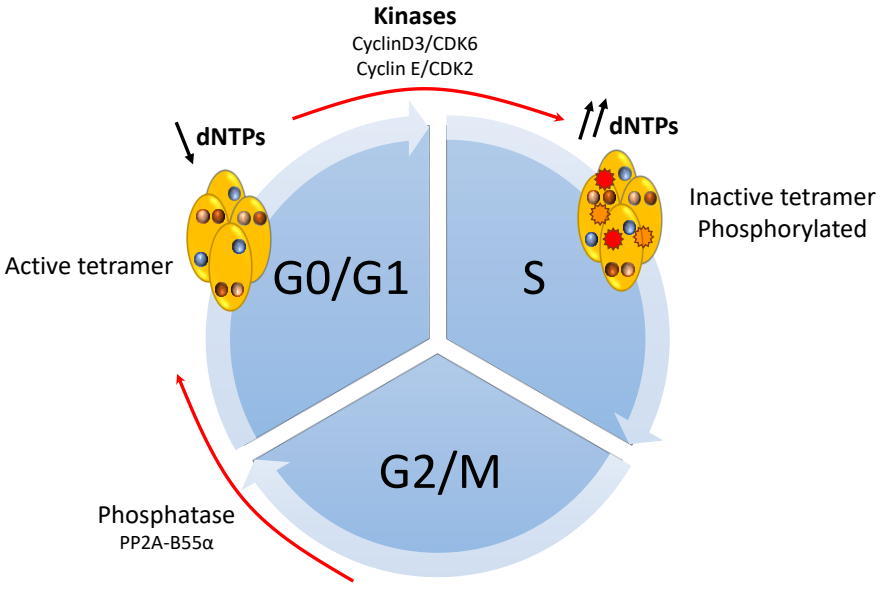


Figure 1.16 Model of SAMHD1 regulation. SAMHD1 is an active tetramer in quiescent cells with low dNTP levels. When cells enter S-phase, activation of CDK2 and CDK6 leads to phosphorylation of SAMHD1 subunits on T592. This destabilizes SAMHD1 tetramers and inactivates the enzyme, allowing dNTP levels to rise. During mitotic exit, the phosphatase PP2A-B55α removes the phosphate group, resulting in an unphosphorylated active SAMHD1 in G0/G1. This determines the restriction function of SAMHD1 and may regulates its dNTPase activity.

phosphorylation was shown to regulate its retroviral activity but not its dNTPase activity (White et al., 2013). This was supported by another study showing that SAMHD1's phosphorylation by cyclin A2/CDK1 regulates its restriction activity (Cribier et al., 2013). In addition, cell-cycle and HIV-1 control are linked to CDK2 and CDK6-dependent phosphorylation of SAMHD1 (Pauls et al., 2014a; Pauls et al., 2014b). It seems that T592 phosphorylation regulates SAMHD1's restriction function but not its dNTPase activity. Phosphorylation also seems to regulate its RNase activity and interferes with HIV-1 restriction (Ryoo et al., 2014). The mechanisms of regulation behind the antiviral and the dNTPase functions of SAMHD1 remain a conundrum.

All together, these studies showed that SAMHD1 is a dual function enzyme that requires GTP or dGTP bound to its allosteric sites to form active stable tetramers. The current model suggests that GTP binds to the allosteric sites in resting cells, allowing SAMHD1 to be active. Catalytically active tetramers are required for its dNTPase and viral restriction activities. SAMHD1 phosphorylation through CDKs inhibits its HIV-1 restriction activity, and its potential RNase activity, but not its dNTPase activity (**Figure 1.16**). Therefore, SAMHD1 is an important enzyme in nucleotide metabolism. The dNTPase function of SAMHD1 suggests that it could affect the cellular concentration of dGTP and therefore play a role in the mechanism of action of PNP inhibitors. Failure to regulate dNTP pools could lead to production of type I IFN (as observed in AGS), cell toxicity and cell death.

1.5 Interferons

Mutations in *SAMHD1*, observed in AGS, trigger the production of type I interferon (IFN). Indeed, nucleic acids can be sensed in the cell by pattern recognition receptors (PRRs) triggering the production of IFNs. IFNs are small proteins called cytokines induced upon viral infections and which contribute to cell defence against viruses and other intracellular pathogens. **Interferons** got their name from the fact that they **interfere** with viral infections by preventing virus spread to neighbouring cells (J.Lindenmann, 1988). There are three main types of interferons (IFN): IFN-α, IFN-β and IFN-γ, and IFN-α/IFN-β are also called type I interferons. Both IFN-α and IFN-β signal through the IFN receptor (IFNAR). Although

the IFN-α family contains 13 subtypes, it is unclear what differs between them since they all signal through the same IFNAR receptor. Binding of type I IFN to their receptor induces signalling through the JAK/STAT signalling pathway and the expression of hundreds of IFN-stimulated genes (ISGs). ISGs encode proteins with anti-viral functions and modulate the immune response (Gibbert et al., 2013; Janeway CA Jr, 2001). This shows that aberrant expression or availability of nucleic acids can trigger PRR signalling and production of type I IFN. This section will focus on toll-like receptor 7 (TLR7), which has been shown to sense oligoribonucleosides (ORN) in the presence of deoxyguanosine (dG) (Shibata et al., 2015).

1.5.1 Interferon production

Sensing of viral DNA or RNA triggers the production of type I IFN (Gao et al., 2013; Rehwinkel et al., 2010; Yoneyama and Fujita, 2009). Viral nucleic acids act as pathogen associated molecular patterns (PAMP) and can be sensed by PRRs. PRRs are germline encoded receptors and therefore are not specific to a particular pathogen (Janeway and Medzhitov, 2002). Nucleic acid PAMPs are sensed by PRRs which can be divided into three main families, toll-like receptors (TLRs), RIG-I like receptors (RLRs) or cytosolic DNA receptors (CDRs) (Kumar et al., 2011b). These receptors recognise specific features of viral RNA or DNA (**Figure 1.17**). Binding through these PRRs induces signalling through their respective adaptor proteins leading to the recruitment of TBK1 and phosphorylation of the

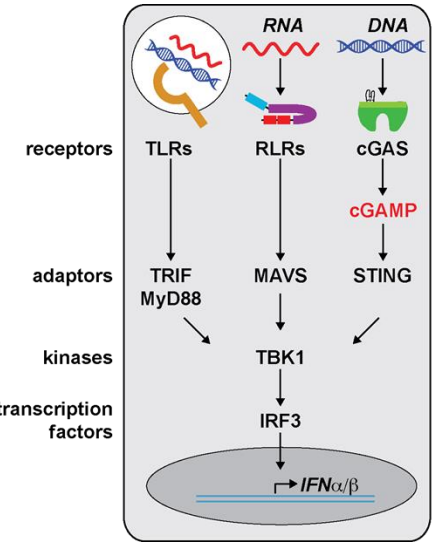
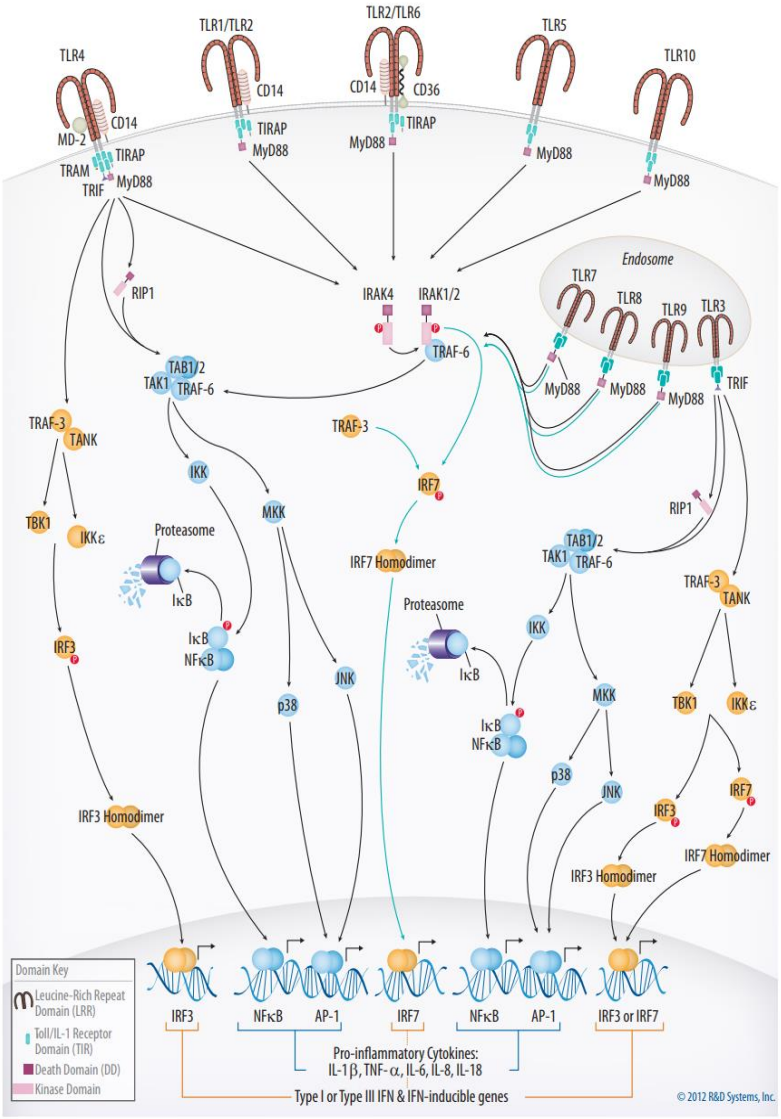


Figure 1.17 Pattern recognition receptors *comprise 3 main families of receptors that can sense viral nucleic acids and induce production of type I IFN: toll-like receptors (TLRs), RIG-I like receptors (RLRs) and cytosolic DNA receptors (CDRs). They signal through different adaptor proteins to induce the recruitment of TBK1 and the phosphorylation of the transcription factor IRF3 that will translocate to the nucleus and induce the production of type I IFN.*

transcription factor IRF3. Phosphorylated IRF3 can translocate to the nucleus and induce the production of type I IFN (Janeway CA Jr, 2001).

1.5.1.1 Toll-like receptors

TLRs are key players of innate immunity and were first discovered and described in Drosophila (Lemaitre et al., 1996). Huge progress has been made over the last two decades, leading to the identification of their specificities and signalling pathways. TLRs are able to recognise various PAMPs and DAMPs to trigger an immune response through different signalling pathways, resulting in the secretion of pro-inflammatory cytokines and chemokines (reviewed in (Kawai and Akira, 2010)). Their ability to sense and to trigger an innate immune response is exploited in vaccine development and cancer therapy. In



Toll-like Receptors (TLRs)		
TLRs	Agonist(s)	Source
TLR1/ TLR2	Triacyl lipopeptides	Bacteria
TLR2	Lipoproteins	Multiple Pathogens
	Peptidoglycan (PGN)	Bacteria
	Porins	Bacteria
	Zymosan	Fungi
	β-Glycan	Fungi
	GPI-mucin	Protozoa
	Envelope glycoproteins	Viruses
TLR2/ TLR6	Diacyl lipopeptides	Bacteria
	Lipoteichoic acid (LTA)	Bacteria
TLR3	Double-stranded RNA	Viruses
	Poly (I:C)	Synthetic analog of double-stranded RNA
TLR4	Lipopolysaccharide (LPS)	Bacteria
	Glycoinositol-phospholipids	Protozoa
	Envelope glycoproteins	Viruses
	Host-derived HMGB1 and HSPs	Endogenous
TLR5	Flagellin	Bacteria
TLR7	Single-stranded RNA	Viruses
TLR8	Single-stranded RNA	Viruses
TLR9	Unmethylated CpG DNA	Bacteria
		Protozoa
		Viruses
	Mitochondrial DNA	Endogenous
TLR10	Unknown	Unknown

Figure 1.18 Toll-like receptors signalling pathways and characteristics *(adapted from R&D Systems)*

addition, they are involved in autoimmunity since they have been proposed to sense endogenous ligands (Marshak-Rothstein, 2006). TLRs are PRRs that are differentially expressed in various cell types and are able to sense bacteria, fungi, viruses and parasites. PAMPs from these organisms will be recognised specifically by a TLR (**Figure 1.18**). TLRs are divided into 6 main families: TLR1, TLR3, TLR4, TLR5, TLR7, and TLR11. The TLR1 family is composed of TLR1, TLR2, TLR6 and TLR10. They are receptors that can be divided into two main groups: cell surface TLRs (TLR 1/2, TLR 2/6, TLR 4, TLR 5 and TLR 10) and endosomal TLRs (TLR3, TLR7, TLR8 and TLR9). The TLR7 family is composed of TLR7, TLR8 and TLR9. Both TLR7 and TLR8 recognise ssRNA whilst TLR9 recognises unmethylated CpG DNA, a short ssDNA that contains dC followed by dG (Lester and Li, 2014). TLRs can signal through myeloid differentiation primary response 88 (MyD88) or TIR-domain containing adaptor inducing IFN-β (TRIF). The MyD88-dependent pathway is activated by all TLRs except TLR3, which only signals through TRIF, whilst TLR4 can signal through both MyD88 and TRIF (**Figure 1.18**). MyD88 contains a Toll-interleukin-1 receptor domain (TIR) domain that can interact with TLR's TIR domains. The death domain (DD) of the protein can interact with IRAK kinases and form a structure called myddosome, allowing the activation of the NF-κB and JNK pathways.

1.5.1.2 Toll-like receptor 7

TLR7 is an endosomal receptor expressed by macrophages, B cells and dendritic cells (Hemmi et al., 2002). Imidazoquinoline compounds, which are tricyclic organic molecules, including imiquimod and R848, can signal through TLR7 and induce the production of IFNα and other cytokines. The expression of TLR7 varies among B cell subsets and naive B cells express more of it than memory B cells, but both express less than dendritic cells (Gururajan et al., 2007). TLR7 agonists mainly target plasmacytoid dendritic cells (pDCs), a cell subset able to quickly produce high amounts of type I IFN (Bao and Liu, 2013). TLR7 agonists have been approved for cancer treatment and are used as adjuvants in vaccine formulations (Kobold et al., 2014). TLR7 has been shown to be involved in the pathogenesis of systemic lupus erythematosus (SLE). Patients with SLE have high levels of small nuclear ribonuclear

proteins (snRNP) (Marshak-Rothstein, 2006). Sensing of snRNPs by pDCs that express endogenous TLR7 leads to secretion of high amount of type I IFNs (Celhar et al., 2012).

A recent paper revealed the tertiary structure of TLR7 in its activated form when the receptor binds to ssRNA and guanosine. The structure includes two binding sites, one for a small ligand and a second one for ssRNA. Zhang et al. showed that TLR7 is a dual sensor synergistically activated by guanosine and uridine-containing ssRNA (Zhang et al., 2016). In another study, dG was signalling through TLR7 only in the presence of uridylic acid (also called poly U, a sequence of 30-40 uridine nucleic acids) to trigger the production of cytokines (Shibata et al., 2015). This illustrates that nucleosides and deoxynucleosides can induce the production of type I IFN through TLR7. It suggests that TLR7 may be involved in sensing dG derivatives and other nucleotides.

1.5.2 Interferon-stimulated genes

Once produced through sensing of viral nucleic acids, type I IFNs bind to the IFNAR receptor in an autocrine and paracrine manner. Activation of IFNAR triggers the JAK and STAT signalling pathway and induces the transcriptional activation of hundreds of interferons stimulated genes (ISGs). Many receptors and proteins involved in positive or negative regulation of the sensing and signalling of type I IFN are ISGs themselves. Among the well-studied ISGs are enzymes such as PKR, oligo adenylate synthetase (OAS), myxovirus resistance protein (Mx), apolipoprotein B mRNA editing enzyme-catalytic polypeptide-like (APOBEC) or tripartite motifs (TRIM), which directly inhibit viral replication. Type I IFN can also stimulate immunity by enhancing proliferation, cytotoxicity and IFN-γ secretion by NK cells. This is an efficient system developed by the host to protect itself from viral infection. SAMHD1 was identified as an ISG as it is upregulated upon the production of type I IFNs (Calonge et al., 2017).

1.5.3 Restrictions factors

SAMHD1 is an ISG and a host restriction factor through its dNTPase activity. Restriction factors are host anti-viral proteins that counteract viral replication. Their actions induce a decrease in virus infectivity, and their expression is linked to innate immunity. They are the

first line of defence against viruses. They usually share common features: they are germline encoded, act cell intrinsically and can be found in many cells. Most restriction factors are ISGs but some also constitutively expressed to act at the early stages of a viral infection (Kluge et al., 2015). Restriction factors often show evidence of positive selection and some viruses have developed strategies to block them to infect their host more efficiently. For instance, HIV-2 protein Vpx that targets SAMHD1 for proteosomal degradation (see section 1.4.2).

1.6 Chronic lymphocytic leukaemia

Cancer cells select for *SAMHD1* mutations and have high dNTP requirements, implying that dNTP regulation by SAMHD1 is a key mechanism that protects against uncontrolled cell division. *SAMHD1* is mutated in some types of cancer, including chronic lymphocytic leukaemia (CLL) (Burns et al., 2017; Clifford et al., 2014; Guieze et al., 2015). Chronic lymphocytic leukaemia is a B cell malignancy characterised by the expression of CD5 at the B cell surface. $CD5^+$ B cells accumulate in the blood, marrow and secondary lymphoid tissues, causing lymphocytosis (an increase of lymphocytes in the blood). The average incidence is higher in the United states and in Europe (0.06%) compared with Asia (0.01%) for reasons that remain unclear (Nabhan et al., 2014). CLL affects more males (~60%) than females (40%). Most people diagnosed with CLL are above 50 years of age and the age pattern is comparable across ethnic backgrounds (**Figure 1.19**).

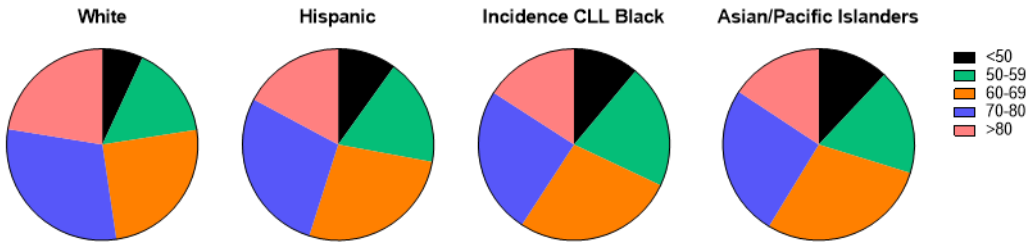


Figure 1.19 Age of CLL patients. Adapted from (Nabhan et al., 2014).

CLL is typically divided into two distinct groups: unmutated or mutated immunoglobulin heavy-chain variable region gene (*IGHV*). These two groups correspond to the stage from which CLL B cells originate. Unmutated *IGHV* patients have higher $CD38^+$ cells, shorter

survival and respond poorly to multiregiment chemotherapy. Patients with mutated *IGHV*, have prolonged survival and require minimal chemotherapy (Damle et al., 1999; Hamblin et al., 1999). These two types of CLL have different clinical courses. One affects naïve B cells (unmutated *IGHV*) and is malignant whilst the other one occurs in memory B cells (mutated *IGHV*) with a benign course. Both groups display different characteristics of their B cell receptor (BCR) signalling. In unmutated *IGHV*, enhanced B cell activation is observed whereas anergy predominates in mutated *IGHV* (Packham et al., 2014). Anergy results from the absence of T cell help and prolonged engagement of the BCR; it is a state of cellular lethargy.

1.6.1 Causes of chronic lymphocytic leukaemia

CLL originates from genetic alterations such as chromosomal deletions, alteration of micro RNA (miRNA) expression, epigenetic modifications, or somatic mutations.

Chromosomal alterations are common and ~80% of CLL patients carry at least one of these 4 deletions in chromosome 13q14.3 (del(13q)), del(11q), del(17p) or trisomy of 12q. These genetic alterations are important predictors of disease progression and survival (Dohner et al., 2000).

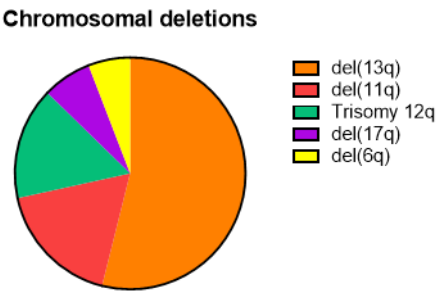


Figure 1.20 Frequencies of chromosomal deletions in CLL

Micro RNAs can contribute to CLL pathogenesis. miRNA are short hairpin RNA, molecules that are involved in gene regulation by binding to target mRNAs leading to translation blockage or mRNA degradation (Tijsterman and Plasterk, 2004). miR15 and miR16 are miRNA located on chromosome 13q14, a region commonly mutated in CLL (**Figure 1.20**). Both miR15 and miR16 show high homology for several genes, including *BCL2* and *MCL1*, which encode anti-apoptotic proteins (Calin et al., 2002). 13q14 deletion occurs in ~65% of CLL patients and is therefore of pathogenic significance. However, patients with 13q14 deletion typically have better prognosis than others due to the presence of a similar miR15/16 cluster on chromosome 3. Mutations in non-coding genes also involve other miRNAs (Kipps et al., 2017).

Epigenetic modifications seem to play a role in development of CLL pathogenesis. CLL B cells display hypomethylated genomic DNA, especially in newly diagnosed and untreated patients (Wahlfors et al., 1992). A more recent study systematically observed variability of the DNA methylation pattern in CLL B cells. The authors proposed that disordered methylation allows cancer cells to search for superior evolutionary adaptive capacity of CLL B cells through genomic instability (Landau et al., 2014). Methylation allows classification into subgroups since mutated or unmutated *IGHV* showed two different methylomes (Kulis et al., 2012). These findings suggest that epigenetics plays an important role in the development of CLL.

Somatic mutations are an important driver for the development of CLL. The development of whole genome sequencing and whole exome sequencing techniques allowed the identification of numerous new mutations in CLL, reflecting its heterogeneity (Landau et al., 2015). Common mutations are in genes involved in DNA damage (*ATM* and *TP53*), mRNA processing (*SF3B1* and *XPO1*), in chromatin modelling (*CHD2* and *ZMYM3*), WNT signalling, Notch signalling, inflammatory pathways and B cell transcription (*EGR2* and *BRAF*), as illustrated in **Figure 1.21**. Some mutations are typically found in all leukaemic cells making them founding mutations (for example *MyD88* or del(13q)) while others are only present in a fraction meaning that they are subclonal mutations (for example *SF3B1* or *NOTCH1*). Initially, 44 somatic mutations were identified in CLL, including mutations in the *SAMHD1* gene (Landau et al., 2015). The most frequent mutations in CLL are *SF3B1, ATM, TP53, NOTCH1*, and *BIRC3*. *SAMHD1* mutations have been identified as driver mutations, meaning they confer an advantage upon the cells, and they are present in ~11% of refractory CLL patients (Clifford et al., 2014; Guieze et al., 2015; Landau et al., 2013; Landau et al., 2015). Since SAMHD1 is involved in dNTP pool regulation and in DNA repair, it is unclear which of these roles confer an advantage to CLL cells when mutated. It is possible that alteration of both dNTP pools and DNA repair lead to increased mutation rate in CLL cells. A recent study showed that SAMHD1 inhibition resulted in elevated dNTP pools which increased mutation rate by enhancing activation-induced deaminase, affecting

immunoglobin hypermutation (Thientosapol et al., 2018). This illustrates how dNTP pools may affect the oncogenic process.

1.6.2 Clinical presentation and diagnosis

CLL is characterised by the chronic expansion of malignant B cells in the blood, lymph nodes and the spleen. Malignant B cells are characterised by the expression of CD19 and the T cell antigen CD5. Most patients are asymptomatic and some patients (~10%) will present symptoms such as unexplained fevers, night sweats or rapid body weight loss. Most patients will develop an adenopathy (enlarged lymph nodes) and some will have hepatosplenomegaly (20-50%).

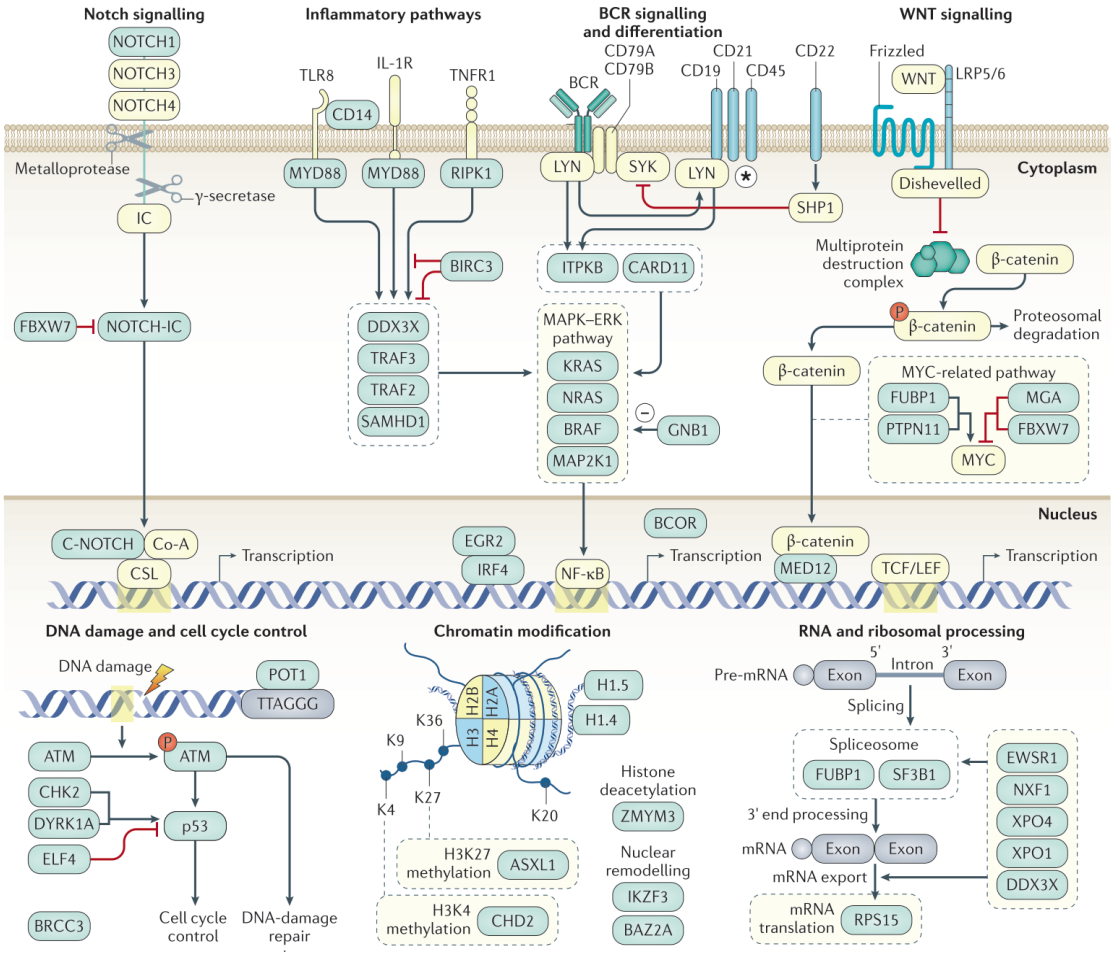


Figure 1.21 Somatic mutations in chronic lymphocytic leukaemia. *Mutations occur in several pathways: Notch signalling, inflammatory pathways, BCR signalling and WNT signalling. Figure from (Kipps et al., 2017).*

CLL is diagnosed when the absolute clonal lymphocyte count is >5000 cells/ mm^3. Symptoms such as autoimmune haemolytic anaemia[1] (1-11% of cases), autoimmune thrombocytopenia[2] (<2%) and hypogammaglobulinemia[3] (8-10%) may be present in patients. In addition, low levels of lipoprotein cholesterol and high levels of β2 globulins are features detected during diagnosis. The diagnosis is usually confirmed by analysing lymphocytes by flow cytometry, where malignant B cells are expressing CD19, CD5 and CD23 (sometimes weak expression of CD20). In approximately 5% of patients malignant B cells infiltrate the lymph nodes, leading to the formation of a small lymphocytic lymphoma (Nabhan and Rosen, 2014). There are two classification systems for CLL: the Rai classification used in the United States, and the Binet classification, mostly used in Europe (**Table 1.4**).

Table 1.4 Chronic lymphocytic leukaemia classification: Rai and Binet stages classification. *Lymphocytosis: lymphocytes > 4000 cells/µl. Anaemia: haemoglobin <10g/dl or. Thrombocytopenia: platelets <100 000cells/µl. Adenopathy: large or swollen lymph nodes. Cytopenia: reduction of mature blood cell numbers. Hepatosplenomegaly: swollen liver and spleen. Adapted from (Kipps et al., 2017; Nabhan and Rosen, 2014)*

Stages	Risk	Clinical features	Overall survival (years)
Rai			
0	Low	Lymphocytosis in peripheral blood and bone marrow only	>10
I/II	Intermediate	Lymphadenopathy ± hepatosplenomegaly	7
III/IV	High	Anemia ± thrombocytopenia	<4
Binet			
A	Low	<3 areas of lymphadenopathy without cytopenia	13
B	Intermediate	>3 areas of lymphadenopathy without cytopenia	8
C	High	Anemia and/or thrombocytopenia	2

1.6.3 Management and treatment

Treatment usually starts when patients present symptoms (night sweats, fatigue, weight loss or fever) and become high risk (Rai stage II/IV or Binet stage C). Several factors are considered when choosing an appropriate therapy, such as the presence of del(17p) or *TP53* mutations and *IGHV* mutational status. Current therapies include chemotherapy, immunochemotherapy and drugs targeting signalling pathways.

[1] rare condition when red blood cells are destroyed quicker than they are replenish
[2] disorder characterised by low platelets counts due to destruction by antibodies
[3] Immune disorder characterised by low counts of all gamma globulins

Chemotherapy alkylating agents induce DNA crosslinks (the most common are chlorambucil, cyclophosphamide or bendamustine), and nucleoside analogues that block DNA synthesis (most commons are fludarabine, pentostatin and cladribine) have been commonly used in the last decades. The nucleoside analogue fludarabine was shown to be more efficient in patients with primary CLL compared with the alkylating agent chlorambucil (Rai et al., 2000). Combination of the nucleoside analogue fludarabine and the alkylating agent cyclophosphamide showed higher efficacy than fludarabine alone (Eichhorst et al., 2006). Fludarabine is administered as the prodrug, 9-β-d-arabinosyl-2-fluoroadenine (F-ara-AMP). After entering the cell, it is phosphorylated to form an ATP chain, and the active compound (F-ara-ATP).The cellular influx of the dephosphorylated prodrug is proven to occur preferentially in active leukaemia cells. The active drug, Fara-ATP, inhibits DNA synthesis by blocking RNR and by intercalating directly into the transcripting DNA strand, stalling RNA translation. These breaks in DNA and interruptions of protein synthesis result in apoptosis (Lukenbill and Kalaycio, 2013). Since fludarabine targets dividing cells, like any chemotherapeutic drug, it also inhibits repair and proliferation of healthy cells. Consequently, patients treated with fludarabine develop myelosuppression and secondary malignancies (Lukenbill and Kalaycio, 2013).

Immunotherapy drugs include mainly monoclonal antibodies targeting CD20 (rituximab, ofatumumab, obinutuzimab) and CD52 (alemtuzumab). Chemoimmunotherapy with fludarabine, cyclophosphamide, and rituximab improves progression free survival and overall survival in patients (Badoux et al., 2011). Moreover, results from a phase III clinical trial suggest that the choice of a specific first-line treatment changes the natural course of CLL (Hallek et al., 2010). Overall, published studies using immunochemotherapy showed longer progression free survival compared with conventional chemotherapy (Kipps et al., 2017). Therefore, the FDA has approved immunochemotherapy has a first-line treatment of patients with CLL.

Drugs targeting the BCR signalling pathway are also being tested. There are Bruton's tyrosine kinase (BTK) inhibitors, phosphatidylinositol 3-kinase (PI3K) inhibitors and spleen tyrosine kinase inhibitors (SYK). Ibrutinib is a BTK inhibitor that has been approved for use in clinical studies. It showed prolonged progression free survival and overall survival as well as improved partial response rate in patients with relapsed CLL (Kim and Dhillon, 2015). It is considered as an emerging treatment option for refractory CLL patient with del(17q) and *TP53* mutations.

Malignant B cells have hyperactivated PI3Kδ which acts downstream of B cell receptor signalling. Therefore, PI3K inhibitors have been developed and are being tested in clinical trials. Idelalisib is the only PI3K inhibitor approved by the FDA, since it showed ~75% overall response rate in CLL patients (Shah and Mangaonkar, 2015). Idelalisib in combination with rituximab showed higher response rate and overall survival than idelalisib or rituximab alone. The combination was considered safe and effective as a new treatment against refractory CLL, including those with poor prognosis. Therefore idelalisib and rituximab were approved for treatment by the FDA in 2014 (Shah and Mangaonkar, 2015). Nonetheless, adverse events of the combination include neutropenia, thrombocytopenia, anaemia, elevation in transaminases, and diarrhoea.

Fostamatinib is an oral SYK inhibitor that causes reduction in lymphadenopathy with concomitant lymphocytosis, an improvement in disease-related cytopenias and relief of disease-related symptoms in most of treated patients with CLL. However, dose-limiting toxicities of fostamatinib treatment include neutropenia, thrombocytopenia and diarrhoea. Other inhibitors of SYK are being evaluated in preclinical and clinical studies (Kipps et al., 2017).

Inhibitors of the anti-apoptotic BCL-2 proteins are also emerging as promising agents against CLL. BCL-2 plays a major role in apoptosis and therefore is an attractive drug target. BH3 mimetic drugs were designed to bind the BH3 domain of anti-apoptotic BCL-2 proteins, releasing their inhibition on the apoptotic BCL-2 proteins and leading to MOMP. Consequently, several inhibitors of BCL-2 proteins are in ongoing clinical trials. Venetoclax

(ABT-199) reached ~80% response rate in CLL, including in relapse/refractory patients or patients with del(17q) (Davids et al., 2013). The most common reported side effects are diarrhoea, neutropenia, fatigue, upper respiratory tract infection, and cough. Venetoclax is the first BCL-2 inhibitor to be approved by the FDA (2016) for CLL with del(17q) that have had prior therapy. Combination therapies with Venetoclax are currently in trials (Cang et al., 2015).

Identifications of genomic mutations in CLL led to a better understanding of CLL development and allowed the identification of new drug targets. The new standard of care for younger CLL patients with good renal function is chemoimmunotherapy with fludarabine, cyclophosphamide and rituximab. Emerging clinical trials using the combination of rituximab with BTK inhibitors or BCL-2 inhibitors in CLL may provide promising alternatives. Identification of somatic mutations, such as in *SAMHD1*, that constitute a founding event in the development of CLL, are important to consider. Identifying the origin of failures to respond to specific therapies remain to be elucidated. Since CLL is very heterogeneous, genetic profiling of the patients' malignant cells may help understanding and predicting treatment efficacy. This approach, combined with the appropriate treatment chosen according to the patient's genetic profile, defines precision oncology. Precision oncology aims to deliver the right treatment, to the right patient at the right time. It is becoming clear that one treatment does not fit all since every cancer presents a unique molecular signature. Understanding the precise mechanism of action of drugs can help to predict how the genetic profile of the patient's cancer will impact treatment efficacy.

1.7 Summary

Maintenance of nucleotide pools by the *de novo* or the salvage pathway is critical to maintain genome integrity. dNTP imbalances can lead to DNA damage and cell death. SAMHD1 is a dNTPase, suggesting that it plays an important role in maintaining balanced dNTP pools in a healthy cell. Several roles for SAMHD1 have been reported so far, including its most studied restriction factor function. However, SAMHD1 is extremely conserved suggesting that its dNTPase function did not evolve to restrict viruses. Accumulation of

nucleic acids can lead to sensing and production of type I IFN which can be toxic to cells if sustained. SAMHD1 prevents the expression and subsequent sensing of LINE-1 retroelements. This is the proposed mechanism of type I IFN production in Aicardi-Goutières syndrome patients with *SAMHD1* mutations. In addition, SAMHD1 is involved in DNA repair, this may explain why it is mutated in cancer cells. Finally, *SAMHD1* mutations are founding events in CLL, suggesting that the protein is important in safeguarding dNTP pools and failure to do so benefits cancer cells.

The involvement of *SAMHD1* mutations in cancer points toward a conserved function of SAMHD1 in nucleotide metabolism through its dNTPase function. It is firmly established that SAMHD1 restricts HIV-1 and other DNA viruses but this could be a side effect of the main protective function of the protein. Regulation of nucleotide pathways in the cell is critical to maintain cell integrity. Failure to regulate the salvage pathway, for example in PNP-deficient patients, leads to the accumulation of dG and dGTP, triggering apoptosis. PNP inhibitors only kill leukaemic cells in a limited number of patients. This suggests that the exact mechanism of action of PNP inhibition and their consequences are not fully understood. SAMHD1 is a recently identified dNTPase and its ability to degrade dGTP could affect the mechanism of action of PNP inhibitors. The PNP inhibitor forodesine was tested in clinical trial against CLL, a condition where *SAMHD1* is mutated recurrently. This highlights the importance of investigating SAMHD1's function in the context of nucleotide metabolism and cell death. Such studies may help to better understand why *SAMHD1* is mutated in cancer cells and to determine the protein's impact on specific treatments with nucleoside analogues. This mechanism at the crossroad of nucleotide metabolism and cell death may be the conserved function of SAMHD1.

The aim of this thesis was therefore to characterise SAMHD1's ancestral function.

Chapter 2. MATERIALS & METHODS

2.1 Mice

Samhd1$^{-/-}$ mice (C57BL/6 background) were described previously (Rehwinkel et al., 2013). This work was performed in accordance with the UK Animals (Scientific Procedures) Act 1986 and institutional guidelines for animal care. This work was approved by a project license granted by the UK Home Office (PPL No. PC041D0AB) and also was approved by the Institutional Animal Ethics Committee Review Board at the University of Oxford. *Tlr7*$^{-/-}$ mice were a kind gift from Caetano Reis e Sousa. *MyD88*$^{-/-}$ mice were a kind gift from Kevin Maloy, originating from Shizuo Akira. *Tlr7*$^{-/-}$ and *MyD88*$^{-/-}$ were on *C57Bl/6* background and were crossed to *Samhd1*$^{-/-}$ mice to obtain *Tlr7*$^{-/-}$ *Samhd1*$^{-/-}$ and *MyD88*$^{-/-}$ *Samhd1*$^{-/-}$.

2.2 Cells

Bone marrow derived macrophages (BMDMs) were prepared from fresh or frozen bone marrow cells from *C57Bl/6* mice of different genotypes. Mice were culled by increasing concentration of CO_2 and death was confirmed by dislocation of the neck. Legs from both sides were collected and kept in RPMI (R10 P/S) medium with 10% foetal calf serum (FCS), 1% L-glutamine and 1% penicillin and streptomycin (P/S). Bones were processed under sterile conditions; disinfected in 70% ethanol for 2 minutes (min) then washed in phosphate buffer saline (PBS). In a petri dish, the ends of each bone were cut with a scalpel. A 10 ml syringe filled with 10 ml of R10 P/S and a 19G needle was inserted into the bones and R10 was injected into the bones to flush out bone marrow cells. This step was repeated until all cells were extracted from each bone. A 10 ml pipette was used to make a single cell suspension which was flushed through a 70 µm cell strainer placed onto a 50ml tube to obtain a single cell suspension. Cells were spun down at 300 g for 5 min and the pellet was resuspend in R10 P/S + 20% L929 supernatant (supernatant from L929 cells in culture, supernatant was collected after 7 days of confluent culture of L929). Supernatant was spun down and filtered through a 0.22 µm filter. One fifth of total bone marrow cells was seeded in 8ml of R10 P/S + 20% L929 in a petri dish on day 0, the leftover cells were spun and resuspend in 4ml of FCS+ 10% dimethyl sulfoxide (DMSO) and 1 ml aliquots were frozen

in Mr frosty boxes. Two days later on day 2, 4 ml R10 + P/S with 40% L929 were added. On day 4, supernatant was discarded and 10 ml of R10 P/S + 20% L929 was carefully added onto the cells. On day 7, BMDMs were washed with PBS, detached with accutase, washed and counted to be used. Cells were seeded in R10 P/S + 20% L929 unless specified otherwise. BMDMs were seeded at 20 000 cells in 200 µl of R10 P/S + 20% L929 per well in a 96-well plate flat bottom in most experiments. Cells were treated appropriately 24h post-seeding.

Mouse embryonic fibroblasts (MEFs) were made by standard protocols from either WT or *Samhd1*$^{-/-}$ mice. Human fibroblasts from AGS patients were collected with approval by a U.K. Multicentre Research Ethics Committee (reference number 04:MRE00/19) and were provided by Y. Crow and G.I. Rice. MEFs were cultured in D10 medium [Dulbecco's modified Eagle medium (DMEM) containing 10% heat-inactivated FCS, P/S, 2 mM L-Glutamine and 20 mM HEPES buffer]. Human fibroblasts, HeLa, B16F10 and MDA MB231 cells were cultured in D10 without P/S. HeLa cells were a gift from M. Way, MDA MB231 cells were from A. Banham and B16F10 cells were provided by V. Cerundolo. Jurkat cells were a gift from S. Davis and originate from the American Type Tissue Collection and were cultured in R10 without P/S. All cells were cultured under 5% CO_2. Human fibroblasts and MEFs were cultured under low oxygen (1.2% O_2).

2.2.1 Generation of *Samhd1*$^{-/-}$ B16F10 cells

sgRNAs were designed to excise exon 2 of mouse *Samhd1* (Gene ID: 56045). Exon 2 is critical to both isoforms of *Samhd1* (**Figure 2.1** and (Rehwinkel et al., 2013)). B16F10 cells were co-transfected with pX458-Ruby-sgRNA-1 and pX458-sgRNA-2 plasmids. GFP-Ruby double positive cells were single cell sorted and clones were expanded. A PCR screening approach was used to identify knock-out cells. PCR-1 was designed to amplify a long fragment (709 bp) from the WT allele and a short fragment (350 bp) from the KO allele using primer 1 fwd and primer 2 rvs (**Figure 2.1**). PCR-2 had a primer located in exon 2 and

amplified a fragment (352 bp) only from the WT allele using primer 2 rvs and primer 3 fwd (**Table 2.5**).

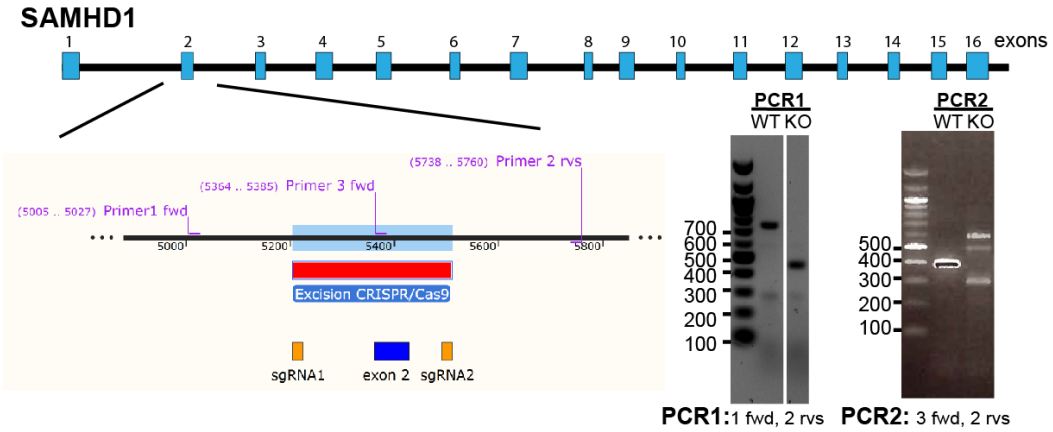


Figure 2.1 SAMHD1 CRISPR/Cas9 strategy in B16F10 cells. *Murine SAMHD1 has 16 exons and exon 2 was taken out using 2 sgRNAs on both sides of exon 2. Taking out exon 2 left 109 initial intact amino acids and lead to an 8 amino acid nonsense frame shift of exon 3, running into a double stop, and abolished more than 80% of the total protein. PCR screening was used to identified Samhd1$^{-/-}$ cells. PCR1 with primer 1 fwd and primer 2 rvs, gives a 756 bp fragment for a WT allele and 449bp fragment for KO allele. PCR2 with primer 3 fwd and primer 2 rvs, gives a band of 397 bp for a WT allele or no band for a KO allele. WT= parental line B16F10, KO= B16F10 Samhd1$^{-/-}$ clone 12.*

2.2.2 Patients' samples

PBMCs from 19 CLL patients recruited into the ADMIRE (n=12) and ARCTIC (n=7) studies (Howard et al., 2017) were retrieved from the Liverpool Bio-Innovation Hub Biobank. Genetic characterisation of the tumour cells for these patients was previously published (Clifford et al., 2014). Informed consent from all patients was obtained in line with the Declaration of Helsinki. The project was covered by the Ethics approval REC 09/H1306/54. PBMCs were thawed in R10 with P/S and 50 U/ml of benzonase, washed twice before being counted and plated. For CellTiter-Glo assay, 50,000 cells were plated in U-bottom 96-well plates. CyTOF experiment was performed using 3,000,000 cells in 12-well non-coated tissue culture plates.

2.3 Plasmids

To generate pMSCVpuro-mSAMHD1, mouse *Samhd1* isoform 1 was PCR amplified. A kozak sequence and N-terminal 3xFLAG-tag were introduced by PCR and the PCR product was cloned into pMSCVpuro using the EcoRI site. This was performed by Jan Rehwinkel and I used the cells expressing pMSCVpuro-mSAMHD1. To generate SAMHD1-deficient

mouse cells, pX458-Ruby-sgRNA-1 and pX458-sgRNA-2 were cloned using pX458-Ruby and pX458, respectively, as described before (Hertzog et al., 2018).

2.4 Western blots

Cells were lysed in NP-40 buffer (150 mM NaCl, 1% NP-40, 50 mM Tris pH 8.0) with protease and phosphatase inhibitors for 20 min on ice, after which lysates were centrifuged at 17,000g for 10 min at 4°C. Supernatant was collected and diluted with sample buffer (with 10% β-Mercaptoethanol) before denaturation at 94°C for 5 min. Samples were loaded on pre-cast 4-12 % gradient Bis-Tris protein gels that were run with MOPS (standard default buffer) or MES (smaller proteins: cleaved-caspase 3) buffer at 120 volts for 2 hours. Transfer to nitrocellulose membranes was performed in transfer buffer (25 mM Tris, 192 mM glycine, 20% methanol) at 30 volts for 3.5 hours. Membranes were blocked in 5% milk powder in Tris buffered saline (TBS) with 1 % Tween-20 (TBST) for 1 hour at room temperature (RT) then washed 5 times for 5 min in TBST. Membranes were incubated with primary antibody in 5 % milk TBST overnight at 4°C, then washed 5 times for 5 min in TBST. ECL or ECL prime substrates were used for signal detection. In some experiments, membranes were stripped (0.2 M glycine, 0.1 % SDS at pH 2.5) for 15 min, washed, blocked and re-probed with a different antibody.

For cytochrome C, lysates were fractionated into cytosolic protein lysate and nuclear/membrane bound protein lysate. Cells were washed and resuspend in lysis buffer (PBS + 0.0025% digitonin with proteases inhibitors) on ice for 10 min then spun at 17 000 g at 4 °C. The supernatant, forming the cytosolic fraction, was collected and kept on ice. The remaining pellet was resuspend into the same volume than the cytosolic fraction (just collected) of RIPA buffer with proteases inhibitors. Cells were incubated on ice for 20 min before being spun at 17 000 g for 10 min. The supernatant collected after centrifugation formed the pellet fraction. Lysates were frozen and stored at -20 °C.

2.5 Viability measurements

CellTiter-Glo, a luminescence assay that measures ATP levels was used. In a 96-well plate seeded with cells, the media was discarded to leave 50 µl of media per well. 50 µl of

CellTiter-Glo reagent at RT was added, mixed to the cells and the plate was incubated for 10 min at RT. 75 µl of this mix was transferred into a 96-well white plate and luminescence was measured using a luminometer and the CellTiter-Glo programme (Promega Glomax). To assess cell viability with crystal violet, cells were stained with 0.5% crystal violet for 20 min, washed 3 times with water and dried overnight before being resuspend in 200 µl methanol and absorbance was measured at 570 nm (ClarioStar) as described in (Feoktistova et al., 2016). For analysis of cell death with the Incucyte live-cell analysis system, Yoyo3 iodide viability die was used at 1/8000 final concentration and images were acquired. The Incucyte was also used to measure confluency and acquire brightfield images over time with a 10x objective.

2.6 Apoptosis assays

The Annexin V/7AAD kit was used to detect apoptotic cells by flow cytometry according to the manufacturer's protocol. Caspase 3/7 Glo was used to measure caspase 3/7 cleavage. For live cell imaging, BMDMs were cultured in a glass chamber coated with Poly-L-lysine at 37°C and 5% CO_2; 100 000 cells were seeded per well in a volume of 300 µl. Culture media were supplemented with 2.5 mM $CaCl_2$, 20 mM HEPES, propidium iodide (3 µl/well) and Annexin V AF488 (1 µl/well). Images were acquired with a Delta Vision microscope with 10x objective lens every 10 min for 24 hours.

2.7 Cell cycle analysis

BMDMs were seeded at 10^6 cells/well in 6-well low attachment plates and were incubated with 10 µM BrdU for 30 min. In pulse chase experiments, cells were incubated with 10 µM BrdU for 15 min, the media was then replaced, and cells were exposed to dG. At appropriate time points, cells were washed and fixed in 70% ethanol and frozen at -20°C. Cells were washed and resuspended in pepsin solution (1 mg/ml in 30 mM HCl) for 30 min at 37°C, spun down and resuspend in 2M HCl for 15 min at RT and washed with PBS. Cells were then blocked with 0.5% BSA, 0.5% Tween-20 in PBS for 30 min at RT, washed and resuspend in FACS buffer with α-BrdU AF488 antibody at 1:100 dilution for 30 min at RT.

Fix Cycle PI/RNAse A staining solution was added to the cells for 30 min at RT. Cells were acquired on a BD LSR II flow cytometer.

2.8 Retroviral vectors

VSV-G-pseudotyped retroviral vectors were produced by plasmid transfection of 293T cells (Bridgeman et al., 2015). HEK293T TLAs cells were cultured in D10 and split 1:4 on day 0. On day 1, the cells were transfected using Fugene HD (1:3), pVSV-G and pSIV3+ (accessory genes) or pSIV4+ (no accessory genes) in OPTIMEM. Details of the transfection are shown in **Table 2.1**. 24h later, the media was replaced with fresh D10. Supernatant containing virus-like particles (VLPs) expressing Vpx protein or not, was collected after 72h. Supernatant was spun down at 300 g for 5 min then transferred onto a vacuum 0.22 μm filter system. After filtration, supernatant containing VLPs was aliquoted and frozen at -80 °C. Vials were single use and were never thawed and frozen again.

Table 2.1. Concentrations of plasmids transfected per 15 mm dish to generate VLP_{vpx} (SIV3+) and VLP_{ctrl} (SIV4+)

Reagent	ug/ dish	ug/ul	*4 (ul)
SIV3+/4+	4	0.5	30
VSV-G	2	1	8
OPTIMEM	300		1200
Fugene HD 1:3	18		72

Retroviral infections were performed in the presence of 8 μg/ml polybrene. Bone marrow cells were transduced three times by spin-infection (2500 rpm, 120 min, 32°C, no brakes) on days 1, 2 and 3 of the 7-day differentiation process with the retroviral vector expressing SAMHD1 or a control vector. For the infection, the media was replaced with the supernatant containing the viral vectors (2ml/ 6-well plate), and replace with fresh media after spin-infection. Cells were seeded into new plates on day 7 and treated with dG on the next day. THP1 cells were transduced by spin infection (2500 rpm, 120 min, 32°C, no brakes), seeded and treated as indicated in the figure legends. Jurkat cells, MDA-MB231 and Hela cells were transduced by adding viral vectors to the culture medium. VLP_{vpx} and VLP_{ctrl} were generated using the SIVmac gag-pol expression vectors SIV3+ and SIV4+(Maelfait et al., 2016). Human SAMHD1 expression constructs pCSHAwtW and pCSHAk11aW were a kind gift from T. Schaller (detailed concentrations are shown in **Table 2.2 Concentrations of plasmids transfected** per 15mm dish to produce pCSW HA SAMHD1 and pCSW HA

SAMHD1 K11A). These were used to generate lentiviruses for reconstitution of Jurkat cells (Bridgeman et al., 2015). Mouse SAMHD1 expression construct pMSCVpuro-mSAMHD1 was used to generate a retroviral vector to transduce bone marrow cells as described earlier (Rehwinkel et al., 2013).

Table 2.2 Concentrations of plasmids transfected *per 15mm dish to produce pCSW HA SAMHD1 and pCSW HA SAMHD1 K11A*

	Plamid nb	vol (ul)	onc (ug/ul	Vol (ul)
pCSW HA SAMHD1	363	4	1	4
VSVG	138	2.5	1	2.5
p8.91	93	2.5	0.7	3.57
OPTIMEM		300		
FUGENE		27		

	Plamid nb	vol (ul)	onc (ug/ul	Vol (ul)
pCSW HA SAMHD1 K11A	364	4	1	4
VSVG	138	2.5	1	2.5
p8.91	93	2.5	0.7	3.57
OPTIMEM		300		
FUGENE		27		

2.9 Reverse transcription and quantitative polymerase chain reaction (RT-qPCR)

Cells were resuspend in RLT buffer from Qiagen RNeasy kit and processed according to manufacturer protocol. RNA was eluted in 30 µl of water and concentration was measured using the nanodrop. Reverse transcription was performed using 100 ng of RNA when possible (or less), RNA was first incubated at 72 °C for 10 min with random hexamers or oligo dT (only for the validation of Micro array). The taqman probes were ordered from Life technologies and are listed in **Table 2.3**.

Table 2.3 List of mouse taqman probes

Gene	Protein	Cat. no.
Gapdh	GAPDH	Mm99999915_g1
Samhd1	SAMHD1	Mm00490121
Rn18S	18S rRNA	Mm03928990_g1
Il28a	IFNL2	Mm04204158_gh
Il6	IL-6	Mm00446191_m1
Ifi44	IFI44	Mm00505670_m1
Ifit1	IFIT1	Mm00515153_m1
Ifit2	IFIT2	Mm00492606_m1
Ifnb1	IFN-b1	Mm00439546_s1
Ifna4	IFN-a4	Mm00833969_s1
Isg20	ISG20	Mm00469585_m1
Socs1	Socs1	Mm00466905_s1
Socs3	Socs3	Mm00545913_s1
Ifng	Ifng	Mm01168134_m1
Tnf	TNF	Mm00492606_m1
Hprt	Hprt	Mm03024075_m1
Ptgs2	PTGS2	Mm00478374_m1
Il12b	IL12b	Mm01288989_m1
Tpbg	TPBG	Mm00495741_s1
Nos2	NOS2	Mm00440502_m1
Cish	CISH	Mm01230623_g1

2.10 Micro array

RNA was extracted using Qiagen RNeasy mini kit as described in section 2.9. RNAs were placed into a 96-well PCR plate and frozen at -80 °C. Samples were processed by the Wellcome Trust centre for human genetics (Oxford, United Kingdom) using the mouse Clariom™ S Assay HT (T). Results were analysed by Stephen Taylor from the CBRG at the Weatherall Institute of Molecular Medicine (WIMM). S.Taylor provided a list of genes showing >2 fold changes between treated and non-treated groups. Data were then exported into graph pad prism 7.0.

2.11 dNTP measurements

Cells from 4 plates (90 × 15 mm) of BMDMs or 3 plates (150 mm × 20 mm) of MEFs were pooled for each sample. Measurements were done on cells from different mice. Cells were treated with deoxynucleosides for a specific time and washed twice with ice-cold NaCl (9 g/L) on ice. Cells were then scraped in 550 µL of ice-cold trichloroacetic acid (15% w/v), $MgCl_2$ (30 mM) solution, collected into an Eppendorf tube, frozen on dry ice and stored at −80 °C. The samples were then shipped on dry ice to A.Chabes and S.Sharma to proceed with the analysis. Cells were thawed on ice and processed as described in (Kong et al., 2018). Briefly, the cell suspension was pulse-vortexed (Intellimixer) at 99 rpm for 10 min at 4°C and centrifuged at 20,000 × g for 1 min at 4°C. The resulting supernatant was then neutralized twice with Freon-Trioctylamine mix (78% v/v - 22%, v/v respectively) by vortexing for 30 sec and centrifugation at 20,000 × g for 1 min. 475 µL of the aqueous phase was pH-adjusted with 1 M ammonium carbonate (pH 8.9), loaded on boronate columns (Affi-Gel Boronate Gel; Bio-Rad), and eluted with a 50 mM ammonium carbonate (pH 8.9) and 15 mM $MgCl_2$ mixture to separate dNTPs from NTPs. The eluates containing dNTPs were adjusted to pH 4.5 and loaded onto an Oasis weak anion exchange (WAX) SPE cartridge. Interfering compounds were eluted off the cartridges in two steps with 1 mL ammonium acetate buffer (pH-adjusted to 4.5 with acetic acid) and 1 mL 0.5% ammonia aqueous solution in methanol (v/v), and the analytes were eluted from the cartridge with 2

mL methanol/water/ammonia solution (80/15/5, v/v/v) into a glass tube and then evaporated to dryness using a centrifugal evaporator at a temperature below 37°C. The residue was reconstituted in 1250 μL ammonium bicarbonate buffer, pH-adjusted to 3.4 and used for the HPLC analysis as described in (Jia et al., 2015). Briefly, nucleotides were isocratically eluted using 0.36 M ammonium phosphate buffer (pH 3.4, 2.5 % v/v acetonitrile) as mobile phase. dNTPs were normalized to total NTP pool of the cells.

2.12 Stimulation, staining and mass cytometry analysis of patient samples

PBMCs were collected 24 hours after treatment with forodesine and dG, and were processed according to the Fluidigm Maxpar® protocol, using Maxpar® reagents. Antibodies are listed in **Table 2.4**. Cells were collected in 15 ml falcon tubes and washed in PBS, using centrifugation at 300 g for 5 min. Cells were resuspend at 10^7/ml in R0 with Cisplatin (1:10,000) and incubated at 37°C for 5 min. Cells were washed with R10 and resuspend in PBS. Staining was performed on 3.10^6 cells/tube. Staining with CD56, CD27, CCR4 and CCR7 was done before fixation. Cells were fixed with Maxpar Fix I Buffer at RT for 10 min then washed with Maxpar Cell Staining Buffer (CSB) and spun at 800 g for 5 min. Cells were barcoded (fluidigm barcoding kit) for 30 min at RT, washed twice in CSB, pooled and counted. All further steps were performed on the pooled sample. Cells were blocked in FcR block diluted in CSB (1:10) for 10 min at RT. Surface staining antibody mix was added to blocking solution and incubated for 30 min at RT. Cells were washed in CSB, resuspend in ice cold methanol added dropwise under the vortex and stored at -80°C overnight. The next day, cells were washed twice with CSB and stained with the intracellular antibody mix for 30 min at RT and stained with the intercalator overnight. The following day, cells were washed with CSB and resuspend in water before acquisition on the Helios mass cytometer (Fluidigm). Samples were normalized, concatenated and de-barcoded using Helios software. Files were analysed with Cytobank.

Table 2.4 List of CyTOF antibodies

target	clone	label	Company	product_id	Location	Owner	ul/sample (55 ul)
CD45	HI30	89Y	Fluidigm	3089003B	surface	Helios lab	0.55
CD11c	Bu15	141Pr	Biolegend	in house	surface	Helios lab	0.28
CD11b (Mac-1)	ICRF44	142Nd	Biolegend	in house	surface	Helios lab	1.1
cld-PARP	F21-852	143Nd	Fluidigm	3143011C	intracellular	Rehwinkel lab	0.55
CD4	RPA-T4	145Nd	Fluidigm	3145001B	surface	Helios lab	1.1
CD20	2H7	147Sm	Fluidigm	3147001B	surface	Helios lab	0.55
dGK	H-3	148Nd	Santa cruz	sc-376267	intracellular	Rehwinkel lab	1.1
CD56 (NCAM)	NCAM16.2	149Sm	Fluidigm	3149021B	surface	Helios lab	1.1
p53	D07	150Nd	Fluidigm	3150024A	intracellular	Rehwinkel lab	1.1
CD123	6H6	151Eu	Biolegend	306027	surface	Rehwinkel lab	0.55
CD27	O323	152Sm	Biolegend	302839	surface	Rehwinkel lab	3.7
pStat1 [Y701]	4a	153Eu	Fluidigm	3153005A	intracellular	Helios lab	1.1
CD38	HIT2	154Sm	Biolegend	303535	surface	Rehwinkel lab	1.1
CD45RA	HI-100	155Gd	Biolegend	304143	surface	Rehwinkel lab	1.1
p38 [T180/Y182]	D3F9	156Gd	Fluidigm	3156002A	intracellular	Helios lab	1.1
SAMHD1	poly	158Gd	Abcam	Ab67820	intracellular	Rehwinkel lab	1.1
CD14	M5E2	160Gd	Fluidigm	3160001B	surface	Helios lab	1.1
pBAD [S112]	40A9	161Dy	Fluidigm	3161006A	intracellular	Rehwinkel lab	1.1
STAT1	MAB1490	163Dy	Bio-Techne	246523	intracellular	Rehwinkel lab	1.1
CD23	EBVCS-5	164 Dy	Fluidigm	3164018B	surface	Rehwinkel lab	1.1
pSAMHD1	D7O2M	165Ho	Cell Signaling	8993OBF	intracellular	Rehwinkel lab	0.55
pNFkBp65 [S529]	K10x	166Er	Fluidigm	3166006A	intracellular	Helios lab	1.1
CD197 (CCR7)	G043H7	167Er	Fluidigm	3167009A	surface	Helios lab	1.1
CD8a	SK1	168Er	Fluidigm	3168002B	surface	Helios lab	1.1
CD24	ML5	169Tm	Fluidigm	3169004B	surface	Rehwinkel lab	1.1
CD3	UCHT1	170Er	Fluidigm	3170001B	surface	Helios lab	0.55
CD19	HIB19	171Yb	Biolegend	302247	surface	Rehwinkel lab	1.1
cld-CASP3	5AE1	172Yb	Fluidigm	3172023A	intracellular	Rehwinkel lab	1.1
CD5	UCHT2	173Yb	Biolegend	300627	surface	Rehwinkel lab	0.55
HLA-DR	L243	174Yb	Fluidigm	3174001B	surface	Helios lab	0.6
CD194 (CCR4)	205410	175Lu	Fluidigm	3175021A	surface	Helios lab	1.1
CD43	eBio84-3C1	176Yb	Invitrogen	14-0439-82	surface	Rehwinkel lab	1.1
CD16	3G8	209Bi	Fluidigm	3209002B	surface	Helios lab	0.55

2.13 Quantification and statistical analysis

All experiments were performed three times or more independently under similar conditions, unless specified otherwise in figure legends. Statistical significance was calculated by unpaired t-test, one-way ANOVA or two-way ANOVA as described in the figure legends. Graph pad prism 7 software was used to generate graphs and to perform statistical analysis.

2.14 Reagents

The reagents used for this work are listed in **Table 2.5**.

Table 2.5. List of reagents

Reagent	Source	Identifier
Antibodies		
Anti-hSAMHD1 (mouse polyclonal)	Abcam	#ab67820
Anti-mSAMHD1 (Rabbit)	(Rehwinkel et al., 2013)	n/a
Anti-mouse AF594 (goat)	Life technologies	#A-11005
Anti-Caspase 3	Cell Signaling	#9661T
Anti-cytochrome C	BD	#556433
Anti-β-actin HRP	Sigma	#A3854
Anti-Rabbit HRP	GE-Healthcare	#NA934V
Anti-Mouse HRP	GE-Healthcare	#NA931V
Anti-gapdh	proteintech	#HRP-60004
Anti-COX IV	Cell Signaling	#11967S
Anti-HA HRP	Cell Signaling	#2999S
Anti-PARP	Cell Signaling	#9542P
Anti-Annexin V AF488	Life technologies	#A13201
Anti-BrdU AF488	Biolegend	#364106
Critical commercial assays		
FITC annexinV / 7AAD detection kit	Biolegend	#640922
Mouse TNF alpha ELISA Ready-SET-Go!	eBioscience	#88-7324-88
CellTiter-Glo Luminescent Cell Viability Assay	Promega	#G7571
Caspase Glo 3/7	Promega	#G6320
TaqMan™ Universal PCR Master Mix	Thermofisher	#4304437
Chemicals, Peptides, and Recombinant Proteins		
Hydroxyurea	Sigma	#H8627-5G
2'-deoxyadenosine monohydrate	Sigma	#D8668-1G
2'-deoxythymidine	Sigma	#T1895-1G
2' deoxyguanosine	MedChemexpress LLC	#HY-17563
2'-deoxycytidine hydrochloride	MedChemexpress LLC	#HY-17564
Etoposide	Sigma	#E1383-25MG
Forodesine hydrochloride	MedChemexpress LLC	#HY-16209
Benzonase	Sigma	#E8263-5KU
Z-VAD-FMK	Enzo Life Sciences	#ALX-260-020-M005
ODN 2088 Control (ODN 20958)	Miltenyi Biotec Ltd	#130-105-821
Imiquimod (R837)	Invivogen	#tlrl-imqs
Recombinant Murine TNF	Peprotech	#315-01A
GSK872	Merck chemicals	#5303890001
YOYO-3 Iodide	Life technologies	#Y3606
Clariom™ S Assay HT	Thermofisher	#902971
Pepsin	Sigma	#77160
FxCycle PI/RNase Staining Solution-100 mL	Life technologies	#F10797
Protease inhibitors	Cell signaling	#871S
Phosphatase inhibitors	Sigma	#P0044
Sample buffer	Life technologies	# NP0007
Novex protein standard	Life technologies	#LC5800
MOPS running buffer	Life technologies	#NP001

MES running buffer	Life technologies	#NP001
NuPAGE™ Antioxidant	Life technologies	#NP0005
Ponceau	Sigma	#P7170
Tween20	Sigma	#P1379
ECL	Perkin Elmer	#NEL104001EA
ECL prime	Sigma	#GERPN2232
Digitonin	Life technologies	#BN2006
Crystal violet	Sigma	#HT90132
Propidium iodide	Sigma	#P4170
4-12% Bis Tris protein gel	Life technologies	#NP0321BOX
FcR block	eBiosciences	#14-9161-73
Plasmids		
pSIV3+	(Negre et al., 2000)	n/a
pSIV4+	(Negre et al., 2000)	n/a
pCMV-VSVG	(Rehwinkel et al., 2013)	n/a
pCSHAwtW	(Schaller et al., 2014)	n/a
pCSHAk11aW	(Schaller et al., 2014)	n/a
p8.91 (packaging plasmid)	(Rehwinkel et al., 2013)	n/a
pMSCVpuro-mSAMHD1	Generated in this study	n/a
pMSCVpuro	Clontech	#634401
pX458-Ruby	(Hertzog et al., 2018)	n/a
pX458	Addgene	#48138, deposited by Dr. Feng Zhang
pX458-Ruby-sgRNA-1	Generated in this study	n/a
pX458-sgRNA-2	Generated in this study	n/a
Oligonucleotides		
mSAMHD1 sgRNA1 fwd: CACCGgaggaactggtagctgtaca	WIMM, Genome Engineering facility	n/a
mSAMHD1 sgRNA1 rvs: AAACtgtacagctaccagttcctcC	WIMM, Genome Engineering facility	n/a
mSAMHD1 sgRNA 2 fwd: CACCgggtgaaccccaagctctt	WIMM, Genome Engineering facility	n/a
mSAMHD1 sgRNA 2 rvs: AAACaagagcttggggttcaccc	WIMM, Genome Engineering facility	n/a
Primer 1 fwd : tgacagtttgcatctaacctctg	In-house	n/a
Primer 2 rvs : tgacagtttgcatctaacctctg	In-house	n/a
Primer 3 fwd : tgacagtttgcatctaacctctg	In-house	n/a
Softwares and algorithms		
Graph pad prism 7	GraphPad softwares	
FlowJo V10	FlowJo, LLC	www.flowjo.com
Cytobank		www.cytobank.org/
Other		
Incucyte Live analysis system	Saortorius	N/A
Attune Nxt flow cytometer	BD	N/A
BD LSR II flow cytometer	BD	N/A
Glo-Max multi detection system	Promega	N/A
250ml bot top filter system 0.22um	Appleton Woods Axygen	Bc502

Chapter 3. SAMHD1 DEFICIENCY PREDISPOSES CELLS TO DEOXYNUCLEOSIDE-TRIGGERED APOPTOSIS

The project started with a serendipitous observation made in the lab: *Samhd1*$^{-/-}$ BMDMs died upon the addition of deoxynucleosides (dNs) to the culture media. I hypothesised that SAMHD1 plays an important role in nucleotide metabolism through its dNTPase activity. A better understanding of this function could lead to new insights into the role of SAMHD1 in Aicardi-Goutières syndrome and cancer, two conditions where *SAMHD1* is mutated.

3.1 *Samhd1*$^{-/-}$ cells die upon exposure to deoxynucleosides

To reproduce the phenotype, BMDMs were treated with an equimolar mix of each deoxyribonucleoside (dN) consisting of 2' deoxyadenosine (dA), 2' deoxycytidine (dC), 2' deoxyguanosine (dG) and 2' deoxythymidine (dT, also called thymidine). Cell viability was measured with CellTiter-Glo (a luminescent based assay) 24h post-treatment and is expressed as percentage of treated versus untreated (% viability vs untreated). As an indirect readout of viability, CellTiter-Glo quantifies the amount of ATP in the cell, an indicator of metabolically active cells. Results showed lower viability of *Samhd1*$^{-/-}$ BMDMs compared with WT BMDMs at 24h post-treatment (**Figure 3.1A**). The same phenotype was observed in MEFs as shown in **Figure 1B**. *Samhd1*$^{-/-}$ MEFs showed a dose-dependent toxicity to dN mix at 48h (**Figure 3.1C**). In addition, reduced viability of *Samhd1*$^{-/-}$ BMDMs upon treatment with dN mix was confirmed by microscopy (**Figure 3.1D**). To determine whether SAMHD1 plays a similar role in human cells, primary human fibroblasts from AGS patients were cultured and treated with dNs for 24h. They were either mutated in *ADAR1*, *IFIH1* (encoding MDA5) or *SAMHD1* (homozygous Q149X). Fibroblasts with mutations in *SAMHD1* showed a significantly reduced viability upon treatment with dNs (**Figure 3.1E**) which was not observed in fibroblasts from healthy controls or AGS patients with mutations in *IFIH1* or *ADAR1*. In addition, mouse *Trex1*$^{+/-}$ BMDMs were treated with dNs (**Figure 3.1F**). *Trex1*$^{+/-}$ BMDMs did not show any sensitivity to dNs. This suggests that the phenotype

was specific to SAMHD1 and that the other genes mutated in AGS (*ADAR1*, *IFIH1* and *TREX1*) do not show sensitivity to dNs.

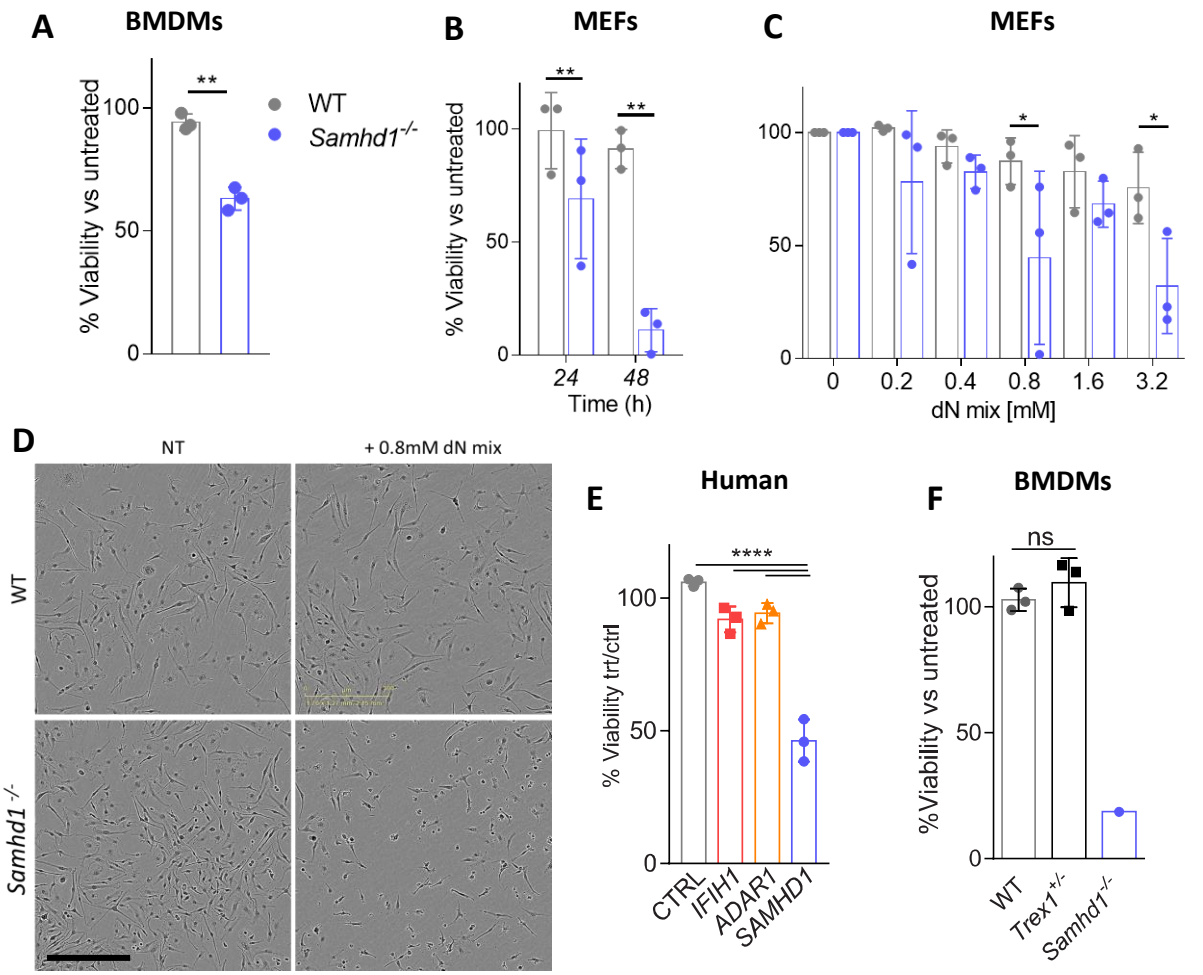


Figure 3.1 Deoxynucleosides are toxic to cells lacking SAMHD1. *(A) Viability (CellTiter-Glo) of BMDMs 24h post-treatment with 0.5 mM of each dN. Dots represent individual wells treated with dN mix, bars represent mean ± SD, paired t-test (**=p<0.005). (B) Viability (CellTiter-Glo) of MEFs treated with 0.8 mM of each dN (dA, dC, dG and dT) at 24h and 48h. Viability is shown as percentage of treated versus untreated. Dots represent individual wells treated with dN mix, bars represent mean ± standard deviation (SD) and two-way ANOVA (*=p<0.05, **=p<0.005, ***=p<0.0005. (C) Viability (CellTiter-Glo) of MEFs at 48h post-treatment with each dNs at indicated concentrations. Dots are cells from individual mice, bars represent mean ± SD and two-way ANOVA (*=p<0.05, **=p<0.005, ***=p<0.0005. (D) Brightfield images of BMDMs 30h post-treatment with 0.8mM dN mix. Scale bar represents 300 μM. (E) Viability of human fibroblasts with mutations in indicated gene 24h after treatment with 0.5 mM mix of dNs. Dots represents different wells of the same cells, bars represent mean ± SD and statistics are one way ANOVA (****=p<0.0001)). (F) Viability (CellTiter-Glo) of BMDMs of indicated genotypes treated with 0.5 mM each dN for 24h. Dots represent cells from individual mice, bars represent mean ± SD and statistics are one way ANOVA. (A-E) are representative of more than 3 independent experiments.*

To determine if toxicity of dNs in *Samhd1*$^{-/-}$ BMDMs correlates with cell death, staining with Annexin V and 7AAD was analysed by flow cytometry. Annexin V is a protein that binds phosphatidylserine, a phospholipid flipping to the outer membrane of apoptotic cells, and 7AAD is a membrane impermeable DNA dye. Apoptotic cells first become positive for

Annexin V, before being positive for the DNA dye 7AAD. Early apoptotic cells only stain positive for Annexin V (AnnexinV$^+$7AAD$^-$ cells) and late apoptotic and necrotic cells are positive for both Annexin V and 7AAD (AnnexinV$^+$7AAD$^+$ cells). BMDMs were treated with dNs for 24h, stained with Annexin V and 7AAD, and analysed on a flow cytometer. Treatment resulted in a significant increase in Annexin V$^+$ 7AAD$^-$ and Annexin V$^+$ 7AAD$^+$ *Samhd1*$^{-/-}$ BMDMs compared with WT BMDMs (**Figure 3.2A-C**). Most of the Annexin V$^+$ cells were also 7AAD$^+$ at 24h meaning that dNs treatment induced cell death by apoptosis or necrosis. This revealed that lower ATP levels measured in previous experiments correlated with cell death as measured in this assay.

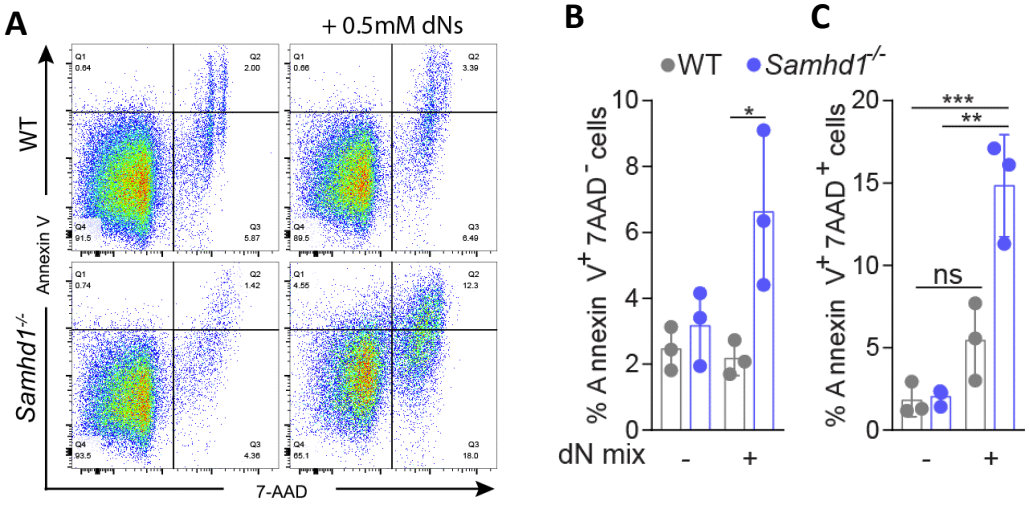


Figure 3.2 dN treatment induces death of Samhd1$^{-/-}$ cells. *(A) Representative FACS plots of Annexin V and 7AAD staining in BMDMs treated with 0.5 mM dNs for 24h. (B) Quantification of Annexin V$^+$7AAD$^-$ in BMDMs 24h post-treatment with 0.5 mM of each dN. (C) Quantification of Annexin V$^+$7AAD$^+$ BMDMs 24h post-treatment with 0.5 mM of each dN. Dots represent biological triplicates, bars represent mean ± SD, two-way ANOVA (***=p<0.0005).*

In order to confirm that SAMHD1 presence was required to protect cells from the toxicity of dN supplementation, *Samhd1*$^{-/-}$ BMDMs were reconstituted with SAMHD1. Bone marrow cells were transduced with a retroviral vector expressing SAMHD1 or a control vector during the first 3 days of the 7 day differentiation process, and cells were then seeded before being treated with dNs for 24h. Reconstitution of *Samhd1*$^{-/-}$ BMDMs with SAMHD1 significantly improved cell viability upon treatment with dNs as compared with non-reconstituted cells (**Figure 3.3A**). Western blot for SAMHD1 confirmed the reconstitution of the protein in *Samhd1*$^{-/-}$ BMDMs transduced with the retrovirus expressing SAMHD1 but not with the control retrovirus (**Figure 3.3B**). These data strongly support the involvement of SAMHD1

in protection against dN-induced cell death in murine and human cells. Taken together, these results demonstrated toxicity of dNs in SAMHD1-deficient cells.

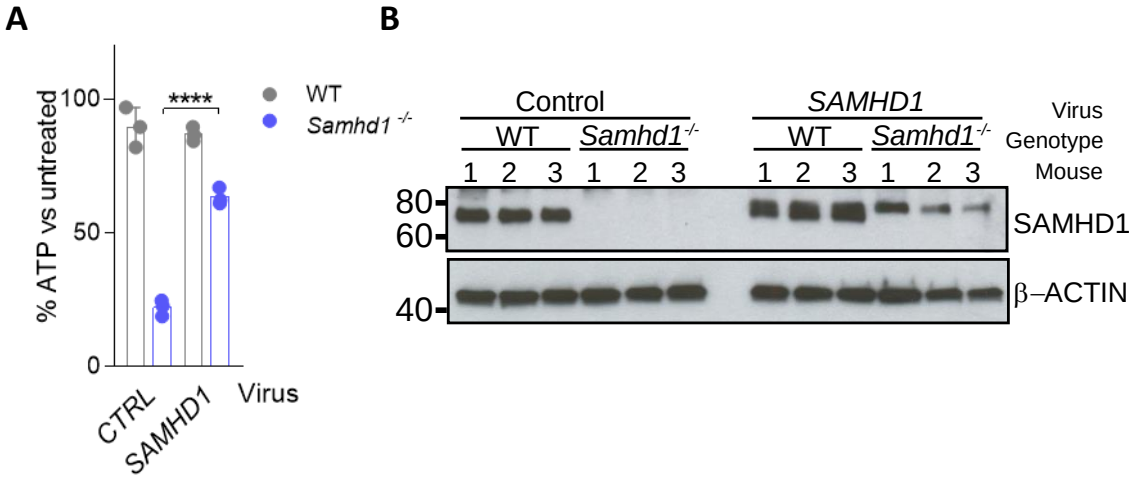


Figure 3.3 SAMHD1 reconstitution protects Samhd1$^{-/-}$ BMDMs from dN-induced cell death*. (A) Viability (CellTiter-Glo) of BMDMs transduced with control retrovirus or retrovirus expressing SAMHD1, and treated with 0.5 mM of each dN for 24h. Transduction was performed by spin infection of bone marrow cells on day 1, 2 and 3 of the culture. Cells were seeded on day 7, and treated the next day for 24h. Dots represent cells from different mice (as shown in (B), error bars represent mean ± SD and statistics are two-way ANOVA (****=p<0.0001). (B) Western Blot of SAMHD1 in BMDMs transduced with SAMHD1 retrovirus or control retrovirus in biological triplicates (sample transduced, shown in A). (A, B) are representative of 3 independent experiments.*

3.2 Deoxyguanosine is the most toxic deoxyribonucleoside to *Samhd1*$^{-/-}$ cells

Next, I wished to determine whether all dNs were equally toxic. *Samhd1*$^{-/-}$ BMDMs were treated with single dNs or with dN combinations and viability was measured at 24h (**Figure 3.4A**). Interestingly, deoxyguanosine (dG) alone was more toxic than a combination of all four dNs together. In addition, when dC was present in the mix of 2-3 dNs together with dG, the toxicity of dG was reduced. In contrast, dC alone showed minimal toxicity compared with dA, dG or dT alone. dG also appeared to be the most toxic to MEFs as measured by crystal violet staining at 24h (**Figure 3.4B, C**). Adherent cells were stained with crystal violet, a dye that binds protein and DNA, while dead cells lost their adherence, resulting in weaker staining of the overall population. Brightfield images of MEFs showed cell death upon dN treatment, with the biggest effect resulting from dG treatment, matching the quantifications with the crystal violet assay (**Figure 3.4D**). Human fibroblasts from an AGS patient with the

SAMHD1 mutation Q149X also showed an increased sensitivity to dG compared with a mix of all four dNs compared with *IFIH1* mutated or control fibroblasts (**Figure 3.4E**).

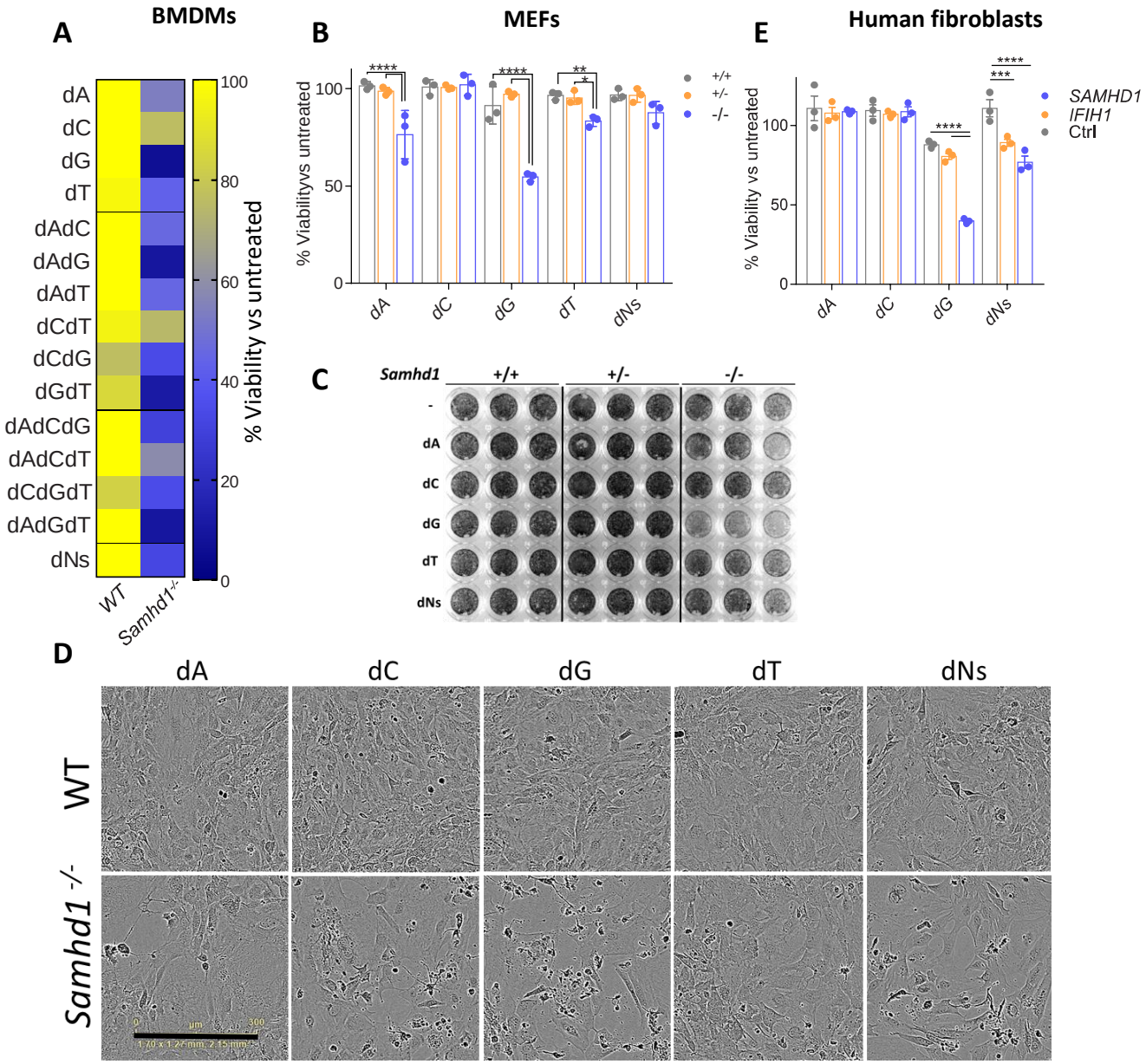


Figure 3.4 dG is the most toxic dN. *(A) Heat map representing mean viability (CellTiter-Glo) of BMDMs treated for 24h with the indicated dNs. (B) Viability of MEFs of indicated genotypes, measured with crystal violet quantification expressed as percentage viability treated vs untreated 30h post-treatment with 0.5 mM of indicated dNs. Dots represent biological triplicates and bars are mean ± SD. Statistics are two-way ANOVA (*=p<0.05, **=p<0.005, ****=p<0.0001). (C) Picture of the crystal violet plate before quantification, each column represents MEFs isolated from a different embryo. (D) Brightfield images of MEFs 24h post-treatment. Scale bar represents 300 μM. (E) Viability (CellTiter-Glo) of human fibroblasts from AGS patients measured 24h post-treatment with 0.5 mM of indicated dNs. Dots represents individual wells, bars are mean ± SD and statistics are two-way ANOVA (***=p<0.0005, ****=p<0.0001). A-D are representative of 3 independent experiments.*

3.3 dG treatment induces an increase in dGTP in *Samhd1*$^{-/-}$ cells

Deoxyguanosine (dG) was the most toxic dN in cells lacking SAMHD1. Early studies reported dG toxicity in lymphoid cells and dGTP was suggested as the toxic metabolite (Chan, 1978; Cohen et al., 1978). Therefore, I hypothesised that dG added onto the cells was transported to the cytoplasm, processed through the nucleotide salvage pathway to be converted into dGTP. SAMHD1-deficient cells would accumulate dGTP, which could then cause toxicity. This meant that dG would be phosphorylated by deoxycytidine kinase (dCK) in the cytoplasm or by deoxyguanosine kinase (dGK) in the mitochondria to form deoxyguanosine monophosphate (dGMP) that is further converted into deoxyguanosine triphosphate (dGTP). dGTP pools in the cytoplasm are transported to the nucleus and the mitochondria to constitute the available dNTP pool in the cell (Berg JM, 2002a). Since SAMHD1 is a dNTPase, I hypothesised that dGTP accumulates in *Samhd1*$^{-/-}$ cells due to lack of degradation by SAMHD1. To test this, dNTP quantifications were performed on cell extracts (analysis performed by our collaborators A. Chabes and S. Sharma at Umeå University). As expected, dNTP levels in BMDMs were higher in *Samhd1*$^{-/-}$ cells compared with WT in resting cells (**Figure 3.5A**). dG treatment induced a 35 fold increase in dGTP 2h post-treatment in *Samhd1*$^{-/-}$ cells but not in WT cells. dNTPs concentrations were similar 4h post-dG treatment. dNTP measurements performed in MEFs two hours post-treatment with dG showed similar results (**Figure 3.5B**). Before treatment, *Samhd1*$^{-/-}$ MEFs had higher levels of dNTPs while *Samhd1*$^{+/-}$ MEFs showed highest concentrations of dCTP followed by dTTP, dATP and dGTP respectively. dG treatment induced a significant increase of dGTP only in *Samhd1*$^{-/-}$ MEFs although the increase of dGTP was lower than in BMDMs. No changes were observed in WT or *Samhd1*$^{+/-}$ MEFs. This suggested that dG was taken up by the cell and converted into dGTP through the salvage pathway. Cells lacking SAMHD1 showed significantly higher dGTP concentrations compared with WT. Interestingly, there was no further increase of dGTP levels after 4h compared with 2h, suggesting that most dG has been phosphorylated already. This suggests that SAMHD1's dNTPase activity protects cells by degrading accumulating dGTP, preventing subsequent toxicity.

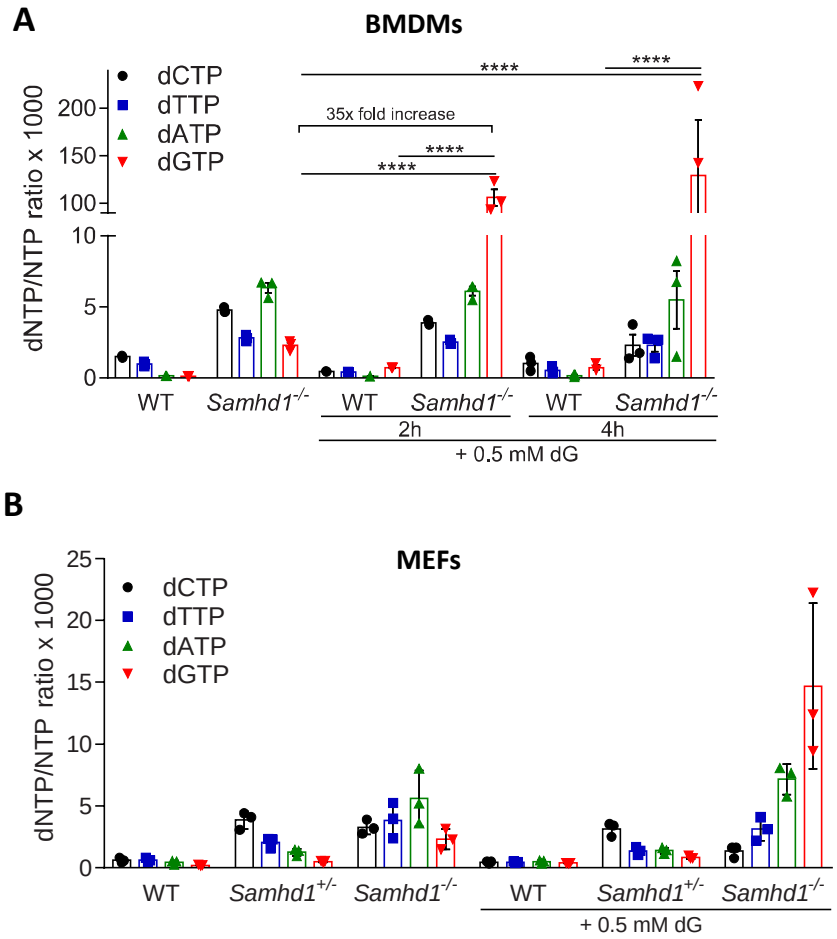


Figure 3.5 dG treatment induces an increase of dGTP in Samhd1$^{-/-}$ cells. *(A) dNTP quantifications in BMDMs treated with dG for the indicated time periods. (B) dNTP quantifications in MEFs of indicated genotypes 2h post-dG treatment. Dots represent cells from individual mice, bars represent mean and ± SD. Statistics are two-way ANOVA (**** =p<0.0001).*

3.4 dG toxicity is independent of genomic DNA replication

Next, I hypothesised that dGTP toxicity was triggering dNTP imbalances leading to DNA damage and cell death during DNA synthesis. Cell cycle analysis using BrdU staining in BMDMs showed that both WT and *Samhd1*$^{-/-}$ had similar cell cycle profiles with ~50% cells in G0/1, ~20% cells in S-phase and ~4% cells in G2/M-phase (**Figure 3.6A**). This meant that BMDMs differentiated from bone marrow cells were still actively dividing after plating on day 7. Cell cycle analysis was performed at several time points post-dG treatment (**Figure 3.6A**). WT BMDMs showed cell cycle arrest in G0/G1 post-dG treatment with cells in S-phase progressing through the cell cycle and dividing, reflected by a decrease in the number of cells in S-phase and an increase in the number of cells in G0/G1. On the other hand, *Samhd1*$^{-/-}$ cells showed a profound loss of S-phase cells as early as 2h post-dG treatment

and a loss of G0/G1 cells. It seemed like both G0/G1 and S-phase cells were dying upon dG treatment in *Samhd1*$^{-/-}$ BMDMs. To track replicating cells post-treatment, a pulse-chase experiment was performed where cells were labelled with BrdU (pulse) before being cultured in media (chase) and treated with dG. Results showed that WT cells in S-phase progressed through S-phase and returned to G0/G1, as shown by a shift of BrdU^{+} cells from right to left (**Figure 3.6B**). However, *Samhd1*$^{-/-}$ cells showed no well-defined BrdU^{+} cells returning to G0/G1 but instead a wide spread of these cells with higher variability of PI and BrdU staining. At later time points, all BrdU^{+} cells disappeared from the culture, most probably having died. This experiment showed that dG treatment triggered a G0/G1 cell cycle arrest in WT cells while it killed *Samhd1*$^{-/-}$ cells in both G0/G1 and S-phase. To determine if dG toxicity was independent of the cell cycle, cells were either cultured in media without FCS (R0) or were pre-treated with hydroxyurea (HU), an inhibitor of RNR (**Figure 3.6D, E**). BrdU staining showed that HU pre-treatment pushed the cells into G0/G1 and triggered cell cycle arrest, with no remaining cells in S-phase (**Figure 3.6C**). Culturing the cells in R0 partially prevented DNA synthesis with a residual proportion of the cells in S-phase. These non-cycling BMDMs were treated with dG and viability was measured after 24h (**Figure 3.6D and E**). Neither culture in R0 nor HU pre-treatment protected *Samhd1*$^{-/-}$ cells from dG toxicity. This showed that dGTP accumulation was toxic independently of DNA synthesis in the nucleus.

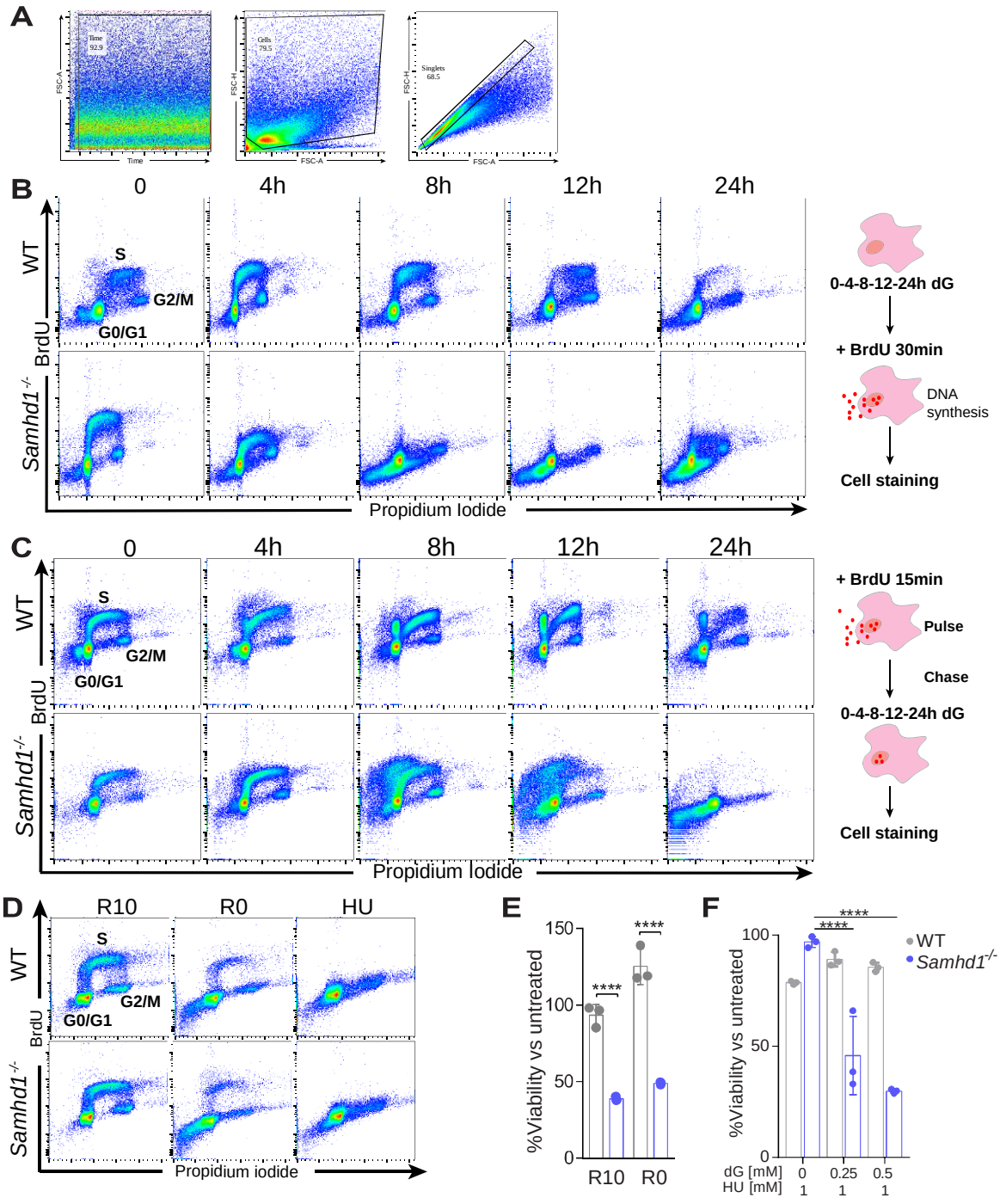


Figure 3.6 dG toxicity is independent of genome replication. *(A) Gating strategy; singlets cells were gated within the time gate, and downstream analysis within that gate are shown in (B-D). (B) BMDMs were treated with 0.5 mM dG for the indicated periods of time. Cells were then labelled with BrdU for 30 min and fixed. Cells were stained with an α-BrdU antibody and PI and analysed by flow cytometry.(C) BMDMs were labelled with BrdU for 15 min and then treated with 0.5 mM dG for the indicated periods of time. Cells were then analysed as in (B). (D-F) After 7 days of conventional culture, BMDMs were grown in medium containing 10% FCS (R10) or in serum-free medium (R0) for 24 hours. Alternatively, BMDMs were treated with 1 mM hydroxyurea (HU) for 8 hours. (C) Cells were analysed as in (B). (E) Cells were treated with 0.5 mM dG for 24 hours and viability was analysed as described in Figure 1A. (F) Cells were treated with 0.5 mM dG for 16 hours and viability was analysed as described in Figure 1A. P-values determined with two-way ANOVA are indicated. **** p<0.0001. Data are representative of three (B, D-F) and two (B) independent experiments, respectively.*

3.5 dGTP overload triggers apoptosis in *Samhd1*$^{-/-}$ cells

Next, I sought to investigate the type of cell death induced by dG treatment. Previous results demonstrated that dG treatment induced an increase of AnnexinV^{+}7AAD^{-} cells in *Samhd1*$^{-/-}$ cells, suggesting cell death by apoptosis. To test this, caspase 3/7 activity was measured 10h post-treatment using the Caspase-Glo® 3/7 assay, a luminescence based assay measuring substrate cleavage by caspases 3/7 (**Figure 3.7A**). An increase in cleaved caspase 3/7 10h post-dG treatment was observed only in *Samhd1*$^{-/-}$ cells. Repeat of this experiment at different time points showed a peak in signal detection 6h post-dG treatment as shown in (**Figure 3.7B)**.

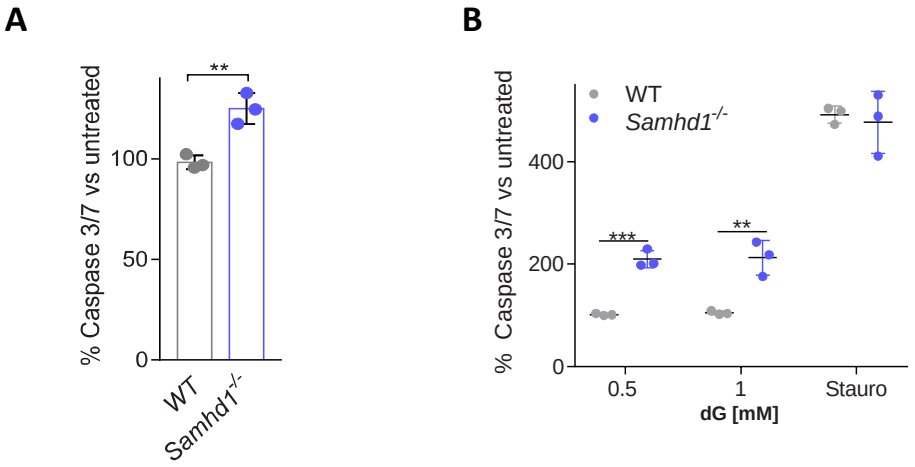


Figure 3.7 Samhd1$^{-/-}$ BMDMs die by apoptosis upon dG treatment. *(A) Percentage of caspase 3/7 (Caspase Glo 3/7) activity versus untreated 10h post-treatment with 0.5 mM dG. Dots represent biological triplicates, bars are means ± SD and statistics are t-test (**=p<0.01). Representative of 3 independent experiments. (B) Raw values of Caspase Glo 3/7 assay on BMDMs 6h post dG treatment. Dots represents individual wells, bars are mean ± SD and statistics are two-way ANOVA (**=p<0.01, ***=p<0.001).*

To further confirm that dG-triggered cell death was apoptosis, widefield fluorescence microscope was used to detect the binding of Annexin V (coupled to Alexa Fluor 488) and staining with propidium iodide (non-permeant DNA dye) in real time post-dG treatment. *Samhd1*$^{-/-}$ BMDMs showed formation of apoptotic bodies as early as 5h post-dG treatment, quickly followed by binding of Annexin V and propidium iodide (**Figure 3.8A**). This particular sequence of events indicated that *Samhd1*$^{-/-}$ BMDMs were dying by apoptosis upon dG treatment. Quantification of Annexin V^{+} PI^{+} cells by microscopy at 24h confirmed our

previous observations: there was an increase of dead cells only in *Samhd1*$^{-/-}$ cells upon dG treatment (**Figure 3.8B**).

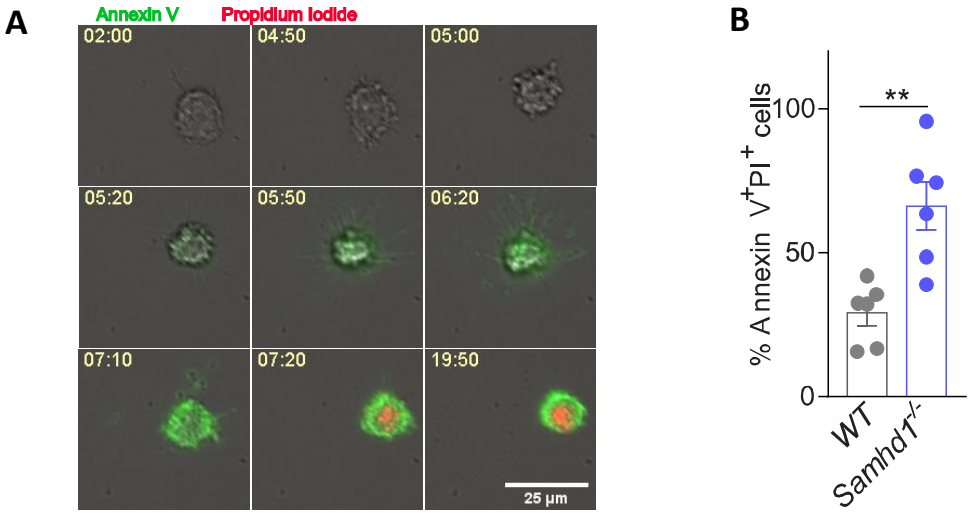


Figure 3.8 Samhd1*$^{-/-}$ *cells become Annexin*$^{+}$*PI*$^{+}$ *post-dG treatment. *(A) Representative images of Samhd1*$^{-/-}$ *BMDMs taken at indicated time points (hours) after treatment with 0.5 mM dG. (B) Quantification of AnnexinV*$^{+}$*PI*$^{+}$ *cells measured by fluorescence on live BMDMs. Dots represent average of individual images of the same well, bars are means, error bars are SD and statistics are t-test (**=p<0.01).*

Cleavage of procaspase 3 in *Samhd1*$^{-/-}$ BMDMs upon dG treatment was confirmed by western blot (**Figure 3.9A**). Procaspase 3 showed similar levels in WT and *Samhd1*$^{-/-}$ and a small reduction only in the positive control (CHX= cyclohexamide + TNF). In contrast, cleaved-caspase 3 was detected only in *Samhd1*$^{-/-}$ cells upon dG treatment. Cleaved-PARP was also detected in *Samhd1*$^{-/-}$ BMDMs post-dG treatment with higher levels at 10h (**Figure 3.9B**). To determine if the cleavage of caspase 3 was triggered by intrinsic apoptosis, release of cytochrome C in the cytoplasm was measured. Cytochrome C is normally present in mitochondria and is released into the cytosol through pore formation when intrinsic apoptosis is triggered. Cell fractionation was performed to separate cytosolic proteins from nuclear, mitochondrial and membrane bound proteins. **Figure 3.9C** shows higher levels of cytochrome C in the cytosolic fraction of *Samhd1*$^{-/-}$ BMDMs compared with WT upon dG treatment. In addition, co-cultures of WT and *Samhd1*$^{-/-}$ BMDMs showed that the reduction of viability post-dG treatment corresponds to the fraction of *Samhd1*$^{-/-}$cells present in the culture (**Figure 3.9D**). This suggested that no soluble factor secreted by *Samhd1*$^{-/-}$cells was

triggering cell death of WT cells. All together, this showed that dG treatment triggered caspase-dependent cell death by intrinsic apoptosis in *Samhd1*$^{-/-}$ cells.

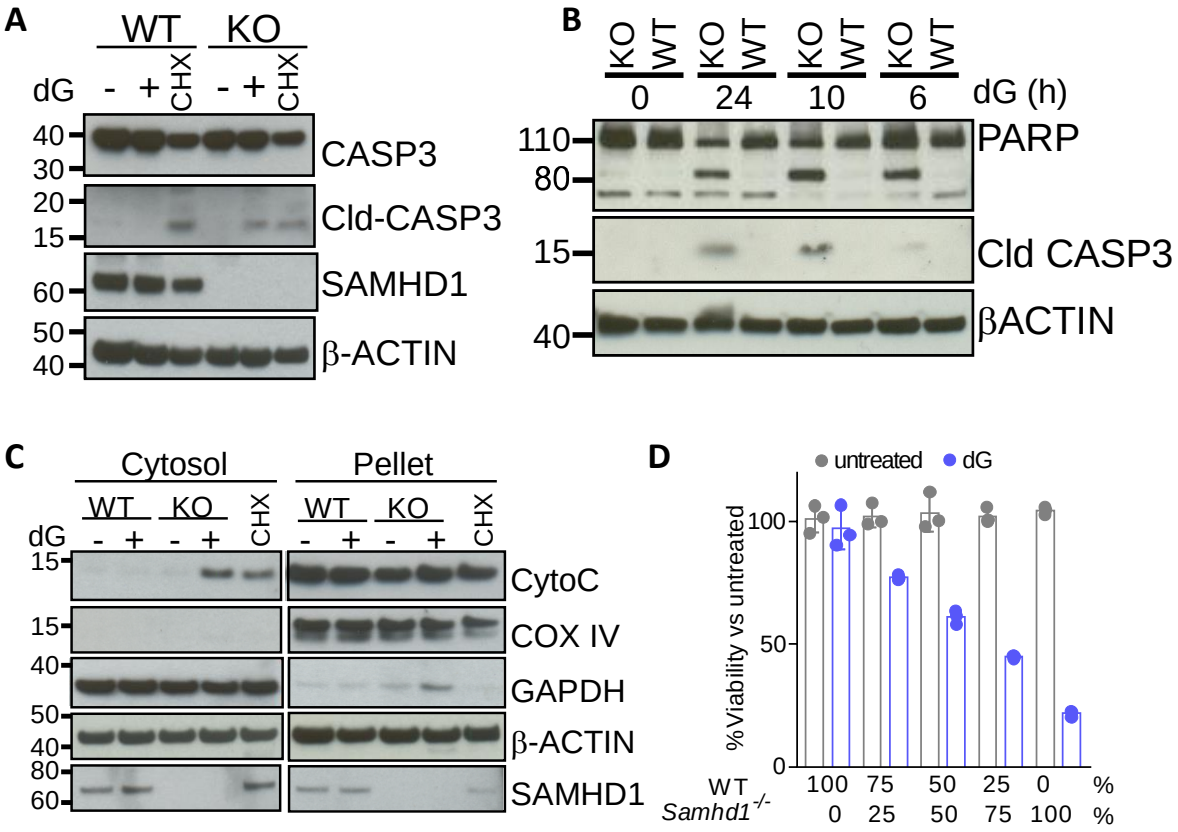


Figure 3.9 Samhd1$^{-/-}$ BMDMs die through caspase-dependent cell death. *(**A**) Western blot of procaspase 3 (CASP3) and cleaved-caspase 3 (Cld-CASP3) in BMDMs 8h post-dG treatment. (**B**) Western blot of PARP and cleaved-PARP (Cld-PARP) in BMDMs at indicated times post-dG treatment. β-ACTIN is used as a loading control. (**C**) Western blot of cytochrome C (CYTO C) 8h post-dG treatment cytosolic and pellet (nuclear, mitochondria and membrane bound) fractions in BMDMs. GAPDH was used as a control for the cytosolic fraction and COX IV (mitochondrial protein) for the pellet fraction. CHX= 1 µg/ml cyclohexamide + 100 ng/ml TNFα. (D) Viability at 24h of WT and Samhd1$^{-/-}$ BMDMs co-culture at indicated percentages post-treatment with 0.5 mM dG versus untreated. Dots represent individual wells, bars are means ± SD. (A-C) are representative of 3 independent experiments, (D) of 2 experiments.*

3.6 Discussion

The aim of this chapter was to investigate a simple observation: the toxicity of dNs in *Samhd1*$^{-/-}$ cells. This interesting observation was repeated numerous times independently, allowing me to confirm the presence of a robust phenotype in mouse and human primary cells.

Further investigation showed that all dNs were toxic in *Samhd1*$^{-/-}$ cells, with dG being the most toxic. This supports an early report of dG toxicity in lymphoid cells (Chan, 1978). A condition called PNP deficiency is characterised by the malfunction of the enzyme PNP, which degrades dG. PNP deficiency is characterised by the accumulation of dG and dGTP in cells, which causes toxicity in T and B cells of PNP-deficient patients (Cohen et al., 1978; Duan et al., 1990; Sidi et al., 1989; Simmonds et al., 1987; Simmonds et al., 1982). Interestingly, combinations of 2 or 3 dNs showed that mixes of dNs were as toxic as dG alone if dG was present in the mix, unless dC was also present. An early study observed a similar reduced toxicity when dC was added with dG (Chan, 1978). I conducted further experiments with dG alone, since it showed the highest toxicity. The toxicity of dG in SAMHD1-deficient cells suggested that the cells were not able to deal with an excess of dGTP and/or imbalances of dNTPs. The accumulation of dGTP observed in SAMHD1-deficient cells upon dG supplementation is similar to the accumulation of dGTP observed in PNP-deficient cells.

Keeping balanced and controlled dNTP pools in cells is important to avoid an increased mutation rates (Kumar et al., 2011a; Kunz et al., 1994). SAMHD1 was shown to be an important regulator of DNA precursor pools in mammalian cells (Franzolin et al., 2013). The authors reported that the absence of SAMHD1 leads to accumulation of cells in G1 phase with oversized dNTP pools and growth arrest. When SAMHD1 was active, dNTP pools normalised and cells could start growing again. This is why SAMHD1 is active in the G0/G1 phase of the cell cycle when cells are quiescent and do not require high levels of dNTPs. In contrast, in S-phase SAMHD1 is inactive leading to an increase of dNTP pools that allows genomic DNA replication (Ruiz et al., 2015). Although it is well established that SAMHD1,

together with RNR, is critical to maintain dNTPs pools, no report has so far described SAMHD1's role in safeguarding the cell against imbalances or excess of dNTPs that otherwise trigger cell death. Thus, the observation that SAMHD1 protects cells against dNTPs imbalances, was novel and worth investigating.

There are two main nucleotide synthesis pathways in the cell, the *de novo* pathway and the salvage pathway (Berg JM, 2002b). The salvage pathway enables the recycling of dNs from apoptotic cells. Transporters and kinases are important to allow dNs to reach the cytoplasm and to be phosphorylated into dNTPs. Therefore, addition of dG to the cell culture media is expected to actively transport dG into the cytoplasm and process it through the salvage pathway. Once in the cell, dG can be phosphorylated into dGMP by deoxycytidine kinase (dCK) in the cytoplasm or deoxyguanosine kinase (dGK) in the mitochondria (Arnér and Eriksson, 1995). Further phosphorylation leads to the generation of dGTP. High levels of dGTP are degraded in the presence of active SAMHD1 whilst SAMHD1-deficient cells are unable to degrade it leading to accumulation of dGTP.

dGK is localised in the mitochondrial matrix. The gene encoding dGK (*DGUOK)*, is not present in the mitochondrial genome, which encodes only 37 genes. Mutations in *DGUOK* cause a rare disease called MTDPS3, one of several mtDNA depletion syndrome diseases (MDSs) (Salviati et al., 2002). Deficiencies in dGK and dTK, both critical enzymes of the salvage pathway in mitochondria, leads to depletion of mtDNA (Wang et al., 2005). This deficiency in dGK causes multiple organ failure and death (Unal et al., 2017). This illustrates the importance of the generation of mitochondrial dGTP pools through dGK. This also demonstrates that dGTP synthesis in the cytosol, through conversion of dG by dCK and the salvage pathway, is not sufficient to produce the mitochondrial dGTP pool. The *de novo* nucleotide synthesis depends on RNR activity, which is regulated by the cell cycle. The functional RNR is composed of two large subunits bound to two small subunits, called RRM1 and RRM2 respectively (Nordlund and Reichard, 2006). RRM1 levels are constant through the cell cycle while levels of RRM2 are regulated through the cell cycle. Cyclin F and its interaction with the Skp1-Cul1-F-box protein ubiquitin ligase complex in G2 leads to

degradation of RRM2, allowing the maintenance of dNTP pools (D'Angiolella et al., 2012). Therefore, it is reasonable to think that the nucleotide salvage pathway within mitochondria plays an important role in maintenance of mtDNA integrity, which is required at any stage of the cell cycle. However, mutations in RNR subunits have been shown to cause mtDNA depletion, showing that *de novo* dNTP synthesis also plays an important role (Bourdon et al., 2007). Mitochondrial transporters of GDP/GTP exist while no transporter of dGTP has been reported yet (Vozza et al., 2004). This suggests that the nucleotide salvage pathway and dGK play a critical role in the mitochondria to generate the dGTP pool. Since RNR is fully active in S-phase, it is reasonable to hypothesise that dGTP would be synthesised *de novo* in S-phase, while it would be salvaged in quiescent cells when RNR is inactive and the dGTP pool is low.

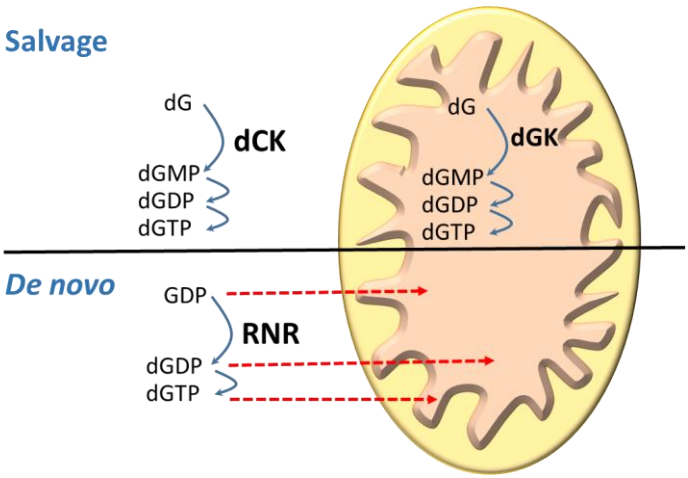


Figure 3.10 Synthesis of dGTP pool. *The salvage pathway phosphorylates dG through dCK (cytosol) or dGK (mitochondrion). De novo pathway depends on RNR, which is regulated throughout the cell cycle, generates dGTP pools in the cytosol. Whilst mitochondrial transporters of GDP and GTP have been described, It has not been shown that dGTP can be transported into mitochondria.*

Samhd1$^{-/-}$ cells displayed higher dNTP levels in my experiments, as reported previously (Behrendt et al., 2013; Franzolin et al., 2013; Rehwinkel et al., 2013; St Gelais et al., 2012). In addition, SAMHD1-deficient MEFs and BMDMs showed a significant increased dGTP levels compared with WT cells. This is consistent with dG being taken up into cells and converted into dGTP via the salvage pathway. It suggests that the absence of SAMHD1 led to the accumulation of dGTP in *Samhd1*$^{-/-}$ cells, and subsequent toxicity. This supports early publications showing dG toxicity through dGTP accumulation in PNP deficient cells (Chan, 1978; Cohen et al., 1978). The authors at the time suggested a model in which dGTP exerts a feedback loop on RNR, leading to reduced dCTP pools, and cell death by dCTP starvation, as illustrated in **Figure 3.11A** (Chan, 1978; Hofer et al., 2012). This model was

supported by the observation that supplementation of dC lead to reduced toxicity of dGTP. In contrast, a more recent publication proposed a model where dGTP toxicity occurs in the mitochondria (Arpaia et al., 2000). Indeed, it is likely that most of the dG conversion into dGTP is happening in the mitochondria, where dGK is located. Severe disease caused by mutations in *DGUOK* supports that dGK is the main enzyme required in the mitochondria to generate the dGTP pool. This is supported by the observation that dGK is more expressed in most tissues, than dCK (Eriksson and Wang, 2008).

The accumulation of dGTP in SAMHD1-deficient cells is most likely the result of dG processing through the salvage pathway. Consequently, dGTP overload may cause a cytotoxic stress and trigger subsequent cell death. High dNTP pools and dNTP imbalances are known to increase mutations rates and induce DNA damage (Kumar et al., 2010). This suggests that the increased dGTP pools may cause toxicity at the replication fork, where DNA damage and mutations can occur. To investigate whether DNA synthesis was required for dGTP toxicity, cell cycle analysis of BMDMs was performed. Around 20% of BMDMs were in S-phase prior to treatment with dG. Loss of *Samhd1*$^{-/-}$ cells following dG treatment from S-phase, G0/G1 and G2/M was observed, suggesting that dG toxicity was not limited to cells in S-phase. On the other hand, upon dG treatment WT cells were able to block cell cycle progression in G0/G1, with cells in S-phase finishing the cycle and returning and remaining in G0/G1. To determine whether dGTP overload was causing replication stress during DNA synthesis, cell cycle progression was stopped. This did not protect *Samhd1*$^{-/-}$ BMDMs from dG-induced toxicity. This key experiment showed that dGTP overload was causing toxicity independently of genomic replication. Indeed, the most probable hypothesis so far was that dGTP imbalances trigger genomic stress at the replication fork, and subsequent cell death. These results demonstrated that dGTP was causing toxicity through a mechanism independent of genomic replication and that the observed protective function of SAMHD1 is unlikely to be its role in DNA repair at the replication fork, as recently described (Coquel et al., 2018; Daddacha et al., 2017).

Purine nucleoside phosphorylase (PNP) deficiency is a disease characterised by the accumulation of dG and dGTP in the cells, causing lymphopenia (Chan, 1978; Cohen et al., 1978; Watson et al., 1981). This condition creates a situation similar to the one observed when supplementing *Samhd1*$^{-/-}$ cells with dG: accumulation of dGTP. Most of the early reports suggest that dGTP causes toxicity in lymphocytes due to a feedback loop on RNR, leading to lower dCTP levels, dNTP starvation and cell death. I named this proposed mechanism **Model A**, shown in **Figure 3.11A** (Boehncke et al., 1994; Cohen et al., 1978; Duan et al., 1990; Sidi et al., 1989). In contrast, another study showed that dGTP toxicity in PNP-deficient cells was due to the increase of dGTP in the mitochondrial compartment and subsequent toxicity; this is **Model B** is illustrated in **Figure 3.11B** (Arpaia et al., 2000). Neither of these two models considered the effect of SAMHD1 since it was unknown at the time. The evidence collected in this chapter showed that SAMHD1 prevents dGTP accumulation when dG is supplemented. This suggests that SAMHD1 could protect PNP-deficient cells from dGTP toxicity, as shown in **Figure 3.11C**.

The mechanism of dGTP toxicity in SAMHD1-deficient cells upon treatment with dG has not been fully investigated. My data showed dG-induced toxicity in *Samhd1*$^{-/-}$ cells despite HU treatment, which blocks RNR and prevents *de novo* dNTP synthesis. Blocking RNR prevented cells to cycle but did not kill WT or *Samhd1*$^{-/-}$ cells within 24 hours. This suggests

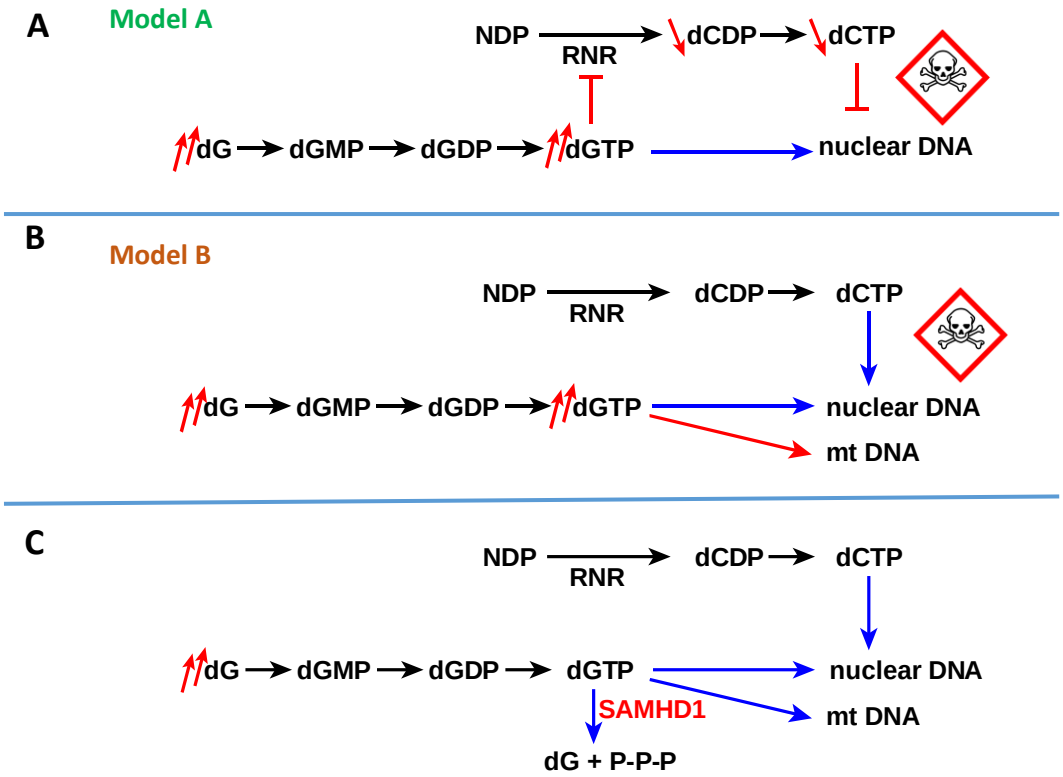


Figure 3.11 Models of dGTP toxicity in PNP-deficient cells. *(A)* ***Model A****, according to (Chan, 1978). Red arrows indicate consequences of dG accumulation. dG is converted into dGTP, which allosterically regulates ribonuclease reductase (RNR). Binding of dGTP to RNR leads to a block of de novo dNTP synthesis, with dCTP pool depletion and subsequent toxicity. (B)* ***Model B*** *of dGTP toxicity according to (Arpaia et al., 2000) where dGTP accumulates in mitochondria, where dGK is located, and causes toxicity and cell death. (C) SAMHD1 prevents dGTP accumulation in PNP-deficient cells and therefore protect cells from dGTP-induced cell death.*

that dNTP starvation through HU block of RNR is not sufficient to induce cell death in 24h. This is against **Model A** which proposes a mechanism of toxicity through dCTP starvation (**Figure 3.11A**). On the other hand, dG toxicity was reduced when combined with dC, suggesting that increased levels of dCTP limits toxicity, perhaps by preventing dCTP starvation. However, blocking *de novo* dNTP synthesis through RNR had no effect on dG-induced toxicity, suggesting that dGTP excess does not cause toxicity through the RNR feedback loop and subsequent dNTP starvation. This is supported by dNTP quantifications which do not show significant increase of dCTP pool 4h post-dG treatment. It will be

interesting to confirm this observation at later time points. In **Model A**, dGTP feeds back on RNR leading to G0/G1 cell cycle arrest and the toxicity is increased in G0/G1 since dGTP cannot be used for DNA synthesis, as it would be in S-Phase (Duan et al., 1990). Altogether, dGTP-induced cell death in SAMHD1-deficient cells supports **Model B** in which dGTP accumulates in mitochondria to cause inhibition of mtDNA repair, mtDNA damage and cell death (**Figure 3.11B**).

Nevertheless, further work is needed to demonstrate dGTP toxicity in the mitochondria. Technical limitations prevented the quantification of dNTP levels in mitochondria (dNTP quantifications were performed by our collaborators and samples were prepared according to their set protocol). It is challenging to measure increased dGTP within the mitochondria and to demonstrate cytotoxicity. Some assays can measure copy numbers of mitochondrial genome (mtDNA) by qPCR, but the toxicity observed is so quick that this may not be an appropriate technique. PCR amplification of mtDNA could give a different profile on an agarose gel, with smears showing up if mtDNA is damaged and thus of different lengths. Evaluating dG toxicity in SAMHD1-deficient cells that lack mtDNA could determine whether mtDNA is required for dGTP toxicity. Such cell lines can be generated by passaging cell lines in ethidium bromide, leading to the loss of their mtDNA (Khozhukhar et al., 2018). These are interesting questions that remained to be addressed. However, this was not investigated further due to time constraints. Focus was made on two other interesting observations instead, detailed in the next results chapters.

Finally, the type of cell death caused by dGTP accumulation was investigated. It was clear that SAMHD1-deficient cells accumulating dGTP died by apoptosis. Apoptosis is a form of programmed cell death characterised by caspase cleavage and formation of apoptotic bodies. Release of cytochrome C in the cytosol confirmed permeabilisation of the mitochondrial membrane. Extrinsic apoptosis can be triggered by binding of a molecule to its death receptor (Tait and Green, 2010). Co-culture experiments suggested that no soluble factor was secreted to trigger programmed cell death of neighbouring cells. Secretion of cytokines and their impact on dG-induced cell death will be further investigated in the next

chapter. Therefore, the data point toward intrinsic apoptosis where danger signals lead to activation of BH3-only proteins that release BAX and BAK, forming pores in the mitochondria. Triggers of intrinsic apoptosis upstream of cytochrome C release have not been investigated. BAX and BAK oligomerisation can be detected technically, but it is challenging to determine whether activation of BH3-only proteins or activation of a death receptor caused it. Crossing our *Samhd1*$^{-/-}$ mice with *BAX*$^{-/-}$ or *BAK*$^{-/-}$ mice, to obtain double mutant could determine if these BMDMs are susceptible do dG-induced cell death, and determine whether BAX and BAK oligomerisation is required. In intrinsic apoptosis, a danger molecule activates BH3-only proteins to induce formation of pores in the mitochondria. It is possible that accumulation of dGTP acts as a danger molecule directly, or that it induces mtDNA damage that can then be sensed to activate BH3-only proteins. In senescent cells, mtDNA damage accumulate and trigger caspase-dependent apoptosis (Laberge et al., 2013). Recently, it has also be shown that pore formation triggers the release of mtDNA that acts as a DAMP, and triggers the production of type I IFN (McArthur et al., 2018). High resolution microscopy could determine whether release of mtDNA occurs when dGTP accumulates and establish whether it is a cause or a consequence of mitochondrial outer membrane permeabilisation. Using cells lacking mitochondria could help to determine if the mitochondrial compartment is required to generate DAMPs upon dGTP accumulation (Ferraresi et al., 2008). However, such cells have been shown to be less susceptible to apoptosis. Therefore, it would be difficult to determine whether reduced cell death is due to their reduced ability to induce apoptosis or because dGTP causes toxicity in the mitochondrial compartment. Several questions remained unanswered and it will be interesting to determine whether dGTP accumulation indirectly triggers intrinsic apoptosis through damage and exposure of mtDNA that then acts as a DAMP to trigger apoptosis.

3.7 Conclusion

Altogether, this chapter demonstrated that SAMHD1 protects cells from dG excess, preventing dGTP overload and intrinsic apoptosis. The mechanism of dGTP toxicity remains unclear. dGTP toxicity was independent of cell replication and genomic DNA synthesis, suggesting that it may act in the mitochondrial compartment. Whether dGTP acts directly as a DAMP or induces damage in the mitochondria that triggers mtDNA release and sensing to induce intrinsic apoptosis, remain to be determined. This unveils a new important role for SAMHD1 in safeguarding cells. SAMHD1 deals with dNTP imbalances and excess to prevent their accumulation and the trigger of intrinsic apoptosis. I established a model in which SAMHD1 is at the crossroads of nucleotide metabolism and cell death (**Figure 3.12**).

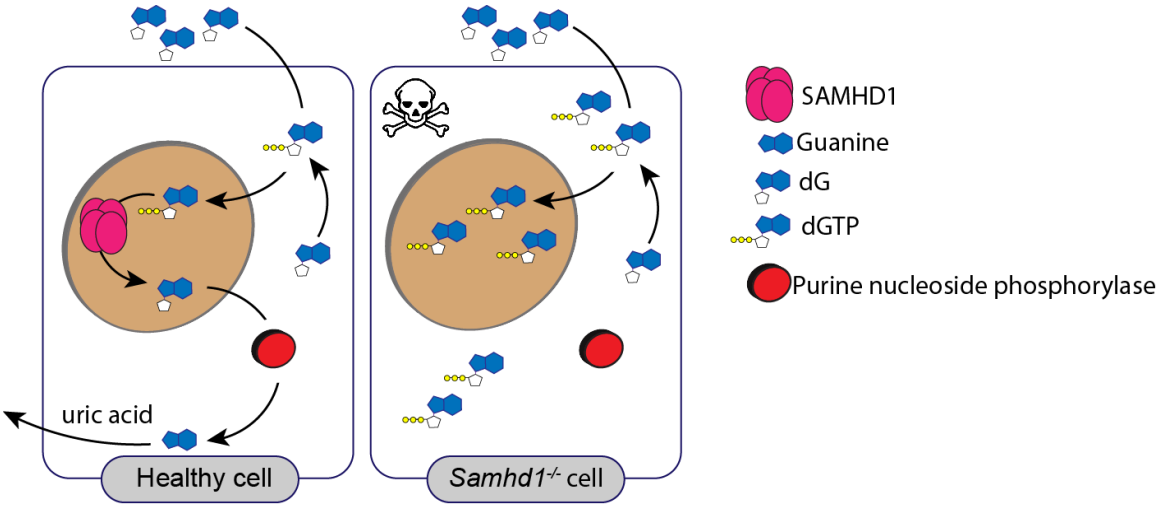


Figure 3.12 SAMHD1 protects cells against dNTP overload. *dG is added to cells, transported in the cytoplasm and converted into dGTP through the nucleotide salvage pathway. In cells lacking SAMHD1 dGTP cannot be degraded, leading to its accumulation, which triggers cell death by intrinsic apoptosis.*

Chapter 4. DEOXYGUANOSINE INDUCES A TLR7-DEPENDENT CYTOKINE RESPONSE

In Chapter 3, I showed that deoxyribonucleosides (dA, dC, dG and dT) are toxic in cells lacking SAMHD1. The highest toxicity was observed with dG, which was phosphorylated through the salvage pathway to form dGTP and accumulated in *Samhd1*$^{-/-}$ cells. The accumulation of dGTP in cells triggered intrinsic apoptosis with the release of cytochrome C into the cytosol and subsequent cleavage of PARP and caspase 3. This was a very consistent and reproducible observation made in different mouse and human cells.

To determine whether dGTP dependent cell death could be rescued by blockade of apoptosis, I used caspase inhibitors. Interestingly, both *Samhd1*$^{-/-}$ as well as WT BMDMs died when pre-treated with the pan-caspase inhibitor z-VAD, followed by dG treatment. Subsequent experiments showed that WT cells were undergoing TNFα-induced necroptosis. BMDMs secreted TNFα upon dG treatment as well as other cytokines. Gene expression analysis confirmed the induction of pro-inflammatory pathways upon dG sensing through TLR7 and MyD88. This chapter describes the investigation of dG-induced cytokine production and its impact on dG-induced cell death in *Samhd1*$^{-/-}$ cells.

4.1 BMDMs produce cytokines upon dG treatment

To test if dG-induced apoptosis of *Samhd1*$^{-/-}$ cells could be prevented, a mini screen of cell death inhibitors was performed in *Samhd1*$^{-/-}$ BMDMs. The pan caspase inhibitor zVAD, RIPK3 inhibitor GSK872, and caspase 2 inhibitor z-DVAD had no effect (**Figure 4.1A**). In contrast, caspase 8 inhibitor z-IEDT, caspase 9 inhibitor z-LEHD and caspase 3 inhibitor DEVD-CHO showed a small but significant increase in viability when used in combination with dG in *Samhd1*$^{-/-}$ BMDMs. However, a clear and complete rescue of dG treated *Samhd1*$^{-/-}$ cells using these inhibitors was not observed over multiple experimental repeats. This is discussed in more detail at the end of this chapter.

To compare the effect of zVAD and dG, the experiment was performed in WT and *Samhd1*$^{-/-}$ BMDMs. The cells were treated with the pan-caspase inhibitor zVAD prior to dG treatment and viability was measured (**Figure 4.1B**). Surprisingly, zVAD did not rescue *Samhd1*$^{-/-}$ cells

from dG-induced apoptosis but zVAD combined with dG triggered the death of WT cells. It has previously been reported that a combination of zVAD and TNFα induces necroptosis (Wu et al., 2011). This is a programmed form of cell death by necrosis which is driven by phosphorylation of MLKL by RIPK3. To determine whether the combination of dG and zVAD induces necroptosis of WT cells, we tested whether the RIPK3 inhibitor GSK872 could prevent the death of these cells. GSK872 significantly increased viability of WT cells treated with zVAD and dG (**Figure 4.1B**). Furthermore, pMLKL was detected by western blot in WT cells upon zVAD and dG treatment which was blocked by GSK872 (**Figure 4.1B**). Overall this strongly suggests that zVAD and dG induce necroptosis in WT cells. It also raises the possibility that TNFα is produced in response to dG, which can then combine with zVAD to induce necroptosis (Wu et al., 2011). In contrast with WT cells, pMLKL was not detected in *Samhd1*$^{-/-}$ cells (**Figure 4.1C**) meaning cell death was still occurring but not by necroptosis. Upon dG treatment and caspase blockade with zVAD, RIPK3 phosphorylate MLKL to induce necroptosis.

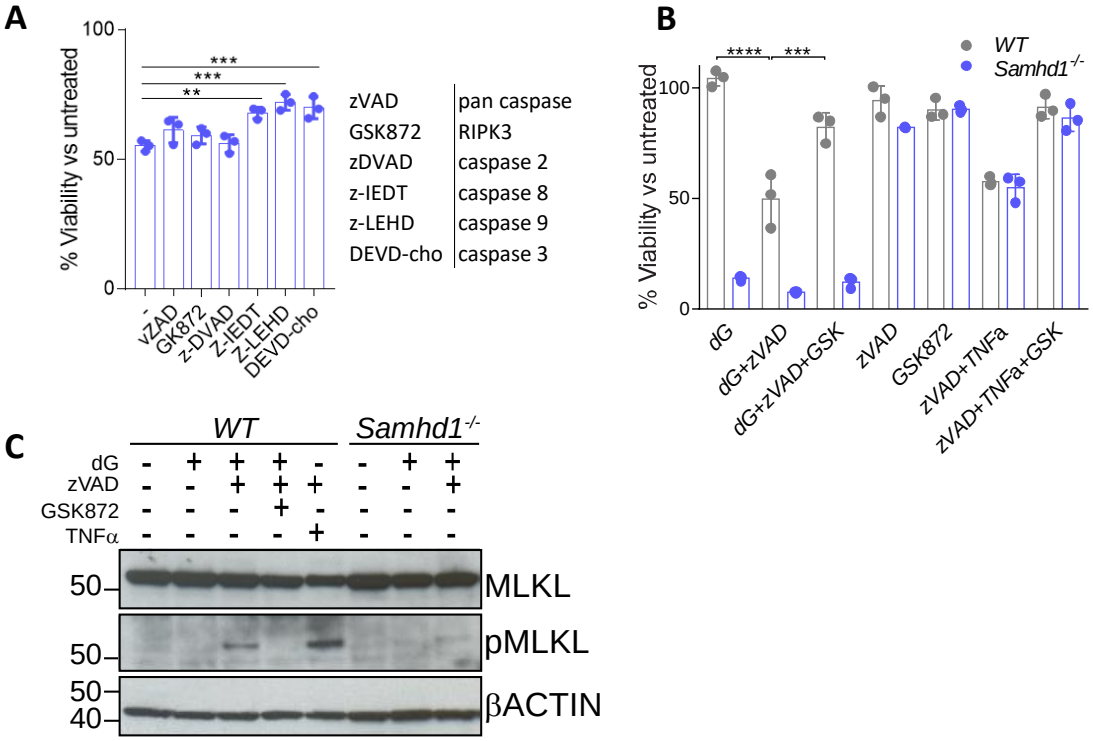


Figure 4.1 z-VAD induces death of dG treated cells. *(A) Viability (CellTiter-Glo) of Samhd1*$^{-/-}$ *BMDMs pre-treated as indicated on the X-axis for 1h with 25 μM zVAD, 10 μM GSK872, 30 μM z-DVAD, 30 μM z-IEDT, 20 μM z-LEHD or 20 μM DEVD-CHO and treated with 0.5 mM dG for 24h. (B) Viability (CellTiter-Glo) 24h post-treatment. Cells were treated with 25 μM zVAD for 2h prior to treatment with 0.5 mM dG. 25 μM zVAD+ 100 ng/ml TNFα was used as a positive control. Bars are mean of triplicates ± SD (C) Western blot of MLKL and phospho-MLKL in BMDMs pre-treated with 25 μM zVAD, 25 μM GSK872 for 1h and treated with 0.5 mM dG for 7h or treated with 25 μM zVAD for 4h and 100 ng/ml TNFα for 4h. (B-C) are representative of 3 independent experiments.*

To determine whether TNFα-induced necroptosis was occurring upon dG treatment, TNFα was measured by ELISA in the supernatant of dG-treated BMDMs (**Figure 4.2**). Both WT and *Samhd1*$^{-/-}$ BMDMs were secreting TNFα as early as 60 min post-dG treatment, and levels increased over time. Interestingly, *Samhd1*$^{-/-}$ cells seemed to produce less TNFα in this early phase.

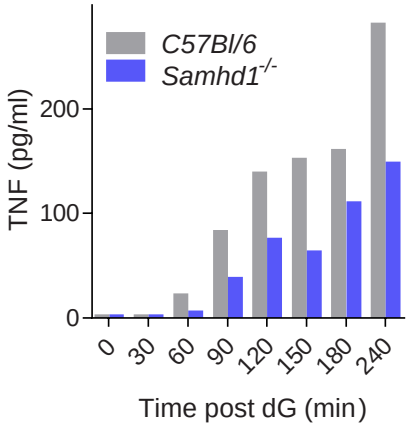


***Figure 4.2 dG-induced TNFα production in WT and Samhd1-/- BMDMs**. TNFα ELISA on supernatant from BMDMs treated with 0.5 mM dG and collected at indicated time points. Bars represent average of technical duplicates. Representative of 2 independent experiments*

4.2 TNFα production upon dG treatment is not caused by endotoxins

These results suggested that BMDMs were producing TNFα upon dG sensing. TNFα is an inflammatory cytokine that can be produced in response to endotoxins. Endotoxins are small molecules derived from bacteria, including lipopolysaccharide (LPS), which can signal through TLR4 and induce cytokine production (Erridge, 2010). It is not uncommon to have traces of endotoxins in reagents, depending on the manufacturing protocols. Therefore, it was important to confirm that TNFα secretion was not due to endotoxin contamination in the compound used. First, the experiment was performed in the presence of polymyxin B (PMB), a compound known to neutralize LPS contamination (Cardoso et al., 2007; Tsuzuki et al., 2001). Second, dG was purchased from a second supplier (MedChem) to compare with the one used so far (SIGMA). A similar decrease in viability of *Samhd1*$^{-/-}$ BMDMs was observed upon treatment with dG from SIGMA or MedChem (**Figure 4.3A**). The supernatant (24h) from these cells was used for TNFα bioassay (HEK-Blue™ TNF-α Cells from Invivogen), where higher absorbance correlates with more TNFα present in the supernatant. PMB reduced the amount of TNFα induced by dG from SIGMA but not from MedChem in both WT and *Samhd1*$^{-/-}$ BMDMs (**Figure 4.3B**). This observation was confirmed by quantifying TNFα present in the supernatant 24h post-dG treatment by ELISA.

PMB was able to almost completely prevent the induction of TNFα by LPS (**Figure 4.3C**). Both compounds were sent to an independent laboratory (Lonza, Belgium) for endotoxin testing and results confirmed that dG from MedChem did not have detectable endotoxin levels whereas dG from SIGMA showed presence of endotoxins (data not shown). Overall this suggested that the observed induction of TNFα production following treatment with dG from MedChem resulted exclusively from a direct dG effect. In contrast, TNFα induction by dG from SIGMA was the result of a combination of dG and contaminating LPS. The compound from SIGMA was discarded and further experiments in this thesis were carried out using dG from MedChem.

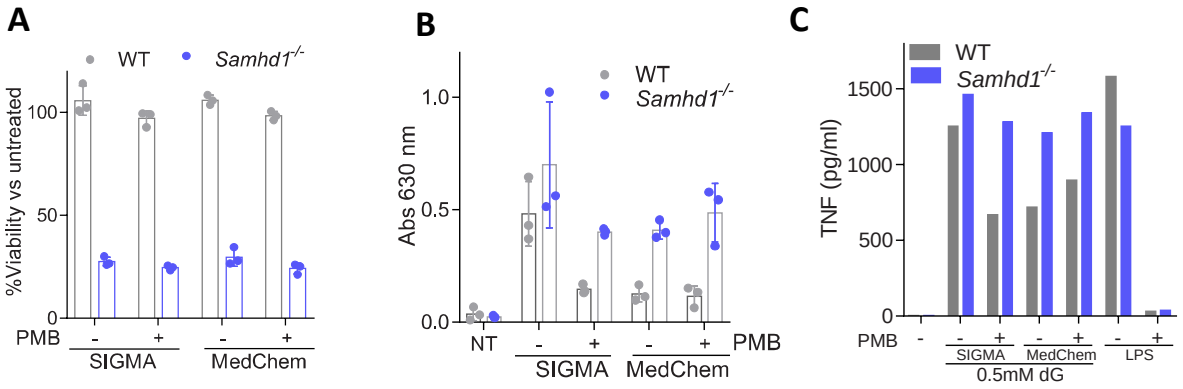


Figure 4.3 dG from Medchem is endotoxin free. *(A) Viability (CellTiter-Glo) of BMDMs treated with 0.5 mM dG from SIGMA or MedChem Polymyxin B was used at 25 μM at the same time than dG treatment. (B) TNFα bioassay on 24h supernatant from (A). The absorbance correlates with the presence of TNFα in the supernatant. (C) TNFα ELISA on supernatant from BMDMs treated with 0.5 mM dG for 24h with or without 25 μM polymyxin B (PMB). (A-B) Dots represent cells from individual mice, bars are means ±SD. (C) Bars represent average of technical duplicates. (A-C) are representative of 3 independent experiments.*

These results raised several important questions:

- What receptor is sensing dG and subsequently triggering TNFα production?
- Are other genes, apart from TNFα, induced upon dG treatment?
- What is the contribution of dG-induced TNFα to cell death or survival?

4.3 TNFα is induced by dG treatment independently of TLR4

In order to further confirm the ability of dG to induce the production of TNFα, the experiment was performed in *Trif*$^{-/-}$ and *Tlr4*$^{-/-}$ BMDMs. TRIF is an adaptor protein downstream of TLR3 and TLR4, and TLR4 is the endotoxins sensor. Therefore, *Trif*$^{-/-}$ and *Tlr4*$^{-/-}$ BMDMs allowed us to confirm that TNFα production was independent of these signalling pathways. Viability of *Trif*$^{-/-}$ and *Tlr4*$^{-/-}$ BMDMs upon dG treatment was similar to WT cells (**Figure 4.4A**). Both *Trif*$^{-/-}$ and *Tlr4*$^{-/-}$ BMDMs were producing TNFα upon dG treatment at levels comparable with WT cells (**Figure 4.4B**), showing that TNFα production was independent of TLR4 and TRIF (**Figure 4.4B**). Importantly, it further confirmed that TNFα production upon treatment with dG from MedChem is not due to endotoxin contamination.

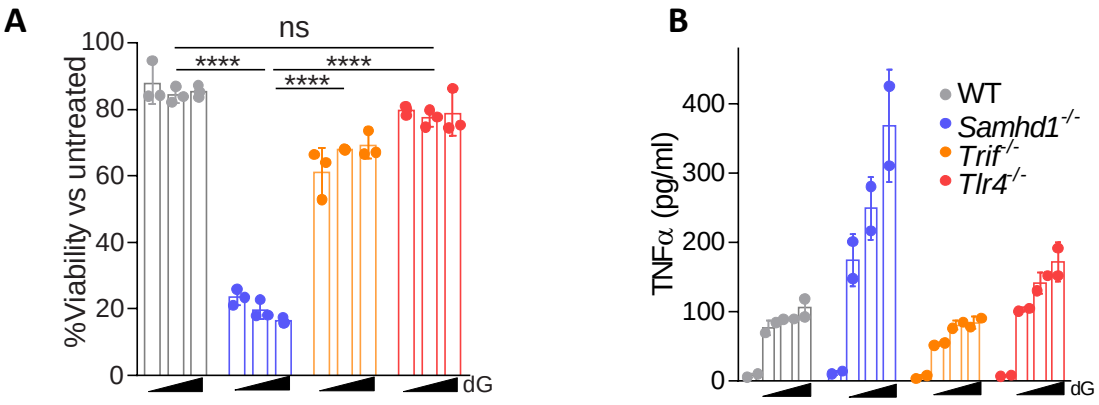


Figure 4.4 dG-induced TNFα production is TRIF and TLR4 independent. *(A) Viability (CellTiter-Glo) of BMDMs 24h post treatment with 0.5 mM dG. Dots are individual wells, bars are mean ± SD, two-way ANOVA (****p<0.0001). (B) TNF ELISA on 24h supernatant from (A). Dots represent average of technical duplicates, bars are mean ± SD.*

Next, I wanted to determine whether dG sensing and signalling was TLR dependent. TLR3 and TLR4 use the adaptor protein TRIF whilst other TLRs use MyD88. Therefore, the experiment was performed in *MyD88*$^{-/-}$, *Trif*$^{-/-}$ and *Trif*$^{-/-}$*MyD88*$^{-/-}$ BMDMs. In addition, *Ifnar*$^{-/-}$ BMDMs were used to check whether type I IFN is required for the cytokine response. Cells were treated with dG and RNA was extracted 3 h post-treatment to measure cytokine expression by qRT-PCR (**Figure 4.5A**). mRNA levels of cytokines *Tnfα* and *Ifnβ* were elevated as well as mRNA levels of IFN stimulated genes (ISGs) *Ifit1* and *Cxcl19* upon dG treatment. This showed that dG induced the production of both cytokines and ISGs. In

contrast, there was no induction of *Tnfα* and *Ifnβ* in *MyD88*$^{-/-}$ and *Trif*$^{-/-}$*MyD88*$^{-/-}$ BMDMs, suggesting that the dG sensor was signalling through the MyD88 adaptor protein. Interestingly, the absence of cytokines post-dG treatment did not hinder survival of these cells (**Figure 4.5B**). The absence of TNFα secretion in *MyD88*$^{-/-}$BMDMs upon dG treatment was confirmed by ELISA (**Figure 4.5C**), with no detectable levels of TNFα observed in the supernatant of *MyD88*$^{-/-}$ and *Trif*$^{-/-}$*MyD88*$^{-/-}$BMDMs upon treatment with dG.

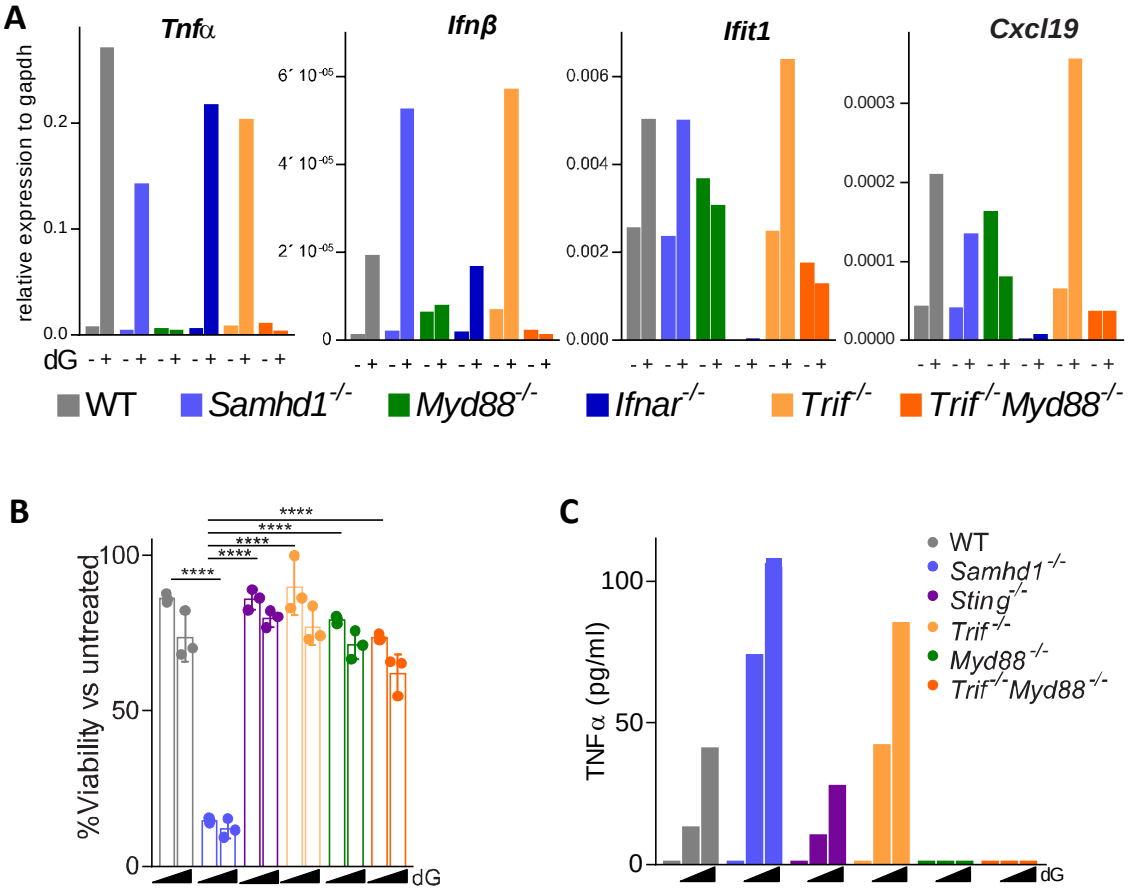


Figure 4.5 dG-induced cytokine production is MyD88 dependent. *(A) BMDMs of the indicated genotypes were treated with 0.5 mM dG for 3 hours. RNA was extracted for RT-qPCR analysis of the indicated mRNAs. Data are relative to Gapdh. (B) BMDMs of the indicated genotypes were treated with dG for 24 hours. Wedges indicate 0.5 or 1 mM dG. P-values determined with two-way ANOVA are indicated. (C) TNFα concentrations were determined as in (B). (A and C) Data from technical duplicates were averaged. (B) Data from triplicate measurements are shown with mean ± SD*

4.4 dG induces a pro-inflammatory response through MyD88

4.4.1 Microarray

To further characterise the response induced by dG sensing in BMDMs, gene expression analysis was performed. DNA microarrays measure expression levels of over 20,000 annotated genes by detecting hybridisation of specific probes to the cDNA of interest. Since the previous section showed a dependency of MyD88 for dG signalling, *MyD88*$^{-/-}$ BMDMs were used as a negative control. In addition to WT and *Samhd1*$^{-/-}$ BMDMs, the experiment was also performed in *Ifnar*$^{-/-}$ cells to determine whether the response observed was dependent on type I IFN signalling.

BMDMs were treated with dG for 3 h, RNA was extracted and reverse transcribed into cDNA before being used for microarray. Transcript expressions that went up or down more than two fold upon dG treatment are shown in a heat map, with each column representing one mouse (**Figure 4.6A**). In total, 538 genes were up or downregulated upon treatment with dG in both WT and *Samhd1*$^{-/-}$ BMDMs. The heat map, representing transcript expression, shows that WT and *Samhd1*$^{-/-}$ BMDMs behaved similarly, with the same genes up or downregulated upon dG treatment. No changes in expression of these genes were observed in *MyD88*$^{-/-}$ BMDMs, supporting the previous observation that dG signalling is dependent on MyD88. *Ifnar*$^{-/-}$ BMDMs showed a similar profile to WT and *Samhd1*$^{-/-}$ cells with a lower amplitude. This suggested that either *Ifnar*$^{-/-}$ cells were less potent at signalling upon dG sensing or that WT or *Samhd1*$^{-/-}$ cells were primed and therefore show a stronger response upon dG treatment.

The 40 most upregulated genes upon treatment in WT and *Samhd1*$^{-/-}$ are shown in **Figure 4.6B**. Very similar gene expression profiles were observed between WT and *Samhd1*$^{-/-}$ BMDMs upon dG treatment. It was interesting to see that many genes of the pro-inflammatory pathways were among the most upregulated genes. In this top 40, few genes were differentially expressed between WT and *Samhd1*$^{-/-}$ cells (**Table 4.1**). These genes, highlighted in bold **Figure 4.6B,** were differentially expressed upon dG treatment in *Samhd1*$^{-/-}$ compared with WT. They encode proteins involved in various processes, their

names, UniProtKB number (used to collect information on these proteins) and function are summarised in **Table 4.1**.

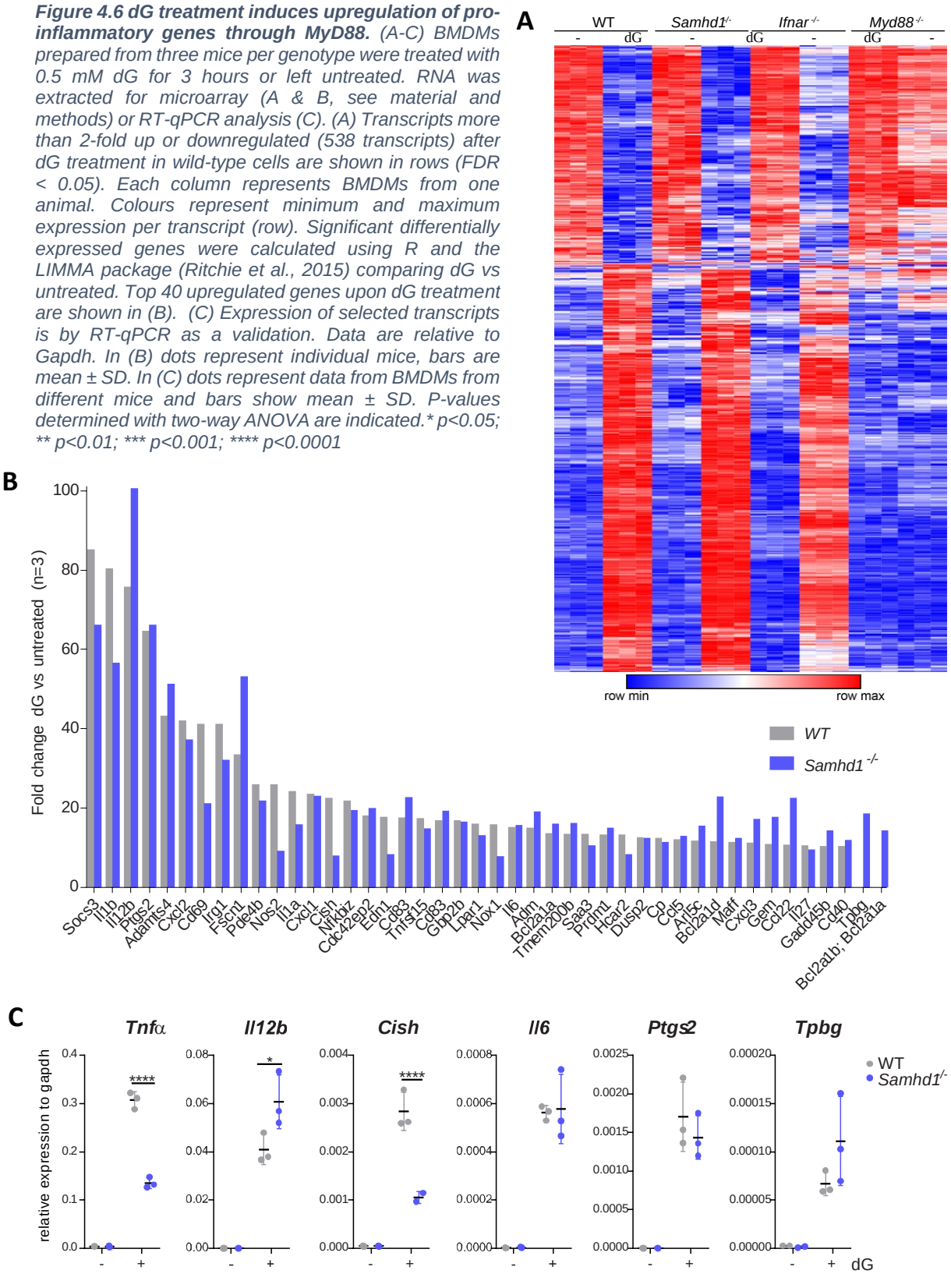


Figure 4.6 dG treatment induces upregulation of pro-inflammatory genes through MyD88. *(A-C) BMDMs prepared from three mice per genotype were treated with 0.5 mM dG for 3 hours or left untreated. RNA was extracted for microarray (A & B, see material and methods) or RT-qPCR analysis (C). (A) Transcripts more than 2-fold up or downregulated (538 transcripts) after dG treatment in wild-type cells are shown in rows (FDR < 0.05). Each column represents BMDMs from one animal. Colours represent minimum and maximum expression per transcript (row). Significant differentially expressed genes were calculated using R and the LIMMA package (Ritchie et al., 2015) comparing dG vs untreated. Top 40 upregulated genes upon dG treatment are shown in (B). (C) Expression of selected transcripts is by RT-qPCR as a validation. Data are relative to Gapdh. In (B) dots represent individual mice, bars are mean ± SD. In (C) dots represent data from BMDMs from different mice and bars show mean ± SD. P-values determined with two-way ANOVA are indicated.* p<0.05; ** p<0.01; *** p<0.001; **** p<0.0001*

Table 4.1 Characteristics of differently expressed genes in WT and Samhd1$^{-/-}$ upon dG treatment

Name	Full name	UniProtKB	Function of the protein encoded
Cd69	Early activation antigen CD69	P37217	receptor expressed at the surface of activated haematopoietic cells
Fscn1	Dascin	Q61553	protein involved in the organization of actin filament bundles and the formation of micro spikes, membrane ruffles, and stress fibres. Also involved in formation ofprotrusions, such as filopodia, and for cell motility and migration
Cish	Cytokine-inducible SH2-containing protein	Q6225	protein of the SOCS family, known to be part of a negative feedback loop of the JAK-STAT signalling pathway, which regulate the immune response
Nos2	nitrite oxide synthase 2	P29477	produces nitrite oxide which is a messenger molecule involve in several process, including tumoricidal and bactericidal actions in macrophages
Saa3	serum amyloid A-3 protein	P04918	encodes a secreted protein which is part of the acute-phase response and acts as a chemoattractant
Il1a	interleukin-1	P01538	encodes IL-1α, a cytokines produced during the inflammatory response by activated macrophages that stimulates thymocyte proliferation through the release of IL-2
Hcar2	hydroxycarboxylic acid receptor 2	Q9EP66	protein which acts as a high affinity receptor for both nicotinic acid and (D)-beta-hydroxybutyrate. HCAR2 can bind GTP, it has a purinergic nucleotide receptor activity and it is a positively regulator neutrophil apoptosis
Ccl22	C-C motif chemokine 22	O88430	chemokine for activated T-lymphocytes that may play an important role in the collaboration of dendritic cells and B-lymphocytes with T-cells in immune responses
Bcl2a1d	A1-d protein	O55179	protein which is a positive regulator of apoptosis involved in several biological processes: release of cytochrome C from mitochondria, mitochondrial fusion, and intrinsic apoptotic signalling pathway in response to DNA damage and extrinsic
Nox1	NADPH oxidase 1	Q8CIZ9	encodes NADPH oxidase 1, a pyridine nucleotide-dependent oxidoreductase that generates superoxide and might conduct H+ ions as part of its electron transport mechanism
Bcl21a	BCL-2 related protein A1	Q07440	negative regulator of apoptotic process by interacting directly with BIM and BID

To validate the microarray results, several of these genes (**Figure 4.6A**) were selected for RT-qPCR. *Socs3 and Ptgs2* showed no significant difference between WT and *Samhd1*$^{-/-}$ BMDMs, in line with the microarray results (**Figure 4.6C**). There was a trend towards increased expression of *Nos2* in WT compared with *Samhd1*$^{-/-}$ BMDMs, which did not reach statistical significance. Higher levels of *Cish* in WT were also supported by the RT-qPCR results. Interestingly, *Tnfα* levels were significantly lower in *Samhd1*$^{-/-}$ cells as measured by RT-qPCR but this was not detected by the microarray. Overall, the RT-qPCR on selected target genes showed similar results as observed by the microarray analysis. This validated the gene expression analysis and therefore confirmed the genes differentially expressed upon dG treatment between WT and *Samhd1*$^{-/-}$ cells.

4.4.2 Gene clustering and pathway analysis

To further investigate the cellular pathways induced upon dG treatment, functional annotation clustering was performed on the gene set shown in **Figure 4.6A** (list of 538 genes). The Database for Annotation, Visualization and Integrated Discovery (DAVID) was

used to perform the analysis (https://david.ncifcrf.gov/). On a given gene set, DAVID is able to identify enriched biological themes and discover enriched functionally-related gene groups.

Functional annotation clustering analysis was performed and the top 20 most enriched clusters are summarised in **Table 4.2**. Among the most enriched relevant pathways were the innate immune system (cluster 1), the TLR pathway and associated pathogens (cluster 2), the transcription regulators (cluster 3, 4 & 5), the inflammatory response with cytokines and chemokines (cluster 6 & 7), the zinc finger proteins, the NF-κB pathway (cluster 13) and the apoptotic pathway (cluster 18). This analysis highlighted the important pathways induced upon exposure to dG. Since most of the pathways activated upon dG treatment were inflammatory, this was consistent with a role for MyD88 in dG sensing as previously observed.

Finally, to support these results, another online tool was used to look at pathway analysis. Reactome, an open-source peer-reviewed pathway data base, was used to have a visual overview (https://reactome.org/). Using the same gene set, it provides a different tool to confirm the enriched gene clusters identified with DAVID, and produces a complete interactive map of the pathways involved. The different pathways are represented in yellow when several genes are significantly present in a pathway (**Figure 4.7**). The most activated pathway was the immune system followed by signal transduction pathway, in agreement with previous findings. To a lesser extent, specific branches of some pathways were also activated such as programmed cell death, cell cycle, disease, transport of molecules, metabolism of proteins and DNA repair.

Table 4.2 Functional annotation clustering of the gene set in Figure 4.6A (https://david.ncifcrf.gov)

Annotation Cluster 1	Enrichment Score: 8.12	Count	p value	Benjamini
	Immunity	36	2.60E-11	1.70E-09
	Innate immune response	31	2.30E-07	3.30E-05
Annotation Cluster 2	Enrichment Score: 6.14			
	Toll-like receptor signaling pathway	19	1.40E-09	6.80E-08
	Leishmaniasis	15	6.10E-09	2.50E-07
	Chagas disease (American trypanosomiasis)	17	8.80E-08	2.00E-06
	Tuberculosis	22	9.60E-08	1.90E-06
	Influenza A	21	2.70E-07	3.90E-06
	Pertussis	14	3.40E-07	4.00E-06
	Inflammatory bowel disease (IBD)	12	1.50E-06	1.60E-05
	Herpes simplex infection	22	1.60E-06	1.50E-05
	Cytosolic DNA-sensing pathway	9	7.40E-04	4.40E-03
	Amoebiasis	11	3.30E-03	1.60E-02
Annotation Cluster 3	Enrichment Score: 5.96			
	domain:Leucine-zipper	19	5.10E-10	6.40E-07
	RNA polymerase II core promoter proximal region sequence-specific DNA binding	31	2.90E-08	6.10E-06
	Transcriptional activator activity, RNA polymerase II core promoter proximal region	21	3.50E-05	3.20E-03
	Transcription factor activity, sequence-specific DNA binding	45	4.10E-05	3.30E-03
	sequence-specific DNA binding	35	7.70E-05	5.40E-03
Annotation Cluster 4	Enrichment Score: 5.19			
	domain:Leucine-zipper	19	5.10E-10	6.40E-07
	DNA-binding region:Basic motif	17	4.40E-06	2.70E-03
	Eukaryotic transcription factor, Skn-1-like, DNA-binding	4	7.80E-03	2.00E-01
Annotation Cluster 5	Enrichment Score: 4.99			
	negative regulation of transcription from RNA polymerase II promoter	46	7.90E-08	1.60E-05
	DNA binding	85	4.30E-07	6.80E-05
	Repressor	32	3.70E-06	8.90E-05
	Nucleus	148	9.10E-06	2.00E-04
	Activator	34	1.30E-05	2.40E-04
	Transcription	73	1.50E-05	2.70E-04
	transcription factor activity, sequence-specific DNA binding	45	4.10E-05	3.30E-03
Annotation Cluster 6	Enrichment Score: 4.77			
	Inflammatory response	25	5.30E-13	7.00E-11
	Cytokine	25	5.90E-11	3.20E-09
	Immune response	28	2.90E-09	9.40E-07
	Cellular response to interferon-gamma	13	1.60E-07	2.70E-05
	Chemotaxis	13	2.00E-06	5.20E-05
	Chemokine interleukin-8-like domain	10	3.20E-06	8.80E-04
	Chemokine signaling pathway	18	1.10E-04	7.60E-04
	Negative regulation by host of viral transcription	5	1.90E-04	8.60E-03
	Positive regulation of natural killer cell chemotaxis	4	3.30E-04	1.40E-02
Annotation Cluster 7	Enrichment Score: 4.15			
	Cytokine	25	5.90E-11	3.20E-09
	Immune response	28	2.90E-09	9.40E-07
	Cytokine-cytokine receptor interaction	26	1.20E-07	2.30E-06
	Cytokines and Inflammatory Response	9	2.50E-04	2.00E-02
	Extracellular space	51	2.70E-02	3.30E-01
	Secreted	47	1.50E-01	5.00E-01
	Signal	89	9.80E-01	1.00E+00
Annotation Cluster 8	Enrichment Score: 3.34			
	Zinc-finger	63	3.30E-05	5.20E-04
	Zinc	76	1.40E-04	2.00E-03
	Metal-binding	107	9.60E-04	1.20E-02
Annotation Cluster 9	Enrichment Score: 3.22			
	Death-like domain	14	2.70E-07	2.20E-04
	Death domain	5	8.40E-03	2.10E-01
Annotation Cluster 10	Enrichment Score: 3.16			
	Defense response to protozoan	11	2.50E-09	9.10E-07
	Adhesion of symbiont to host	5	5.20E-05	2.80E-03
	Defense response to Gram-positive bacterium	10	7.10E-04	2.50E-02
	Symbiont-containing vacuole membrane	4	8.10E-04	5.60E-02
	Guanylate-binding protein, C-terminal	4	4.40E-03	1.40E-01
	Cellular response to interferon-beta	4	9.10E-02	7.20E-01
	GTPase activity	8	3.20E-01	9.20E-01
Annotation Cluster 11	Enrichment Score: 3.1			
	Positive regulation of tumor necrosis factor production	9	1.40E-04	6.60E-03
	Positive regulation of xenophagy	4	5.70E-04	2.10E-02
	Cellular response to peptidoglycan	3	6.40E-03	1.40E-01
Annotation Cluster 12	Enrichment Score: 3.04			
	Caspase Recruitment	7	2.60E-05	4.30E-03
	cellular response to muramyl dipeptide	4	1.70E-04	7.90E-03
	positive regulation of JNK cascade	9	4.60E-04	1.80E-02
	positive regulation of xenophagy	4	5.70E-04	2.10E-02
	positive regulation of stress-activated MAPK cascade	5	1.60E-03	4.90E-02
	CARD domain binding	3	1.30E-02	2.20E-01
	positive regulation of monocyte chemotactic protein-1 production	3	2.20E-02	3.30E-01
Annotation Cluster 13	Enrichment Score: 3.02			
	I-kappaB kinase/NF-kappaB signaling	11	5.00E-09	1.30E-06
	NF-kappa-B/Rel/Dorsal	4	1.40E-04	1.50E-02
	Rel homology domain	4	1.60E-03	7.80E-02
	Immunoglobulin E-set	9	6.20E-03	1.70E-01
	domain:RHD	3	2.30E-02	7.10E-01
	Cell surface receptor IPT/TIG	4	3.70E-02	5.00E-01
	p53-like transcription factor, DNA-binding	4	9.40E-02	7.40E-01
Annotation Cluster 14	Enrichment Score: 2.98			
	SH2 domain	11	1.80E-04	2.30E-03
Annotation Cluster 15	Enrichment Score: 2.95			
	Caspase Recruitment	7	2.60E-05	4.30E-03
	domain:CARD	6	1.50E-04	6.00E-02
Annotation Cluster 16	Enrichment Score: 2.94			
	Extrinsic apoptotic signaling pathway in absence of ligand	10	1.10E-06	1.10E-04
	Intrinsic apoptotic signaling pathway in response to DNA damage	11	1.10E-06	1.20E-04
	release of cytochrome c from mitochondria	6	4.90E-04	1.90E-02
	Blc2 family	4	3.50E-03	1.30E-01
	Channel activity	4	4.30E-03	1.10E-01
	Mitochondrial fusion	4	1.20E-02	2.30E-01
	Mitochondrial outer membrane	10	1.60E-02	2.70E-01
	Apoptosis regulator, Bcl-2, BH2 motif, conserved site	3	1.90E-02	3.40E-01
	BH domain binding	3	3.30E-02	3.50E-01
Annotation Cluster 17	Enrichment Score: 2.77			
	positive regulation of interleukin-10 production	6	2.70E-04	1.10E-02
	positive regulation of interleukin-12 production	6	4.90E-04	1.90E-02
	negative regulation of interleukin-17 production	3	3.80E-02	4.60E-01
Annotation Cluster 18	Enrichment Score: 2.69			
	Mitogen-activated protein (MAP) kinase phosphatase	6	2.00E-06	8.40E-04
	Dual specificity phosphatase	7	9.40E-05	1.10E-02
	Rhodanese-like domain	6	2.60E-04	2.10E-02
	Dual specificity phosphatase, catalytic domain	7	4.10E-04	3.00E-02
Annotation Cluster 19	Enrichment Score: 2.54			
	Cytokines and Inflammatory Response	9	2.50E-04	2.00E-02
	IL-10 Anti-inflammatory Signaling Pathway	5	7.40E-03	1.30E-01
	Cytokine Network	6	1.30E-02	1.90E-01
Annotation Cluster 20	Enrichment Score: 2.47			
	Ankyrin repeat	15	1.90E-03	9.00E-02



Figure 4.7 Pathway analysis of the gene set in Figure 4.6A (https://reactome.org/)

4.5 dG-induced cytokine production is TLR7-dependent

It has previously been reported that TLR7 is able to bind guanosine, or dG in combination with poly U, an artificial form of RNA containing exclusively uracil repeats (Gentile et al., 2015; Shibata et al., 2015). This suggested that TLR7 may be sensing dG and triggering the production of cytokines. To test this hypothesis, *Tlr7*$^{-/-}$ BMDMs were treated with dG and assessed for viability and cytokine production. *Tlr7*$^{-/-}$ BMDMs showed slightly lower viability than WT cells upon dG treatment but significantly higher viability than *Samhd1*$^{-/-}$ cells (**Figure 4.8A**). *Tlr7*$^{-/-}$ BMDMs did not produce TNFα upon dG treatment while WT and *Samhd1*$^{-/-}$ cells did (**Figure 4.8B**). To confirm that *Tlr7*$^{-/-}$ cells were not able to respond to TLR7 stimuli, cells were treated with TLR7 ligand R837 (Lee et al., 2003). *Tlr7*$^{-/-}$ BMDMs did not produce TNFα upon stimulation with R837 and responded to the dsDNA poly I:C, a TLR3 ligand (Zhou et al., 2013b). dG-induced cytokine production was confirmed by RT-qPCR. WT and *Samhd1*$^{-/-}$ BMDMs showed increased levels of TNFα, IFNβ and IL6 post-dG treatment while there was no induction *Tlr7*$^{-/-}$ cells (**Figure 4.8C**). These experiments revealed that dG was signalling through TLR7 to induce production of cytokines and type I IFN.

To determine if cytokines and type I IFN were required to induce apoptosis of *Samhd1*$^{-/-}$ cells upon dG treatment, TLR7 signalling was blocked using the TLR7 antagonist ODN20958 (ODN). Viability of WT and *Samhd1*$^{-/-}$ BMDMs was measured post-treatment and showed similar levels whether or not ODN was used with dG treatment (**Figure 4.8D**). To confirm that ODN was efficiently blocking TLR7, a TNFα ELISA was performed on supernatants from these cells (**Figure 4.8E**). Blocking of TLR7 using ODN completely prevented TNFα production following administration of R837. However, ODN and dG treatment showed a low residual TNFα production. This suggested that partially reducing cytokines production did not affect dG-induced apoptosis in *Samhd1*$^{-/-}$ cells.

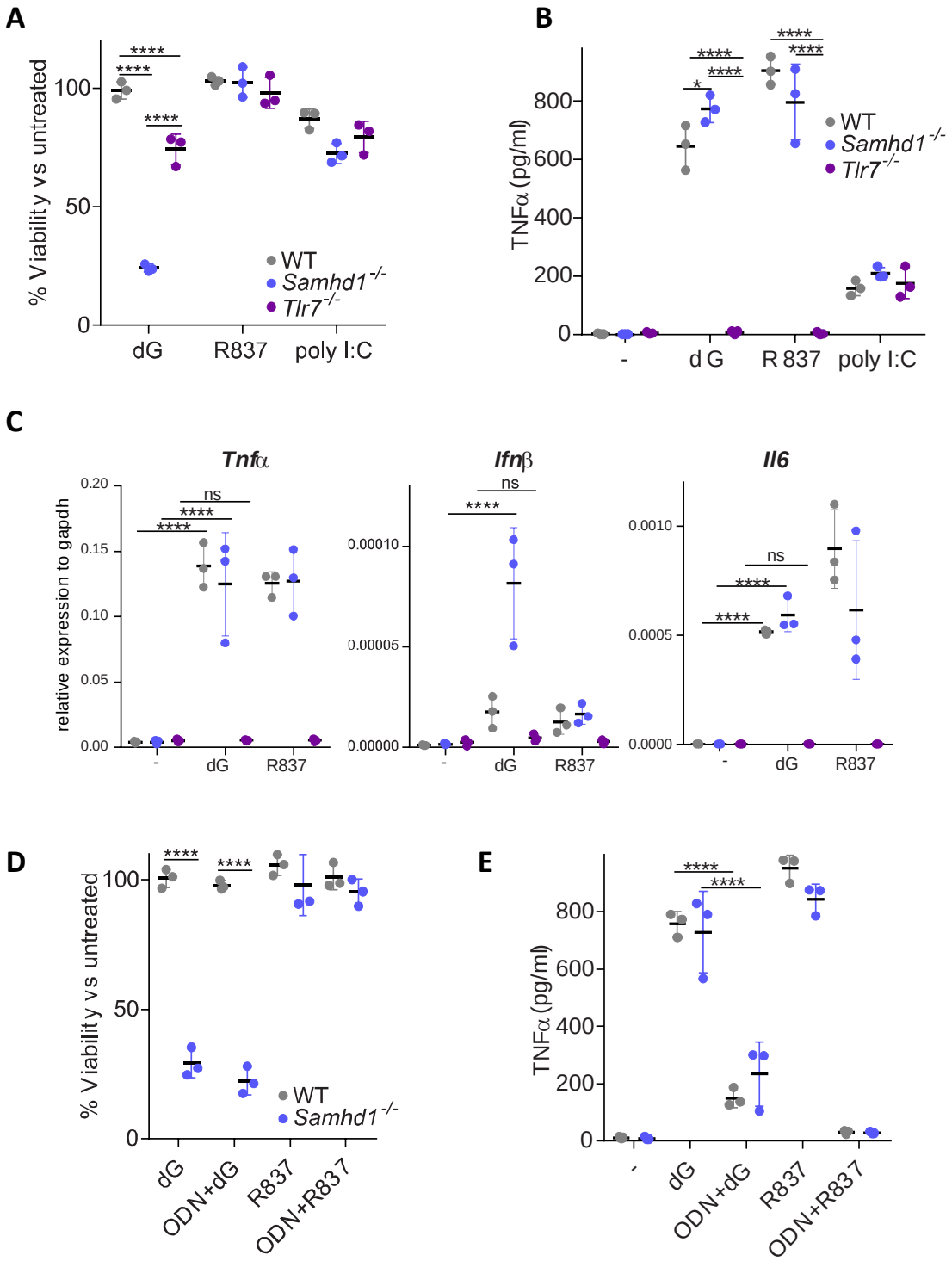


Figure 4.8 dG signals through TLR7 to induce cytokine production. *(A-C) BMDMs of the indicated genotypes were treated for 24 hours (A, B) or 6 hours (C) with 0.5 mM dG, 1 µg/ml R837 or 1 µg/ml poly I:C. Cell viability (A), TNFα production (B) and induction of selected mRNAs (C) were determined as in* ***Figure 4.5B****, c and a. (D, E) BMDMs were pre-treated or not with 2 µM ODN 20958 for 1 hour. Cells were then treated for 24 hours with 0.5 mM dG or 1 µg/ml R837. Cell viability (D) and TNFα production (E) were determined as in* ***Figure 4.5B****. Data are representative of three independent experiments. In A-E, dots represent BMDMs from individual mice and mean ± SD is shown. P-values determined with two-way ANOVA are indicated. ns p≥0.05; * p<0.05; ** p<0.01; *** p<0.001; **** p<0.0001*

4.6 Cytokine production and dG-induced apoptosis are independent events

To investigate whether the cytokine production impacts dG-induced cell death, double knock out mice are ideal. Our *Samhd1*$^{-/-}$ mice were crossed with *Tlr7*$^{-/-}$ and *MyD88*$^{-/-}$ mice to generate double knock out mice. The viability of *Samhd1*$^{-/-}$, *Samhd1*$^{-/-}$*Tlr7*$^{-/-}$ and *Samhd1*$^{-/-}$*MyD88*$^{-/-}$ BMDMs was significantly reduced 24 post-treatment with dG (**Figure 4.7A**). At a low doses of 125 µM and greater, the double knockouts showed reduced viability compared with *Samhd1*$^{-/-}$ BMDMs. *MyD88*$^{-/-}$ and *Tlr7*$^{-/-}$ BMDMs also had slightly reduced viability upon treatment compared with WT cells, but significantly higher viability than *Samhd1*$^{-/-}$ cells. This suggested that cytokines produced upon dG sensing helped both WT and *Samhd1*$^{-/-}$ cells to survive dG treatment. Crystal violet staining confirmed that *Samhd1*$^{-/-}$*Tlr7*$^{-/-}$ and *Samhd1*$^{-/-}$ had reduced viability upon dG treatment (**Figure 4.9B**). TNFα ELISA on supernatant from BMDMs 24h post-treatment showed that neither *Samhd1*$^{-/-}$*Tlr7*$^{-/-}$ or *Samhd1*$^{-/-}$*MyD88*$^{-/-}$ were producing TNFα upon dG treatment (**Figure 4.9C**). These data showed that dG-induced cytokines are not required to induce apoptosis in *Samhd1*$^{-/-}$ cells. Moreover, cytokines produced upon dG-mediated stimulation of TLR7 seem to promote cell survival.

To determine whether *Samhd1*$^{-/-}$*Tlr7*$^{-/-}$ were still dying by apoptosis upon dG treatment, I analysed cleaved-PARP and cleaved-caspase 3 by western blot, using cyclohexamide and TNFα combination as a positive control (**Figure 4.10A, B**). Both *Samhd1*$^{-/-}$*Tlr7*$^{-/-}$ and *Samhd1*$^{-/-}$ cells showed detectable levels of cleaved-PARP and cleaved-caspase 3. This showed that cytokines were not required for inducing dG-induced cell death by apoptosis since *Samhd1*$^{-/-}$*Tlr7*$^{-/-}$ double knockout BMDMs were still dying by apoptosis upon dG treatment. In addition, it showed increased levels of both cleaved-PARP and cleaved-caspase 3 in *Samhd1*$^{-/-}$*Tlr7*$^{-/-}$ compared to *Samhd1*$^{-/-}$. This increase correlated with reduced viability (**Figure 4.9A, B**) as measured with CellTiter-Glo and crystal violet assays. These data showed that cytokine production upon dG treatment through TLR7 is not required to induce apoptosis of *Samhd1*$^{-/-}$ cells.

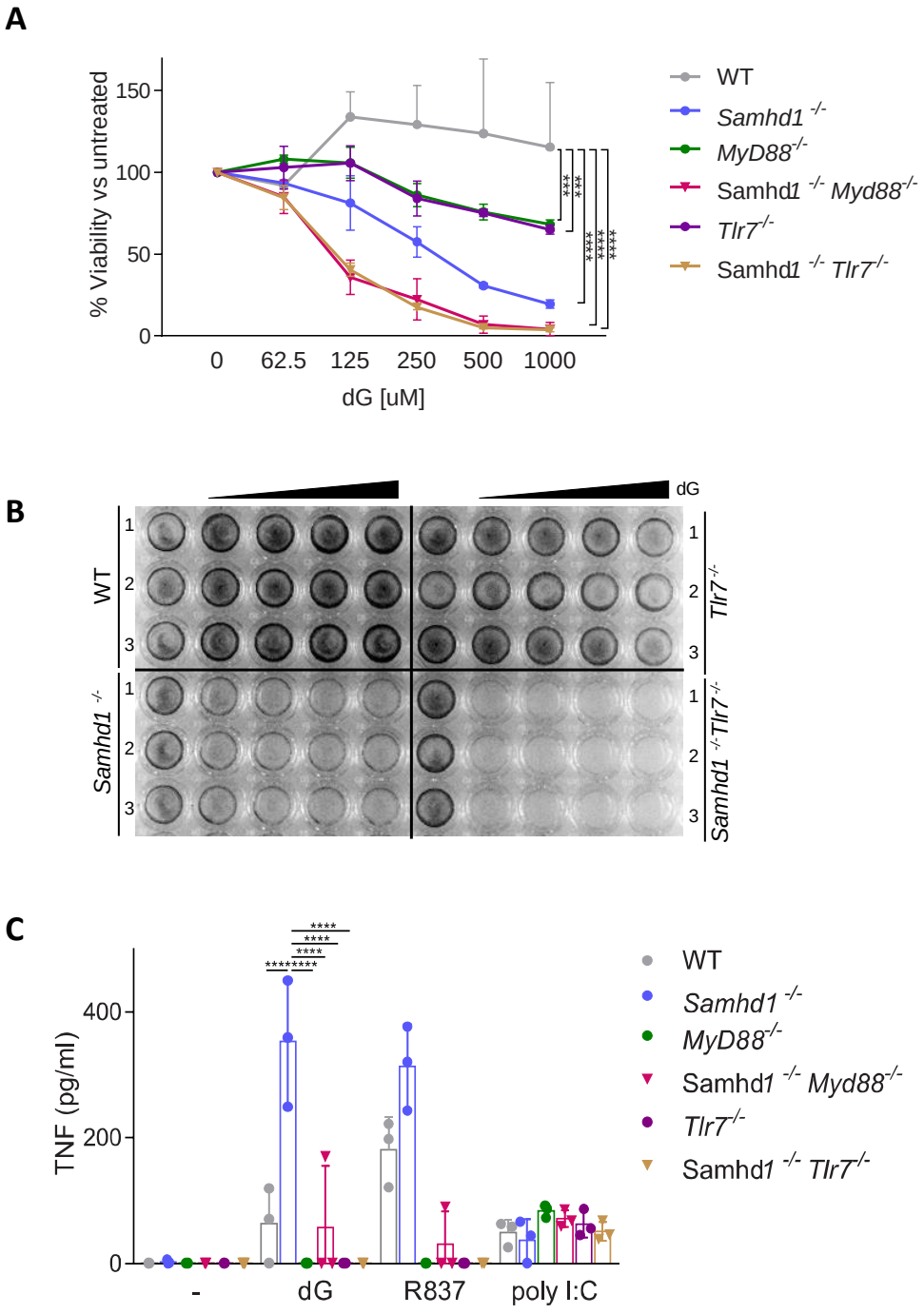


Figure 4.9 Cytokines do not contribute to dG-induced apoptosis. *(A) Viability (CellTiter-Glo) of BMDMs treated with indicated concentrations of dG for 24h. Dots represent mean of biological triplicates ±SD, two-way ANOVA (***p<0.001, ****p<0.0001). (B) Crystal violet staining of BMDMs treated with 0.25, 0.5, 0.75 or 1 mM dG for 24h. (C) TNFα ELISA on 24h supernatant of BMDMs untreated (NT) or treated with 0.5 mM dG, 1 µg/ml R837 or 1 µg/ml poly I:C. Dots represent technical duplicates of individual mice, bars are means ±SD, two-way ANOVA (****p<0.0001). (A-C) are representative of 3 independent experiments.*

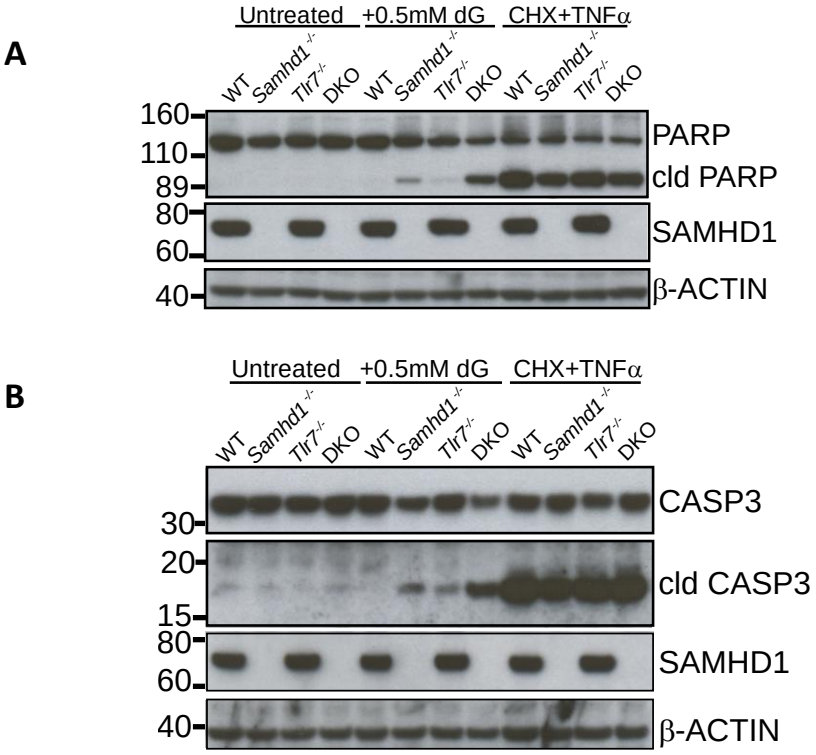


Figure 4.10 Samhd1$^{-/-}$Tlr7$^{-/-}$ BMDMs die by apoptosis upon dG treatment*. (A-B) Western blot of cleaved-PARP and cleaved-caspase 3 in BMDMs 8h post-treatment with 0.5 mM dG. Blots are representative of 2 independent experiments.*

4.7 Discussion

In this chapter, I investigated the cytokine production phenomenon occurring upon dG treatment. First, I showed that caspase inhibitors could not rescue *Samhd1*$^{-/-}$ BMDMs from dG-induced apoptosis. Single inhibitors often fail to rescue cells, pushing cells towards a different type of cell death due to crosstalk between the numerous cell death pathways (Nikoletopoulou et al., 2013). Moreover, combinations of inhibitors often lead to toxicity of some of these inhibitors and can make the interpretation of results difficult. Results from **Chapter 3** clearly demonstrated that dG induces cell death by intrinsic apoptosis, thus the decision was taken not to pursue blocking dG-induced apoptosis in *Samhd1*$^{-/-}$ cells. Instead, I focussed on an interesting new observation: dG induces the production of TNFα in BMDMs. The pan-caspase inhibitor zVAD, in combination with dG, triggered the death of WT and *Samhd1*$^{-/-}$ BMDMs, suggesting that cells were dying by TNFα-induced necroptosis. Indeed, TNFα is a cytokine that can trigger cell death through activation of death receptors. This illustrates an alternative death pathway triggered when apoptosis is blocked by the pan-caspase inhibitor zVAD in the presence of dG. Therefore it became important to investigate how the presence of TNFα impacted dG-induced apoptosis in SAMHD1-deficient cells.

Secretion of TNFα upon dG treatment was observed in both WT and *Samhd1*$^{-/-}$ cells. Interestingly, WT cells initially produced more TNFα than *Samhd1*$^{-/-}$ BMDMs. At later stages, *Samhd1*$^{-/-}$ BMDMs secreted higher levels of TNFα compared with WT. SAMHD1-deficient macrophages have been shown to display an IFN signature, suggesting that they may have a higher activation threshold (Behrendt et al., 2013; Rehwinkel et al., 2013). This could explain why the initial production of TNFα is lower in *Samhd1*$^{-/-}$ cells. This also suggested that TNFα production was maintained over time in *Samhd1*$^{-/-}$ BMDMs. It is possible that dying *Samhd1*$^{-/-}$ BMDMs released TNFα, contributing to the phenotype.

TNFα secretion was not due to the presence of endotoxins, as confirmed by a commercial laboratory testing (Lonza), experiments in the presence of polymyxin B, and the results in *Tlr4*$^{-/-}$ BMDMs. Further experiments were carried out with dG from Medchem, which was

tested endotoxin free and which maintained TNFα secretion with polymyxin B. This highlighted the importance of purchasing endotoxin free compounds, testing them if not sold as such, and considering the impact of any trace of endotoxins in the observed phenotype.

The production of TNFα independently of TLR4 also suggested that dG was sensed through a different cell receptor. I further showed that TNFα secretion was dependent on MyD88, suggesting sensing of dG by a PRR. The production of TNFα and other cytokines was confirmed by microarray and was completely dependent on MyD88. Characterising gene expression allowed me to address several important questions. Firstly, it defined the amplitude of the response triggered in BMDMs upon dG treatment and it demonstrated that the response was similar in both WT and *Samhd1*$^{-/-}$cells. 538 genes were differentially expressed upon dG treatment in WT and *Samhd1*$^{-/-}$ BMDMs supporting the sensing and signalling of dG. Secondly, it allowed the identification of transcripts that were differentially up or downregulated between WT and *Samhd1*$^{-/-}$ BMDMs. Although the amplitude of the response was very similar in both, some genes differed. The transcription factor CISH, involved in cytokine signalling, was among the genes that had a lower increase in *Samhd1*$^{-/-}$ compared with WT. This may explain the fact that *Samhd1*$^{-/-}$ cells are not able to respond with the same amplitude as WT cells. Several inflammatory genes were indeed less upregulated in *Samhd1*$^{-/-}$ cells: *Cd69, Il1b, Cish, Nos2, Saa3, Hcar2 and Nox1*. This supports the hypothesis that *Samhd1*$^{-/-}$ BMDMs are less sensitive to dG stimuli due to a higher activation threshold required. On the other hand, expression of mRNA encoding the anti-apoptotic proteins BCL21A was significantly higher in *Samhd1*$^{-/-}$ cells, suggesting that cells produced more BCL21A proteins to prevent the initiation of apoptosis. However, higher levels of anti-apoptotic proteins were not sufficient to protect *Samhd1*$^{-/-}$ cells from dGTP toxicity, since apoptosis is triggered upon dG treatment.

Analysis of the microarray gene set using two independent tools, DAVID and Reactome, allowed me to identify the main pathways activated upon dG sensing. dG sensing through MyD88 triggered an activation of the innate immune response causing the production of cytokines and chemokines via the NF-κB pathway. The sensing of dG also activated the

TLR pathway, suggesting that the PRR sensing dG may be a TLR receptor. Interestingly, the programmed cell death pathway was engaged 3h post-dG sensing suggesting that the cells were at a critical stage where the balance of pro and anti-apoptotic signals could trigger cell death. Overall, gene expression analysis revealed that dG induces a pro-inflammatory response similar in both in WT and *Samhd1*$^{-/-}$ BMDMs through the MyD88 adaptor protein. This suggested that the cytokines produced upon dG sensing were unlikely to play a role in the death phenotype of SAMHD1-deficient cells.

Next, I established that no cytokines were produced upon dG treatment of *Tlr7*$^{-/-}$ BMDMs, identifying TLR7 as the dG sensor. This was not surprising, since guanine nucleoside analogues have been shown to induce type I IFN and exert anti-viral activities specifically through TLR7 (Lee et al., 2003). This was supported by another study reporting that TLR7 can bind guanosine and dG in the presence of oligoribonucleotides (ORN) to strengthen the interaction (Shibata et al., 2015). Structural analysis of TLR7 later revealed that it is a dual receptor for guanosine and ssRNA (Zhang et al., 2016). Nonetheless, signalling of dG alone through TLR7 in macrophages has not been reported. However, the data presented here do not unequivocally support the claim that dG signals alone through TLR7. Indeed, several reasons could explain the presence of ORNs in the culture.

First, ORNs may come from foetal calf serum (FCS), a known source of RNA containing extra vesicles. Extracellular RNAs present in FCS are a concern in extra vesicles studies and they are challenging to get rid of even after several hours of ultracentrifugation (Tosar et al., 2017). Furthermore, conditioned media from L929 cells was used at 20% to grow and differentiate BMDMs. Despite filtration of this conditioned medium, it is possible that ORNs were present in this supernatant. A preliminary experiment comparing BMDMs grown either in media with 20% L929 in media or with recombinant macrophage colony stimulating factor (M-CSF), showed reduced production of TNFα by the M-CSF differentiated cells (data not shown). These cells also displayed a slower maturation and lower proliferation on day 7, which could explain the amplitude of TNFα production rather than the presence of ORNs in L929 conditioned media. This was not further investigated due to time constraints. To

address these questions in the future, it will be important to determine whether ORNs are present in L929 conditioned media or in FCS. FCS-free media are commercially available and could be used when dG is added. Growing macrophages in media without FCS may affect their proliferation and differentiation. BMDMs could be grown in culture medium with L929 conditioned media and seeded in FCS-free media with M-CSF.

Second, ORNs could originate from dead cells. However, dG is signalling through TLR7 quickly, as revealed by the production of TNFα from 60 min onwards. Cell death however, occurs from 6h upon dG treatment, suggesting that potential release of ORNs from dead cells is only available then. Signalling of dG through TLR7 preceded cell death, therefore it seems unlikely that ORNs released from dead cells are involved for dG signalling. In contrast, TNFα production was maintained over time in *Samhd1*$^{-/-}$ cells, supporting that at later stages ORNs are released and could signal with dG. Nevertheless, dG molecules may have all been internalised by the cell at that time. To determine whether dying cells produce extra cellular vesicles containing ORNs, the supernatant from the culture could be stained with Annexin V, which will detect the presence of lipid phosphatidylserine, present on the membrane of vesicles (Kastelowitz and Yin, 2014).

To further test whether dG is signalling alone through TLR7, poly U could be added to the cells with dG, or other ORNs to determine if the signalling of dG through TLR7 can be enhanced. In addition, RNase treatment could be applied to the media to digest any potential RNA contaminants. A preliminary experiment showed that treatment with RNase I had no effect on TNFα production whilst RNase A induced a small reduction (data not shown). Repeating the experiment with appropriate doses of RNase, different RNases as well as a positive control to show the efficacy of the RNase will be required. This may be a straightforward way to determine whether the presence of ORNs affects dG sensing through TLR7.

A TLR7 antagonist (ODN20958) was used to block cytokine production by *Samhd1*$^{-/-}$ cells treated with dG and to determine whether cytokine production influences cell death. Although the antagonist completely prevented TNFα production upon stimulation with TLR7

ligand (R837), it did not fully block dG-induced TNFα secretion. Despite the fact that the TLR7 inhibitor did not have an effect on dG-induced apoptosis in *Samhd1*$^{-/-}$ BMDMs, it was difficult to conclude that cytokines had no effect due to the possible incomplete block of TLR7 receptor. TLR7 is an endosomal receptor, so it is possible that TLR7 bound to its antagonist was recycled and that the ODN was used up while there was still some dG present in the culture medium able to signal through TLR7 at a later stage. Alternatively, *Samhd1*$^{-/-}$ cells dying upon dG treatment may release cytokines that could signal through different receptors to induce TNFα production. Overall, these data showed that partial blockade of TNFα secretion using a TLR7 antagonist did not affected the survival or death of WT and *Samhd1*$^{-/-}$ BMDMs, respectively. This suggested that the cytokines produced upon dG treatment did not play a role in apoptosis induced by dGTP overload in *Samhd1*$^{-/-}$ cells.

To decorticate the involvement of TLR7 in dG-induced apoptosis, *Samhd1*$^{-/-}$*Tlr7*$^{-/-}$ double knock-out mice were generated. No TNFα production upon dG sensing was observed in *Samhd1*$^{-/-}$*Tlr7*$^{-/-}$ BMDMs and they were sensitive to dG-induced apoptosis. This was further confirmed in *Samhd1*$^{-/-}$*MyD88*$^{-/-}$ BMDMs that displayed similar phenotype than *Samhd1*$^{-/-}$ *Tlr7*$^{-/-}$, and *Samhd1*$^{-/-}$ cells. This affirmed that the TLR7 antagonist ODN20958 was not entirely efficient at blocking dG signalling through TLR7. The absence of cytokine production in *Samhd1*$^{-/-}$*Tlr7*$^{-/-}$ and *Samhd1*$^{-/-}$*MyD88*$^{-/-}$ supported that dG was solely sensed through the TLR7/MyD88 pathway. Therefore, *Samhd1*$^{-/-}$ *Tlr7*$^{-/-}$ BMDMs were used to study apoptosis induced by dGTP overload in SAMHD1-deficient cells. *Samhd1*$^{-/-}$*Tlr7*$^{-/-}$ BMDMs died by apoptosis upon dG treatment, similarly to *Samhd1*$^{-/-}$ BMDMs. This demonstrated that cytokine production and cell death induced in *Samhd1*$^{-/-}$ cells were two independent phenomena. The absence of cytokine production did not protect *Samhd1*$^{-/-}$ cells from dG-induced apoptosis. Interestingly, cytokines produced upon dG treatment had a small pro-survival effect in both WT and *Samhd1*$^{-/-}$ cells, compared to *Tlr7*$^{-/-}$ and *MyD88*$^{-/-}$. It suggests that cytokine induction through dG sensing actually enhances cell survival. This is

consistent with the induction of pro-survival molecules downstream of TNF receptor and NF-KB signalling (Ting and Bertrand, 2016).

TLR7 is located at the endosomal membrane and can sense ssRNA, chemical ligands, guanosine and its derivatives (Shibata et al., 2015; Zhang et al., 2016). TLR7 is also located at the cell surface of macrophages, DCs and B cells where it can be targeted to prevent inflammation and autoimmunity (Kanno et al., 2015). It will be interesting to investigate dG-induced apoptosis in SAMHD1-deficient cells that do not express TLR7. For example, murine T cell lines have been shown to not express TLR7 (Applequist et al., 2002). This would help to support that dG solely trigger through TLR7 and that dGTP accumulates and trigger apoptosis in these cells in absence of cytokine production.

4.8 Conclusion

In summary, the data in this chapter demonstrate that dG is sensed through TLR7, signalling through its adaptor protein MyD88. dG sensing induces rapid release of TNFα and other cytokines by BMDMs. The innate immune pathway was the main pathway activated, inducing upregulation of numerous cytokines and chemokines. Importantly, this pro-inflammatory response had no effect on dG-induced apoptosis. dG sensing by TLR7 in BMDMs has not been described, although it is known that dG can signal through TLR7 in macrophages only when in combination with poly U (Shibata et al., 2015). Altogether this investigation revealed that the cytokine production induced upon dG treatment is independent of dG-induced apoptosis observed in SAMHD1-deficient cells.

Chapter 5. DEOXYGUANOSINE KILLS SAMHD1-DEFICIENT CANCER CELLS

Previous chapters characterised a phenotype where SAMHD1 protects cells against dGTP overload and cell death by intrinsic apoptosis. Interestingly, dG triggered cytokine production through TLR7 and MYD88 in BMDMs. The cytokines had only a minor effect on survival and dG-induced cytokine production was totally independent of the death phenomenon. In this chapter, I sought to investigate whether dG can also induce toxicity in cancer cell lines. As described in the introduction, SAMHD1 is regulated by cyclin-dependent kinase (CDK)-mediated phosphorylation (Cribier et al., 2013; Pauls et al., 2014b). According to the current model, CDKs phosphorylate SAMHD1 (pSAMHD1) in cycling cells, which become unstable tetramers, reducing SAMHD1's activity. Therefore, in the established model SAMHD1's dNTPase function is high in resting cells and low in cycling cells. Here, I investigated whether highly proliferative cancer cells also suffer from dG-induced apoptosis. This would help to determine whether the dNTPase protective function of SAMHD1 is active in cycling cells. Since *SAMHD1* mutations have been observed in CLL (Clifford et al., 2014; Guieze et al., 2015), in colon cancer (Rentoft et al., 2016) and in T-cell prolymphocytic leukaemia (Johansson et al., 2018), it was particularly relevant to determine if dG could induce toxicity in cancer cells lacking SAMHD1.

5.1 SAMHD1-depleted cancer cell lines are sensitive to dG

First, I wanted to determine whether dG treatment induced toxicity in cancer cells. To address this, cervical carcinoma cell line (HeLa), and acute monocytic cell line (THP1) were used. To knock down SAMHD1 in these lines, lentivirus-like particles expressing Vpx (VLP_{vpx}) or not (VLP_{ctrl}) were produced. Vpx is a protein expressed by HIV-2 that targets SAMHD1 for proteosomal degradation (Hrecka et al., 2011; Laguette et al., 2011). Infection with VLP_{vpx} is a commonly used system in human cells *in vitro* to knock down SAMHD1 expression. HeLa cells were infected with VLP_{vpx} or VLP_{ctrl} for several hours and treated with dNs (**Figure 5.1A**). HeLa cells infected with VLP_{vpx}, in which SAMHD1 was targeted for degradation, showed reduced viability compared to VLP_{ctrl} treated cells upon dN treatment. THP1 cells infected with VLP_{vpx} displayed similar results with lower viability upon dN

treatment (**Figure 5.1B**). This showed that knocking down SAMHD1 rendered HeLa and THP1 cells sensitive to dN-induced cell death, consistent with our previous observations in primary cells.

Brightfield images of HeLa cells presented a healthy layer of growing non-infected (NI) or VLP_{ctrl} infected cells 12h post-dG treatment (**Figure 5.1C**). In contrast, VLP_{vpx} infected HeLa showed sparse dying cells characterized by the loss of structure and rounded shape. SAMHD1 staining by flow cytometry confirmed the knock down efficiency using VLP_{vpx} (**Figure 5.1D, E**). This shows that SAMHD1-depleted HeLa and THP1 cells are sensitive to dG overload. This further suggested that SAMHD1 is protective in cycling cells.

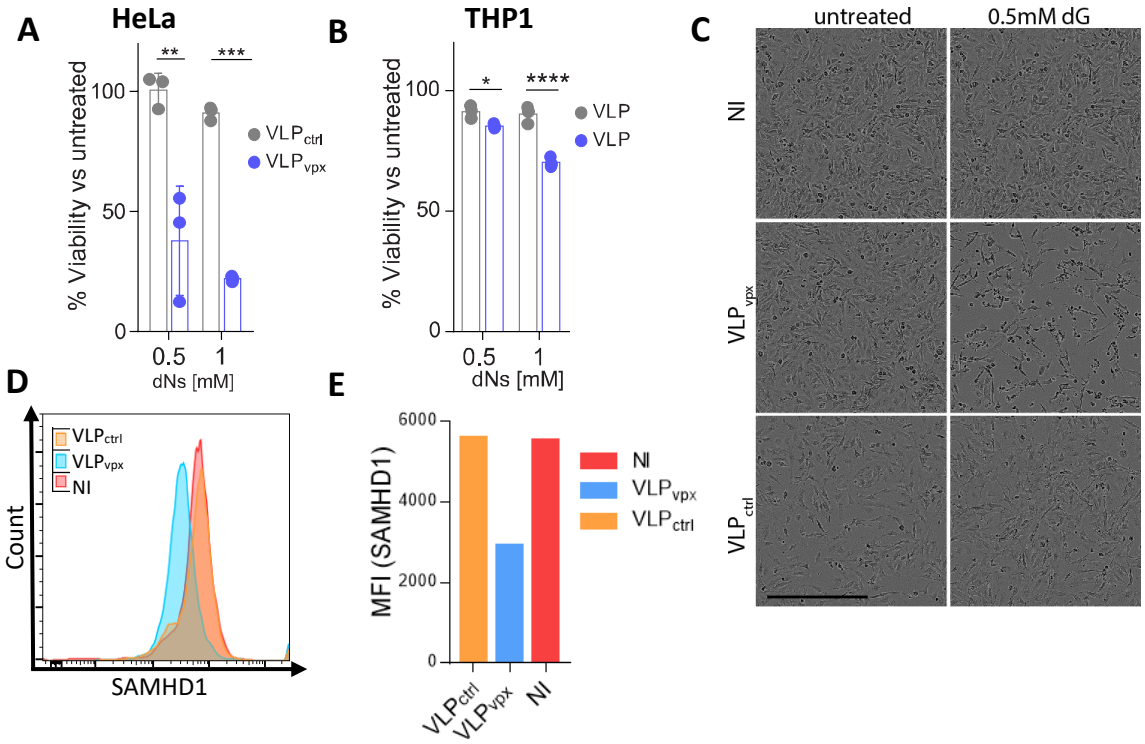


Figure 5.1 Vpx-targeted cells are sensitive to dNs and dG treatment. *(A-B) HeLa cells (A) and THP1 cells (B) were infected with virus-like particles containing Vpx (VLP_{vpx}) or not (VLP_{ctrl}). After 24 hours, cells were treated with 0.5 mM of each dN for an additional 24 hours. Cell viability was assessed with CellTiter-Glo. (C) Brightfield images of HeLa cells infected with VLP_{vpx} or VLP_{ctrl} and treated with 0.5 mM dG for 12h, scale bar represents 300 μM. (D) Histograms of SAMHD1 staining of HeLa cells (NI), infected with VLP_{vpx} or VLP_{ctrl}. (E) Mean fluorescence intensity (MFI) of SAMHD1 staining of HeLa cells shown in (A) and (D). (A-B) are representative of 3 independent experiments, dots represent technical duplicates, bars are mean ± SD. (C-E) are representative of 2 independent experiments. P-values determined with two-way ANOVA are indicated. ** p<0.01; *** p<0.001.*

To determine whether this was a consistent phenotype among different cancer lines, the breast cancer line MDA-MB231 was used. MDA-MB231 cells were infected with VLP_{vpx} or VLP_{ctrl} and treated with 0.5 mM dG. Cell death was observed only in MDA-MB231 infected with VLP_{vpx} 10h post-dG treatment (**Figure 5.2A**). Confluency measurements over time post-dG treatment supported this observation in VLP_{vpx}-treated MDA-MB231 showing a decline in confluency over time (**Figure 5.2B**). Experiments in HeLa, THP1 and MDA-MB231 cells consistently showed that SAMHD1-depleted cells were dying upon treatment with dG whilst had no effect in uninfected cells. This demonstrated that dG-induced apoptosis occurs in cancer cell lines when SAMHD1 is knocked down and it suggests that SAMHD1 is protective in highly proliferative cancer cells.

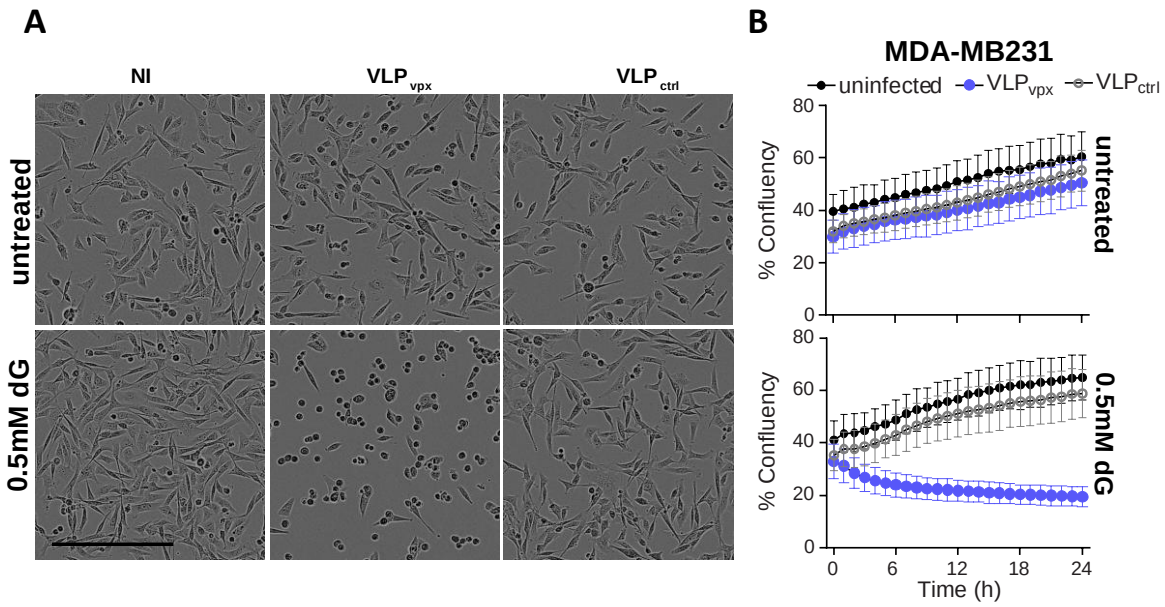


Figure 5.2 SAMHD1-depleted MDA-MB231 cells die upon dG treatment. *(A) MDA-MB231 cells were uninfected (NI) or were infected with virus-like particles containing Vpx (VLP_{vpx}) or not (VLP_{ctrl}). After 24 hours, cells were treated with 0.5 mM dG and Brightfield images were acquired after an additional 10h. (B) MDA-MB231 were treated as in (C) and confluency was monitored after dG addition using an in-incubator imaging system (Incucyte). The mean of 9 measurements ± SD is shown. This is representative of 2 independent experiments.*

5.2 Jurkat cells are highly sensitive to dG treatment

Jurkat cells, a leukaemic T-cell line, are known to not express SAMHD1 (Ballana et al., 2014). Jurkat cells were therefore a good model test whether cells lacking SAMHD1 are more sensitive to dG treatment. According to my model, the absence of SAMHD1 in Jurkat cells should lead to hypersensitivity to dG treatment, causing the accumulation of dGTP in the cells with subsequent toxicity and cell death by apoptosis.

Jurkat cells were treated with a range of dG concentrations from 0.05 to 0.8 mM. Cell viability was assessed with CellTiter-Glo and showed reduced viability upon treatment with 0.05 mM dG, a low dose of dG (**Figure 5.3A**). This was 10 times less than the dose of dG used so far in previous experiments in mouse and human primary cells and cancer cell lines. To determine whether the absence of SAMHD1 was responsible for the sensitivity to dG treatment, the cells were reconstituted with SAMHD1. Jurkat cells were infected with a lentivirus expressing SAMHD1 or SAMHD1 K11A, mutated in its nuclear localisation signal resulting in cytoplasmic localisation (Schaller et al., 2014). Low viability of Jurkat cells was observed upon dG treatment (**Figure 5.3B**). A significant increase in viability was observed when the cells where expressing either SAMHD1 or SAMHD1 K11A. Western blot confirmed that both proteins were expressed similarly (**Figure 5.3C**). This established that the absence of SAMHD1 renders Jurkat cells hypersensitive to dG treatment while its expression protects them from dG-induced cell death.

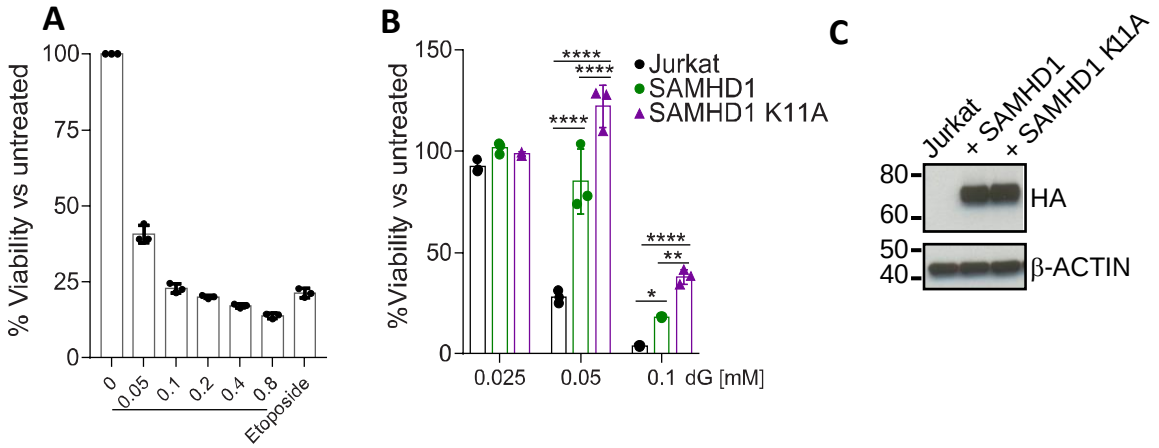


Figure 5.3 Jurkat cells are hypersensitive to dG treatment. *(A) Jurkat cells were treated for 20 hours with dG as indicated or with 25 μM Etoposide. Cell viability was determined with CellTiter-Glo. (B-C) Jurkat cells were reconstituted with HA-tagged wild-type or K11A mutant SAMHD1 using a lentiviral vector. (B) Cells were then treated with dG for 48 hours. Cell viability was determined with CellTiter-Glo. (C) SAMDH1 levels in total cell extracts were determined by Western blot. β-Actin served as a loading control. (A-C) are representative of 3 independent experiments. Two-way ANOVA, *p<0.05, **p<0.01, ****p<0.0001.*

5.3 *Samhd1*$^{-/-}$ B16F10 cells die upon dG treatment

dG treatment killed human cancer cell lines. Next, I wanted to test whether this was also happening in a murine cancer cell line *in vitro* to use *in vivo* in a cancer model. Since Vpx targets only human SAMHD1, this system could not be used in mouse cells. A *Samhd1*$^{-/-}$ murine cancer cell line was therefore generated using CRISPR/Cas9 technology.

5.3.1 Choosing a cancer model

Melanoma murine cancer line B16F10 offered several advantages as an *in vivo* subcutaneous growth tumour model (Overwijk and Restifo, 2001). First, our colleagues at the WIMM from Professor Vincenzo Cerundolo's group had B16F10 cells expressing the OVA peptide coupled to GFP. This meant that the adaptive immune response could be analysed with assays such as tetramer staining and ELISPOT assays. Second, it is fast growing cancer model *in vivo*; within approximately 20 days post-injection of the inoculum, tumour sizes should have reached the limit allowed in our project licence and the animals would have to be culled. Third, it does not require highly specialised skills to work with that model and techniques are easy to learn. Finally, the tumour is black due to melanin pigments in the cells. This makes it easily trackable under a pink shaved skin. Once the tumour is big enough, it can be monitored through the skin using a calliper without anaesthesia of the animal.

B16F10 are tetraploid cells meaning that SAMHD1 needs to be knock out on all four alleles (Baroja et al., 1998). This reduces the probability of obtaining a full KO and therefore increased the number of clones to be screened. Moreover, B16F10 tumours are poorly immunogenic, this means that strong stimuli are required to induce an immunogenic response. Therefore, weak treatment strategies may not work with that model (Overwijk and Restifo, 2001).

5.3.2 Validation of *Samhd1*$^{-/-}$ B16F10 cells

Samhd1$^{-/-}$ B16F10 cells were generated by C.Cursi (see details in section 2.2.1) and I tested them for dG-induced apoptosis to determine whether the phenotype could be observed in a murine melanoma cancer line. Brightfield images showed dying *Samhd1*$^{-/-}$ B16F10 cells upon dG treatment (**Figure 5.4A**). In addition, confluency measurements 20h post-treatment showed *Samhd1*$^{-/-}$ cells with reduced confluency compared with WT (**Figure 5.4B**). dG-induced apoptosis was confirmed by measuring Annexin V and 7AAD positive cells (**Figure 5.4C** and **D**). *Samhd1*$^{-/-}$ cells had increased levels of early apoptotic cells (AnnexinV^{+}7AAD^{-}) and late apoptotic/necrotic cells (AnnexinV^{+}7AAD^{+}) post-dG treatment. These data support a model in which the absence of SAMHD1 renders murine cancer cells sensitive to dG-induced apoptosis. This demonstrates that my observation extends to a murine cancer cell line.

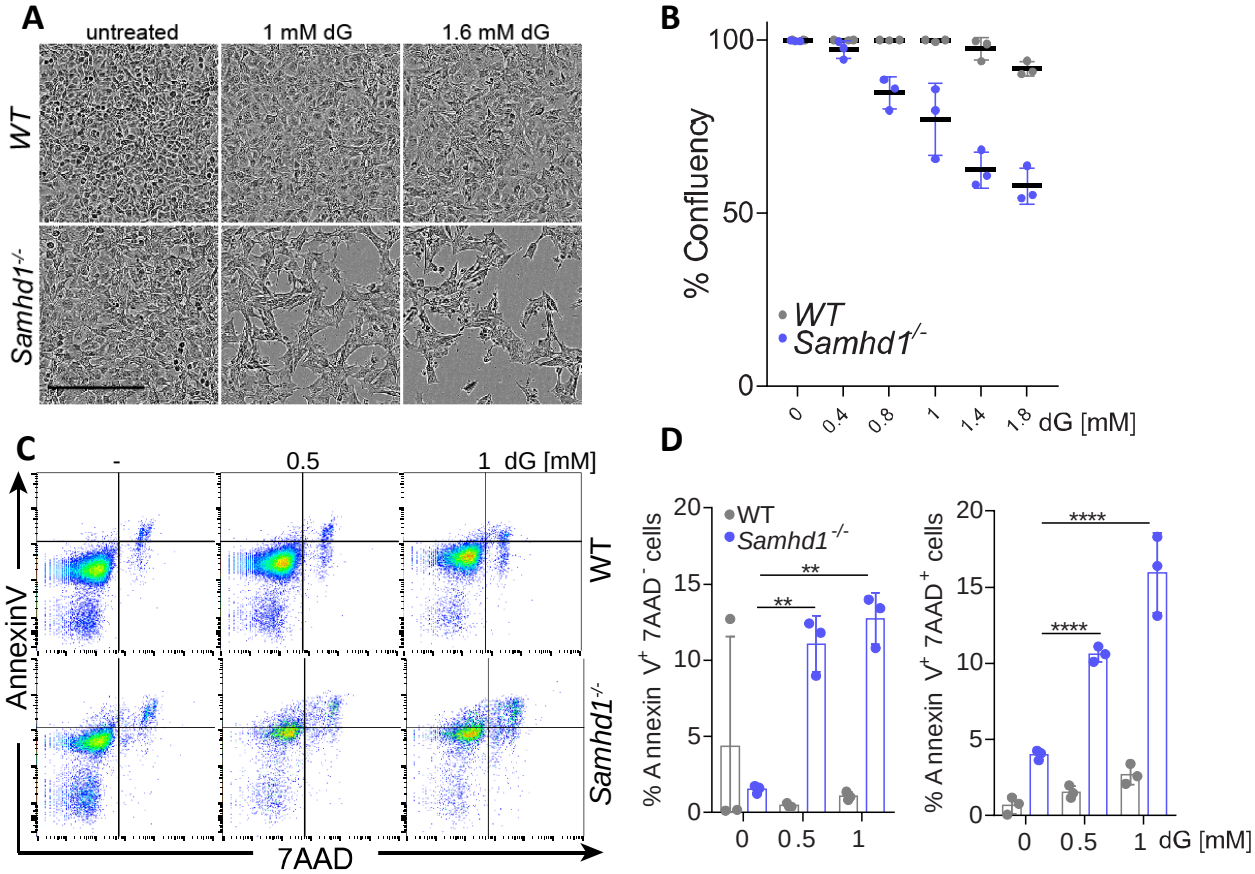


***Figure 5.4 Samhd1*$^{-/-}$ *B16F10 cells die upon dG treatment**. (A) Brightfield images of B16F10 cells 20 hours post-dG treatment (from the experiment in **Figure 5.4B**). Scale bar represents 300 μM. (B) Confluency measurements over time of B16F10 cells treated with indicated doses of dG for 20h. (C-D) Cells were stained with annexin V and 7AAD 20h post-dG treatment and analysed by flow cytometry. Representative FACS plots are shown in panel (C), Annexin V^{+} 7AAD^{-} and Annexin V^{+} 7AAD^{+} cells were quantified in panel (D). (A-D) are representative of 2 independent experiments.*

5.4 *Samhd1*$^{-/-}$ melanoma cancer model *in vivo*

Samhd1$^{-/-}$ B16F10 cells were generated and validated *in vitro*. They showed a robust phenotype, similar to the previously observed loss of viability of human and mouse primary cells as well as human cancer cell lines upon treatment with dG. *Samhd1*$^{-/-}$ B16F10 were used to induce subcutaneous melanoma tumours *in vivo* and to investigate whether dG treatment could be used to kill cancer cells *in vivo*.

5.4.1 *Samhd1*$^{-/-}$ melanoma grow slower than WT melanoma

First, tumour growth rates were measured to determine whether there were any differences in tumour growth between *Samhd1*$^{+/+}$, *Samhd1*$^{+/-}$, *Samhd1*$^{-/-}$ tumours in *C57Bl6* mice. As a control, cells from the inoculum were plated *in vitro* and confluency was measured over time. Confluency growth curves showed similar profiles between *Samhd1*$^{+/+}$, *Samhd1*$^{+/-}$, and *Samhd1*$^{-/-}$ B16F10 cells (**Figure 5.5A**). This confirmed that concentrations of each cell suspension injected in mice were similar between the groups and that their growth rates were similar *in vitro*. Cells (1.5 10^5) shown in **Figure 5.5A** were injected subcutaneously into the left shaved side (above the leg) of mice under anaesthesia. Tumour sizes were measured daily once detectable and tumour volume was calculated assuming the tumour was a cylinder multiplying tumour length by squared tumour width divided by two (LxW^2)/2. Ten mice per group were injected with 1.5 10^5 cells B16F10 of *Samhd1*$^{+/+}$, *Samhd1*$^{+/-}$, or *Samhd1*$^{-/-}$ genotype. Surprisingly, *Samhd1*$^{+/+}$ and *Samhd1*$^{+/-}$ tumours grew faster than *Samhd1*$^{-/-}$ tumours (**Figure 5.5B** and **C**). The humane end point was revealed when the tumour had a volume larger than 864mm^3, as described in our project license. Median time before reaching the endpoint for mice receiving *Samhd1*$^{-/-}$ cells was was 25.5 days compared with 19 and 21 days for *Samhd1*$^{+/+}$ and *Samhd1*$^{+/-}$ cells respectively. From day 14 post-injection, *Samhd1*$^{+/+}$ tumours became significantly bigger than *Samhd1*$^{-/-}$ tumours (**Figure 5.5D**). This difference was most striking at day 19. *Samhd1*$^{+/-}$ tumours behaved similarly to *Samhd1*$^{+/+}$tumours. Survival curves were plotted using tumour volume to define the end point (>864mm^3). Mean time to the endpoint was significantly higher in mice with *Samhd1*$^{-/-}$ tumours compared with *Samhd1*$^{+/+}$ tumours (**Figure 5.5E**). The same results

were observed in 3 independent experiments (**Figure 5.5** and PBS treated groups in **Figure 5.6**). This was surprising because *in vitro* confluency measurements showed that *Samhd1*$^{-/-}$ B16F10 cells were growing at the same rate over a 24h period.

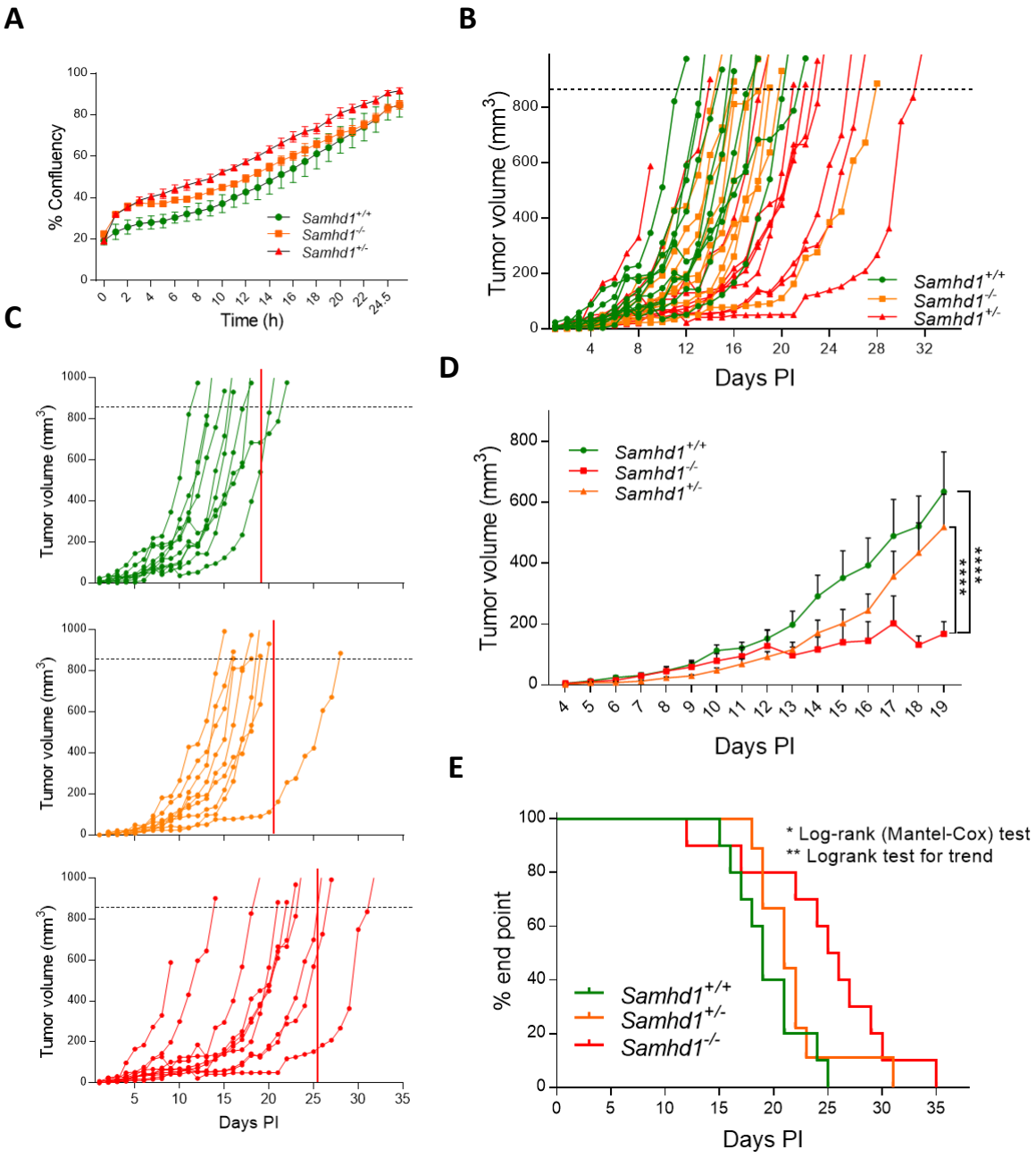


Figure 5.5 Samhd1$^{-/-}$ B16F10 tumours grow slower than Samhd1$^{+/+}$ and Samhd1$^{+/-}$ in C57Bl6 mice. *(A) Confluency measurements in vitro of B16F10 cells of indicated genotypes inoculated in (B-E). Dots are means of technical triplicates ± SD. (B-C) Growth measurements of B16F10 tumours of indicated genotypes over time. In (C), vertical red line represents mean days until the end point (>864mm3). Each line represent a different mouse, n=10 per group. (D) Tumour growth curves from the same experiment than (B-C), dots represent mean and error bars are SEM. Two-way ANOVA, ****p<0.0001. (E) Survival curve of mice shown in (B-D), the end point is tumour volume > 864 mm^3. Statistics of survival curves in Prism 7: Log-rank (Mantel-Cox) *p=0.0257, Logrank test for trend **p=0.0071, Gehan-Breslow-Wilcoxon test *p=0.0434*

5.4.2 dG treatment had no effect on WT B16F10 tumours

Next, I wanted to test whether dG treatment could have an effect on tumour growth. *Samhd1*$^{+/+}$ or *Samhd1*$^{-/-}$ B16F10 tumours were induced and were injected intratumorally with 5 mM dG when big enough. Intratumoral injections were chosen to deliver the compound directly in a small volume into the tumour. The dose of dG (5 mM was the highest fully soluble dose of dG in PBS) was higher than the final concentration used *in vitro*, considering that it may be diluted in fluids present within the tumour. Typically tumours were big enough to be injected when tumour volume was >100 mm^3. Since there was variability in tumour growth within a group, it was challenging to decide when to inject the groups since it was not logistically feasible to inject mice individually on different days.

The first experiment was performed by injecting *Samhd1*$^{+/+}$ B16F10 tumour cells subcutaneously at day 0 followed by two intratumoral injections at days 11 and 14, with PBS or 5 mM dG to test if dG treatment has an effect on tumour growth in this control group. A minimum number of ten mice per group was used to start with, due to variation in tumour growth within a group (illustrated in **Figure 5.5**). Tumour sizes on injection day are represented in **Figure 5.6A** and tumours out of the red box were excluded to avoid bias, since they were bigger on injection day. Intratumoral injections were performed on day 11 and day 14 post-injection of the inoculum. There were no further injections due to high tumours sizes and the injected volume became insignificant. No difference in tumour growth was observed between PBS and dG treated *Samhd1*$^{+/+}$ B16F10 tumour (**Figure 5.6B**). Survival curves to the end point (tumour volume >864mm^3) showed no significant difference between PBS and dG treated *Samhd1*$^{+/+}$ B16F10 tumour (**Figure 5.6C**). This suggested that dG treatment had no effect on *Samhd1*$^{+/+}$ tumour growth. There was no difference in tumour growth post-injection (day 20 and day 23) with PBS or dG (**Figure 5.6D**).

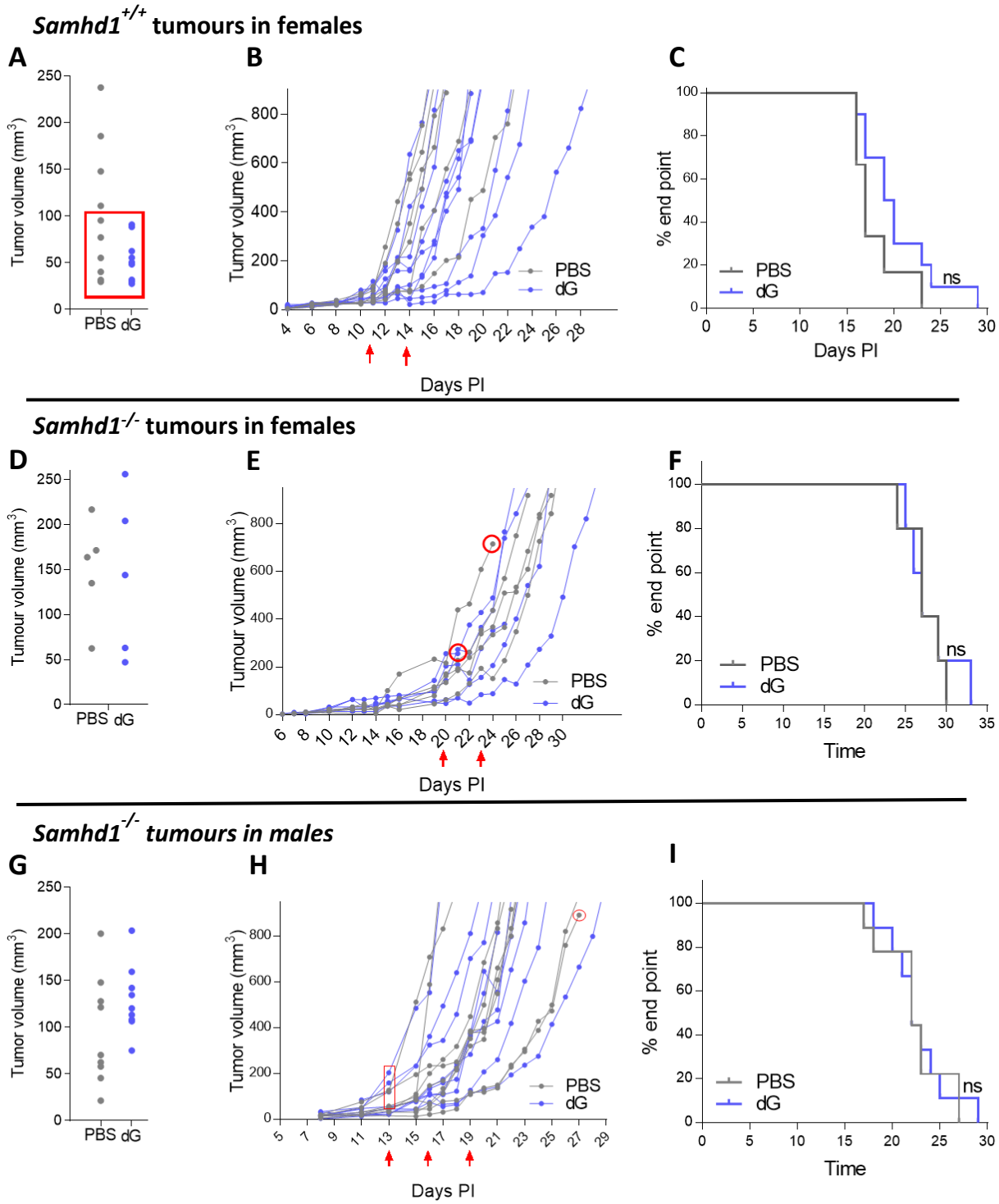


Figure 5.6. dG treatment has no effect on tumour growth. *(A-C) Samhd1$^{+/+}$ B16F10 melanoma tumours in female C57Bl6 mice received intratumoral injection twice with 5 mM dG or PBS 72h apart, on day 11 and day 14 post tumour injection. (A) Tumour volume on the day of the first injection. Only dots in the red rectangle are represented in figure (B) and (C). (B) Tumour growth over time, arrow represent intratumoral injection of dG or PBS, lines represent individual mice. (C) Survival curve of mice shown in (B). Dots represent individual mice, n=6 in PBS group and n=10 in dG treated group. (D-F) Samhd1$^{-/-}$ B16F10 melanoma tumours in female C57Bl6 mice. (D) Tumour volume on the day of the first injection. (E) Tumour growth as in (B). (F) Survival curve of mice shown in (E), n=5 per group. (G-I) Samhd1$^{-/-}$ B16F10 melanoma tumours in male C57Bl6 mice. (G) Tumour volume on the day of the first injection. (H) Tumour growth as in (B). (I) Survival curve of mice shown in (E), n=9 per group. In (E and H) red circles represent mice culled before end point due to sickness. In (A) the red box represents mice that are plotted in (B and C). In (H), the red box represents mice that received their first intratumoural injection on day 13.*

5.4.3 dG treatment had no effect on *Samhd1*$^{-/-}$ melanoma

Similar experiments were performed with *Samhd1*$^{-/-}$ B16F10 cells in either females (**Figure 5.6D**, **E** and **F**) or males (**Figure 5.6G**, **H** and **I**). First, females were treated with intratumoral injection of PBS or dG. *Samhd1*$^{-/-}$ tumours grew slower (**Figure 5.6D**) which was consistent with the previous experiment (**Figure 5.5**). Choosing the day of treatment was challenging due to high variability in tumour sizes (**Figure 5.6E**). In this experiment tumours were bigger on injection day compared with my previous experiment in WT tumours (**Figure 5.6D**). Two mice (red circles in **Figure 5.6E**), one in each group, became sick and had to be culled before tumour volume reached 864mm^3. Survival curves did not show a significant difference between PBS or dG-treated tumours (**Figure 5.6F**), suggesting dG treatment had no effect on *Samhd1*$^{-/-}$ tumours.

The experiment was also performed in *C57Bl6* males, with *Samhd1*$^{-/-}$ B16F10 cells injected to induce a melanoma tumour. Again, tumour sizes were variable on injection day (**Figure 5.6G**) and the animals represented in the red box (**Figure 5.6H)** received their first intratumoral injection on day 13 (and day 16) since tumour sizes were big, while the others were treated on day 16 and day 19. Tumour growth and survival curves did not show any significant difference between dG-treated and PBS control group (**Figure 5.6H** and **I**). This was consistent with the experiment in females.

5.5 Discussion

HeLa, THP1 and MDA-MB231 cells with Vpx mediated SAMHD1 depletion showed sensitivity to dNs and dG treatment. Therefore, highly proliferative human cancer cell lines lacking SAMHD1 are sensitive to dGTP overload. This suggests that SAMHD1's dNTPase function is highly active in cycling cells which challenges the current model of SAMHD1's regulation.

According to the current model, SAMHD1 does not restrict HIV-1 in cycling cells (Baldauf et al., 2012; Cribier et al., 2013; Descours et al., 2012). SAMHD1 is tightly regulated by phosphorylation throughout the cell cycle, which relies on cyclin D3, CDK6 and CDK2 (Pauls et al., 2014a; Pauls et al., 2014b; Ruiz et al., 2015). However, other reports observed different consequences of SAMHD1's phosphorylation on its restriction activity and its dNTPase activity. According to some, phosphorylated SAMHD1 (pSAMHD1) prevents its HIV-1 restriction function but does not affect its dNTPase activity in cycling cells (Cribier et al., 2013; White et al., 2013). Other manuscripts report that phosphorylation of SAMHD1 through cell cycle regulation affects dNTP pools and HIV-1 restriction (Cribier et al., 2013; Pauls et al., 2014a; Pauls et al., 2014b; Ruiz et al., 2015; Wittmann et al., 2015). Although it is not entirely clear which function(s) of SAMHD1 is regulated by phosphorylation, it was generally accepted, that phosphorylation of SAMHD1 in cycling cells leads to the inactivation of its restriction function and its dNTPase (**Figure 5.7A**). In contrast, a recent report indicates that the dNTPase function of the protein persists during S-phase when SAMHD1 is phosphorylated (Tramentozzi et al., 2018). This challenges the current model and suggests that SAMHD1's restriction function is regulated by phosphorylation through the cell cycle, while its dNTPase is not. The active dNTPase function of SAMHD1 in cycling cells observed in my experiments, protecting from dGTP accumulation, supports this latest publication.

Data in this chapter demonstrated that SAMHD1's dNTPase activity is functional in cycling cells, allowing SAMHD1 to protect cancer cells against dGTP overload. dGTP binds SAMHD1's allosteric site and is the most potent stimulator of its dNTPase activity (Powell et al., 2011). Only GTP or dGTP (but not other dNTPs) can bind SAMHD1's allosteric site I. GTP is the most likely binder due to its abundance (cellular levels of GTP ~1000 time higher dGTP) and NTPs concentrations remain relatively constant throughout the cell cycle (Amie et al., 2013; Hansen et al., 2014; Koharudin et al., 2014; Miazzi et al., 2014). It is possible that temporary high dGTP levels in WT cells promote the formation of active tetramers through binding of allosteric sites and therefore overcome the instability of pSAMHD1 tetramers (**Figure 5.7C**). I propose a model in which SAMHD1's dNTPase activity may be regulated by its phosphorylation depending on the cell cycle, with dNTPs concentrations also affecting the formation of active tetramers. In this model, abundance of dNTPs, especially dGTP which is SAMHD1's most potent activator, would overcome the formation of pSAMHD1 unstable tetramers happening during cell cycle progression (**Figure**

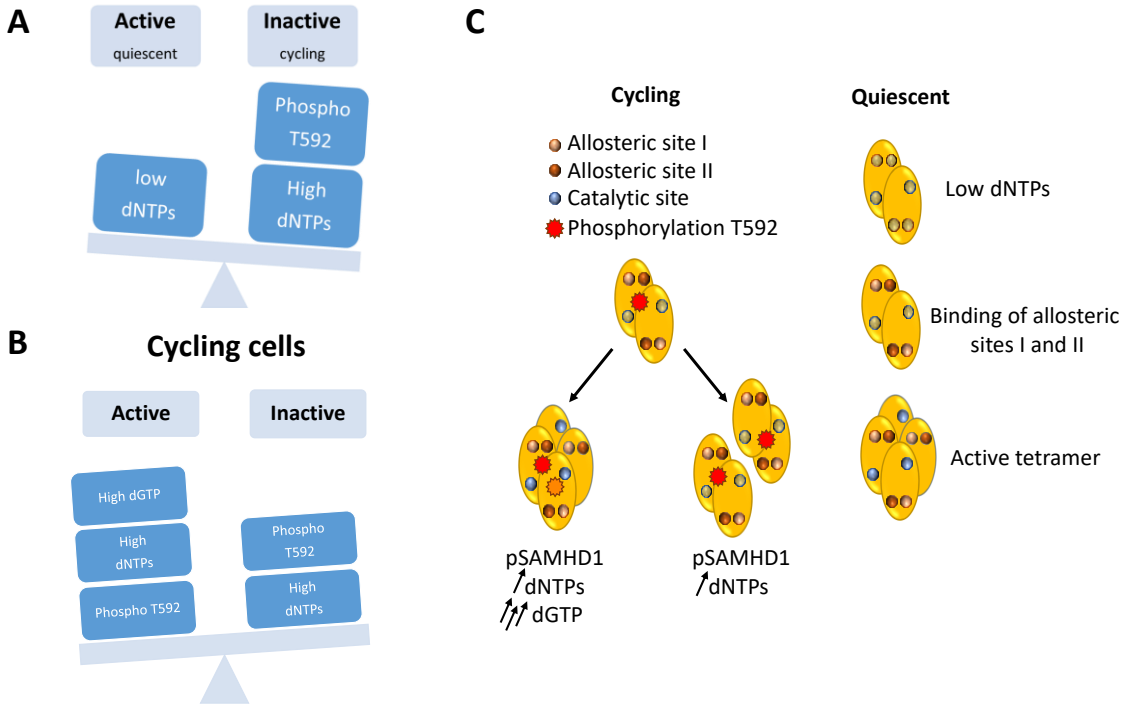


Figure 5.7 SAMHD1 regulation. *(A) Current model of SAMHD1 regulation. SAMHD1 is active in quiescent cells where low dNTPs bind to allosteric sites, allowing the formation of an active stable tetramer. SAMHD1's dNTPase is active and degrades dNTPs, maintaining low dNTP pools. SAMHD1 is phosphorylated on T592 in cycling cells, preventing tetramer formation. SAMHD1 is therefore inactive and dNTP levels increase. (B) In the new model proposed here, cycling cells with high concentration of dGTP in addition to high dNTP pools and despite phosphorylation of T592, allow the formation of active tetramers. SAMHD1 is active and degrades dGTP. (C) Detailed activation model of SAMHD1. In cycling cells, high concentration of dGTP could allow formation of SAMHD1 tetramers despite phosphorylation on T592.*

5.7B). This could be a safety mechanism when dNTP pools are rising in cycling cells, due to SAMHD1's inactivity. Above a certain threshold of dNTPs or imbalances, binding of dNTPs to allosteric sites may promote the formation of active tetramers despite SAMHD1's phosphorylation (**Figure 5.7C**). This would activate SAMHD1's dNTPase and therefore avoid toxically high dNTP pools. Although this model explains my results, evidences lack to support it. Additional experiments are required to investigate these mechanisms. Defining SAMHD1 tetramer formation in cancer cell lines and SAMHD1 phosphorylation would address these questions. Sensitive antibodies exist to detect pSAMHD1, they can be used for western blot or flow cytometry. Using SAMHD1 published mutants may help investigating these questions, although this would mean working in overexpression systems.

Jurkat T cells which do not express SAMHD1, presented hypersensitivity to dG treatment. Jurkat cells were dying by apoptosis with a dose of dG 10 times lower (0.05 mM) than the one used on other cell lines (0.5 mM). It is not clear why Jurkat cells, despite not expressing SAMHD1, are 10 times more sensitive than SAMHD1-depleted cells. It suggests that another enzyme involved in the synthesis of dGTP from dG is more active, or that Jurkat cells are more sensitive to dGTP accumulation. Quantification of dGTP will allow to determine whether or not they have a more efficient nucleotide salvage pathway and consequently synthesise and accumulate dGTP faster. Evidences in PNP deficient patients, which cells accumulate dG and dGTP suggests that this mechanism is particularly toxic in T-cells (Cohen et al., 1978; Simmonds et al., 1987; Simmonds et al., 1982). This was attributed to high expression of dCK, one of the enzyme that phosphorylate dG. It is possible that the hypersensitivity of Jurkat cells is due to higher expression of dCK and dGK. This could be tested by western blot with antibodies against these proteins. Expression of SAMHD1 in Jurkat cells increased viability and decreased apoptosis, showing that SAMHD1 protected Jurkat cells from dG-induced apoptosis. Interestingly, a SAMHD1 cytosolic mutant appeared to show a slightly increased protective effect. Since WT SAMHD1 is located in the nucleus, excess dGTP has to diffuse to the nucleus to be

degraded by SAMHD1. Molecules smaller than 60kDa have been shown to diffuse freely through nuclear pore complexes to reach the nucleus (Wang and Brattain, 2007). It is likely that dGTP excess occurs in the mitochondria and in the cytosol where dGK and dCK are located, respectively. Cytosolic location of SAMHD1 K11A mutant may allow a direct degradation of dGTP in the cytosol, preventing dGTP overload to reach the nucleus. Our results also show that SAMHD1 is not required in the nucleus to have a protective effect, excluding a protective role of SAMHD1 in DNA repair but supporting a protective effect from its dNTPase function. It would be interesting to quantify dNTP pools in the cytosol and in the mitochondria to determine if SAMHD1's location has an effect on these dNTP pools. In addition, immunofluorescence to confirm SAMHD1's location and to determine whether SAMHD1 forms specific structures upon dG treatment would be elegant.

Next, dG-induced apoptosis was tested in CRISPR/Cas9 generated murine cancer cells lacking SAMHD1. *Samhd1*$^{-/-}$ B16F10 cells were sensitive to dG-induced apoptosis *in vitro* which was consistent with our model in which SAMHD1 is required to protect against dG induced apoptosis in mouse and human cells. This demonstrated that both human and murine SAMHD1-deficient cancer cell lines are sensitive to dG-induced apoptosis.

Higher dNTP pools in SAMHD1-deficient cells were expected to give an advantage to highly proliferative cells. When used *in vivo*, *Samhd1*$^{-/-}$ tumours grew slower than WT melanoma. This is consistent with a report showing that the absence of SAMHD1, leads to higher dNTP pools and consequently, inhibition of cell cycle progression (Franzolin et al., 2013). Since cancer cell lines often acquire mutations that can dysregulate cell cycle progression checkpoints, the effect of high dNTP pools may vary between cancer lines. dNTP levels can slow down or speed up replication by tuning fork progression. Therefore, any change within the tumour will directly have an effect on tumour growth (Poli et al., 2012). The growth rate of WT and *Samhd1*$^{-/-}$ cells was similar *in vitro* but different *in vivo,* suggesting an effect of the tumour micro-environment. Factors such as increased mutation rates or secretion of cytokines may impact growth of WT and *Samhd1*$^{-/-}$ tumours.

Higher dNTP pools with deficient repair mechanisms, which cancer cells tend to acquire selective mutations for, increase mutation rates which may give the tumour a selective advantage (Rentoft et al., 2016). In addition, *SAMHD1* mutations tend to be selected upon treatment with chemotherapy since it was shown to be recurrently mutated in chronic lymphocytic leukaemia (Clifford et al., 2014; Guieze et al., 2015), suggesting that *SAMHD1* mutations give CLL cells a competitive advantage. It would be interesting to sequence both WT and *Samhd1*$^{-/-}$ tumours to determine whether they accumulate more mutations overtime than WT. In addition, a recent publication showed that SAMHD1 acts at stalled replication forks to prevent IFN induction (Coquel et al., 2018). This could be happening in *Samhd1*$^{-/-}$ tumours, leading to type I IFN production and boosting of the anti-tumour immune response by rendering the tumour more immunogenic. The B16F10 tumour model is a fast growing model and the immune system of the host may already be overwhelmed. It would be interesting to inject a smaller inoculum to see if the immune system could keep tumour growth under control and increase the mean time to the end point. Alternatively, knocking out cGAS in *Samhd1*$^{-/-}$ B16F10 cells should prevent production of type I IFN and therefore abolish this mechanism. If this were true, *Samhd1*$^{-/-}$*cGAS*$^{-/-}$ B16F10 tumours would grow at similar rates than WT.

Disappointingly, dG treatment *in vivo* did not slow down tumour growth or increase survival of the dG-treated group. This was unexpected due to a robust *in vitro* phenotype showing dG-induced apoptosis in *Samhd1*$^{-/-}$ B16F10 cells, but there are several possible explanations. First, whatever mechanism lead to the slower growth of *Samhd1*$^{-/-}$ tumours may have had an impact on the effect of dG treatment that was not predicted *in vitro*. It is not clear why *Samhd1*$^{-/-}$ melanoma tumours grew slower, it is hard to hypothesise whether it could have had an impact or not. Second, intratumoral injections may not be not the best way of delivering the drug. They can sometimes perforate the membrane in which the tumour cells sit and disrupt the whole structure. The tumour core is under high pressure in solid tumours, which explains why a perforation of the membrane can be disruptive, and cause occasional bleeding. Third, B16F10 melanoma tumours grow extremely fast, and

quickly develop a necrotic centre, due to lack of oxygen of the cells localized in the tumour core (this was obvious when animals were culled and tumours studied). This context of cell death may have had an impact on the treatment efficacy since it was hard to determine from what tumour volume necrotic centres started to form. In addition, our project licence allowed us intratumoral injections 72h apart. Since B16F10 are fast growing tumour, only 2 or 3 injections were possible until the tumour became too big to be injected. Daily injections may have increased the chances of detecting an effect. Fourth, dG treatment may have had only a minor effect since the injection volume was very small. Tumours were growing fast, thus the immune system may have had already been overwhelmed and therefore any effect wouldn't make a difference. Injecting in smaller tumours would solve that problem, although it is technically challenging. Alternatively, intravenous or intraperitoneal injections would allow earlier treatment of the mice. Finally, since B16F10 tumours have low immunogenicity, the cell death induced by dG treatment (if it happened) may not have been enough to boost anti-tumour immunity. Although these *in vivo* experiments were carried out with a single *Samhd1*$^{-/-}$ clone, the functional validation of that clone suggests that something is fundamentally different between culturing the line *in vitro* and developing tumours *in vivo*.

Identifying the reason(s) why *Samhd1*$^{-/-}$ tumours grow slower is the first step to better understand the potential impact of dG on these tumours. Our observation support a recent publication where SAMHD1 KO THP1 cells transplanted into SCID mice showed reduced tumour growth (Kodigepalli et al., 2018). The authors observed that these tumour secreted more TNFα and suggests that this pro inflammatory cytokine stimulated cell death, leading to reduced tumour growth. Interestingly, culture of these SAMHD1 KO THP1 cells *in vitro* showed the opposite effect and displayed increase cell proliferation and apoptosis. To test if the same is happening with *Samhd1*$^{-/-}$ B16 tumours, TNFα western blot on tumour extracts could be performed. Deeper analysis of the tumour micro-environment and its impact on SAMHD1 activity in WT tumour is critical to determine whether dG treatment is expected to have an effect *in vivo*. B16F10 melanoma may not be the best tumour model to observe the effect of dG treatment. SAMHD1 is mutated in leukaemia, thus using *in vivo* models of

leukaemias may be more appropriate to see an effect of dG treatment. There are four main types of leukaemia in human: acute and chronic myeloid leukaemia (AML and CML), acute lymphoblastic leukaemia (ALL) and chronic lymphocytic leukaemia (CLL). Since *SAMHD1* mutations have been observed in CLL and T cell prolymphocytic leukaemia, it will be particularly relevant to choose among available models for these (Clifford et al., 2014; Johansson et al., 2018). New Zealand black mice would be a good model since they develop spontaneous CLL in old mice. Transgenic mice overexpressing TCL-1 mimic human CLL and could be used, but they show delayed disease progression which is not ideal (Kohnken et al., 2017). Xenograft models, in which human cells are injected into immunocompromised mice to avoid rejection of the cells could be an option. These models are often used to characterise tumour growth rate, biological behaviour, biomarkers and response to drug. Established NOD/scid/gcnull (NSG) mice xenografted with human CLL cells was shown to recapitulated the human host microenvironment in CLL and have been successfully used to assess therapy efficacy (Herman et al., 2013). The appropriate cancer model may show dG-induced apoptosis in SAMHD1-deficient tumours cells *in vivo*. All of these proposed model take time to generate and were therefore not developed during my D.Phil.

5.6 Conclusion

This chapter demonstrates that dG-induced apoptosis extends to human and mouse cancer cell lines. It was particularly important to show a protective effect in highly dividing cells since it remains unclear whether SAMHD1's dNTPase function is active throughout the cell cycle. This challenges the current model and views on SAMHD1 regulation. I propose a model in which high dGTP concentration can overcome the destabilisation of SAMHD1 tetramer formation caused by its phosphorylation in cycling cells. This could explain how cancer cells, mostly with inactive pSAMHD1, could form stable active tetramers under high dGTP concentrations. This would explain the active dNTPase function of SAMHD1 in cycling cells with high dGTP levels, allowing dGTP degradation and thus safeguarding the cells against dGTP toxicity.

Chapter 6. SAMHD1 MUTATED CELLS ARE KILLED BY FORODESINE AND DEOXYGUANOSINE

The previous chapter demonstrated that dG-induced apoptosis also occurred in cancer cells lacking SAMHD1. The phenotype was robust, and observed in different human and murine cancer cell lines. To develop my project, I investigated the relevance of this mechanism in physiological settings.

Rare disorders can be caused by defects in enzymes involved in purine and pyrimidine metabolism. For example, purine nucleoside phosphorylase (PNP) is the enzyme responsible for the degradation of guanosine, inosine and their deoxy counterparts. PNP is a key enzyme of the nucleotide salvage pathway, involved in purine metabolism. PNP deficiency leads to the accumulation of all four of its substrates (including dG) and causes T-cell lymphopenia (Mansouri et al., 2012; Papinazath et al., 2011). Consequently, PNP inhibitors have been explored to treat B cell and T cell leukaemias. Forodesine, also called BCX-1777 or Immucilin-H, is the most potent PNP inhibitor identified to date. Forodesine was shown to inhibit growth of malignant T-cells (Kicska et al., 2001). When initially developed, the authors claimed that forodesine does not kill or inhibit the growth of malignant B cells. Kicska et al. reported that forodesine blocks growth and induces apoptosis in malignant T cells through the accumulation of dG that becomes phosphorylated, triggering the accumulation of dGTP and the inhibition of ribonuclease reductase (Kicska et al., 2001). By blocking PNP, forodesine triggers the accumulation of dG and dGTP in the cell, a similar situation that dG supplementation of *Samhd1*$^{-/-}$ cells. Forodesine's toxicity in T cells has been attributed to high expression of dGK, the enzyme that phosphorylates dG (Balakrishnan et al., 2006; Osborne and Scott, 1983). Malignant T cells express high levels of dGK leading to high levels of dGTP. In this chapter, a key role of SAMHD1 in forodesine's mode of action is uncovered. I exploited this novel finding to kill CLL cells carrying *SAMHD1* loss-of-function mutations. This chapter demonstrates the relevance of this novel role of SAMHD1 by demonstrating its relevance on clinical samples.

6.1 *Samhd1*$^{-/-}$ BMDMs are more sensitive to forodesine than WT cells

Accumulation of dG in the cell can be triggered by forodesine, a PNP inhibitor used as anti-cancer agent against B cell and T cell leukaemia (Balakrishnan et al., 2006; Bantia et al., 2001; Gandhi and Balakrishnan, 2007; Gandhi et al., 2005). This suggests that dGTP overload created by adding dG to cells may mimic treating cells with forodesine. SAMHD1-deficient cells were sensitive to dG treatment, suggesting that they could be more sensitive to forodesine treatment. I hypothesised that SAMHD1 is a key enzyme that limits forodesine's toxicity in cells. To test whether SAMHD1 is important in that context, *Samhd1*$^{-/-}$ BMDMs were treated with dG and forodesine. Viability of BMDMs was measured 24h post-treatment with forodesine, dG or a combination of both. Neither WT nor *Samhd1*$^{-/-}$ BMDMs showed toxicity at low doses of dG or forodesine (**Figure 6.1A**). Reduced viability of *Samhd1*$^{-/-}$ BMDMs was measured with a higher dose of dG (40 µM) or when combination of low doses of forodesine (1 µM) and dG (10 µM) were used. This indicated a synergy between forodesine and dG, which is in line with previous *in vitro* work. Different combinations of forodesine and dG were used and each compound was titrated one at a time. Results confirmed that a low dose of dG with a low dose of forodesine resulted in low viability of *Samhd1*$^{-/-}$BMDMs (**Figure 6.1B**). At 10 µM dG, increasing forodesine concentration did not increase toxicity. In contrast, with 1 µM forodesine, there was a dose-dependent toxicity of dG and a correlation between the amount of dG added and the toxicity observed. This showed that forodesine sensitised *Samhd1*$^{-/-}$ BMDMs to dG-induced toxicity.

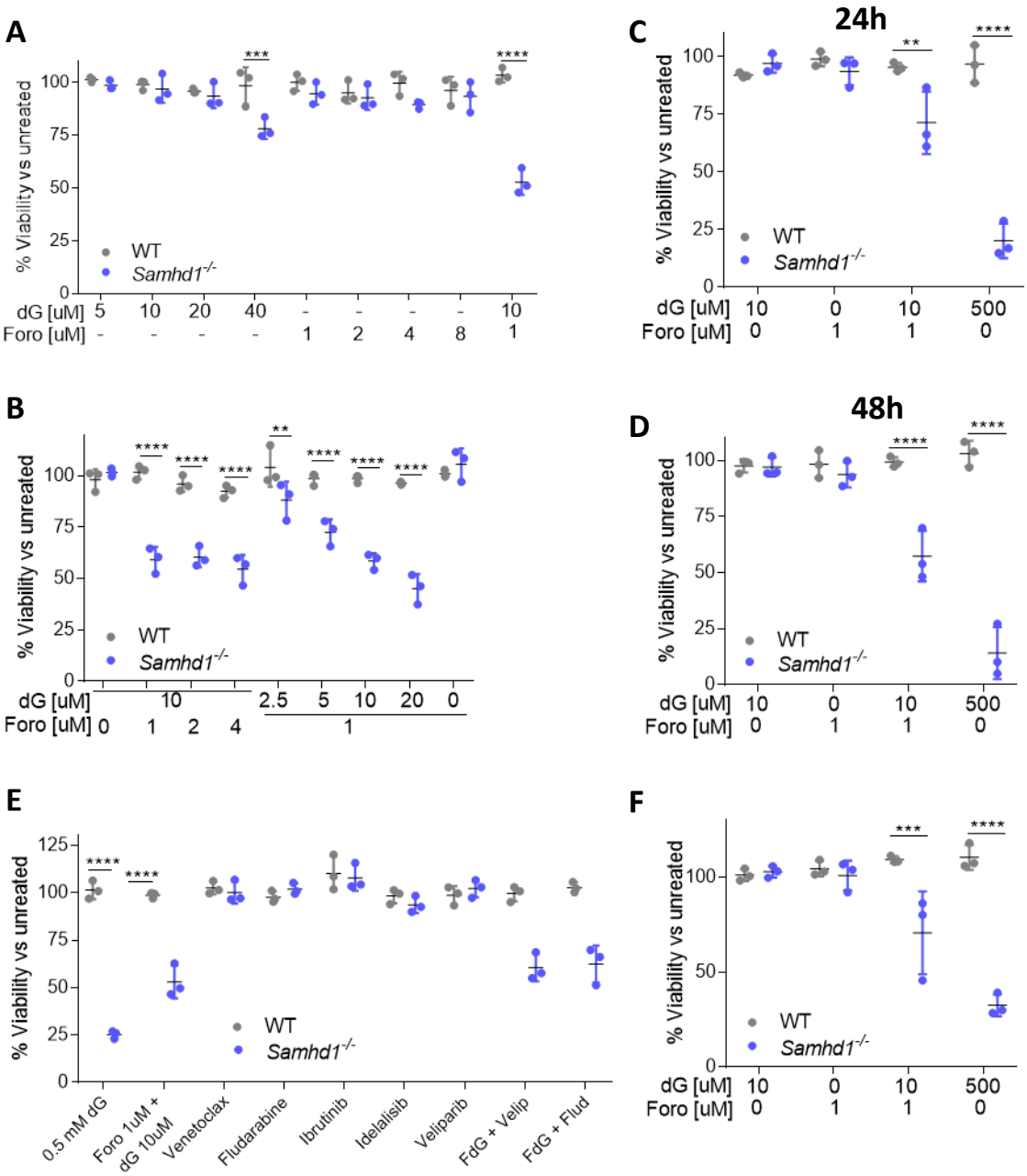


Figure 6.1 Samhd1$^{-/-}$ BMDMs die upon treatment with forodesine and dG. *(A-B) Viability (CellTiter-Glo) of BMDMs treated with indicated doses of dG and Forodesine at 24h. (C-D) Viability (CellTiter-Glo) was tested after 24 or 48 hours.(E) Viability of BMDMs was measured 24h post-treatment with 0.5 mM dG, 10 µM dG and 1 µM Forodesine, or CLL drugs 1 µM Venetoclax, 1 µM Fludarabine, 1 µM Ibrutinib, 1 µM Idelalisib or 1 µM Veliparib. (F) BMDMs treated for 24 hours with dG and Forodesine were fixed and stained with crystal violet. After washing, cell-associated dye was solubilised and quantified by absorbance at 570 nm. For each genotype, values from untreated control cells were set to 100%. (A-C) Representative of 3 independent experiments. (A-F) Dots are cells from individual mice, bars are mean ± SD. Two-way ANOVA, **p<0.01, ***P<0.001, ****p<0.0001.*

To compare the phenotype of dG toxicity previously observed with the effect of forodesine and dG at low concentrations, the experiment was repeated with 1 µM forodesine and 10 µM dG alone or in combination, in parallel with 0.5 mM dG treatment. Forodesine or dG alone had no effect on viability, as previously observed, whilst combination of both showed a toxicity similar to the high dose of dG used previously (**Figure 6.1C** and **D**). This was supported by viability measured with crystal violet staining (**Figure 6.1F**). Importantly, toxicity was only observed in *Samhd1*$^{-/-}$ BMDMs with no effect on WT BMDMs. In order to show the specificity of forodesine and dG toxicity in *Samhd1*$^{-/-}$cells, BMDMs were treated with different drugs also used against CLL (**Figure 6.1E**). None of the other CLL drugs tested (venetoclax, fludarabine, ibrutinib, idelalisib and veliparib) showed cytotoxicity in WT or *Samhd1*$^{-/-}$ BMDMs, demonstrating the specificity of SAMHD1's protection in forodesine's specific mechanism of action. These results showed that SAMHD1 protects specifically against forodesine and dG treatment.

To determine whether reduced viability correlated with induction of apoptosis, *Samhd1*$^{-/-}$ BMDMs were treated with either a low dose of forodesine, a low dose of dG, combination of both or a high dose of dG as in previous experiments. Cleaved-caspase 3 and cleaved-PARP were detected in *Samhd1*$^{-/-}$ BMDMs treated with the combination of forodesine and dG, as well as with 0.5 mM dG (**Figure 6.2A, B**). Levels of cleaved-PARP were similar than with high dose of dG whilst lower levels of cleaved-caspase 3 were detected when the combination was used compared with high dose of dG. These data confirmed that combination of forodesine and dG act synergistically to induce cell death by apoptosis only in *Samhd1*$^{-/-}$ BMDMs.

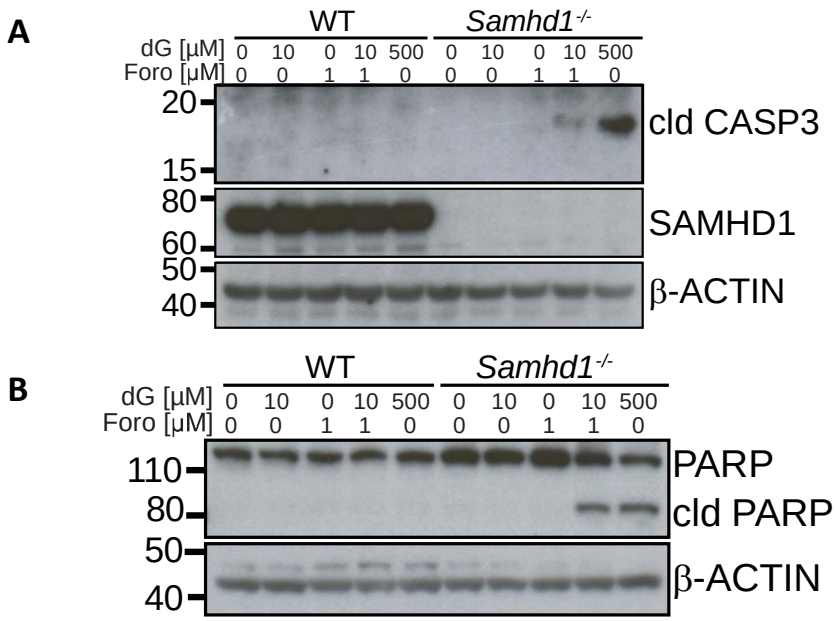


Figure 6.2 Forodesine and dG treatment induces apoptosis in Samhd1$^{-/-}$ BMDMs. *(A) Western blot of cleaved-caspase 3 upon treatment with dG or forodesine at indicated doses. (B) Western blot of cleaved-PARP upon treatment with dG or forodesine at indicated doses. Cld=cleaved. This experiment was performed once.*

6.2 Jurkat cells are sensitive to dG and forodesine treatment

Next, Jurkat cells were reconstituted with a lentiviral vector expressing SAMHD1 or the SAMHD1 K11 cytosolic mutant and treated with forodesine and dG. Viability measured with CellTiter-Glo was reduced in Jurkat cells treated with the combination of forodesine and dG but not when they were used independently (**Figure 6.3A**). The toxicity of forodesine and dG treatment was abolished when Jurkat cells were expressing SAMHD1 or SAMHD1 K11. This indicated that SAMHD1 had a protective effect against forodesine and dG treatment.

To confirm that lower viability of Jurkat cells correlated with induction of apoptosis, staining with Annexin V and 7AAD was performed.. Annexin V and 7AAD staining showed an increase of early apoptotic cells (AnnexinV^{+}7AAD^{-}) in Jurkat cells upon treatment with forodesine and dG (**Figure 6.3A, B** and **C**). In contrast, when SAMHD1 WT or mutant K11A were expressed, no apoptotic cells were detected post-treatment. As previously observed, low doses of forodesine or dG alone did not have an effect on the viability of Jurkat cells. These data showed that Jurkat cells are sensitive to forodesine and dG treatment. SAMHD1 expression in protected Jurkat cells from forodesine and dG-induced apoptosis. The unclear localisation of SAMHD1 appears to be dispensable for this protective effect.

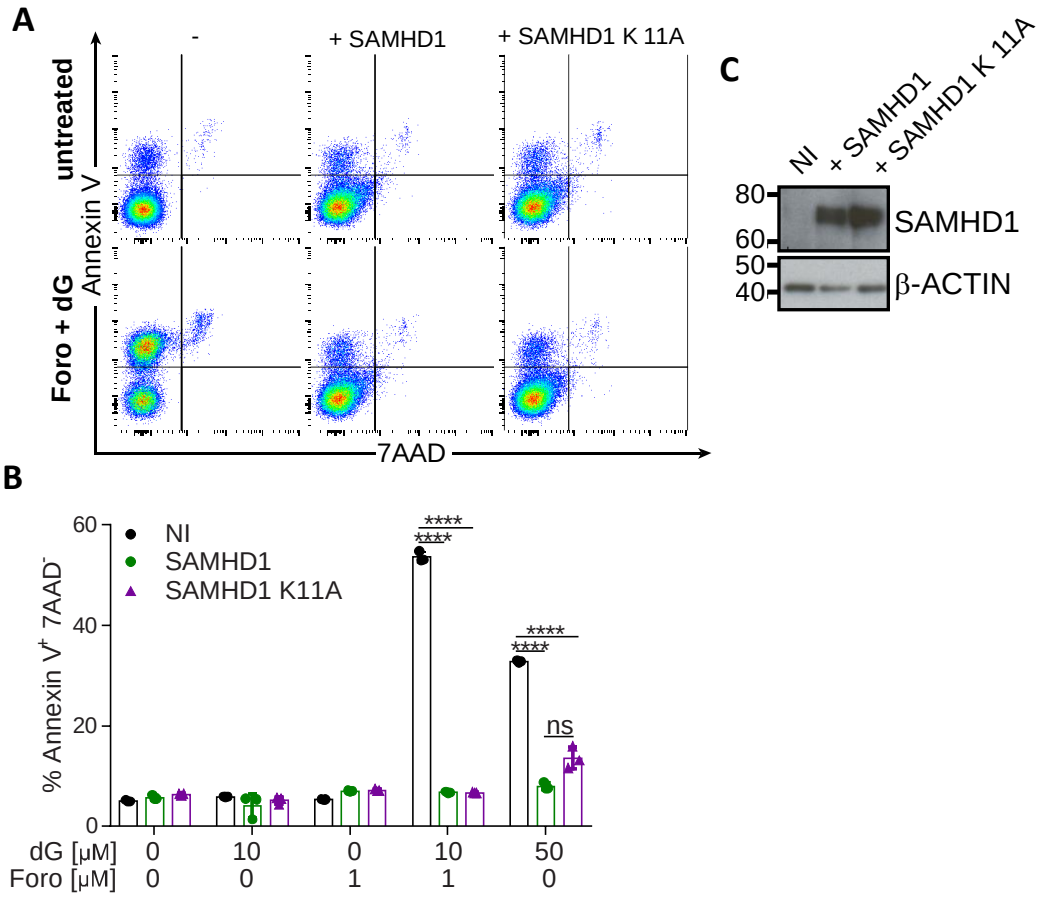


Figure 6.3 Jurkat cells are sensitive to forodesine and dG treatment. *(A-C) Cells were treated for 18 hours with dG and Forodesine, then stained with annexin V and 7AAD and analysed by flow cytometry. Representative FACS plots are shown in panel (A) and Annexin V⁺ 7AAD⁻ cells were quantified in panel (b). (C) SAMDH1 levels in total cell extracts were determined by Western blot. β-Actin served as a loading control. This is representative of 3 independent experiments. Dots are cells from individual wells, bars are mean ± SD. Two-way ANOVA, ****p<0.0001.*

6.3 Vpx-treated PBMCs showed limited sensitivity to forodesine and dG

Next, a collaboration with Dr Jenny Klintman (Anna Schuh's laboratory) was set up to secure PBMCs from CLL patients carrying *SAMHD1* mutations. Since CLL samples were human PBMCs, it was important to test forodesine and dG toxicity in PBMCs. This section shows the effect of forodesine and dG treatment in VLP_{vpx} treated PBMCs. It describes the optimisation of mass cytometry (CyTOF) to assess SAMHD1 expression and treatment efficacy.

6.3.1 Low efficiency of Vpx-mediated degradation of SAMHD1 in PBMCs

Lentiviral vectors coated with the envelope protein VSV-G and containing Vpx (VLP_{vpx}) were produced, as previously described (Besnier et al., 2002). Resting PBMCs were infected with VLP_{vpx} to degrade SAMHD1 or with VLP_{ctrl}. Five hours after infection, the medium was replaced and PBMCs were treated with forodesine and dG. After treatment, apoptosis was quantified by flow cytometry using Annexin V and 7AAD staining. According to side scatter and forward scatter, lymphocytes and monocytes, which differ in size, were gated (**Figure 6.4A**). There was no change in the frequencies of monocytes and lymphocytes upon treatment with forodesine, dG or combination, whether they were left uninfected, infected with VLP_{vpx} or VLP_{ctrl} (**Figure 6.4B** and **D**). Within the lymphocyte population, there was an increase of early apoptotic ($AnnexinV^{+}7AAD^{-}$) cells in VLP_{vpx} infected PBMCs upon treatment with forodesine and dG (**Figure 6.4C**). Neither the uninfected or VLP_{ctrl} infected PBMCs showed significant changes post-treatment. It is important to note that although there were significantly more $AnnexinV^{+}7AAD^{-}$ cells in VLP_{vpx} infected PBMCs, the results from the 3 PBMCs donors showed a high degree of variation. No difference in the frequency of monocytes was observed upon treatment (**Figure 6.4D**). Nevertheless, VLP_{vpx} infected monocytes showed an increase of $annexinV^{+}7AAD^{-}$ cells upon treatment with forodesine and dG (**Figure 6.4E**). These experiments have been repeated 3 times independently and similar results were observed: minor or no increase of apoptotic cells in VLP_{vpx} treated PBMCs upon treatment with forodesine and dG. Previously, VLP_{vpx} was very effective at infecting cancer cell lines but it showed limitations in human PBMCs. The limited efficacy of

forodesine and dG treatment in PBMCs suggested that only a minority of cells had depleted SAMHD1.

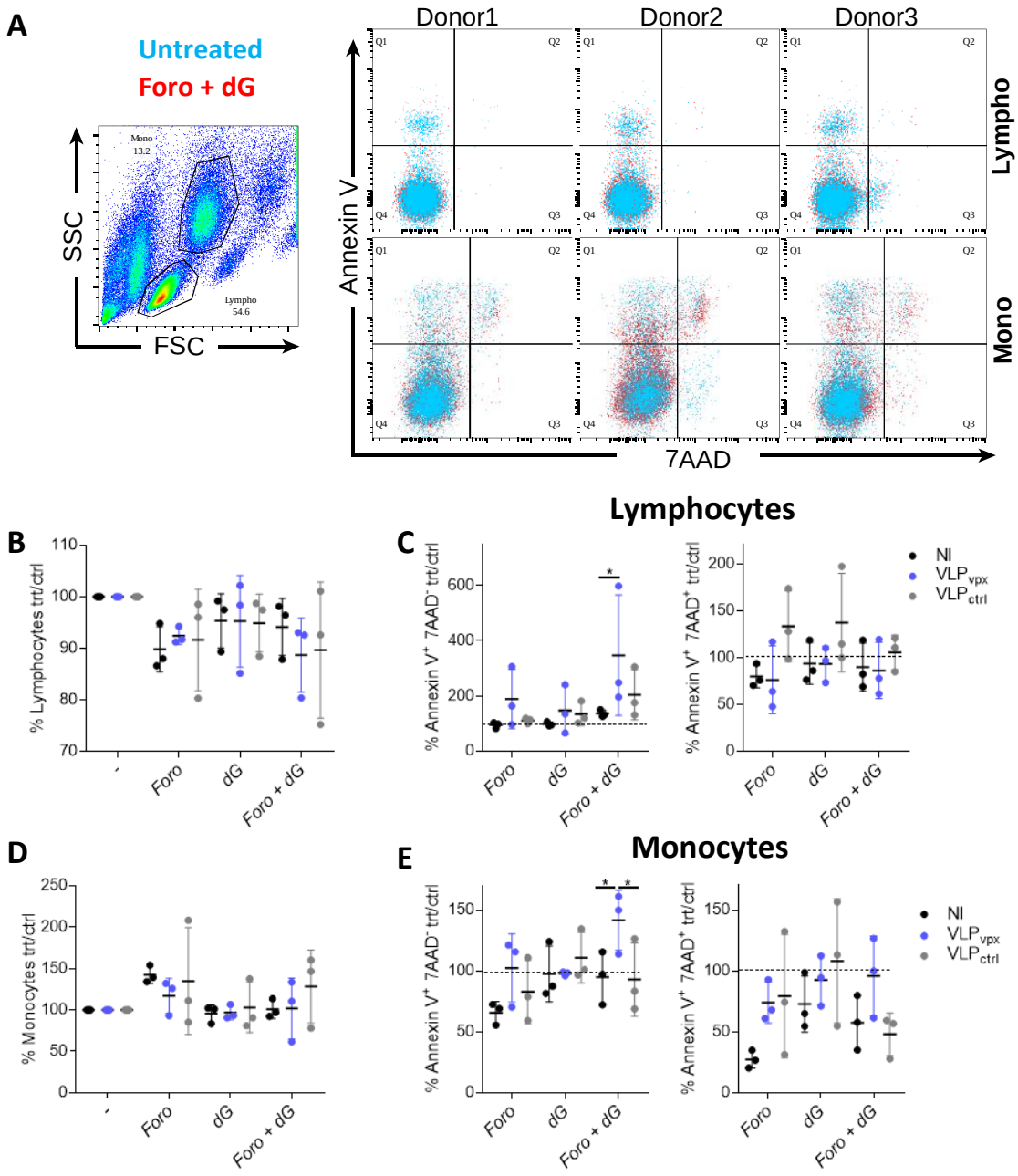


Figure 6.4 VLP$_{vpx}$ infected PBMCs showed limited sensitivity to forodesine and dG treatment. *(A) FACS plot of VLP$_{vpx}$ infected PBMCs with gating strategy of monocytes and lymphocytes. Cells were rested 17h after thawing, infected with VLPs for 7h, and treated for 18h. Annexin V and 7 AAD staining 18h post-treatment with 2 µM forodesine and 20 µM dG (red) or untreated (blue) in lymphocytes or monocytes as gated in (A). (B) Frequency of lymphocytes gated as in (A) 18h post treatment with 2 µM forodesine, 20 µM dG or combination of both at that dose. (C) Quantification of AnnexinV$^+$7AAD$^-$ and AnnexinV$^+$7AAD$^+$ cells uninfected (NI), infected with VLP$_{vpx}$ or with VLP$_{ctrl}$ in lymphocytes as gated in (A). (D) Frequency of monocytes gated as in (A) treated as in (B). (E) Quantification as in (C) in lymphocytes. Dots represent cells from a different donor, bars are means ± SD. P-values are two-way ANOVA, *, p<0.05. Representative plots of 3 independent experiments.*

6.3.2 CyTOF optimization on human PBMCs

Single cell mass cytometry (CyTOF) was developed and optimized on human PBMCs in order to use on PBMCs from CLL patients (see next section 6.4). I tested my CyTOF panel and investigated whether the low efficacy of forodesine and dG treatment in PBMCs was due to low infectivity of VLP_{vpx} (and therefore little degradation of SAMHD1). CyTOF is a technique based on inductively coupled plasma mass spectrometry and time of flight mass spectrometry used for the determination of the properties of cells (Bandura et al., 2009). CyTOF can detect up to 40 metals simultaneously and is not limited by spill over between channels as is the case in conventional flow cytometry. Using this cutting edge technology to characterise single cells allowed to overcome the heterogeneity of PBMCs. First, I needed to optimise the technology in order to use it on CLL patients' samples (see section 6.4.3). PBMCs are composed of a variety of cell types, each expressing different surface markers and potentially different levels of SAMHD1. To explain the limited sensitivity of VLP_{vpx} infected PBMCs to forodesine and dG treatment it was important to determine which populations were targeted by VLP_{vpx}.

The panel used included 22 lineage markers (including CLL markers CD5, CD19, CD27, CD43, CD20), 2 death markers (cleaved-PARP and cleaved-caspase 3), 3 inflammatory markers (phosphorylated p65 NFκB [S529], phosphorylated p38 MAPK [T180/Y182] and phosphorylated Stat1 [Y701]), as well as an antibody against SAMHD1 and pSAMHD1 (antibodies are listed in **Table 6.1**). A panel created by Dr Rachel Rigby, a postdoctoral researcher in the lab was used as a starting point. From this panel originally designed for staining on fresh blood, unwanted markers were removed to create space for the antibodies of interest: SAMHD1, pSAMHD1, cld-PARP, cld-CASPASE 3, pBad, CD5, CD43, CD23, p53, phospho p38, phospho p65 NFκB and DGUOK. For some antibodies (including SAMHD1 and pSAMHD1), several clones were tested by flow cytometry to identify the most suitable. The antibodies clones and the metals they were conjugated to are presented in **Table 6.1**. All antibodies were titrated to determine the optimal concentration for the CyTOF

protocol. Once the CyTOF panel was designed, it was validated with the experiments presented in this section.

Table 6.1 CyTOF panel for PBMCs

target	clone	label	Location
CD45	HI30	89Y	surface
CD11c	Bu15	141Pr	surface
CD11b (Mac-1)	ICRF44	142Nd	surface
cld-PARP	F21-852	143Nd	intracellular
CD4	RPA-T4	145Nd	surface
CD20	2H7	147Sm	surface
dGK	H-3	148Nd	intracellular
CD56 (NCAM)	NCAM16.2	149Sm	surface
p53	D07	150Nd	intracellular
CD123	6H6	151Eu	surface
CD27	O323	152Sm	surface
pStat1 [Y701]	4a	153Eu	intracellular
CD38	HIT2	154Sm	surface
CD45RA	HI-100	155Gd	surface
p38 [T180/Y182]	D3F9	156Gd	intracellular
SAMHD1	poly	158Gd	intracellular
CD14	M5E2	160Gd	surface
pBAD [S112]	40A9	161Dy	intracellular
STAT1	246523	163Dy	intracellular
CD23	EBVCS-5	164 Dy	surface
pSAMHD1	D7O2M	165Ho	intracellular
pNFkBp65 [S529]	K10x	166Er	intracellular
CD197 (CCR7)	G043H7	167Er	surface
CD8a	SK1	168Er	surface
CD24	ML5	169Tm	surface
CD3	UCHT1	170Er	surface
CD19	HIB19	171Yb	surface
cld-CASP3	5AE1	172Yb	intracellular
CD5	UCHT2	173Yb	surface
HLA-DR	L243	174Yb	surface
CD194 (CCR4)	205410	175Lu	surface
CD43	eBio84-3C1	176Yb	surface
CD16	3G8	209Bi	surface

Cells were gated to exclude calibration beads, then single cells were selected based on the intercalator staining, a cationic nucleic acid intercalator that contains natural-abundance iridium (191Ir and 193Ir). Within these single cells, live cells were negative for cisplatin, a viability agent that reacts with protein nucleophiles and are accessible only in dying cells with compromised membrane (**Figure 6.5A)**. T-Distributed Stochastic Neighbor Embedding (tSNE) plots are two dimensional representations of multi-parameter analysis where each dot represents a single cell. The tSNE algorithm uses a nonlinear dimensional reduction to allow visualization of the data (Van Der Maaten, 2008). tSNE plots were used to visualise SAMHD1 and pSAMHD1 expression in cells (**Figure 6.5B** and **C**). SAMHD1 was broadly expressed with high expression in most cell types and lower levels in $CD19^+$ cells, which are B-cells. It was particularly high in $CD56^+$ and $CD14^+$ compartments which are NK cells and monocytes, respectively. Interestingly, monocytes ($CD14^+$) were very high for SAMHD1

staining and were also well stained for pSAMHD1. Other subsets had variable levels of pSAMHD1, mostly low and very low. Interestingly, monocytes that expressed high levels of pSAMHD1 also had high levels of dGK (**Figure 6.5B**). dGK seemed to be specifically expressed in monocytes. The broad expression of SAMHD1 in most PBMCs subsets explained why forodesine and dG treatment did not have an effect on healthy PBMCs. These data validated CyTOF as a powerful technique to detect SAMHD1 and pSAMHD1 levels.

Next, VLP_{vpx} efficacy was assessed by determining SAMHD1 expression in uninfected, VLP_{vpx} or VLP_{ctrl} infected PBMCs. It became clear that VLP_{vpx} were only degrading SAMHD1 in a specific cell population: mostly $CD14^+$ monocytes (**Figure 6.6A** and **Figure 6.5C**). VLP_{vpx} also decreased the expression of pSAMHD1. Interestingly, monocytes in VLP-

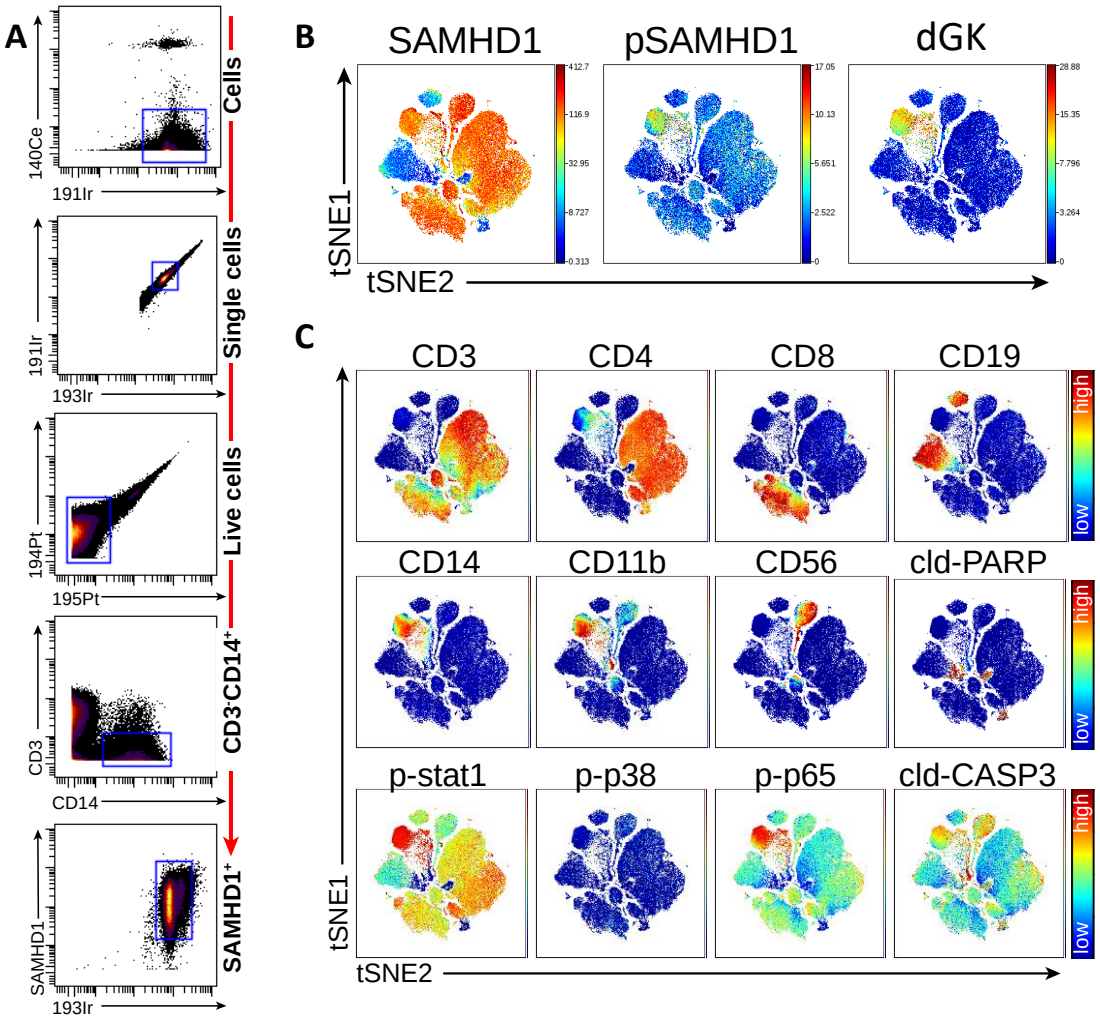


Figure 6.5 Mass cytometry detects SAMHD1 and pSAMHD1 in PBMCs. *(A) Gating strategy (B) tSNE plots generated with 22 lineage markers of healthy PBMCs. Legends represent signal intensity of indicated antibody. (C) Same tSNE plot than (B) coloured by indicated channels. Representative plots of 3 independent experiments.*

infected PBMCs shifted on the map, meaning that the expression of some markers used to generate the tSNE map must have changed. Quantification of $CD14^+$ monocytes showed a reduction in their frequency upon treatment with forodesine and dG in uninfected, VLP_{vpx} and VLP_{ctrl} infected PBMCs. VLP_{vpx} infected PBMCs had lower frequency of $CD14^+$ monocytes compared with uninfected and VLP_{ctrl} , suggesting that degrading SAMHD1 in these cells killed them. The absence of a population on the map would be represented by a dot free area. It is important to note that if the same cells are expressing different markers upon treatment, they can move spatially on the map. A similar observation was made in another experiment at a different time point, where upon VLP_{vpx} infection, tSNE plots showed a reduction of the $CD14^+$ compartment but not with VLP_{ctrl} (**Figure 6.7A** and **B**). The targeted compartment expressed high levels of CD14, CD11b, CD11c, HLA-DR, CD16 and CD56 which are monocytes, dendritic cells (DCs) and NK cells. There was a clear loss of $CD16^+$ cells upon VLP_{vpx} and the remaining cells had lower levels of SAMHD1 compared

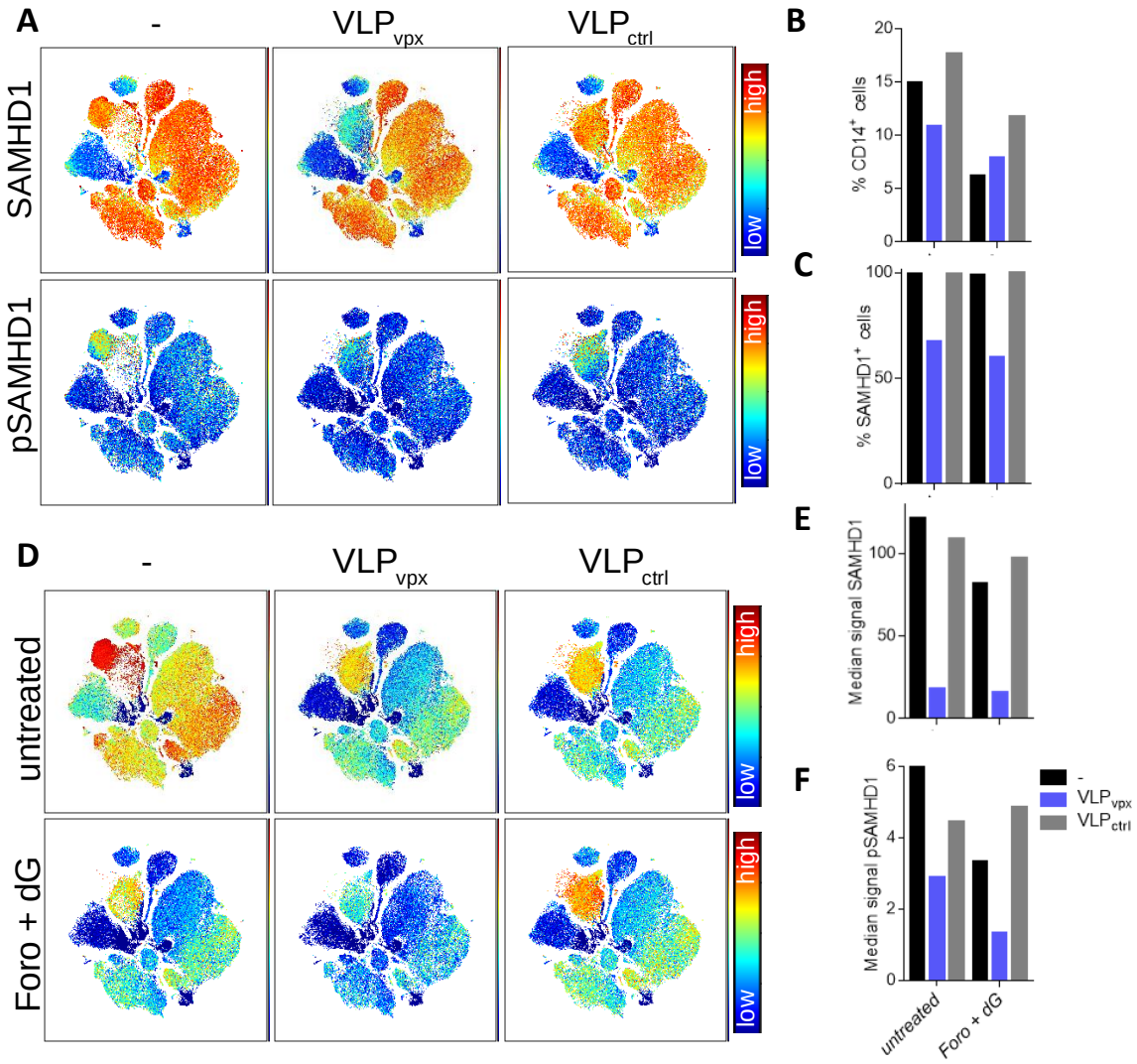


Figure 6.6 Vpx degrades SAMHD1 only in monocytes. *(A) tSNE plots coloured by SAMHD1 or pSAMHD1 staining intensity, gated on live cells in PBMCs. (B) Frequency of CD14⁺ cells in live PBMCs untreated or treated with 2 µM forodesine and 20 µM dG for 24h. (C) Frequency of SAMHD1⁺ cells in CD14⁺ population, untreated or treated as in (B). (D) tSNE plots coloured by pSTAT1 expression gated on live cells in PBMCs untreated or treated with 2 µM forodesine and 20 µM dG for 24h. (E) Median signal intensity of SAMHD1 staining in CD14⁺ cells, untreated or treated as in (B). (F) Median signal intensity of pSAMHD1 staining in CD14⁺ cells, untreated or treated as in (B). Representative plots of 3 independent experiments.*

with VLP_{ctrl} (**Figure 6.6D**). Furthermore, depletion of SAMHD1 induced a reduction of myeloid cells. Interestingly, the cell population sensitive to VLP_{vpx} treatment also had high expression of STAT1, pSTAT1 and p-p65 NF-κB (these markers were not used to generate the tSNE plots). Only in VLP_{vpx} infected PBMCs treated with forodesine and dG, the myeloid cells were reduced, with a complete loss of NK cells. Lower expression of SAMHD1 was also observed in other cell populations. The experiment was performed three times at 12h, 18h and 24h. No effect of forodesine and dG was observed 12h post-treatment (data not

shown) while at 18h (**Figure 6.7**) and 24h (**Figure 6.5** and **Figure 6.6**) loss of myeloid cells upon forodesine and dG treatment in VLP_{vpx} infected PBMCs was evident.

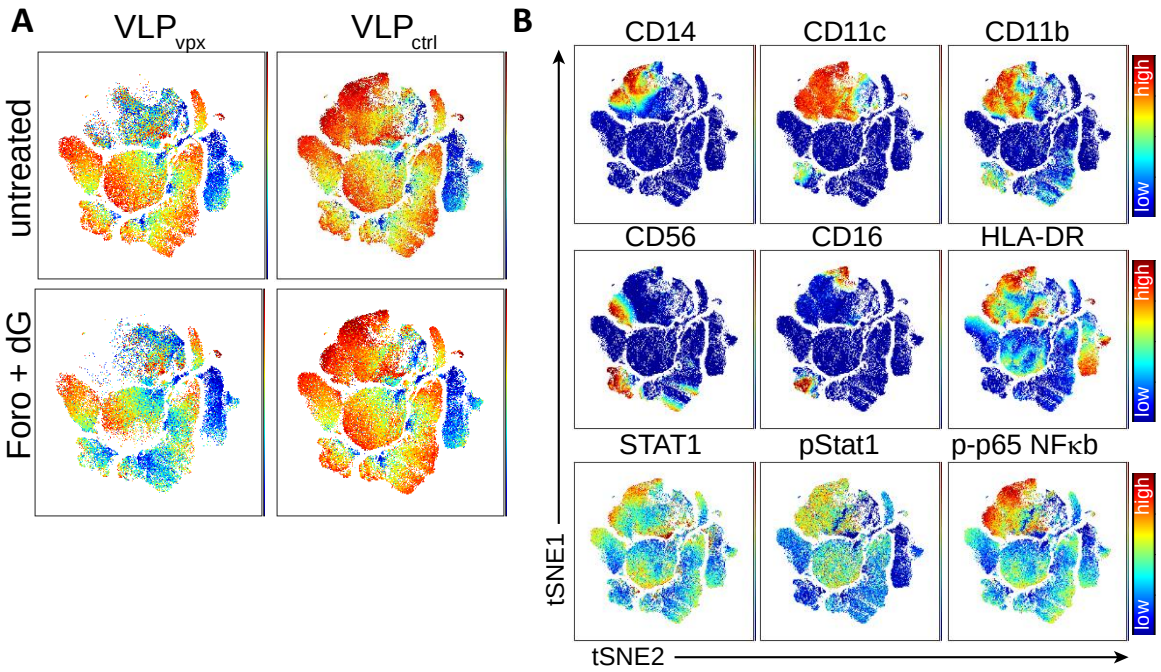


Figure 6.7 VLP_{vpx} degrade SAMHD1 in monocytes. *(A) tSNE plots of SAMHD1 expression in PBMCs thawed and rested for 3h, infected with VLPs for 5h and left untreated or treated with 2 µM forodesine and 20 µM dG for 18h. (B) Same tSNE analysis than (A) with expression of indicated markers in VLP_{ctrl} untreated cells.*

Strikingly, $CD14^+$ cells displayed high expression of pSTAT1 when untreated and the signal was reduced upon treatment with forodesine and dG. Treatment with VLPs seemed to have affected pSTAT1 levels in $CD14^+$ cells (**Figure 6.6D**). In that experiment, although the decrease of myeloid cells was obvious, no increase of cleaved-PARP or cleaved-caspase 3 was detectable. This suggested that 24h post-treatment was too late to detect these markers of apoptosis, which is in contradiction previous studies using that time point (Alonso et al., 2009; Gandhi et al., 2005).

All together, these data validated the staining panel and demonstrated the pertinence of using CyTOF on human PBMCs to detect SAMHD1 as well as the apoptotic markers cleaved-PARP and cleaved-caspase 3. This highlighted the limited efficacy of VLP_{vpx} treatment in healthy PBMCs and explained the lack of toxicity of forodesine and dG treatment.

6.4 CLL patients with *SAMHD1* mutations are more sensitive to forodesine and dG treatment

To test whether *SAMHD1*-mutated CLL cancer cells responded better to forodesine treatment, we collaborated with Anna Schuh at the John Radcliffe hospital (Oxford, UK) who has previously shown that *SAMHD1* is mutated in CLL (Clifford et al., 2014; Guieze et al., 2015). Anna Schuh and Jenny Klintman helped us obtaining clinical samples with *SAMHD1* mutations. PBMCs from 20 CLL patients with CLL recruited into the ADMIRE (n=12) and ARCTIC (n=7) studies (Howard et al., 2017) were retrieved from the Liverpool Bio-Innovation Hub Biobank. Genetic characterisations of the patients' tumour cells were previously published (Clifford et al., 2014). From these samples, 5 samples could not be processed due to extremely low viability upon thawing (**Figure 6.8A**) and one was excluded after sequencing did not match the information received from the biobank about that particular patient. In addition, PBMCs from three healthy donors were used as controls in the CyTOF experiment. Patient's characteristics are shown in **Table 6.2** and details of *SAMHD1* mutated cells are shown in **Table 6.3**. In total, 14 patient samples were processed and analysed, 4 in the *ATM* mutated group, 6 in the *TP53* mutated group and 4 in the *SAMHD1* mutated (*SAMHD1*^{mut}) group. Samples from *ATM* and *TP53* groups were pooled into a *SAMHD1*^{nonmut} group (also marked as *ATM/TP53*).

Table 6.2 Genetic characteristics of CLL patients

Sample ID	*Del17p*	*TP53*	*SAMHD1*	*del11q (ATM)*	Group
ADM224				y	*SAMHD1*^{nonmut}
ADM295				y	
ARC138				y	
ARC554				y	
ADM013		y			*SAMHD1*^{nonmut}
ADM020		y			
ARC334		y			
ADM181	y	y			
ADM216	y	y			
ARC603	y	y			
ADM007			y		*SAMHD1*^{mut}
ADM069			y		
ADM210			y		
ADM228			y		

Table 6.3 SAMHD1 mutations of CLL patients. *Y=yes, N=no, NA= non applicable, cnLOH= copy neutral loss of heterozygosity, CNLoss= copy number*

Sample ID	Exon	Nucleotide	Amino Acid	SAMHD1 locus
ADM007	exon5	T602A	I201N	cnLOH
ADM007	exon5	A617G	H206R	cnLOH
ADM007	exon11	G1165A	A389T	cnLOH
ADM069	exon4	G434A	R145Q	cnLOH
ADM210	exon15	1694_1705del	565_569del	CNLoss
ADM228	exon15	G1715A	W572X	cnLOH

Several assays were performed on these samples in order to validate my observations. Viability was assessed post-treatment using CellTiter-Glo, a measure of metabolic activity (ATP levels), as in previous experiments. Staining with Annexin V and 7AAD was also performed post-treatment with forodesine and dG. In addition, cell lysates were collected post-treatment for western blot. Some cells were also frozen in buffer for further RNA extraction if required. Finally, CyTOF was the main assay where cells were treated, stained and analysed 24h post-treatment with forodesine and dG.

6.4.1 Viability assessed by CellTiter-Glo

Viability was assessed 24h post-treatment with forodesine and dG. First, viability upon thawing of PBMCs was measured and cells with viability lower than 20% were not used (**Figure 6.8A**). CellTiter-Glo analysis was performed on PBMCs treated with forodesine and dG for 24h or 48h. The dose of forodesine and dG used was slightly higher (2 µM forodesine and 20 µM dG) than the one used in previous experiment in BMDMs but similar to the one used in my PBMC experiments. This was to match concentrations used in previous *in vitro* studies with forodesine on CLL PBMCs (Alonso et al., 2009; Balakrishnan et al., 2010a). At 24h, viability of *SAMHD1*^{mut} cells was significantly lower compared with cells in the *SAMHD1*^{nonmut} group upon forodesine and dG treatment (**Figure 6.8B**). In addition, *SAMHD1*^{mut} cells showed a significant decrease in viability only when treated with the combination of forodesine and dG and not with each compound alone. Similar results were observed at 48h, with *SAMHD1*^{nonmut} group showing a small reduction of viability upon forodesine and dG treatment (**Figure 6.8C**). This meant that most of the toxicity from

forodesine and dG treatment already happened within the first 24h, since no further decrease of viability was observed in the *SAMHD1*^{mut} group. On the other hand, cells in the *SAMHD1*^{nonmut} group showed a slightly lower viability upon treatment with forodesine and dG at 48h, suggesting that some cells were dying between 24 and 48h. These results showed a profound effect of forodesine and dG treatment on CLL PBMCs from the *SAMHD1*^{mut} group but not in the *SAMHD1*^{nonmut} group. This was reflected by low viability, as measured by ATP levels (CellTiter-Glo), a correlate of metabolic activity and therefore viability. It suggested that only *SAMHD1* mutated CLL cells were responding to treatment with forodesine and dG.

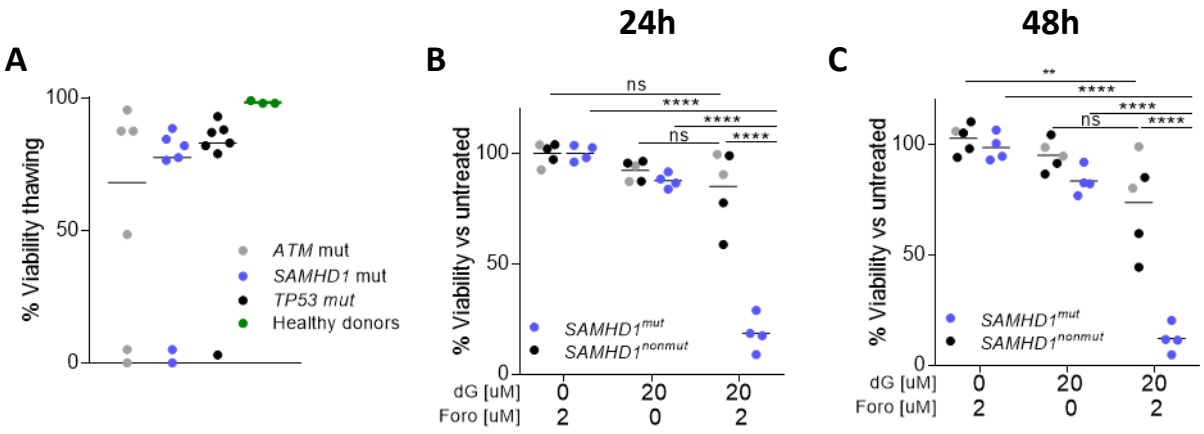


Figure 6.8 SAMHD1 mutated CLL cells are sensitive to forodesine and dG treatment. *(A) Viability of PBMCs upon thawing of vials, measured by Countess (ThermoFisher). (B-C) Viability of PBMCs from CLL patients thawed, rested for 3h, and treated with forodesine or dG at indicated concentration for 24h (B) or 48h (C). Dots represent cells from different patients, black dots are ATM mutated cells, grey are TP53 mutated cells and blue are SAMHD1 mutated cells. Bars are means and statistics are two-way ANOVA. ns,p>0.05, **p<0.01, ****p<0.0001.*

6.4.1.1 Viability measured by flow cytometry

To confirm cell death, staining with Annexin V and 7AAD was performed 48h post-treatment. Flow cytometry analysis showed numerous dead cells in the culture and only a small population in the gate represented in **Figure 6.9A,** which defined as “live cells”. Manual gating was used to identify this population, which according to forward scatter (FSC) and side scatter (SSC) features represents live cells. When gating on this population, no positive signal for Annexin V could be detected upon forodesine and dG treatment, suggesting the staining did not work. It became clear when looking at the live cell gates that the live population was totally depleted upon forodesine and dG treatment in the *SAMHD1*^{mut} group but not in the *SAMHD1*^{nonmut} control group. Therefore, detection of Annexin V^{+} cells was not possible with no cells left in that gate. Earlier time points would have probably allowed the detection of early apoptotic cells (Annexin V^{+}) upon treatment. Numerous dead cells were observed upon thawing of PBMCs, which is a common feature of clinical samples (personal information from Anna Schuh and Jenny Klintman), with CLL PBMCs known to grow poorly *in vitro*. A considerable loss of live cells was observed in *SAMHD1*^{mut} group compared with *SAMHD1*^{nonmut} upon forodesine and dG treatment (**Figure 6.9B**). Treatment with forodesine or dG alone did not have an effect. These results support the reduction of metabolic activity measured by CellTiter-Glo (**Figure 6.8)**. This showed that reduction in ATP levels correlated to the depletion of the live cells upon forodesine and dG treatment.

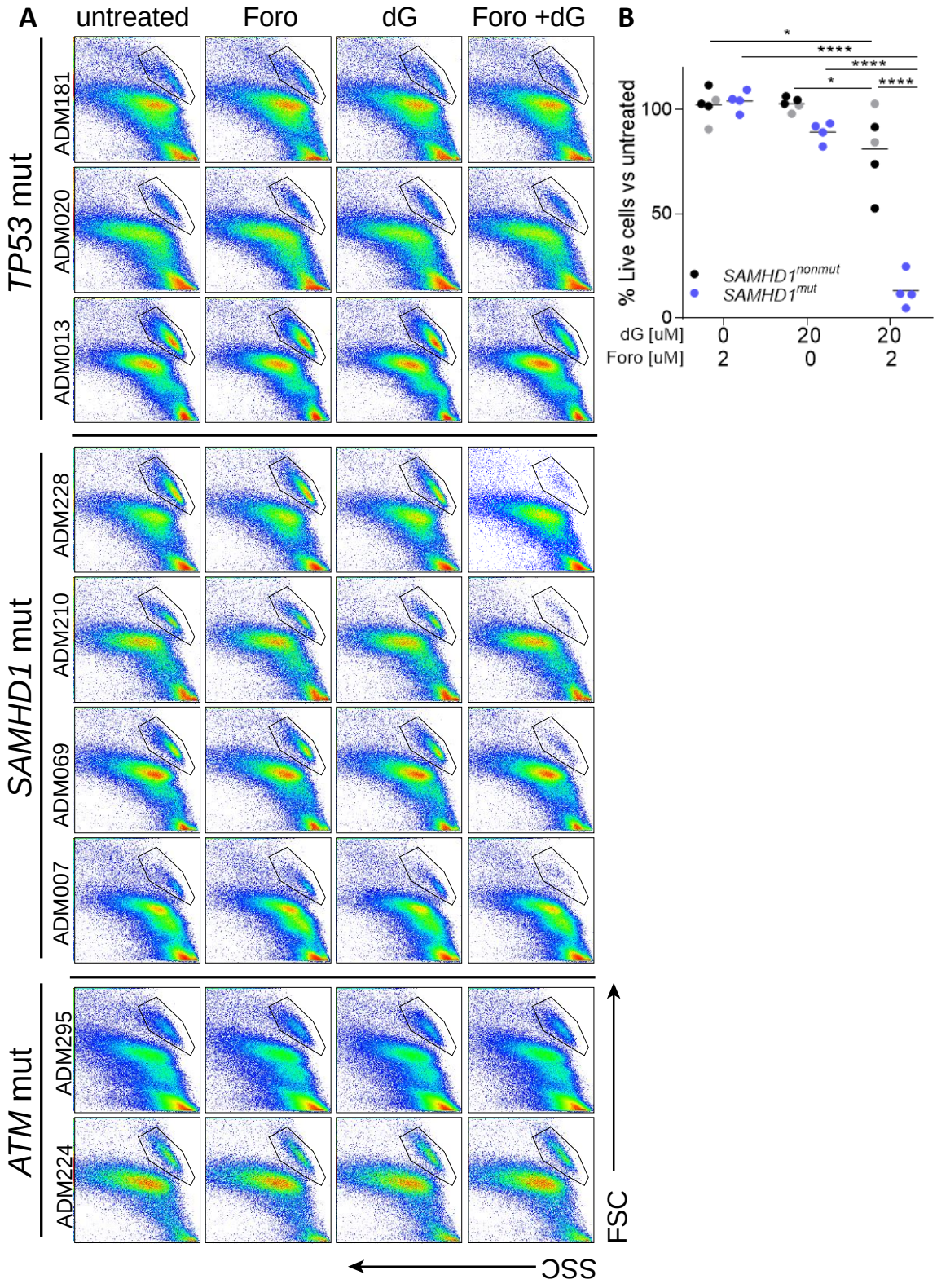


Figure 6.9 Forodesine and dG treatment kills SAMHD1 mutated cells. *(A) FACS plot of PBMCs 48h post treatment with 2 µM forodesine and 20 µM dG. (B) Quantification of live cells shown in gate represented in (A), untreated is set to 100%. Dots represent cells from patients, bars are means and statistics are two-way ANOVA. *p<0.05, ****p<0.0001.*

6.4.2 Viability assessed by western blot

Cell lysates from CLL patient samples were prepared 8h post-forodesine and dG treatment. Western blot of PARP, cleaved-PARP and cleaved-caspase 3 are shown in **Figure 6.10A** and **Figure 6.10B**. Each patient already showed detectable levels of cleaved-PARP when untreated. This reflects the flow cytometry data with numerous dead cells (**Figure 6.9A**). It suggested that cleaved-PARP was present in cells that were dead or dying upon thawing of the cells. Since levels of cleaved-PARP were already high, any increase in cleaved-PARP levels upon forodesine and dG treatment was difficult to detect. The sample ADM069 (*SAMHD1* mutated) showed decreased levels of full length PARP but no increase of cleaved-PARP. Sample ADM228, with *SAMHD1* mutation, is the only sample which showed a clear increase in cleaved-PARP levels upon forodesine and dG treatment (**Figure 6.10A**). Caspase 3 western blot showed similar results. Samples ADM069 and ADN210 from the *SAMHD1*^{mut} group showed a reduction in total caspase 3 levels but cleaved-caspase 3 was not detectable. Patient ADM228 with a *SAMHD1* mutation showed low cleaved-caspase 3 levels upon forodesine and dG treatment (**Figure 6.10B**). High background of cleaved-PARP made the detection of any change difficult. The sensitivity of cleaved-caspase 3 western blot reached its limit and its detection was too weak to interpret. Overall, this

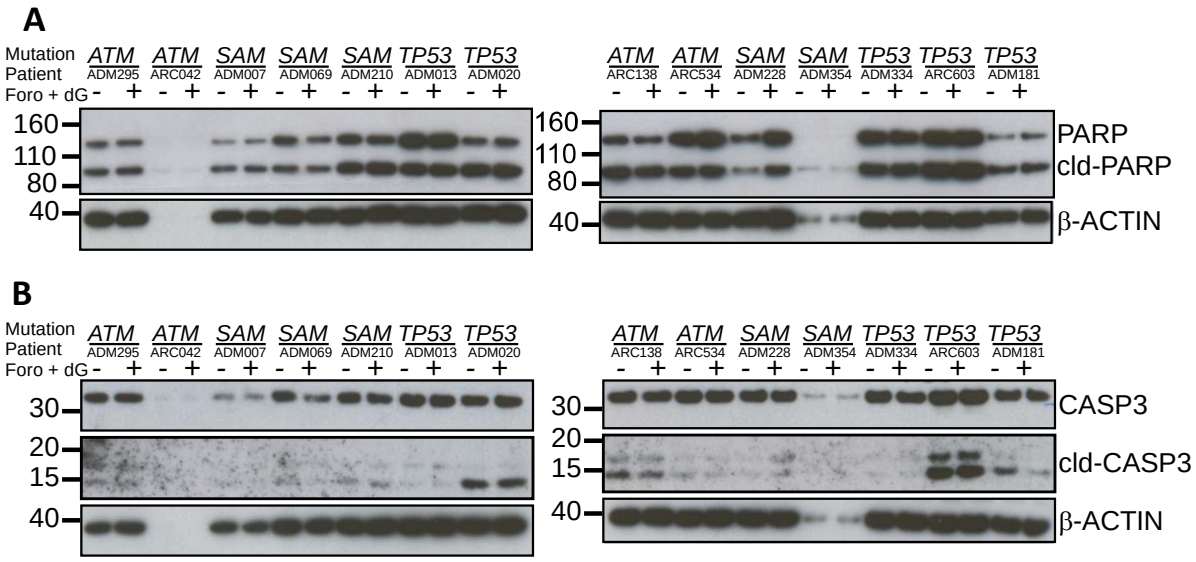


Figure 6.10 Detection of cleaved-PARP and cleaved-caspase 3 upon forodesine and dG treatment. *(A) Western blot of PARP and cleaved-PARP 8h post treatment with 2 µM forodesine and 20 µM dG or untreated in PBMCs from CLL patients with the indicated mutations. (B) Western blot of caspase 3 cleaved-caspase 3.*

supported the presence of dead cells upon thawing of the PBMCs, as observed previously with flow cytometry. It revealed the limitations of looking at cell death in total PBMCs by western blot, especially when most of them are already dead in the culture. Therefore, these data did not allow me to strengthen my observations.

6.4.3 Assessment of forodesine and dG toxicity with CyTOF

CyTOF is a powerful technique that I optimized with human PBMCs (see section 6.3.2). Here, CyTOF was used to characterize CLL PBMCs, to assess SAMHD1 expression and to identify the cell populations affected by forodesine and dG treatment.

Patients' CLL PBMCs were thawed, rested for a few hours and treated for 24h (2 µM forodesine and 20 µM dG). First, CLL B cells were identified as shown in **Figure 6.11A**. CLL B cells are characterised by the expression of both CD5 and CD19, whilst healthy B cells express only $CD19^+$. Quantification of CLL $CD5^+CD19^+$ B cells showed no difference in the frequency of $CD5^+CD19^+$ cells between the *ATM/TP53* and *SAMHD1* mutated groups (**Figure 6.11B**). Frequencies of $CD5^+CD19^+$ cells were variable within each group. In

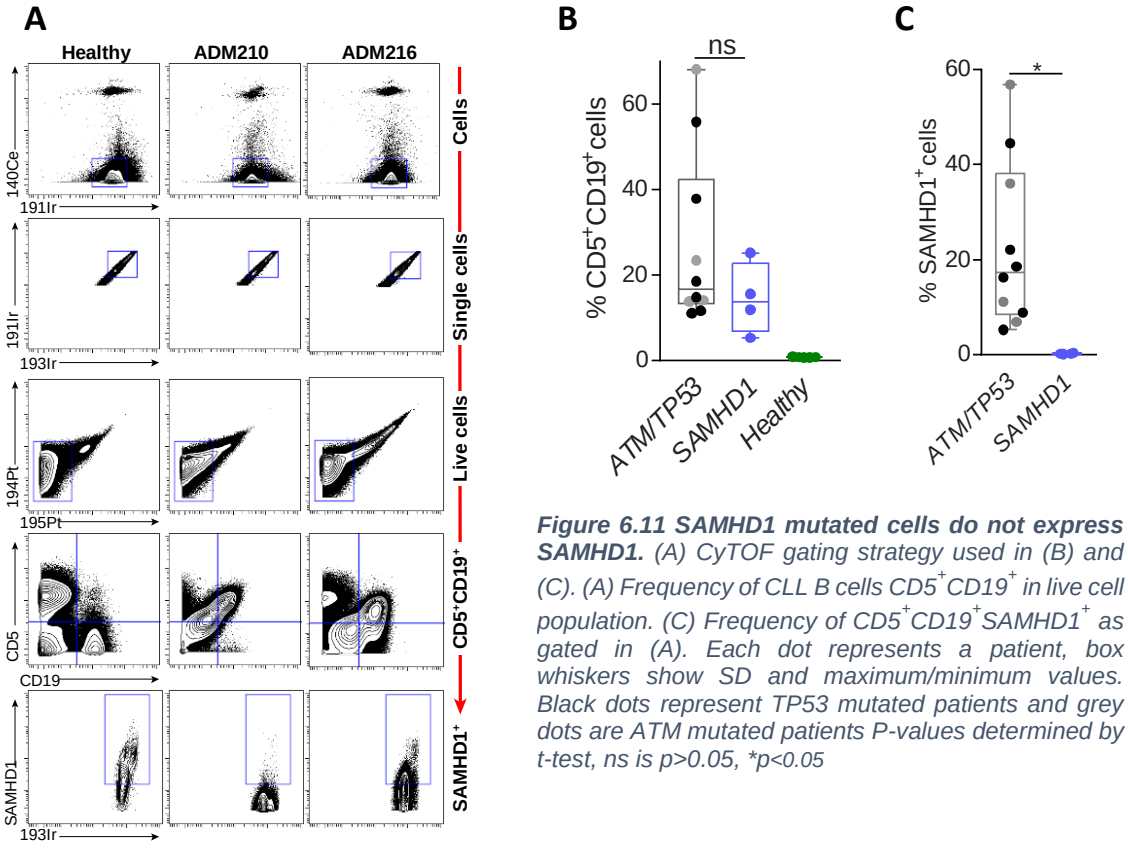


Figure 6.11 SAMHD1 mutated cells do not express SAMHD1. *(A) CyTOF gating strategy used in (B) and (C). (A) Frequency of CLL B cells $CD5^+CD19^+$ in live cell population. (C) Frequency of $CD5^+CD19^+SAMHD1^+$ as gated in (A). Each dot represents a patient, box whiskers show SD and maximum/minimum values. Black dots represent TP53 mutated patients and grey dots are ATM mutated patients P-values determined by t-test, ns is p>0.05, *p<0.05*

$CD5^+CD19^+$ cells, levels of $SAMHD1^+$ cells were variable within the *ATM/TP53* group with no differences between these two groups (**Figure 6.11B**). Importantly, all samples from the *SAMHD1* mutated group showed no detectable levels of SAMHD1 (**Figure 6.11C**), testifying that no functional SAMHD1 protein was expressed in these cells.

Next, tSNE plots were used to visualise CLL B cells. Due to the heterogeneity of the PBMCs from CLL patients, one tSNE analysis was performed per patient. Indeed, CLL cells are different between patients and running one tSNE analysis with all samples together resulted in representations were each patient's cells occupy a small different area of the plot. The tSNE analysis run used the default settings of perplexity, a knob that determines the numbers of nearest neighbours, and iterations, which represent the number of adjustments in the placement of events. PBMCs from healthy donors were characterized by very distinct islands, each representing a different cell population with all populations present in each donor (**Figure 6.12**). This was consistent with previous experiments. B cells were $CD19^+$ and also expressed low levels of SAMHD1. CLL samples displayed a different tSNE map, with a main island of cells that were mostly CD5 bright and CD19 bright, representing CLL B cells. Cells bright for CD5 and CD19 were also bright for SAMHD1 in *ATM* and *TP53* mutated patients. Samples from the *SAMHD1* mutated group did not show expression of SAMHD1, confirming that mutations in *SAMHD1* were loss-of-function with no protein expressed. When comparing tSNE plots between untreated and treated (2 µM forodesine and 20 µM dG), it was clear that the *SAMHD1* mutated group showed a loss of CLL B cells but other groups were unaffected (**Figure 6.12**). Using manual gating, the frequency of CLL B cells was compared between untreated and treated. The gating strategy was similar as before (**Figure 6.11A**). There was a significant decrease of $CD5^+CD19^+$ cells in the *SAMHD1* mutated group but not in the *ATM/TP53* group upon treatment (**Figure 6.13A** and **B**). Within the CLL B cells ($CD5^+CD19^+$ cells), a significant increase in median intensity of cleaved-PARP (**Figure 6.13C**) and cleaved-caspase 3 (**Figure 6.13D**) was detected upon forodesine and dG treatment only in *SAMHD1* mutated cells. No change was observed in the *ATM/TP53* control group.

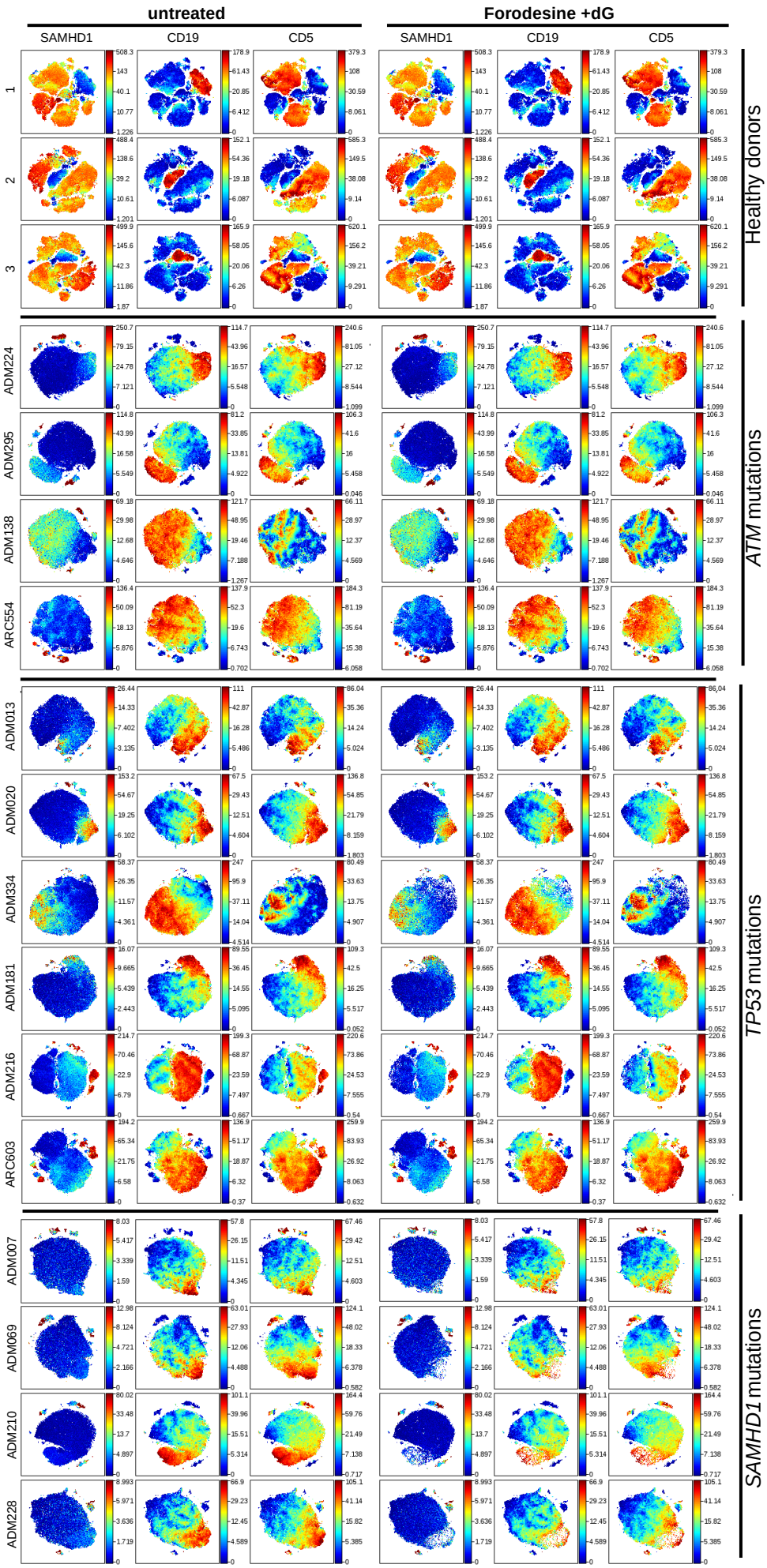


Figure 6.12 Loss of CD5⁺CD19⁺ cells in SAMHD1 mutated cells upon forodesine and dG treatment. *tSNE maps of healthy donors or PBMCs from CLL patients untreated or treated with 2 μM forodesine and 20 μM dG for 24h. One tSNE was generated per patient (untreated and forodesine + dG) on live cells using proportional sampling of 100 000 cells, 1000 iterations and 30 perplexity.*

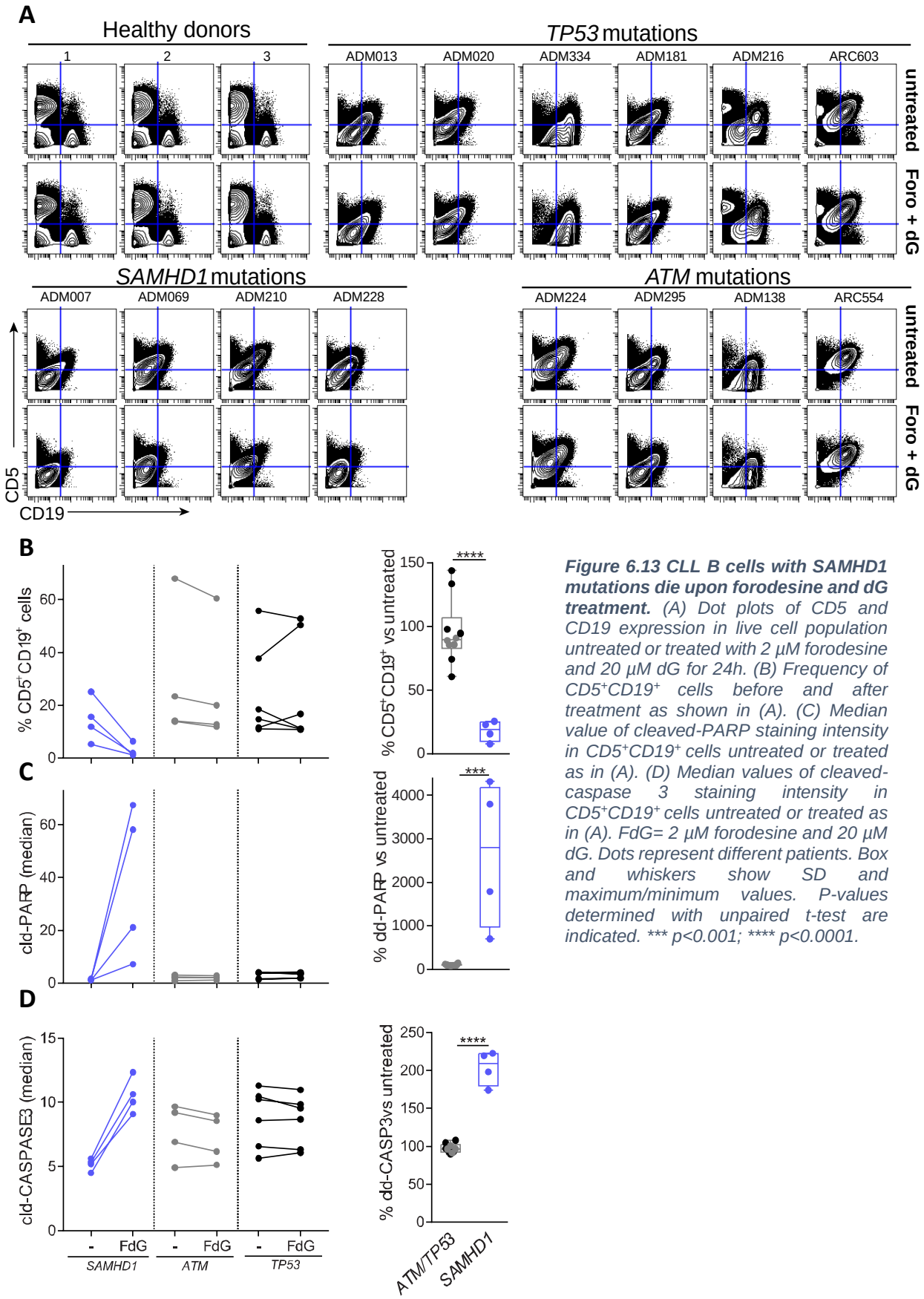


Figure 6.13 CLL B cells with SAMHD1 mutations die upon forodesine and dG treatment. *(A) Dot plots of CD5 and CD19 expression in live cell population untreated or treated with 2 μM forodesine and 20 μM dG for 24h. (B) Frequency of $CD5^+CD19^+$ cells before and after treatment as shown in (A). (C) Median value of cleaved-PARP staining intensity in $CD5^+CD19^+$ cells untreated or treated as in (A). (D) Median values of cleaved-caspase 3 staining intensity in $CD5^+CD19^+$ cells untreated or treated as in (A). FdG= 2 μM forodesine and 20 μM dG. Dots represent different patients. Box and whiskers show SD and maximum/minimum values. P-values determined with unpaired t-test are indicated. *** p<0.001; **** p<0.0001.*

Interestingly, CLL B cells appeared to have two populations differentiated by intracellular markers. The tSNE algorithm did not separate them since it uses only surface markers. When looking at the expression of phosphorylated p65 NFκB (p-p65 NFκB), phosphorylated p38 MAPK (p-p38 MAPK) and phosphorylated Stat1 (p-Stat1) two distinct populations became apparent (**Figure 6.14A**). I defined an "active" population characterised by high NFκB, MAPK and JAK/STAT (pSTAT1) signalling and an "inactive" population characterised by low expression of these markers. Representative examples of patients CLL B cells with either *ATM*, *TP53* or *SAMHD1* mutations showed that active and inactive CLL B cells were found in each group (**Figure 6.14A**). This was confirmed for each patient, although in some cases the inactive population was much smaller than the active one (data not shown). tSNE plots before and after forodesine and dG treatment clearly showed that *SAMHD1* mutated active B cells are lost 24h post-treatment (**Figure 6.14A**). This was consistent in all 4 *SAMHD1* mutated patients, in which active and inactive populations were also identified (**Figure 6.14B**). Heatmap analysis confirmed higher levels of p-p65 NFκB, p-p38 MAPK, p-Stat1 as well as CD27 in the active population. Surprisingly, although the inactive population was the only one remaining 24h post-treatment, these cells expressed higher levels of cleaved-PARP and cleaved-caspase 3, suggesting that they were dying. This suggested that both active and inactive CLL B cells lacking SAMHD1 were sensitive to forodesine and dG toxicity, albeit with different kinetics. Importantly, this demonstrated that forodesine and dG treatment can kill SAMHD1-deficient CLL B cells independently of their status.

All together these data revealed that forodesine and dG treatment killed *SAMHD1* mutated CLL B cells but had no effect when SAMHD1 was present.

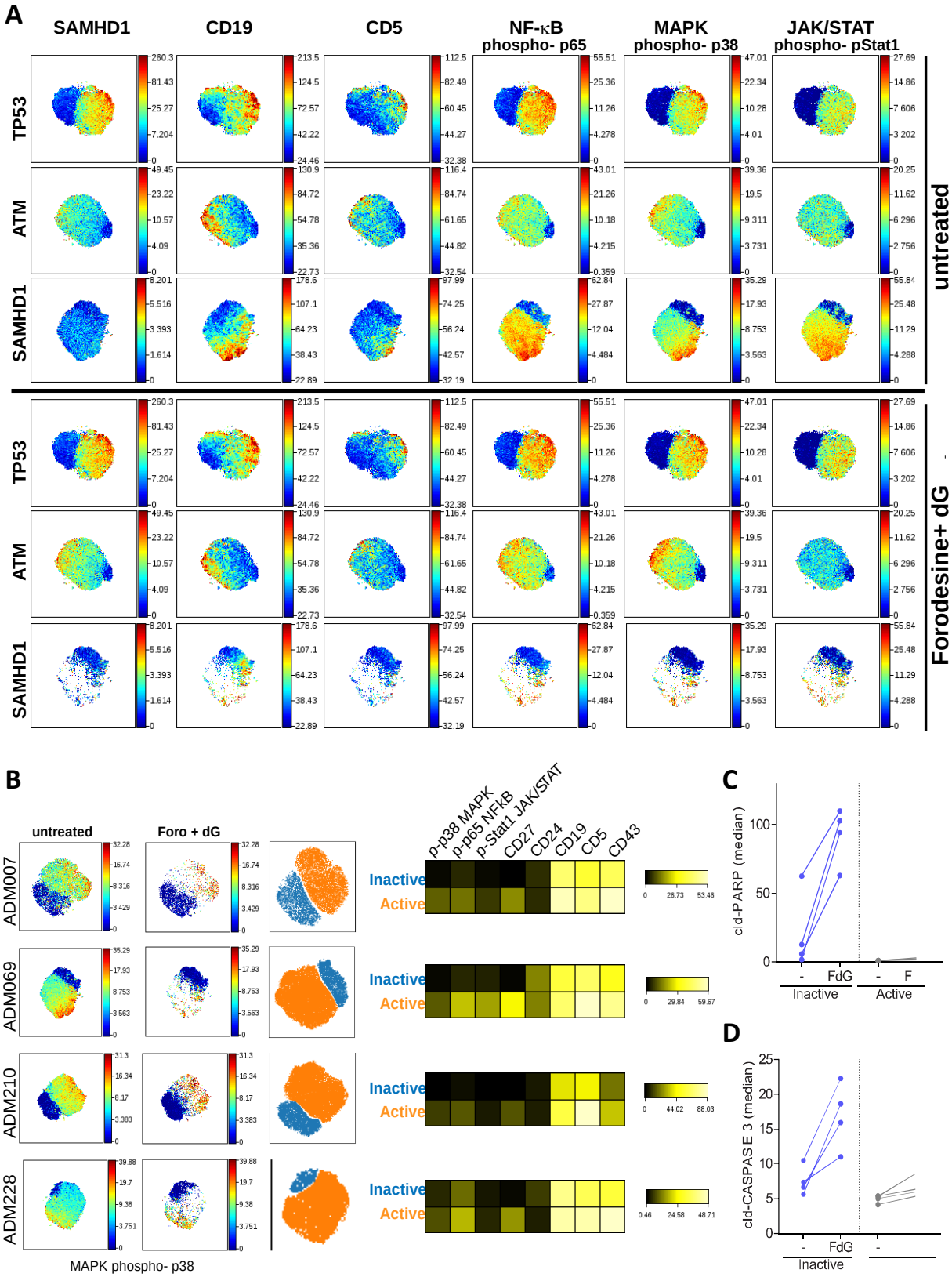


Figure 6.14 CLL B cells are active or inactive. *(A) tSNE maps generated on live CD5⁺CD19⁺ cells (as gated in Figure 6.11A) untreated or treated with 2 µM forodesine and 20 µM dG for 24h, one tSNE analysis per patient. One patient per group is represented. (B) tSNE maps of SAMHD1 mutated patients coloured by the phosphor-p38 MAPK channel, treated or untreated. From these tSNE plots, manual gating defined an inactive and an active population. Heatmaps represent expression of indicated channels in inactive and active CD5⁺CD19⁺ cells. (C-D) Intensity staining of the cleaved-PARP (C) or cleaved-caspase 3 (D) channel in active or inactive CLL B cells untreated or treated with 2 µM forodesine and 20 µM dG for 24h.*

6.5 Discussion

In this chapter, SAMHD1's role in forodesine treatment was investigated. A combination of forodesine and dG was used to kill *Samhd1*$^{-/-}$ BMDMs and had no effect on WT cells. Forodesine is a PNP inhibitor that prevents the degradation of dG, which is then converted into dGTP by dGK and dCK. Forodesine is used as an anti-cancer agent since the accumulation of dGTP in the cell is toxic. This suggested that dGTP would accumulate more efficiently in SAMHD1-deficient cells and trigger cell death by apoptosis. In line with previous studies, neither dG nor forodesine alone showed toxicity in my experiments (Balakrishnan et al., 2006). The combination of forodesine and dG showed strong toxicity by inducing apoptosis in *Samhd1*$^{-/-}$ but not in WT BMDMs. This supported a synergy of forodesine and dG *in vitro* to enhance the cytotoxic effect of the drug, as previously reported (Bantia et al., 2001). *In vivo*, treatment of forodesine was shown to trigger elevation of dG in the plasma, increasing the lifespan of SCID mice transplanted with human peripheral blood lymphocytes, a model of human immune function (Bantia et al., 2001). The authors chose this particular transplant model claiming that mouse T cells do not accumulate dGTP as human T cells do. It would be interesting to determine if the variable efficacy of forodesine between mouse and human T cells is due to different expression levels of SAMHD1 or dCK/dGK in these cells. Bantia et al. showed that forodesine has to be combined with dG *in vitro*, to mimic the elevation of plasma dG observed *in vivo* and to cause toxicity. The elevation of plasma dG was also observed in leukaemic patients, and the combination of forodesine and dG has been used *in vitro* in later studies (Alonso et al., 2009; Balakrishnan et al., 2006). It is not entirely clear how dG concentration raises in the blood of patients treated with forodesine. Early studies on PNP-deficiency revealed that erythrocytes accumulates dGTP (Cohen et al., 1978; Gabrio et al., 1956). This suggests that erythrocytes do not express SAMHD1, which is supported by their lack of nucleus. It will be interesting to test whether erythrocytes express SAMHD1 by staining with an antibody against SAMHD1 by flow cytometry or western blot. I speculate that erythrocytes accumulate dG and dGTP when PNP inhibitors are used, triggering their transport outside of the cell, and rising the concentration of dG and dGTP in the blood. Since erythrocytes do not contain

mitochondria, the absence of toxicity of PNP inhibitors in the cells supports the hypothesis of mitochondria dysfunction as the origin of dG-induced apoptosis. My results demonstrate that forodesine and dG killed SAMHD1-deficient BMDMs.

To validate these findings, the human T cell line Jurkat was used. Jurkat cells do not express SAMHD1 and were ten times more sensitive to forodesine and dG treatment compared with SAMHD1-deficient BMDMs. Hypersensitivity of Jurkat cells to dG, compared with mouse and human SAMHD1-deficient cells, suggests that dGTP accumulates more in these cells. This is in line with reports suggesting that human T cells express higher levels of dCK and dGK, supported by lymphopenia observed in PNP deficient patients (Simmonds et al., 1982). Indeed, dCK is known to be important in T cell and B cell development (Toy et al., 2010). To test whether Jurkat cells express higher levels of dGK and dCK, RT-qPCR and western blot could be performed. When SAMHD1 was expressed in Jurkat cells, no cell death was observed upon forodesine and dG treatment. Both WT SAMHD1 (nuclear) and the cytosolic mutant SAMHD1 K11A protected the cells efficiently against forodesine and dG treatment. Interestingly, the K11A mutant seemed to show slightly better protection, suggesting that degrading dGTP in the cytosol is slightly more efficient than in the nucleus. This makes sense since the conversion of dG into dGTP happens in the mitochondria and the cytosol (Jüllig and Eriksson, 2000). It will be interesting to determine whether dGTP accumulation happens in the mitochondria or in the cytosol. This will show whether dCK or dGK is mostly responsible for the conversion of dG into dGMP (and subsequently dGTP). dNTP quantifications on mitochondrial and cytosolic fractions could address this question. These data demonstrate that the combination of forodesine and dG kills SAMHD1-deficient human cancer cell lines by apoptosis. Expression of SAMHD1 protected them from this toxicity.

The finding that SAMHD1 plays a critical role in limiting forodesine's mechanism of toxicity is new and could explain the limited efficacy of forodesine in clinical trials. The early studies on PNP deficiency and PNP inhibitors were performed before the discovery of SAMHD1

and the characterisation of its dNTPase function. Therefore my data suggest that SAMHD1 limits the toxicity of forodesine.

The next step to determine the clinical relevance of these findings was to determine whether SAMHD1 can protect against forodesine toxicity in patient's samples. Since *SAMHD1* is mutated in CLL, PBMCs from CLL patients with or without *SAMHD1* mutations were obtained to test SAMHD1's protection against forodesine and dG efficacy *in vitro*. The first step was to determine whether forodesine and dG would have an effect on SAMHD1-deficient PBMCs. Since PBMCs mostly express SAMHD1, VLP_{vpx} were used to target SAMHD1 for degradation and to sensitize the cells to forodesine and dG treatment. Vpx-targeted PBMCs showed a significant increase of early apoptotic cells upon treatment with forodesine and dG, compared with controls. However, in PBMCs, the phenotype was not as strong as previously observed. Limited efficacy of forodesine and dG treatment may be due to restricted infection of some cell subsets with VLP_{vpx} to some subsets. If only a small fraction of the cells were depleted for SAMHD1, only these were expected to die upon forodesine and dG treatment.

Viability assessment, by quantifying at ATP levels or apoptotic cells in total PBMCs, showed only weak evidences of cell death of VLP_{vpx} treated PBMC upon forodesine and dG treatment. This illustrates the limitations of the CellTiter-Glo assay when measuring the average of all cells in a well. Indeed, PBMCs contain various different cell types, that may react differently or not to forodesine and dG treatment. Specific efficacy of treatment in a small population, can be missed when using a technique measuring bulk PBMCs. Therefore, a different approach needed to be used to overcome these drawbacks. Single cell techniques are key to better understand mechanisms that affect specific cell populations within PBMCs. CyTOF was chosen as a powerful technique to investigate the cytotoxicity of forodesine and dG treatment in CLL samples and was first tested on healthy PBMCs.

The antibody panel was designed, optimised and tested on healthy PBMCs infected with VLP_{vpx} or VLP_{ctrl} and treated with forodesine and dG. tSNE maps showed the heterogeneity of SAMHD1 expression in PBMCs, with the lowest expression in B cells and the highest

expression in myeloid cells. Interestingly, SAMHD1 was more phosphorylated in monocytes and levels were low in other cell types. This is consistent with resting PBMCs being non-cycling, and thus SAMHD1 not being phosphorylated and active. It suggests that monocytes were not expressing active SAMHD1 since its phosphorylation prevents the formation of stable active tetramers. This was the first time SAMHD1 and its phosphorylation were evaluated with CyTOF in PBMCs. It highlighted the power of the technique and it justified its use to investigate the toxicity of forodesine and dG in clinical samples. Infection of resting PBMCs with VLP_{vpx} induced reduction of SAMHD1 expression only in monocytes. CyTOF revealed that Vpx efficacy was limited to monocytes, demonstrating how a bulk technique such as CellTiter-Glo can underestimate the loss of viability in specific cell subsets by looking at average measurements. Surprisingly, VLP infection induced a reduction in the levels of pSTAT1 in several subsets. This underscores the importance of control vectors to distinguish VLP and Vpx-related effects. Treatment of VLP_{vpx} infected PBMCs with forodesine and dG only had a minor effect. Monocytes appeared to be the target population of Vpx, but the infection with VLPs induced loss of these monocytes. Hence, it was challenging to assess any loss of monocytes upon forodesine and dG treatment. Nonetheless, these experiments successfully validated my CyTOF panel. CyTOF allowed to look deeper in cell populations expressing SAMHD1 and to assess the effect of forodesine and dG treatment on specific subsets. To summarise, these data unveiled that:

- SAMHD1 is expressed in PBMCs with heterogeneous expression in different cell types. B cells have lowest levels of SAMHD1.
- Monocytes have high levels of pSAMHD1 compared with all other populations.
- VLP_{vpx} infection reduced SAMHD1 expression in myeloid cells.
- VLP_{vpx} infection induced partial loss of myeloid cells.
- Forodesine and dG treatment induced loss of myeloid cells.
- Forodesine and dG had no effect on cell populations expressing SAMHD1

The panel allowed me to quantify SAMHD1 expression and its phosphorylation at a single cell level. These data showed that VLP_{vpx} targeted myeloid cells which then die upon

treatment with forodesine and dG. This supports our model in which forodesine and dG kills SAMHD1 deficient cells and validate the technique.

Next, I investigated the toxicity of forodesine and dG treatment in clinical samples from CLL patients carrying *SAMHD1* mutations. PBMCs from CLL patients with *SAMHD1* mutations showed depletion of CLL B cells in response to forodesine and dG. On the other hand, cells mutated in *ATM* or *TP53* remained unaffected. ATP levels were not reduced when forodesine and dG were used alone and only their combination reduced viability of *SAMHD1* mutated cells. CyTOF confirmed that CLL B ($CD5^+CD19^+$) cells with *SAMHD1* mutations did not show detectable levels of SAMHD1, meaning that they were loss-of function mutations. At 24h, more than half of the $CD5^+CD19^+$ cells in the *SAMHD1* mutated group were depleted upon forodesine and dG treatment.

Identification of an active and an inactive population in CLL B cells highlighted different kinetics of forodesine and dG toxicity. At 24h, the active population had died in *SAMHD1*-mutated CLL B cells, while the inactive cells remained. Interestingly, the remaining inactive population showed elevated levels of cleaved-PARP and cleaved-caspase 3, both hallmarks of apoptosis. This suggested that the remaining inactive CLL B cells were initiating apoptosis and therefore they would probably be dead at a later time point. Forodesine and dG treatment may follow different kinetics of cytotoxicity in the active and inactive populations. This supports the hypothesis that SAMHD1-deficient CLL B cells die by apoptosis upon forodesine and dG treatment, independently of their signalling status. These experiments on clinical samples confirmed that SAMHD1 is an enzyme that limits forodesine and dG efficacy.

The identification of an active B cell population with these characteristics is not surprising. CLL B cells have been reported to have an altered MAPK-Erk signalling pathway (Shukla et al., 2018). Constitutive activation of p38 MAPK has been shown to be critical for their survival (Ringshausen et al., 2004). In addition, mutation in *NFKBIE* encoding IκBε, a negative regulator of the NFκB signalling pathway, were reported in ~10% of advanced stage CLL patients and are associated with poor outcome (Damm et al., 2014; Mansouri et al.,

2015). Phosphorylation of Stat1 is a hallmark of active JAK/STAT signalling, found downstream of the B cell receptor signalling pathway, which can be constitutively activated in CLL (Rozovski et al., 2014). JAK/STAT inhibitors are a class of drugs being developed that targets this pathway to kill leukaemic cells. The CLL B cell population I defined as active gather all these characteristics. The existence of an inactive population suggests that drug inhibitors targeting the signalling of NFκB, MAPK or JAK/STAT will be limited to this active population, which may not be ideal. It will be interesting to track these active and inactive compartment before and after therapy. Forodesine and dG seem to act on both active and inactive CLL B cells that carry *SAMHD1* mutations with different kinetics. This may constitute an advantage when using PNP inhibitors instead of inhibitors of these signalling pathways. The loss of the active population is profound: depleted within 24h, while the inactive population displayed the hallmarks of apoptosis at 24h, suggesting that they need more time to accumulate dGTP and engage the cell death process. It is not clear why the active population has faster kinetics. I could hypothesise that the background levels of proteins involved in programmed cell death are higher, such as caspases and BCL-2 proteins. Another explanation could be that the the enzymes of the nucleotide salvage pathway are upregulated in the active population, resulting in a faster conversion and accumulation of dGTP in these cells.

These results suggested that the limited efficacy of forodesine in clinical trials is attributed to SAMHD1. I hypothesise that patients with CLL or T-ALL who responded well to forodesine treatment in previous clinical trials carry a *SAMHD1* loss-of-function mutations. *SAMHD1* is mutated in 11% of refractory CLL and 20% of T-cell prolymphocytic leukaemia (Clifford et al., 2014; Johansson et al., 2018). In CLL, the response rate to forodesine in trials correlates with the percentages of patients expected to carry *SAMHD1* mutations.

These findings suggest that forodesine should only be aimed at leukaemic patients with *SAMHD1* loss-of-function mutations where a potent toxicity is predicted. This new important role of SAMHD1 in forodesine treatment adds to the knowledge that can be used in precision oncology, the molecular profiling of tumours to identify targetable alterations

(Schwartzberg et al., 2017). It has become clear that one treatment does not fit for all cancers and therefore delivering the right treatment to the right patient at the right dose and at the right time is key. Better understanding the mechanisms of action of each drug with a comprehensive understanding of the pathway involved is essential to develop precision medicine. Identifying the role of SAMHD1 in forodesine treatment together with the identification of *SAMHD1* mutations in some leukaemias, may become relevant in the clinic.

The first step to validate this discovery will be to set up a clinical trial enrolling only leukaemic patients with *SAMHD1* mutations to treat with forodesine. Patients' stratification according to their genetic profile should be developed. It is important to mention that it is not possible to predict the impact of a mutation in *SAMHD1*, therefore, detection of the protein by flow cytometry or western blot should be used to confirm its presence or absence. There are good antibodies available for SAMHD1. However, a quick an easy assay available in the clinic, to test for SAMHD1 expression and function, remained to be developed. A successful trial would encourage the development of an easy screening test in the clinic to determine SAMHD1 expression or activity in leukaemic cells. This could be used to predict patients respond to forodesine.

In summary, these data showed that SAMHD1 plays a major role in protecting cells against forodesine and dG *in vitro* and *ex vivo*.

6.6 Conclusion

This chapter divulged that SAMHD1 protects cells against forodesine and dG treatment. In addition, forodesine and dG had a profound effect on PBMCs from CLL patients with *SAMHD1* mutations. In our model, forodesine induces the accumulation of dG and dGTP, as observed in PNP deficient patients (Chan, 1978; Cohen et al., 1978; Simmonds et al., 1987). In SAMHD1-deficient cells, the excess of dGTP cannot be degraded and becomes toxic (**Figure 6.15**).

Since forodesine and dG were used *in vitro* to mimic the effect of forodesine treatment alone in patients, it suggests that forodesine treatment will be extremely potent in CLL patients with *SAMHD1* loss-of-function mutations. The presence of functional SAMHD1 in many patients probably explains why forodesine showed limited efficacy in clinical trials. A new clinical trial looking at forodesine efficacy in a cohort of leukaemic patients with *SAMHD1* loss-of-function mutations is the obvious next step. If this is confirmed, forodesine could be used as precision medicine in leukaemic patients carrying a *SAMHD1* loss-of-function mutation.

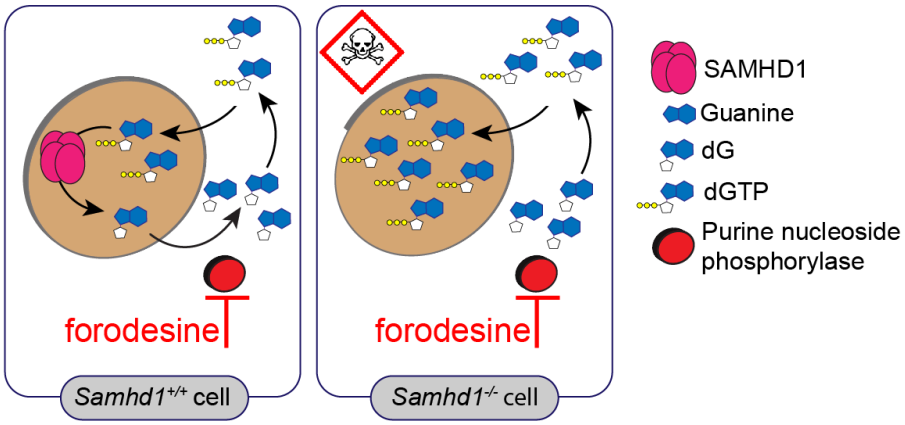


Figure 6.15 Model of forodesine toxicity in SAMHD1-deficient cells.

Chapter 7. CONCLUSIONS AND FUTURE WORK

Summary

The work presented in this thesis aimed to identify and characterise SAMHD1's ancestral function in dNTP metabolism. The overall picture that emerges from this work is a novel important role for SAMHD1 in safeguarding cells against dNTP-induced cell death. In the absence of SAMHD1 and its dNTPase function, upon supplementation of dNs, dNTPs accumulate in the cell to cause intrinsic apoptosis. Interestingly, dGTP appeared to be the most toxic dNTP for reasons that remain to be elucidated. The phenotype of dG-induced apoptosis in SAMHD1-deficient cells was observed in murine and human cells, including primary cells and transformed cells. This suggested a conserved mechanism of protection by SAMHD1 against dNTP overload induced cell death. Another new observation, namely dG sensing by TLR7 that triggered an immune response, was also investigated. Cytokine production resulting from dG signalling had no effect on dG-induced apoptosis. I connected SAMHD1's mechanism of protection against dG treatment with the mechanism of action of forodesine, a purine nucleoside phosphorylase (PNP) inhibitor. PNP is the enzyme responsible for the degradation of dG in the cell. PNP inhibitors have been used as anti-cancer agents to trigger accumulation of dG and dGTP in the cell and subsequent toxicity. Forodesine has been tested in clinical trials against leukaemia, which showed limited efficacy for reasons that remain unknown. Both low dose of forodesine and dG and high dose of dG induced dGTP-induced apoptosis of SAMHD1-deficient cells. A synergy between dG and forodesine was observed in cells lacking SAMHD1, identifying SAMHD1 as a key enzyme which limits forodesine's toxicity. Importantly, the combination of dG and forodesine selectively killed SAMHD1-deficient CLL B cells.

SAMHD1 was identified as a restriction factor for HIV, and has been studied extensively in the context of lentiviral infections since then (Hrecka et al., 2011; Laguette et al., 2011). SAMHD1 is highly conserved from marine invertebrates to man (Rice et al., 2009), whereas lentiviruses evolved more recently. This suggests that restriction of lentiviral infections is an adaptation of SAMHD1's biochemical activity to degrade dNTPs, which perhaps has a more

ancestral function in cellular dNTP metabolism. I propose that SAMHD1's ancestral function is to safeguard the cell death from dNTP excess that could trigger intrinsic apoptosis. Indeed, my data demonstrated that intracellular dNTP concentrations were only marginally altered in WT cells exposed to extracellular dNs, while SAMHD1-deficient cells accumulated large dNTP pools. Concomitantly, cells lacking SAMHD1 succumbed to apoptotic cell death.

SAMHD1 protects cells against dNTP overload

My investigation revealed that all four dNs were toxic in SAMHD1-deficient cells, with dG being the most toxic. dG was converted to dGTP. Most likely, this involved the nucleotide salvage pathway and was initiated by the action of dGK and dCK which convert dG into dGMP, located in the mitochondria and in the cytoplasm, respectively. Higher cytotoxicity of dG compared with other dNs may be related to baseline dGTP concentrations that are lower than those of the three other dNTPs (dTTP>dATP>dCTP>dGTP). These results are consistent with the dNTP pool asymmetry consistently observed in mammalian cells, with similar dNTP ratios (Mathews and Ji, 1992). This results in particularly pronounced dNTP imbalances upon dG feeding. dNTP pools are highly controlled and dNTP imbalances can enhance mutagenesis, stimulate genomic recombination, cause chromosomal abnormality, induce DNA breaks and cause cell death (Kunz et al., 1994; Reichard, 1988). Increase of one dNTP results in the depletion of other dNTPs through RNR, and subsequent cell cycle arrest. However, dNTP imbalances with no limiting dNTPs, even at mutagenic concentrations, does not trigger cell cycle arrest (Kumar et al., 2010). Mitochondrial dNTP pools are distinct from the nuclear dNTP pools with a higher spontaneous mutation rate (Marcelino and Thilly, 1999). Interestingly, dNTP ratios are different in the mitochondria with dGTP being the most abundant (Mathews, 2006). Therefore, the accumulation of dGTP caused by dG feeding in SAMHD1-deficient cells may have different consequences in the nucleus and in the mitochondria. The mitochondrial localisation of dGK suggests that dG is converted into dGTP in the mitochondria and therefore that imbalanced dGTP pools cause cytotoxicity in the mitochondria. dGTP-toxicity was independent of genomic replication,

excluding an effect of dGTP imbalance on genomic DNA and supporting an effect on the mitochondrial genome.

In addition, dGTP allosterically regulates RNR, preventing dCTP production through the *de novo* pathway (Moore and Hurlbert, 1966). Consistent with this idea is our observation that the toxicity of dG was reduced when added together with dC, providing dCTP via the salvage pathway. Interestingly, dGTP's mechanism of toxicity was independent of DNA synthesis. This suggested that regulation of RNR by dGTP and subsequent downregulation of dNTP synthesis by RNR and dNTP starvation is not the mechanism of toxicity. It is possible that dNTP imbalances disrupt replication or repair of mitochondrial DNA, resulting in mitochondrial stress and subsequent apoptosis (Arpaia et al., 2000; Franzolin et al., 2015). Alternatively, dGTP might be involved more directly in the activation of apoptosis, as reported for dATP (Reubold et al., 2009; White et al., 2017). Nonetheless, the precise molecular mechanism by which dNTP imbalances in SAMHD1-deficient cells result in apoptosis remains to be fully elucidated.

Deoxyguanosine induces a TLR7-dependent cytokine response

Cell death induced by dG in SAMHD1-deficient cells was accompanied by detectable levels of cleaved-PARP and cleaved-caspase 3. The release of cytochrome C from mitochondria into the cytosol was also detected, indicative of cell-intrinsic apoptosis. Attempts to block apoptosis with inhibitors failed and the combination of the pan caspase inhibitor zVAD with dG treatment caused TNFα-induced necroptosis in WT cells with minimal effects on *Samhd1*$^{-/-}$ cells. Gene expression analysis post-dG treatment revealed the upregulation of hundreds of genes in a MyD88-dependent manner in both WT and *Samhd1*$^{-/-}$ BMDMs and TLR7 was identified as the dG sensor. Earlier work by others determined the crystal structure of TLR7 and revealed that this receptor recognises guanosine and poly U at two distinct sites (Zhang et al., 2016). In addition, combination of dG and poly U was shown to activate the NFκB pathway and to induce IFNα and IL-12p40 production in mouse DCs as well as IL-12p40 production in BMDMs (Shibata et al., 2015). Therefore, our observation that dG signals alone through TLR7 is an unexpected observation that contradicts this

paper. Additional experiments are required to exclude the presence of ORNs in the culture media, which could contribute to the signalling of dG through TLR7. The identification of TLR7 as the dG sensor allowed me to determine the impact of cytokine production on dG-induced apoptosis. dG-induced apoptosis was observed in *Samhd1*$^{-/-}$*Myd88*$^{-/-}$ and *Samhd1*$^{-/-}$*Tlr7*$^{-/-}$cells, similarly to what was seen in *Samhd1*$^{-/-}$ cells, showing that the cytokines were not impacting the cell death phenotype. This is supported by the observation that the human cancer lines used, which are unlikely to express TLR7, were able to induce dG-triggered apoptosis. Nevertheless, the absence of cytokine production in cancer cell lines upon dG treatment remains to be confirmed. It will be interesting to test other cell types expressing TLR7 such as B cells and pDCs, to determine whether they can also sense dG alone. The investigation of the TLR7-dependent cytokine production upon dG sensing concluded that the cytokine production was not required for dG-induced apoptosis in SAMHD1-deficient cells. Therefore, future experiments were carried out without considering dG sensing by TLR7 and subsequent cytokine production.

Deoxyguanosine kills SAMHD1-deficient cancer cells

SAMHD1 also protected cancer cells from dG-induced apoptosis *in vitro*. This revealed that its dNTPase function was active in dividing cells, in line with the idea that SAMHD1's dNTPase activity is not regulated by phosphorylation in cycling cells (Tramentozzi et al., 2018; White et al., 2013). The well described mechanism of SAMHD1 phosphorylation through the cell cycle regulates its anti-viral activity (Badia et al., 2016; Cribier et al., 2013; Pauls et al., 2014a; Pauls et al., 2014b; Schott et al., 2018), but it remains unclear whether it also controls its dNTPase activity (Goldstone et al., 2011; Lahouassa et al., 2012; St Gelais et al., 2012). My data demonstrated that SAMHD1 protects cells from dG-induced apoptosis independently of the cell cycle. This supports the recent publication showing that SAMHD1's dNTPase function is not regulated by phosphorylation and the cell cycle (Tramentozzi et al., 2018). I propose that in the presence of high dNTPs, or dNTP imbalances (especially of dGTP), binding of dNTPs to allosteric sites overcomes T592 phosphorylation that may otherwise destabilise and inactivate the enzyme. Nevertheless, it

will be interesting to characterise SAMHD1's phosphorylation status in treated cells to confirm this hypothesis. Therefore, the protective role of SAMHD1 against dGTP accumulation is not limited to a specific phase of the cell cycle.

These findings were not supported *in vivo* by the B16F10 melanoma tumour model. Although SAMHD1-deficient B16F10 melanoma cell were sensitive to dG-induced apoptosis *in vitro*, their tumour growth was not reduced by dG treatment. The use of SAMHD1-deficient melanoma tumours revealed a slower growth of these tumours compared with WT, which was an interesting observation. Elevated dNTP levels impact genome integrity by increasing mutagenesis (Bester et al., 2011; Reichard, 1988; Wheeler et al., 2005). This should confer cancer cells an advantage, unless persistent stalling of replications forks slows down fork progression and triggers cell death. On the other hand, it has been shown that SAMHD1-deficient cells release ssDNAs from stalled replication forks; they accumulate in the cytosol and are sensed by the cGAS-STING pathway (Coquel et al., 2018). This novel mechanism induces the production of type I IFN through the cGAS-STING pathway in SAMHD1-deficient cells and therefore could result in higher immunogenicity of *Samhd1*$^{-/-}$ B16F10 tumour cells, and reduced tumour growth. It would be interesting to reduce the inoculum to test if the host immune system can prevent the establishment of SAMHD1-deficient tumours compared with WT. A mouse model of leukaemic cancers would be more appropriate since *SAMHD1* mutations are present in CLL and T-cell prolymphocytic leukaemia (Clifford et al., 2014; Johansson et al., 2018). Mouse lines that spontaneously develop leukaemia are currently the best models despite being time consuming (Kohnken et al., 2017). The proto-oncogene T-cell leukaemia 1 (TCL1) is expressed in pre-B cells and early T-cell precursors. The Eμ TCL1 (also called TCL1-tg) transgenic mouse model has been used as CLL model (Bresin et al., 2016; Gorgun et al., 2009). These mice spontaneously develop CLL and injection of their CLL cells into recipient mice can be used to test the effect of cancer treatment *in vivo* (Carter et al., 2017). Crossing Eμ TCL1 with our *Samhd1*$^{-/-}$ mice would generate the ideal mouse model to study the effect of dG (or forodesine) treatment on *Samhd1*$^{-/-}$ CLL cells. The Eμ TCL1 mice can be

purchased and crossed with our *Samhd1*$^{-/-}$ to obtain double knock out mice, which will eventually develop CLL. The process would take ~8 months (mice breeding and CLL development in knock out mice), after which *Samhd1*$^{-/-}$ CLL cells could be transferred into recipient mice and the experiments performed (another 2-3 months). This constitutes a reliable model of SAMHD1-deficient CLL. Previous studies treating CLL patients with forodesine observed the elevation of dG in the plasma of these patients. Therefore, it will be interesting to determine whether it also happens *in vivo*, and the impact it would have on different immune cell. Taken together, SAMHD1 safeguards cancer cells from dGTP-induced apoptosis *in vitro*.

Deoxyguanosine synergises with forodesine to kill SAMHD1-deficient cancer cells

The PNP inhibitor forodesine is used as anti-leukaemic agent. Inhibiting PNP results in the accumulation of dG and dGTP, which is toxic to cells (Alonso et al., 2009; Balakrishnan et al., 2006; Gandhi and Balakrishnan, 2007; Gandhi et al., 2005). Therefore, using forodesine results in the same situation as feeding dG to SAMHD1-deficient cells. Forodesine was developed more than a decade ago when SAMHD1's function was unknown. I bridge the two phenomena and hypothesised that SAMHD1 limits forodesine efficacy. This is particularly relevant since forodesine has been tested in clinical trials against CLL, a disease presenting *SAMHD1* mutations in ~11% of cases (Clifford et al., 2014). These clinical trials reported beneficial effects of forodesine in some but not all patients with B or T cell malignancies (Alonso et al., 2009; Balakrishnan et al., 2006; Balakrishnan et al., 2013; Balakrishnan et al., 2010b; Dummer et al., 2014; Gandhi and Balakrishnan, 2007; Gandhi et al., 2005; Makita et al., 2018; Ogura et al., 2012), an observation that thus far has lacked an explanation. I demonstrated that PBMCs from CLL patients with *SAMHD1* loss-of-function mutations responded well to forodesine compared with the control group. The CyTOF analysis revealed that CLL B cells identified by CD19 and CD5 staining contained two sub-populations of cells, distinguishable by their expression of CD27 and phosphorylation of p65, p38 and STAT1. Activation of NFκB, MAP kinase and STAT signalling pathways have been reported in CLL (Frank et al., 1997; Herishanu et al., 2011;

Ringshausen et al., 2004; Shukla et al., 2018) whilst CD27 is upregulated in response to B cell receptor engagement (Lafarge et al., 2015). Therefore, the identification of “active” and “inactive” populations in CLL B cells is not surprising. Interestingly, forodesine and dG killed the “active” population within 24h, and also induced an increase of the apoptotic markers in the “inactive” cells. This suggests that the inactive cells are in the process of dying by apoptosis and that they respond to forodesine and dG treatment with different kinetics than the “active” cells. As such, forodesine may have an advantage over other CLL drugs that inhibit B cell receptor signalling and thus target only “active” cells.

The cartoon below (**Figure 7.1**) presents the model that emerged from this work. It describes a novel role for SAMHD1’s dNTPase function in safeguarding cells against dNTP imbalances that otherwise trigger apoptosis. This mechanism was exploited to specifically induce apoptosis in CLL B cells with *SAMHD1* loss-of-function mutations. The role of SAMHD1 in the mechanism of toxicity of forodesine is novel and suggests that SAMHD1 may be responsible for the limited efficacy of forodesine in clinical trials.

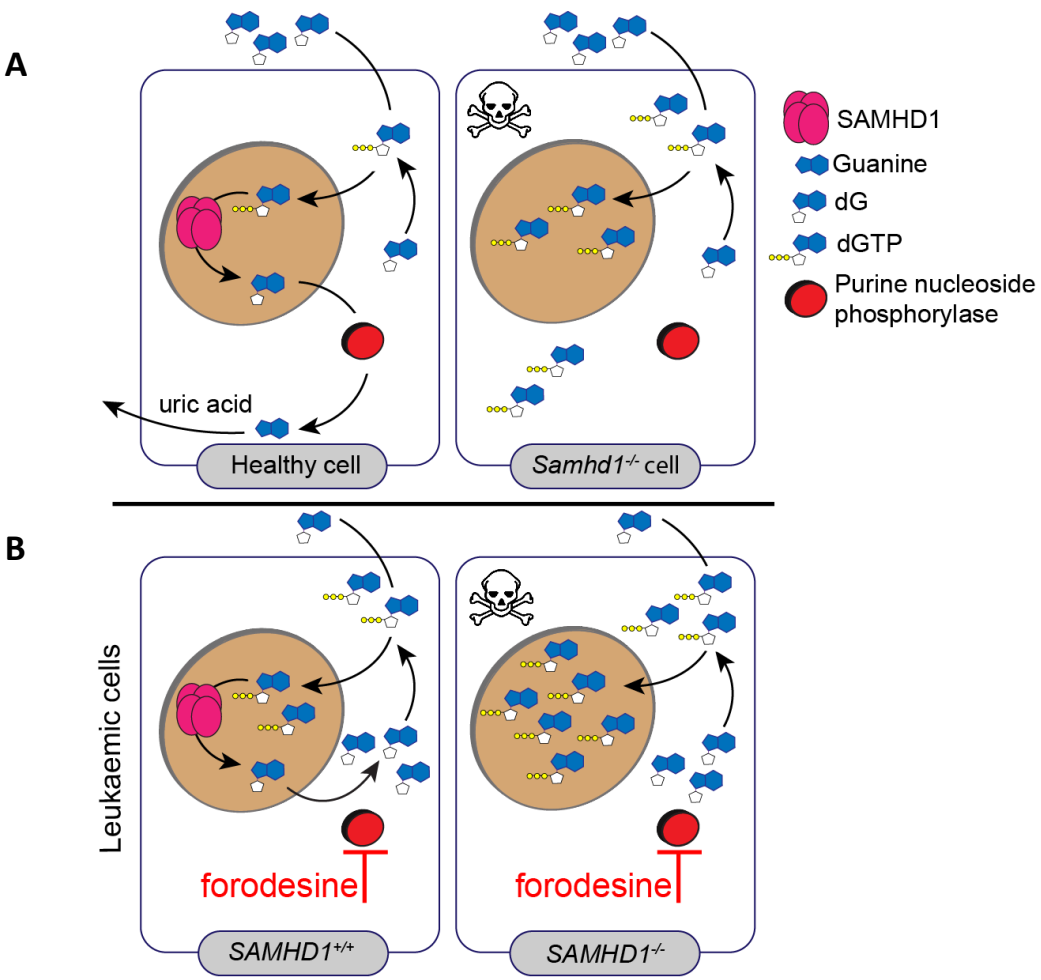


***Figure 7.1 Model of SAMHD1's mechanism of protection against dGTP**. (A) dG enters the cell and is converted to dGTP through the salvage pathway. In WT cells, SAMHD1 degrades dGTP while dGTP accumulates in SAMHD1-deficient cells. Accumulation of dGTP triggers cell intrinsic apoptosis, independently of genomic DNA synthesis. (B) In a leukaemic cell, forodesine triggers limited accumulation of dG and dGTP. Because dGTP is degraded by SAMHD1, cytotoxicity is limited. In a leukaemic cell without functional SAMHD1, PNP inhibitors trigger accumulation of dG and dGTP. Since dGTP is not degraded, the toxicity is enhanced.*

This finding suggested that only patients with *SAMHD1* loss-of-function mutations respond well to forodesine treatment. Developing *in vivo* models of leukaemia would allow to determine whether this mechanism is specific to CLL or if it can be extended to other types of leukaemia. The time line of my project did not allow to develop a more appropriate *in vivo* model (for example the Eμ TCL1 mic model discussed above). In addition, a clinical trial enrolling only these patients should be set up to confirm the finding and to validate my model in a clinical setting. An increase of dG is detected in the blood of patients upon forodesine treatment, suggesting that it will be efficient against any SAMHD1-deficient circulating cells

(Balakrishnan et al., 2006; Balakrishnan et al., 2010b). It will be interesting to determine whether it could also be used against solid tumours carrying *SAMHD1* mutations (Rentoft et al., 2016). The elevation of dG in the blood suggests that cells in the bloodstream accumulate dG intracellularly and flush it out in the blood (Balakrishnan et al., 2006; Balakrishnan et al., 2010b). Marrow stromal cells have been shown to limit the effect of forodesine on CLL cells (Balakrishnan et al., 2010a). In addition, erythrocytes where shown to accumulate dGTP in PNP-deficient patients (Simmonds et al., 1982). Since erythrocytes express PNP, this suggests that their accumulation of dGTP may be due to the absence of SAMHD1 (Gabrio et al., 1956). Therefore, it would be important to determine whether erythrocytes express SAMHD1, something that has not been reported yet. Establishing that erythrocytes do no express SAMHD1 and are responsible for the elevation of dG in the blood is of great interest. Indeed, patients undergoing chemotherapy can have lower erythrocytes counts. Therefore, it would be important to use forodesine only in patients with acceptable erythrocyte counts to allow the increase of dG in the blood when forodesine is used. In addition, testing the mechanism with other PNP inhibitors will strengthen the model. Two other PNP inhibitors are commercially available: 9-deazaguanine and 8-aminoguanosine. There are only a limited number of old publications reporting their use. These inhibitors will be tested with or without dG in WT and SAMHD1-deficient cells.

According to this new role of SAMHD1, stratification of leukaemic patients based on their *SAMHD1* genotype or expression levels should be used in the clinic. Testing the survival of PBMCs *ex vivo* upon forodesine and dG treatment, together with α-SAMHD1 antibodies would be suitable for rapid clinical assays to identify patients with SAMHD1 deficiency.

Overall, I have uncovered an important role of SAMHD1 in protecting cells against dNTP imbalance that otherwise triggers apoptotic cell death. These findings allowed me to selectively ablate SAMHD1-mutated transformed cells using a combination treatment involving forodesine and dG. In future, forodesine may be developed into a precision medicine for a subset of leukaemia patients with *SAMHD1* loss-of-function mutations in which strong efficacy is predicted.

This work suggests that SAMHD1's ancestral function may be to protect cells against dNTP imbalances. Such physiological conditions are occurring in cancer therapy with the PNP inhibitor forodesine. This novel role of SAMHD1 demonstrated how the dNTPase limits the efficacy of forodesine and therefore could be used as a precision medicine in cancer patients with *SAMHD1* loss-of-function mutations.

Bibliography

Aglietti, R.A., and Dueber, E.C. (2017). Recent Insights into the Molecular Mechanisms Underlying Pyroptosis and Gasdermin Family Functions. Trends in Immunology *38*, 261-271.

Ahmad, S., Mu, X., Yang, F., Greenwald, E., Park, J.W., Jacob, E., Zhang, C.Z., and Hur, S. (2018). Breaching Self-Tolerance to Alu Duplex RNA Underlies MDA5-Mediated Inflammation. Cell *172*, 797-810 e713.

Ahn, J., Hao, C., Yan, J., DeLucia, M., Mehrens, J., Wang, C., Gronenborn, A.M., and Skowronski, J. (2012). HIV/simian immunodeficiency virus (SIV) accessory virulence factor Vpx loads the host cell restriction factor SAMHD1 onto the E3 ubiquitin ligase complex CRL4DCAF1. The Journal of biological chemistry *287*, 12550-12558.

Alonso, R., Lopez-Guerra, M., Upshaw, R., Bantia, S., Smal, C., Bontemps, F., Manz, C., Mehrling, T., Villamor, N., Campo, E.*, et al.* (2009). Forodesine has high antitumor activity in chronic lymphocytic leukemia and activates p53-independent mitochondrial apoptosis by induction of p73 and BIM. Blood *114*, 1563-1575.

Amie, S.M., Bambara, R.A., and Kim, B. (2013). GTP is the primary activator of the anti-HIV restriction factor SAMHD1. The Journal of biological chemistry *288*, 25001-25006.

Antes, A., Tappin, I., Chung, S., Lim, R., Lu, B., Parrott, A.M., Hill, H.Z., Suzuki, C.K., and Lee, C.G. (2010). Differential regulation of full-length genome and a single-stranded 7S DNA along the cell cycle in human mitochondria. Nucleic Acids Res *38*, 6466-6476.

Antonucci, J.M., St Gelais, C., de Silva, S., Yount, J.S., Tang, C., Ji, X., Shepard, C., Xiong, Y., Kim, B., and Wu, L. (2016). SAMHD1-mediated HIV-1 restriction in cells does not involve ribonuclease activity. Nature medicine *22*, 1072-1074.

Applequist, S.E., Wallin, R.P.A., and Ljunggren, H.G. (2002). Variable expression of Toll-like receptor in murine innate and adaptive immune cell lines. International immunology *14*, 1065-1074.

Aravind, L., and Koonin, E.V. (1998). The HD domain defines a new superfamily of metal-dependent phosphohydrolases. Trends Biochem Sci *23*, 469.

Arnér, E.S.J., and Eriksson, S. (1995). Mammalian deoxyribonucleoside kinases. Pharmacology & Therapeutics *67*, 155-186.

Arpaia, E., Benveniste, P., Di Cristofano, A., Gu, Y., Dalal, I., Kelly, S., Hershfield, M., Pandolfi, P.P., Roifman, C.M., and Cohen, A. (2000). Mitochondrial Basis for Immune Deficiency. The Journal of Experimental Medicine *191*, 2197.

Aye, Y., Li, M., Long, M.J., and Weiss, R.S. (2015). Ribonucleotide reductase and cancer: biological mechanisms and targeted therapies. Oncogene *34*.

Badia, R., Angulo, G., Riveira-Munoz, E., Pujantell, M., Puig, T., Ramirez, C., Torres-Torronteras, J., Marti, R., Pauls, E., Clotet, B.*, et al.* (2016). Inhibition of herpes simplex virus type 1 by the CDK6 inhibitor PD-0332991 (palbociclib) through the control of SAMHD1. The Journal of antimicrobial chemotherapy *71*, 387-394.

Badoux, X.C., Keating, M.J., Wang, X., O'Brien, S.M., Ferrajoli, A., Faderl, S., Burger, J., Koller, C., Lerner, S., Kantarjian, H.*, et al.* (2011). Fludarabine, cyclophosphamide, and rituximab chemoimmunotherapy is highly effective treatment for relapsed patients with CLL. Blood *117*, 3016-3024.

Bailey, L.J., and Doherty, A.J. (2017). Mitochondrial DNA replication: a PrimPol perspective. Biochem Soc Trans *45*, 513-529.

Balakrishnan, K., Burger, J.A., Quiroga, M.P., Henneberg, M., Ayres, M.L., Wierda, W.G., and Gandhi, V. (2010a). Influence of bone marrow stromal microenvironment on forodesine-induced responses in CLL primary cells. Blood *116*, 1083-1091.

Balakrishnan, K., Nimmanapalli, R., Ravandi, F., Keating, M.J., and Gandhi, V. (2006). Forodesine, an inhibitor of purine nucleoside phosphorylase, induces apoptosis in chronic lymphocytic leukemia cells. Blood *108*, 2392-2398.

Balakrishnan, K., Ravandi, F., Bantia, S., Franklin, A., and Gandhi, V. (2013). Preclinical and clinical evaluation of forodesine in pediatric and adult B-cell acute lymphoblastic leukemia. Clinical lymphoma, myeloma & leukemia *13*, 458-466.

Balakrishnan, K., Verma, D., O'Brien, S., Kilpatrick, J.M., Chen, Y., Tyler, B.F., Bickel, S., Bantia, S., Keating, M.J., Kantarjian, H*., et al.* (2010b). Phase 2 and pharmacodynamic study of oral forodesine in patients with advanced, fludarabine-treated chronic lymphocytic leukemia. Blood *116*, 886-892.

Baldauf, H.M., Pan, X., Erikson, E., Schmidt, S., Daddacha, W., Burggraf, M., Schenkova, K., Ambiel, I., Wabnitz, G., Gramberg, T*., et al.* (2012). SAMHD1 restricts HIV-1 infection in resting CD4(+) T cells. Nature medicine *18*, 1682-1687.

Ballana, E., Badia, R., Terradas, G., Torres-Torronteras, J., Ruiz, A., and Pauls, E. (2014). SAMHD1 specifically affects the antiviral potency of thymidine analog HIV reverse transcriptase inhibitors. Antimicrob Agents Chemother *58*.

Bandura, D.R., Baranov, V.I., Ornatsky, O.I., Antonov, A., Kinach, R., Lou, X., Pavlov, S., Vorobiev, S., Dick, J.E., and Tanner, S.D. (2009). Mass cytometry: technique for real time single cell multitarget immunoassay based on inductively coupled plasma time-of-flight mass spectrometry. Analytical chemistry *81*, 6813-6822.

Bantia, S., Miller, P.J., Parker, C.D., Ananth, S.L., Horn, L.L., Kilpatrick, J.M., Morris, P.E., Hutchison, T.L., Montgomery, J.A., and Sandhu, J.S. (2001). Purine nucleoside phosphorylase inhibitor BCX-1777 (Immucillin-H)—a novel potent and orally active immunosuppressive agent. International immunopharmacology *1*, 1199-1210.

Bantia, S., Montgomery, J.A., Johnson, H.G., and Walsh, G.M. (1996). In vivo and in vitro pharmacologic activity of the purine nucleoside phosphorylase inhibitor BCX-34: the role of GTP and dGTP. Immunopharmacology *35*, 53-63.

Bantia, S., Parker, C., Upshaw, R., Cunningham, A., Kotian, P., Kilpatrick, J.M., Morris, P., Chand, P., and Babu, Y.S. (2010). Potent orally bioavailable purine nucleoside phosphorylase inhibitor BCX-4208 induces apoptosis in B- and T-lymphocytes--a novel treatment approach for autoimmune diseases, organ transplantation and hematologic malignancies. International immunopharmacology *10*, 784-790.

Bao, M., and Liu, Y.J. (2013). Regulation of TLR7/9 signaling in plasmacytoid dendritic cells. Protein & cell *4*, 40-52.

Baroja, A., de la Hoz, C., Alvarez, A., Vielba, R., Sarrat, R., Aréchaga, J., and de Gandarias, J.M. (1998). Polyploidization and exit from cell cycle as mechanisms of cultured melanoma cell resistance to methotrexate. Life Sciences *62*, 2275-2282.

Behrendt, R., Schumann, T., Gerbaulet, A., Nguyen, L.A., Schubert, N., and Alexopoulou, D. (2013). Mouse SAMHD1 has antiretroviral activity and suppresses a spontaneous cell-intrinsic antiviral response. Cell reports *4*.

Beloglazova, N., Flick, R., Tchigvintsev, A., Brown, G., Popovic, A., Nocek, B., and Yakunin, A.F. (2013). Nuclease activity of the human SAMHD1 protein implicated in the Aicardi-Goutieres syndrome and HIV-1 restriction. The Journal of biological chemistry *288*, 8101-8110.

Benitez-Guijarro, M., Lopez-Ruiz, C., Tarnauskaite, Z., Murina, O., Mian Mohammad, M., Williams, T.C., Fluteau, A., Sanchez, L., Vilar-Astasio, R., Garcia-Canadas, M.*, et al.* (2018). RNase H2, mutated in Aicardi-Goutieres syndrome, promotes LINE-1 retrotransposition. The EMBO journal *37*.

Berg JM, T.J., Stryer L. (2002a). Biochemistry, 5th edn (New York: W H Freeman).

Berg JM, T.J., Stryer L. (2002b). Purine Bases Can Be Synthesized de Novo or Recycled by Salvage Pathways. In Biochemestry 5th edition (New York: W H Freeman).

Bergsbaken, T., Fink, S.L., and Cookson, B.T. (2009). Pyroptosis: host cell death and inflammation. Nat Rev Microbiol *7*, 99-109.

Besnier, C., Takeuchi, Y., and Towers, G. (2002). Restriction of lentivirus in monkeys. Proc Natl Acad Sci U S A *99*, 11920-11925.

Bester, A.C., Roniger, M., Oren, Y.S., Im, M.M., Sarni, D., Chaoat, M., Bensimon, A., Zamir, G., Shewach, D.S., and Kerem, B. (2011). Nucleotide deficiency promotes genomic instability in early stages of cancer development. Cell *145*, 435-446.

Boehncke, W.H., Gilbertsen R, B., Hemmer, J., and Sterry, W. (1994). Evidence for a Pathway Independent from 2′-Deoxyguanosine and Reversible by IL-2 by which Purine Nucleoside Phosphorylase Inhibitors Block T-Cell Proliferation. Scandinavian Journal of Immunology *39*, 327-332.

Bourdon, A., Minai, L., Serre, V., Jais, J.P., Sarzi, E., Aubert, S., Chretien, D., de Lonlay, P., Paquis-Flucklinger, V., Arakawa, H.*, et al.* (2007). Mutation of RRM2B, encoding p53-controlled ribonucleotide reductase (p53R2), causes severe mitochondrial DNA depletion. Nat Genet *39*, 776-780.

Bresin, A., D'Abundo, L., Narducci, M.G., Fiorenza, M.T., Croce, C.M., Negrini, M., and Russo, G. (2016). TCL1 transgenic mouse model as a tool for the study of therapeutic targets and microenvironment in human B-cell chronic lymphocytic leukemia. Cell Death & Disease *7*, e2071.

Bridgeman, A., Maelfait, J., Davenne, T., Partridge, T., Peng, Y., Mayer, A., Dong, T., Kaever, V., Borrow, P., and Rehwinkel, J. (2015). Viruses transfer the antiviral second messenger cGAMP between cells. Science (New York, NY) *349*, 1228-1232.

Brown, N.C., and Reichard, P. (1969). Role of effector binding in allosteric control of ribonucleoside diphosphate reductase. Journal of Molecular Biology *46*, 39-55.

Burns, A., Alsolami, R., Becq, J., Timbs, A., Bruce, D., Robbe, P., Vavoulis, D., Cabes, M., Dreau, H., Taylor, J.*, et al.* (2017). Whole-genome sequencing of chronic lymphocytic leukaemia reveals distinct differences in the mutational landscape between IgHVmut and IgHVunmut subgroups. Leukemia.

Bzowska, A., Kulikowska, E., and Shugar, D. (2000). Purine nucleoside phosphorylases: properties, functions, and clinical aspects. Pharmacology & Therapeutics *88*, 349-425.

Calin, G.A., Dumitru, C.D., Shimizu, M., Bichi, R., Zupo, S., Noch, E., Aldler, H., Rattan, S., Keating, M., Rai, K.*, et al.* (2002). Frequent deletions and down-regulation of micro- RNA genes miR15 and miR16 at 13q14 in chronic lymphocytic leukemia. Proc Natl Acad Sci U S A *99*, 15524-15529.

Calonge, E., Bermejo, M., Diez-Fuertes, F., Mangeot, I., González, N., Coiras, M., Jiménez Tormo, L., García-Perez, J., Dereuddre-Bosquet, N., Le Grand, R.*, et al.* (2017). Different Expression of Interferon-Stimulated Genes in Response to HIV-1 Infection in Dendritic Cells Based on Their Maturation State. Journal of virology *91*, e01379-01316.

Cang, S., Iragavarapu, C., Savooji, J., Song, Y., and Liu, D. (2015). ABT-199 (venetoclax) and BCL-2 inhibitors in clinical development. Journal of Hematology & Oncology *8*, 129.

Cardoso, L.S., Araujo, M.I., Goes, A.M., Pacifico, L.G., Oliveira, R.R., and Oliveira, S.C. (2007). Polymyxin B as inhibitor of LPS contamination of Schistosoma mansoni recombinant proteins in human cytokine analysis. Microb Cell Fact *6*, 1.

Carter, M.J., Cox, K.L., Blakemore, S.J., Turaj, A.H., Oldham, R.J., Dahal, L.N., Tannheimer, S., Forconi, F., Packham, G., and Cragg, M.S. (2017). PI3Kdelta inhibition elicits anti-leukemic effects through Bim-dependent apoptosis. Leukemia *31*, 1423-1433.

Castro, M., Carrillo, R., Garcia, F., Sanz, P., Ferrer, I., Ruiz-Sala, P., Vega, A.I., Ruiz Desviat, L., Perez, B., Perez-Cerda, C.*, et al.* (2014). Thirteen years experience with selective screening for disorders in purine and pyrimidine metabolism. Nucleosides Nucleotides Nucleic Acids *33*, 233-240.

Celhar, T., Magalhães, R., and Fairhurst, A.M. (2012). TLR7 and TLR9 in SLE: when sensing self goes wrong. Immunologic Research *53*, 58-77.

Chan, T.-s. (1978). Deoxyguanosine toxicity on lymphoid cells as a cause for immunosuppression in purine nucleoside phosphorylase deficiency. Cell *14*, 523-530.

Chen, Z., Zhu, M., Pan, X., Zhu, Y., Yan, H., Jiang, T., Shen, Y., Dong, X., Zheng, N., Lu, J.*, et al.* (2014). Inhibition of Hepatitis B virus replication by SAMHD1. Biochemical and biophysical research communications *450*, 1462-1468.

Cho, Y., Challa, S., Moquin, D., Genga, R., Ray, T.D., Guildford, M., and Chan, F.K.-M. (2009). Phosphorylation-Driven Assembly of the RIP1-RIP3 Complex Regulates Programmed Necrosis and Virus-Induced Inflammation. Cell *137*, 1112-1123.

Chung, H., Calis, J.J.A., Wu, X., Sun, T., Yu, Y., Sarbanes, S.L., Dao Thi, V.L., Shilvock, A.R., Hoffmann, H.H., Rosenberg, B.R.*, et al.* (2018). Human ADAR1 Prevents Endogenous RNA from Triggering Translational Shutdown. Cell.

Clifford, R., Louis, T., Robbe, P., Ackroyd, S., Burns, A., Timbs, A.T., Wright Colopy, G., Dreau, H., Sigaux, F., Judde, J.G.*, et al.* (2014). SAMHD1 is mutated recurrently in chronic lymphocytic leukemia and is involved in response to DNA damage. Blood *123*, 1021-1031.

Cohen, A., Gudas, L.J., Ammann, A.J., Staal, G.E.J., and Martin, D.W., Jr. (1978). Deoxyguanosine Triphosphate as a Possible Toxic Metabolite in the Immunodeficiency Associated with Purine Nucleoside Phosphorylase Deficiency. The Journal of Clinical Investigation *61*, 1405-1409.

Conry, R.M., Bantia, S., Turner, H.S., Barlow, D.L., Allen, K.O., LoBuglio, A.F., Montgomery, J.A., and Walsh, G.M. (1998). Effects of a novel purine nucleoside phosphorylase inhibitor, BCX-34, on activation and proliferation of normal human lymphoid cells. Immunopharmacology *40*, 1-9.

Cookson, B.T., and Brennan, M.A. (2001). Pro-inflammatory programmed cell death. Trends in Microbiology *9*, 113-114.

Coquel, F., Silva, M.J., Techer, H., Zadorozhny, K., Sharma, S., Nieminuszczy, J., Mettling, C., Dardillac, E., Barthe, A., Schmitz, A.L.*, et al.* (2018). SAMHD1 acts at stalled replication forks to prevent interferon induction. Nature.

Cotruvo, J.A., and Stubbe, J. (2011). Class I Ribonucleotide Reductases: Metallocofactor Assembly and Repair In Vitro and In Vivo. Annual Review of Biochemistry *80*, 733-767.

Cribier, A., Descours, B., Valadao, A.L., Laguette, N., and Benkirane, M. (2013). Phosphorylation of SAMHD1 by cyclin A2/CDK1 regulates its restriction activity toward HIV-1. Cell reports *3*, 1036-1043.

Crow Yanick, J., Chase Diana, S., Lowenstein Schmidt, J., Szynkiewicz, M., Forte Gabriella, M.A., Gornall Hannah, L., Oojageer, A., Anderson, B., Pizzino, A., Helman, G.*, et al.* (2015). Characterization of human disease phenotypes associated with mutations in TREX1, RNASEH2A, RNASEH2B, RNASEH2C, SAMHD1, ADAR, and IFIH1. American Journal of Medical Genetics Part A *167*, 296-312.

Crow, Y.J., Hayward, B.E., Parmar, R., Robins, P., Leitch, A., Ali, M., Black, D.N., van Bokhoven, H., Brunner, H.G., Hamel, B.C.*, et al.* (2006a). Mutations in the gene encoding the 3'-5' DNA exonuclease TREX1 cause Aicardi-Goutieres syndrome at the AGS1 locus. Nat Genet *38*, 917-920.

Crow, Y.J., Leitch, A., Hayward, B.E., Garner, A., Parmar, R., Griffith, E., Ali, M., Semple, C., Aicardi, J., Babul-Hirji, R.*, et al.* (2006b). Mutations in genes encoding ribonuclease H2 subunits cause Aicardi-Goutieres syndrome and mimic congenital viral brain infection. Nat Genet *38*, 910-916.

Crow, Y.J., and Livingston, J.H. (2008). Aicardi-Goutieres syndrome: an important Mendelian mimic of congenital infection. Developmental medicine and child neurology *50*, 410-416.

Crow, Y.J., and Manel, N. (2015). Aicardi-Goutieres syndrome and the type I interferonopathies. Nature reviews Immunology *15*, 429-440.

Czabotar, P.E., Lessene, G., Strasser, A., and Adams, J.M. (2014). Control of apoptosis by the BCL-2 protein family: implications for physiology and therapy. Nat Rev Mol Cell Biol *15*, 49-63.

Daddacha, W., Koyen, A.E., Bastien, A.J., Head, P.E., Dhere, V.R., Nabeta, G.N., Connolly, E.C., Werner, E., Madden, M.Z., Daly, M.B.*, et al.* (2017). SAMHD1 Promotes DNA End Resection to Facilitate DNA Repair by Homologous Recombination. Cell reports *20*, 1921-1935.

Dale, R.C., Gornall, H., Singh-Grewal, D., Alcausin, M., Rice, G.I., and Crow, Y.J. (2010). Familial Aicardi-Goutieres syndrome due to SAMHD1 mutations is associated with chronic arthropathy and contractures. American journal of medical genetics Part A *152a*, 938-942.

Damle, R.N., Wasil, T., Fais, F., Ghiotto, F., Valetto, A., Allen, S.L., Buchbinder, A., Budman, D., Dittmar, K., Kolitz, J.*, et al.* (1999). Ig V gene mutation status and CD38

expression as novel prognostic indicators in chronic lymphocytic leukemia. Blood *94*, 1840-1847.

Damm, F., Mylonas, E., Cosson, A., Yoshida, K., Della Valle, V., Mouly, E., Diop, M., Scourzic, L., Shiraishi, Y., Chiba, K.*, et al.* (2014). Acquired initiating mutations in early hematopoietic cells of CLL patients. Cancer Discov *4*, 1088-1101.

Davids, M.S., Pagel, J.M., Kahl, B.S., Wierda, W.G., Miller, T.P., Gerecitano, J.F., Kipps, T.J., Anderson, M.-A., Huang, D.C.S., Rudersdorf, N.K.*, et al.* (2013). Bcl-2 Inhibitor ABT-199 (GDC-0199) Monotherapy Shows Anti-Tumor Activity Including Complete Remissions In High-Risk Relapsed/Refractory (R/R) Chronic Lymphocytic Leukemia (CLL) and Small Lymphocytic Lymphoma (SLL). Blood *122*, 872.

Decherchi, S., Berteotti, A., Bottegoni, G., Rocchia, W., and Cavalli, A. (2015). The ligand binding mechanism to purine nucleoside phosphorylase elucidated via molecular dynamics and machine learning. Nat Commun *6*, 6155.

Degterev, A., Boyce, M., and Yuan, J. (2003). A decade of caspases. Oncogene *22*, 8543-8567.

Degterev, A., Huang, Z., Boyce, M., Li, Y., Jagtap, P., Mizushima, N., Cuny, G.D., Mitchison, T.J., Moskowitz, M.A., and Yuan, J. (2005). Chemical inhibitor of nonapoptotic cell death with therapeutic potential for ischemic brain injury. Nature chemical biology *1*, 112-119.

Descours, B., Cribier, A., Chable-Bessia, C., Ayinde, D., Rice, G., Crow, Y., Yatim, A., Schwartz, O., Laguette, N., and Benkirane, M. (2012). SAMHD1 restricts HIV-1 reverse transcription in quiescent CD4(+) T-cells. Retrovirology *9*, 87.

Dohner, H., Stilgenbauer, S., Benner, A., Leupolt, E., Krober, A., Bullinger, L., Dohner, K., Bentz, M., and Lichter, P. (2000). Genomic aberrations and survival in chronic lymphocytic leukemia. The New England journal of medicine *343*, 1910-1916.

Duan, D.S., Nagashima, T., Hoshino, T., Waldman, F., Pawlak, K., and Sadee, W. (1990). Mechanisms of 2'-deoxyguanosine toxicity in mouse T-lymphoma cells with purine nucleoside phosphorylase deficiency and resistance to inhibition of ribonucleotide reductase by dGTP. Biochem J *268*, 725-731.

Dummer, R., Duvic, M., Scarisbrick, J., Olsen, E.A., Rozati, S., Eggmann, N., Goldinger, S.M., Hutchinson, K., Geskin, L., Illidge, T.M.*, et al.* (2014). Final results of a multicenter phase II study of the purine nucleoside phosphorylase (PNP) inhibitor forodesine in patients with advanced cutaneous T-cell lymphomas (CTCL) (Mycosis fungoides and Sezary syndrome). Ann Oncol *25*, 1807-1812.

Durham, J.P., and Ives, D.H. (1969). Deoxycytidine kinase. I. Distribution in normal and neoplastic tissues and interrelationships of deoxycytidine and 1-beta-D-arabinofuranosylcytosine phosphorylation. Molecular pharmacology *5*, 358-375.

Eichhorst, B.F., Busch, R., Hopfinger, G., Pasold, R., Hensel, M., Steinbrecher, C., Siehl, S., Jager, U., Bergmann, M., Stilgenbauer, S.*, et al.* (2006). Fludarabine plus cyclophosphamide versus fludarabine alone in first-line therapy of younger patients with chronic lymphocytic leukemia. Blood *107*, 885-891.

Eriksson, S., and Wang, L. (2008). Molecular Mechanisms of Mitochondrial DNA Depletion Diseases Caused by Deficiencies in Enzymes in Purine and Pyrimidine Metabolism. Nucleosides, Nucleotides and Nucleic Acids *27*, 800-808.

Erridge, C. (2010). Endogenous ligands of TLR2 and TLR4: agonists or assistants? J Leukoc Biol *87*, 989-999.

Evans, G.B., Furneaux, R.H., Gainsford, G.J., Schramm, V.L., and Tyler, P.C. (2000). Synthesis of Transition State Analogue Inhibitors for Purine Nucleoside Phosphorylase and N-Riboside Hydrolases. Tetrahedron *56*, 3053-3062.

Fasullo, M., and Endres, L. (2015). Nucleotide salvage deficiencies, DNA damage and neurodegeneration. International journal of molecular sciences *16*, 9431-9449.

Feoktistova, M., Geserick, P., and Leverkus, M. (2016). Crystal Violet Assay for Determining Viability of Cultured Cells. Cold Spring Harb Protoc *2016*, pdb prot087379.

Fernandes-Alnemri, T., Wu, J., Yu, J.W., Datta, P., Miller, B., Jankowski, W., Rosenberg, S., Zhang, J., and Alnemri, E.S. (2007). The pyroptosome: a supramolecular assembly of ASC dimers mediating inflammatory cell death via caspase-1 activation. Cell death and differentiation *14*, 1590-1604.

Ferraresi, R., Troiano, L., Pinti, M., Roat, E., Lugli, E., Quaglino, D., Taverna, D., Bellizzi, D., Passarino, G., and Cossarizza, A. (2008). Resistance of mtDNA-depleted cells to apoptosis. Cytometry A *73*, 528-537.

Fink, S.L., and Cookson, B.T. (2006). Caspase-1-dependent pore formation during pyroptosis leads to osmotic lysis of infected host macrophages. Cellular microbiology *8*, 1812-1825.

Frank, D.A., Mahajan, S., and Ritz, J. (1997). B lymphocytes from patients with chronic lymphocytic leukemia contain signal transducer and activator of transcription (STAT) 1 and STAT3 constitutively phosphorylated on serine residues. J Clin Invest *100*, 3140-3148.

Franzolin, E., Pontarin, G., Rampazzo, C., Miazzi, C., Ferraro, P., Palumbo, E., Reichard, P., and Bianchi, V. (2013). The deoxynucleotide triphosphohydrolase SAMHD1 is a major regulator of DNA precursor pools in mammalian cells. Proc Natl Acad Sci U S A *110*, 14272-14277.

Franzolin, E., Salata, C., Bianchi, V., and Rampazzo, C. (2015). The Deoxynucleoside Triphosphate Triphosphohydrolase Activity of SAMHD1 Protein Contributes to the Mitochondrial DNA Depletion Associated with Genetic Deficiency of Deoxyguanosine Kinase. The Journal of biological chemistry *290*, 25986-25996.

Gabrio, B.W., Huennekens, F.M., and Nurk, E. (1956). Erythrocyte metabolism. I. Purine nucleoside phosphorylase. The Journal of biological chemistry *221*, 971-981.

Galmarini, C.M., Mackey, J.R., and Dumontet, C. (2002). Nucleoside analogues and nucleobases in cancer treatment. Lancet Oncol *3*.

Gandhi, V., and Balakrishnan, K. (2007). Pharmacology and mechanism of action of forodesine, a T-cell targeted agent. Semin Oncol *34*, S8-12.

Gandhi, V., Kilpatrick, J.M., Plunkett, W., Ayres, M., Harman, L., Du, M., Bantia, S., Davisson, J., Wierda, W.G., Faderl, S.*, et al.* (2005). A proof-of-principle pharmacokinetic, pharmacodynamic, and clinical study with purine nucleoside phosphorylase inhibitor immucillin-H (BCX-1777, forodesine). Blood *106*, 4253-4260.

Gao, D., Wu, J., Wu, Y.T., Du, F., Aroh, C., Yan, N., Sun, L., and Chen, Z.J. (2013). Cyclic GMP-AMP synthase is an innate immune sensor of HIV and other retroviruses. Science (New York, NY) *341*, 903-906.

Gentile, F., Deriu, M.A., Licandro, G., Prunotto, A., Danani, A., and Tuszynski, J.A. (2015). Structure Based Modeling of Small Molecules Binding to the TLR7 by Atomistic Level Simulations. Molecules *20*, 8316-8340.

Gibbert, K., Schlaak, J.F., Yang, D., and Dittmer, U. (2013). IFN-alpha subtypes: distinct biological activities in anti-viral therapy. British journal of pharmacology *168*, 1048-1058.

Giblett, E., Ammann, A., Sandman, R., Wara, D., and Diamond, L. (1975). NUCLEOSIDE-PHOSPHORYLASE DEFICIENCY IN A CHILD WITH SEVERELY DEFECTIVE T-CELL IMMUNITY AND NORMAL B-CELL IMMUNITY. The Lancet *305*, 1010-1013.

Gifford, R.J. (2012). Viral evolution in deep time: lentiviruses and mammals. Trends Genet *28*, 89-100.

Goldstone, D.C., Ennis-Adeniran, V., Hedden, J.J., Groom, H.C., Rice, G.I., Christodoulou, E., Walker, P.A., Kelly, G., Haire, L.F., Yap, M.W.*, et al.* (2011). HIV-1 restriction factor SAMHD1 is a deoxynucleoside triphosphate triphosphohydrolase. Nature *480*, 379-382.

Gorgun, G., Ramsay, A.G., Holderried, T.A.W., Zahrieh, D., Le Dieu, R., Liu, F., Quackenbush, J., Croce, C.M., and Gribben, J.G. (2009). Eμ-TCL1 Mice Represent a Model for Immunotherapeutic Reversal of Chronic Lymphocytic Leukemia-Induced T-Cell Dysfunction. Proceedings of the National Academy of Sciences of the United States of America *106*, 6250-6255.

Guieze, R., Robbe, P., Clifford, R., de Guibert, S., Pereira, B., Timbs, A., Dilhuydy, M.S., Cabes, M., Ysebaert, L., Burns, A.*, et al.* (2015). Presence of multiple recurrent mutations confers poor trial outcome of relapsed/refractory CLL. Blood *126*, 2110-2117.

Guo, H., Callaway, J.B., and Ting, J.P. (2015). Inflammasomes: mechanism of action, role in disease, and therapeutics. Nature medicine *21*, 677-687.

Gururajan, M., Jacob, J., and Pulendran, B. (2007). Toll-Like Receptor Expression and Responsiveness of Distinct Murine Splenic and Mucosal B-Cell Subsets. PloS one *2*, e863.

Hallek, M., Fischer, K., Fingerle-Rowson, G., Fink, A.M., Busch, R., Mayer, J., Hensel, M., Hopfinger, G., Hess, G., von Grünhagen, U.*, et al.* (2010). Addition of rituximab to fludarabine and cyclophosphamide in patients with chronic lymphocytic leukaemia: a randomised, open-label, phase 3 trial. The Lancet *376*, 1164-1174.

Hamblin, T.J., Davis, Z., Gardiner, A., Oscier, D.G., and Stevenson, F.K. (1999). Unmutated Ig V(H) genes are associated with a more aggressive form of chronic lymphocytic leukemia. Blood *94*, 1848-1854.

Hansen, E.C., Seamon, K.J., Cravens, S.L., and Stivers, J.T. (2014). GTP activator and dNTP substrates of HIV-1 restriction factor SAMHD1 generate a long-lived activated state. Proc Natl Acad Sci U S A *111*, E1843.

Hemmi, H., Kaisho, T., Takeuchi, O., Sato, S., Sanjo, H., Hoshino, K., Horiuchi, T., Tomizawa, H., Takeda, K., and Akira, S. (2002). Small anti-viral compounds activate immune cells via the TLR7 MyD88–dependent signaling pathway. Nature immunology *3*, 196.

Herishanu, Y., Perez-Galan, P., Liu, D., Biancotto, A., Pittaluga, S., Vire, B., Gibellini, F., Njuguna, N., Lee, E., Stennett, L.*, et al.* (2011). The lymph node microenvironment promotes B-cell receptor signaling, NF-kappaB activation, and tumor proliferation in chronic lymphocytic leukemia. Blood *117*, 563-574.

Herman, S.E., Sun, X., McAuley, E.M., Hsieh, M.M., Pittaluga, S., Raffeld, M., Liu, D., Keyvanfar, K., Chapman, C.M., Chen, J.*, et al.* (2013). Modeling tumor-host interactions of chronic lymphocytic leukemia in xenografted mice to study tumor biology and evaluate targeted therapy. Leukemia *27*, 2311-2321.

Herold, N., Rudd, S.G., Ljungblad, L., Sanjiv, K., Myrberg, I.H., Paulin, C.B., Heshmati, Y., Hagenkort, A., Kutzner, J., Page, B.D.*, et al.* (2017a). Targeting SAMHD1 with the Vpx protein to improve cytarabine therapy for hematological malignancies. Nature medicine.

Herold, N., Rudd, S.G., Sanjiv, K., Kutzner, J., Bladh, J., Paulin, C.B.J., Helleday, T., Henter, J.I., and Schaller, T. (2017b). SAMHD1 protects cancer cells from various nucleoside-based antimetabolites. Cell Cycle, 0.

Herrmann, A., Wittmann, S., Thomas, D., Shepard, C.N., Kim, B., Ferreiros, N., and Gramberg, T. (2018). The SAMHD1-mediated block of LINE-1 retroelements is regulated by phosphorylation. Mob DNA *9*, 11.

Hertzog, J., Dias Junior, A.G., Rigby, R.E., Donald, C.L., Mayer, A., Sezgin, E., Song, C., Jin, B., Hublitz, P., Eggeling, C.*, et al.* (2018). Infection with a Brazilian isolate of Zika virus generates RIG-I stimulatory RNA and the viral NS5 protein blocks type I IFN induction and signaling. Eur J Immunol *48*, 1120-1136.

Ho, M.-C., Shi, W., Rinaldo-Matthis, A., Tyler, P.C., Evans, G.B., Clinch, K., Almo, S.C., and Schramm, V.L. (2010). Four generations of transition-state analogues for human purine nucleoside phosphorylase. Proceedings of the National Academy of Sciences *107*, 4805.

Hofer, A., Crona, M., Logan, D.T., and Sjoberg, B.M. (2012). DNA building blocks: keeping control of manufacture. Critical reviews in biochemistry and molecular biology *47*, 50-63.

Hofmann, H., Logue, E.C., Bloch, N., Daddacha, W., Polsky, S.B., Schultz, M.L., Kim, B., and Landau, N.R. (2012). The Vpx Lentiviral Accessory Protein Targets SAMHD1 for Degradation in the Nucleus. Journal of virology *86*, 12552-12560.

Hollenbaugh, J.A., Gee, P., Baker, J., Daly, M.B., Amie, S.M., Tate, J., Kasai, N., Kanemura, Y., Kim, D.H., Ward, B.M.*, et al.* (2013). Host factor SAMHD1 restricts DNA viruses in non-dividing myeloid cells. PLoS pathogens *9*, e1003481.

Holler, N., Zaru, R., Micheau, O., Thome, M., Attinger, A., Valitutti, S., Bodmer, J.-L., Schneider, P., Seed, B., and Tschopp, J. (2000). Fas triggers an alternative, caspase-8–independent cell death pathway using the kinase RIP as effector molecule. Nature immunology *1*, 489.

Howard, D.R., Munir, T., McParland, L., Rawstron, A.C., Milligan, D., Schuh, A., Hockaday, A., Allsup, D.J., Marshall, S., Duncombe, A.S.*, et al.* (2017). Results of the randomized phase IIB ARCTIC trial of low-dose rituximab in previously untreated CLL. Leukemia *31*, 2416-2425.

Hrecka, K., Hao, C., Gierszewska, M., Swanson, S.K., Kesik-Brodacka, M., and Srivastava, S. (2011). Vpx relieves inhibition of HIV-1 infection of macrophages mediated by the SAMHD1 protein. Nature *474*.

Hu, S., Li, J., Xu, F., Mei, S., Le Duff, Y., Yin, L., Pang, X., Cen, S., Jin, Q., Liang, C.*, et al.* (2015). SAMHD1 Inhibits LINE-1 Retrotransposition by Promoting Stress Granule Formation. PLoS genetics *11*, e1005367.

J.Lindenmann, A.I. (1988). Virus interference: I. The interferon. By Alick Isaacs and Jean Lindenmann, 1957. CA: a cancer journal for clinicians *38*, 280-290.

Janeway CA Jr, T.P., Walport M, et al. (2001). Induced innate responses to infection. In Immunobiology: The Immune System in Health and Disease (New York: Garland Science).

Janeway, C.A., Jr., and Medzhitov, R. (2002). Innate immune recognition. Annual review of immunology *20*, 197-216.

Ji, X., Tang, C., Zhao, Q., Wang, W., and Xiong, Y. (2014). Structural basis of cellular dNTP regulation by SAMHD1. Proc Natl Acad Sci U S A *111*, E4305-4314.

Ji, X., Wu, Y., Yan, J., Mehrens, J., Yang, H., and DeLucia, M. (2013). Mechanism of allosteric activation of SAMHD1 by dGTP. Nat Struct Mol Biol *20*.

Jia, S., Marjavaara, L., Buckland, R., Sharma, S., and Chabes, A. (2015). Determination of deoxyribonucleoside triphosphate concentrations in yeast cells by strong anion-exchange high-performance liquid chromatography coupled with ultraviolet detection. Methods in molecular biology (Clifton, NJ) *1300*, 113-121.

Johansson, P., Klein-Hitpass, L., Choidas, A., Habenberger, P., Mahboubi, B., Kim, B., Bergmann, A., Scholtysik, R., Brauser, M., Lollies, A.*, et al.* (2018). SAMHD1 is recurrently mutated in T-cell prolymphocytic leukemia. Blood Cancer J *8*, 11.

Jüllig, M., and Eriksson, S. (2000). Mitochondrial and submitochondrial localization of human deoxyguanosine kinase. Eur J Biochem *267*, 5466-5472.

Kanno, A., Tanimura, N., Ishizaki, M., Ohko, K., Motoi, Y., Onji, M., Fukui, R., Shimozato, T., Yamamoto, K., Shibata, T.*, et al.* (2015). Targeting cell surface TLR7 for therapeutic intervention in autoimmune diseases. Nature Communications *6*, 6119.

Karch, J., Kanisicak, O., Brody, M.J., Sargent, M.A., Michael, D.M., and Molkentin, J.D. (2015). Necroptosis Interfaces with MOMP and the MPTP in Mediating Cell Death. PloS one *10*, e0130520.

Kastelowitz, N., and Yin, H. (2014). Exosomes and microvesicles: identification and targeting by particle size and lipid chemical probes. Chembiochem *15*, 923-928.

Kato, H., Takeuchi, O., Sato, S., Yoneyama, M., Yamamoto, M., Matsui, K., Uematsu, S., Jung, A., Kawai, T., Ishii, K.J.*, et al.* (2006). Differential roles of MDA5 and RIG-I helicases in the recognition of RNA viruses. Nature *441*, 101-105.

Kawai, T., and Akira, S. (2010). The role of pattern-recognition receptors in innate immunity: update on Toll-like receptors. Nature immunology *11*, 373-384.

Kayagaki, N., Stowe, I.B., Lee, B.L., O'Rourke, K., Anderson, K., Warming, S., Cuellar, T., Haley, B., Roose-Girma, M., Phung, Q.T.*, et al.* (2015). Caspase-11 cleaves gasdermin D for non-canonical inflammasome signalling. Nature *526*, 666-671.

Khozhukhar, N., Spadafora, D., Rodriguez, Y., and Alexeyev, M. (2018). Elimination of Mitochondrial DNA from Mammalian Cells. Current protocols in cell biology *78*, 20.11.21-20.11.14.

Kicska, G.A., Long, L., Horig, H., Fairchild, C., Tyler, P.C., Furneaux, R.H., Schramm, V.L., and Kaufman, H.L. (2001). Immucillin H, a powerful transition-state analog inhibitor of purine nucleoside phosphorylase, selectively inhibits human T lymphocytes. Proc Natl Acad Sci U S A *98*, 4593-4598.

Kim, B., Nguyen, L.A., Daddacha, W., and Hollenbaugh, J.A. (2012). Tight interplay among SAMHD1 protein level, cellular dNTP levels, and HIV-1 proviral DNA synthesis kinetics in

human primary monocyte-derived macrophages. The Journal of biological chemistry *287*, 21570-21574.

Kim, E.S., and Dhillon, S. (2015). Ibrutinib: A Review of Its Use in Patients with Mantle Cell Lymphoma or Chronic Lymphocytic Leukaemia. Drugs *75*, 769-776.

Kim, E.T., White, T.E., Brandariz-Nunez, A., Diaz-Griffero, F., and Weitzman, M.D. (2013). SAMHD1 restricts herpes simplex virus 1 in macrophages by limiting DNA replication. Journal of virology *87*, 12949-12956.

Kipps, T.J., Stevenson, F.K., Wu, C.J., Croce, C.M., Packham, G., Wierda, W.G., O'Brien, S., Gribben, J., and Rai, K. (2017). Chronic lymphocytic leukaemia. Nat Rev Dis Primers *3*, 16096.

Kluge, S.F., Sauter, D., and Kirchhoff, F. (2015). SnapShot: Antiviral Restriction Factors. Cell *163*, 774-774.e771.

Kobold, S., Wiedemann, G., Rothenfußer, S., and Endres, S. (2014). Modes of action of TLR7 agonists in cancer therapy. Immunotherapy *6*, 1085-1095.

Kodigepalli, K.M., Bonifati, S., Tirumuru, N., and Wu, L. (2018). SAMHD1 modulates in vitro proliferation of acute myeloid leukemia-derived THP-1 cells through the PI3K-Akt-p27 axis. Cell Cycle, 1-14.

Koharudin, L.M., Wu, Y., DeLucia, M., Mehrens, J., Gronenborn, A.M., and Ahn, J. (2014). Structural basis of allosteric activation of sterile alpha motif and histidine-aspartate domain-containing protein 1 (SAMHD1) by nucleoside triphosphates. The Journal of biological chemistry *289*, 32617-32627.

Kohnken, R., Porcu, P., and Mishra, A. (2017). Overview of the Use of Murine Models in Leukemia and Lymphoma Research. Front Oncol *7*, 22.

Kong, Z., Jia, S., Chabes, A.L., Appelblad, P., Lundmark, R., Moritz, T., and Chabes, A. (2018). Simultaneous determination of ribonucleoside and deoxyribonucleoside triphosphates in biological samples by hydrophilic interaction liquid chromatography coupled with tandem mass spectrometry. Nucleic Acids Res.

Kovacs, S.B., and Miao, E.A. (2017). Gasdermins: Effectors of Pyroptosis. Trends in Cell Biology *27*, 673-684.

Kretschmer, S., Wolf, C., Konig, N., Staroske, W., Guck, J., Hausler, M., Luksch, H., Nguyen, L.A., Kim, B., Alexopoulou, D.*, et al.* (2015). SAMHD1 prevents autoimmunity by maintaining genome stability. Annals of the rheumatic diseases *74*, e17.

Kulis, M., Heath, S., Bibikova, M., Queirós, A.C., Navarro, A., Clot, G., Martínez-Trillos, A., Castellano, G., Brun-Heath, I., Pinyol, M.*, et al.* (2012). Epigenomic analysis detects widespread gene-body DNA hypomethylation in chronic lymphocytic leukemia. Nature Genetics *44*, 1236.

Kumar, D., Abdulovic, A.L., Viberg, J., Nilsson, A.K., Kunkel, T.A., and Chabes, A. (2011a). Mechanisms of mutagenesis in vivo due to imbalanced dNTP pools. Nucleic Acids Res *39*, 1360-1371.

Kumar, D., Viberg, J., Nilsson, A.K., and Chabes, A. (2010). Highly mutagenic and severely imbalanced dNTP pools can escape detection by the S-phase checkpoint. Nucleic Acids Res *38*.

Kumar, H., Kawai, T., and Akira, S. (2011b). Pathogen recognition by the innate immune system. International reviews of immunology *30*, 16-34.

Kunz, B.A., and Kohalmi, S.E. (1991). Modulation of Mutagenesis by Deoxyribonucleotide Levels. Annual Review of Genetics *25*, 339-359.

Kunz, B.A., Kohalmi, S.E., Kunkel, T.A., Mathews, C.K., McIntosh, E.M., and Reidy, J.A. (1994). Deoxyribonucleoside triphosphate levels: A critical factor in the maintenance of genetic stability. Mutation Research/Reviews in Genetic Toxicology *318*, 1-64.

Laberge, R.M., Adler, D., DeMaria, M., Mechtouf, N., Teachenor, R., Cardin, G.B., Desprez, P.Y., Campisi, J., and Rodier, F. (2013). Mitochondrial DNA damage induces apoptosis in senescent cells. Cell Death &Amp; Disease *4*, e727.

Lafarge, S.T., Hou, S., Pauls, S.D., Johnston, J.B., Gibson, S.B., and Marshall, A.J. (2015). Differential expression and function of CD27 in chronic lymphocytic leukemia cells expressing ZAP-70. Leuk Res *39*, 773-778.

Laguette, N., Sobhian, B., Casartelli, N., Ringeard, M., Chable-Bessia, C., Segeral, E., Yatim, A., Emiliani, S., Schwartz, O., and Benkirane, M. (2011). SAMHD1 is the dendritic- and myeloid-cell-specific HIV-1 restriction factor counteracted by Vpx. Nature *474*, 654-657.

Lahouassa, H., Daddacha, W., Hofmann, H., Ayinde, D., Logue, E.C., and Dragin, L. (2012). SAMHD1 restricts the replication of human immunodeficiency virus type 1 by depleting the intracellular pool of deoxynucleoside triphosphates. Nature immunology *13*.

Lamkanfi, M., and Dixit, Vishva M. (2014). Mechanisms and Functions of Inflammasomes. Cell *157*, 1013-1022.

Landau, D.A., Carter, S.L., Stojanov, P., McKenna, A., Stevenson, K., and Lawrence, M.S. (2013). Evolution and impact of subclonal mutations in chronic lymphocytic leukemia. Cell *152*.

Landau, D.A., Clement, K., Ziller, M.J., Boyle, P., Fan, J., Gu, H., Stevenson, K., Sougnez, C., Wang, L., Li, S*., et al.* (2014). Locally disordered methylation forms the basis of intratumor methylome variation in chronic lymphocytic leukemia. Cancer cell *26*, 813-825.

Landau, D.A., Tausch, E., Taylor-Weiner, A.N., Stewart, C., Reiter, J.G., Bahlo, J., Kluth, S., Bozic, I., Lawrence, M., Böttcher, S*., et al.* (2015). Mutations driving CLL and their evolution in progression and relapse. Nature *526*, 525.

Lee, J., Chuang, T.-H., Redecke, V., She, L., Pitha, P.M., Carson, D.A., Raz, E., and Cottam, H.B. (2003). Molecular basis for the immunostimulatory activity of guanine nucleoside analogs: Activation of Toll-like receptor 7. Proceedings of the National Academy of Sciences *100*, 6646.

Lemaitre, B., Nicolas, E., Michaut, L., Reichhart, J.-M., and Hoffmann, J.A. (1996). The Dorsoventral Regulatory Gene Cassette spätzle/Toll/cactus Controls the Potent Antifungal Response in Drosophila Adults. Cell *86*, 973-983.

Leon, J., Sakumi, K., Castillo, E., Sheng, Z., Oka, S., and Nakabeppu, Y. (2016). 8-Oxoguanine accumulation in mitochondrial DNA causes mitochondrial dysfunction and impairs neuritogenesis in cultured adult mouse cortical neurons under oxidative conditions. Scientific reports *6*, 22086.

Leshinsky-Silver, E., Malinger, G., Ben-Sira, L., Kidron, D., Cohen, S., Inbar, S., Bezaleli, T., Levine, A., Vinkler, C., Lev, D*., et al.* (2011). A large homozygous deletion in the

SAMHD1 gene causes atypical Aicardi-Goutieres syndrome associated with mtDNA deletions. Eur J Hum Genet *19*, 287-292.

Lester, S.N., and Li, K. (2014). Toll-Like Receptors in Antiviral Innate Immunity. Journal of Molecular Biology *426*, 1246-1264.

Li, J., and Yuan, J. (2008). Caspases in apoptosis and beyond. Oncogene *27*, 6194-6206.

Li, N., Zhang, W., and Cao, X. (2000). Identification of human homologue of mouse IFN-γ induced protein from human dendritic cells. Immunology Letters *74*, 221-224.

Liao, W., Bao, Z., Cheng, C., Mok, Y.K., and Wong, W.S. (2008). Dendritic cell-derived interferon-gamma-induced protein mediates tumor necrosis factor-alpha stimulation of human lung fibroblasts. Proteomics *8*, 2640-2650.

Lukenbill, J., and Kalaycio, M. (2013). Fludarabine: A review of the clear benefits and potential harms. Leukemia Research *37*, 986-994.

Maelfait, J., Bridgeman, A., Benlahrech, A., Cursi, C., and Rehwinkel, J. (2016). Restriction by SAMHD1 Limits cGAS/STING-Dependent Innate and Adaptive Immune Responses to HIV-1. Cell reports.

Makita, S., Maeshima, A.M., Maruyama, D., Izutsu, K., and Tobinai, K. (2018). Forodesine in the treatment of relapsed/refractory peripheral T-cell lymphoma: an evidence-based review. Onco Targets Ther *11*, 2287-2293.

Mansouri, A., Min, W., Cole, C.J., Josselyn, S.A., Henderson, J.T., van Eede, M., Henkelman, R.M., Ackerley, C., Grunebaum, E., and Roifman, C.M. (2012). Cerebellar abnormalities in purine nucleoside phosphorylase deficient mice. Neurobiology of disease *47*, 201-209.

Mansouri, L., Sutton, L.A., Ljungstrom, V., Bondza, S., Arngarden, L., Bhoi, S., Larsson, J., Cortese, D., Kalushkova, A., Plevova, K.*, et al.* (2015). Functional loss of IkappaBepsilon leads to NF-kappaB deregulation in aggressive chronic lymphocytic leukemia. J Exp Med *212*, 833-843.

Marcelino, L.A., and Thilly, W.G. (1999). Mitochondrial mutagenesis in human cells and tissues. Mutation Research/DNA Repair *434*, 177-203.

Marshak-Rothstein, A. (2006). Toll-like receptors in systemic autoimmune disease. Nature reviews Immunology *6*, 823-835.

Mathews, C.K. (2006). DNA precursor metabolism and genomic stability. FASEB journal : official publication of the Federation of American Societies for Experimental Biology *20*, 1300-1314.

Mathews, C.K. (2015). Deoxyribonucleotide metabolism, mutagenesis and cancer. Nat Rev Cancer *15*, 528-539.

Mathews, C.K., and Ji, J. (1992). DNA precursor asymmetries, replication fidelity, and variable genome evolution. BioEssays *14*, 295-301.

McArthur, K., Whitehead, L.W., Heddleston, J.M., Li, L., Padman, B.S., Oorschot, V., Geoghegan, N.D., Chappaz, S., Davidson, S., San Chin, H.*, et al.* (2018). BAK/BAX macropores facilitate mitochondrial herniation and mtDNA efflux during apoptosis. Science (New York, NY) *359*.

McIlwain, D.R., Berger, T., and Mak, T.W. (2013). Caspase functions in cell death and disease. Cold Spring Harbor perspectives in biology *5*, a008656.

Medeiros, A.C., Soares, C.S., Coelho, P.O., Vieira, N.A., Baqui, M.M.A., Teixeira, F.R., and Gomes, M.D. (2018). DNA damage response signaling does not trigger redistribution of SAMHD1 to nuclear foci. Biochemical and biophysical research communications *499*, 790-796.

Miao, E.A., Leaf, I.A., Treuting, P.M., Mao, D.P., Dors, M., Sarkar, A., Warren, S.E., Wewers, M.D., and Aderem, A. (2010). Caspase-1-induced pyroptosis is an innate immune effector mechanism against intracellular bacteria. Nature immunology *11*, 1136-1142.

Miazzi, C., Ferraro, P., Pontarin, G., Rampazzo, C., Reichard, P., and Bianchi, V. (2014). Allosteric Regulation of the Human and Mouse Deoxyribonucleotide Triphosphohydrolase Sterile -Motif/Histidine-Aspartate Domain-containing Protein 1 (SAMHD1), Vol 289.

Miles, R.W., Tyler, P.C., Furneaux, R.H., Bagdassarian, C.K., and Schramm, V.L. (1998). One-Third-the-Sites Transition-State Inhibitors for Purine Nucleoside Phosphorylase. Biochemistry *37*, 8615-8621.

Mizushima, N., Yoshimori, T., and Ohsumi, Y. (2011). The role of Atg proteins in autophagosome formation. Annual review of cell and developmental biology *27*, 107-132.

Montgomery John, A. (1993). Purine nucleoside phosphorylase: A target for drug design. Medicinal Research Reviews *13*, 209-228.

Moore, E.C., and Hurlbert, R.B. (1966). Regulation of mammalian deoxyribonucleotide biosynthesis by nucleotides as activators and inhibitors. The Journal of biological chemistry *241*, 4802-4809.

Morita, M., Stamp, G., Robins, P., Dulic, A., Rosewell, I., Hrivnak, G., Daly, G., Lindahl, T., and Barnes, D.E. (2004). Gene-targeted mice lacking the Trex1 (DNase III) 3'-->5' DNA exonuclease develop inflammatory myocarditis. Mol Cell Biol *24*, 6719-6727.

Nabhan, C., Aschebrook-Kilfoy, B., Chiu, B.C.H., Smith, S.M., Shanafelt, T.D., Evens, A.M., and Kay, N.E. (2014). The impact of race, ethnicity, age and sex on clinical outcome in chronic lymphocytic leukemia: a comprehensive Surveillance, Epidemiology, and End Results analysis in the modern era. Leukemia & Lymphoma *55*, 2778-2784.

Nabhan, C., and Rosen, S.T. (2014). Chronic lymphocytic leukemia: a clinical review. Jama *312*, 2265-2276.

Negre, D., Mangeot, P.E., Duisit, G., Blanchard, S., Vidalain, P.O., Leissner, P., Winter, A.J., Rabourdin-Combe, C., Mehtali, M., Moullier, P.*, et al.* (2000). Characterization of novel safe lentiviral vectors derived from simian immunodeficiency virus (SIVmac251) that efficiently transduce mature human dendritic cells. Gene therapy *7*, 1613-1623.

Nikoletopoulou, V., Markaki, M., Palikaras, K., and Tavernarakis, N. (2013). Crosstalk between apoptosis, necrosis and autophagy. Biochimica et biophysica acta *1833*, 3448-3459.

Ogura, M., Tsukasaki, K., Nagai, H., Uchida, T., Oyama, T., Suzuki, T., Taguchi, J., Maruyama, D., Hotta, T., and Tobinai, K. (2012). Phase I study of BCX1777 (forodesine) in patients with relapsed or refractory peripheral T/natural killer-cell malignancies. Cancer Sci *103*, 1290-1295.

Oh, C., Ryoo, J., Park, K., Kim, B., Daly, M.B., Cho, D., and Ahn, K. (2018). A central role for PI3K-AKT signaling pathway in linking SAMHD1-deficiency to the type I interferon signature. Scientific reports *8*, 84.

Osborne, W.R., and Scott, C.R. (1983). The metabolism of deoxyguanosine and guanosine in human B and T lymphoblasts. A role for deoxyguanosine kinase activity in the selective T-cell defect associated with purine nucleoside phosphorylase deficiency. Biochem J *214*, 711-718.

Ostertag, E.M., and Kazazian Jr, H.H. (2001). Biology of Mammalian L1 Retrotransposons. Annual Review of Genetics *35*, 501-538.

Overwijk, W.W., and Restifo, N.P. (2001). B16 as a Mouse Model for Human Melanoma. Current protocols in immunology / edited by John E Coligan [et al] *CHAPTER*, Unit-20.21.

Packham, G., Krysov, S., Allen, A., Savelyeva, N., Steele, A.J., Forconi, F., and Stevenson, F.K. (2014). The outcome of B-cell receptor signaling in chronic lymphocytic leukemia: proliferation or anergy. Haematologica *99*, 1138-1148.

Papinazath, T., Min, W., Sujiththa, S., Cohen, A., Ackerley, C., Roifman, C.M., and Grunebaum, E. (2011). Effects of purine nucleoside phosphorylase deficiency on thymocyte development. Journal of Allergy and Clinical Immunology *128*, 854-863.e851.

Pasparakis, M., and Vandenabeele, P. (2015). Necroptosis and its role in inflammation. Nature *517*, 311-320.

Pauls, E., Badia, R., Torres-Torronteras, J., Ruiz, A., Permanyer, M., Riveira-Munoz, E., Clotet, B., Marti, R., Ballana, E., and Este, J.A. (2014a). Palbociclib, a selective inhibitor of cyclin-dependent kinase4/6, blocks HIV-1 reverse transcription through the control of sterile alpha motif and HD domain-containing protein-1 (SAMHD1) activity. AIDS *28*, 2213-2222.

Pauls, E., Ruiz, A., Badia, R., Permanyer, M., Gubern, A., and Riveira-Munoz, E. (2014b). Cell cycle control and HIV-1 susceptibility are linked by CDK6-dependent CDK2 phosphorylation of SAMHD1 in myeloid and lymphoid cells. J Immunol *193*.

Pokatayev, V., Hasin, N., Chon, H., Cerritelli, S.M., Sakhuja, K., Ward, J.M., Morris, H.D., Yan, N., and Crouch, R.J. (2016). RNase H2 catalytic core Aicardi-Goutieres syndrome-related mutant invokes cGAS-STING innate immune-sensing pathway in mice. J Exp Med *213*, 329-336.

Poli, J., Tsaponina, O., Crabbe, L., Keszthelyi, A., Pantesco, V., Chabes, A., Lengronne, A., and Pasero, P. (2012). dNTP pools determine fork progression and origin usage under replication stress. The EMBO journal *31*, 883-894.

Powell, R.D., Holland, P.J., Hollis, T., and Perrino, F.W. (2011). Aicardi-Goutieres syndrome gene and HIV-1 restriction factor SAMHD1 is a dGTP-regulated deoxynucleotide triphosphohydrolase. The Journal of biological chemistry *286*, 43596-43600.

Qiao, F., and Bowie, J.U. (2005). The Many Faces of SAM. Science's STKE *2005*, re7.

Rai, K.R., Peterson, B.L., Appelbaum, F.R., Kolitz, J., Elias, L., Shepherd, L., Hines, J., Threatte, G.A., Larson, R.A., Cheson, B.D.*, et al.* (2000). Fludarabine compared with chlorambucil as primary therapy for chronic lymphocytic leukemia. The New England journal of medicine *343*, 1750-1757.

Ramesh, V., Bernardi, B., Stafa, A., Garone, C., Franzoni, E., Abinun, M., Mitchell, P., Mitra, D., Friswell, M., Nelson, J.*, et al.* (2010). Intracerebral large artery disease in Aicardi-Goutieres syndrome implicates SAMHD1 in vascular homeostasis. Developmental medicine and child neurology *52*, 725-732.

Rehwinkel, J., Maelfait, J., Bridgeman, A., Rigby, R., Hayward, B., Liberatore, R.A., Bieniasz, P.D., Towers, G.J., Moita, L.F., Crow, Y.J.*, et al.* (2013). SAMHD1-dependent retroviral control and escape in mice. The EMBO journal *32*, 2454-2462.

Rehwinkel, J., Tan, C.P., Goubau, D., Schulz, O., Pichlmair, A., Bier, K., Robb, N., Vreede, F., Barclay, W., Fodor, E.*, et al.* (2010). RIG-I detects viral genomic RNA during negative-strand RNA virus infection. Cell *140*, 397-408.

Reichard, P. (1988). Interactions between deoxyribonucleotide and DNA synthesis. Annu Rev Biochem *57*.

Reijns, M.A., Rabe, B., Rigby, R.E., Mill, P., Astell, K.R., Lettice, L.A., Boyle, S., Leitch, A., Keighren, M., Kilanowski, F.*, et al.* (2012). Enzymatic removal of ribonucleotides from DNA is essential for mammalian genome integrity and development. Cell *149*, 1008-1022.

Reijns, M.A.M., Bubeck, D., Gibson, L.C.D., Graham, S.C., Baillie, G.S., Jones, E.Y., and Jackson, A.P. (2011). The Structure of the Human RNase H2 Complex Defines Key Interaction Interfaces Relevant to Enzyme Function and Human Disease. The Journal of biological chemistry *286*, 10530-10539.

Rentoft, M., Lindell, K., Tran, P., Chabes, A.L., Buckland, R.J., Watt, D.L., Marjavaara, L., Nilsson, A.K., Melin, B., Trygg, J.*, et al.* (2016). Heterozygous colon cancer-associated mutations ofSAMHD1have functional significance. Proceedings of the National Academy of Sciences, 201519128.

Reubold, T.F., Wohlgemuth, S., and Eschenburg, S. (2009). A new model for the transition of APAF-1 from inactive monomer to caspase-activating apoptosome. The Journal of biological chemistry *284*, 32717-32724.

Rice, G.I., Bond, J., Asipu, A., Brunette, R.L., Manfield, I.W., Carr, I.M., Fuller, J.C., Jackson, R.M., Lamb, T., Briggs, T.A.*, et al.* (2009). Mutations involved in Aicardi-Goutieres syndrome implicate SAMHD1 as regulator of the innate immune response. Nat Genet *41*, 829-832.

Ringshausen, I., Dechow, T., Schneller, F., Weick, K., Oelsner, M., Peschel, C., and Decker, T. (2004). Constitutive activation of the MAPkinase p38 is critical for MMP-9 production and survival of B-CLL cells on bone marrow stromal cells. Leukemia *18*, 1964-1970.

Ritchie, M.E., Phipson, B., Wu, D., Hu, Y., Law, C.W., Shi, W., and Smyth, G.K. (2015). limma powers differential expression analyses for RNA-sequencing and microarray studies. Nucleic Acids Res *43*, e47.

Rozovski, U., Wu, J.Y., Harris, D.M., Liu, Z., Li, P., Hazan-Halevy, I., Ferrajoli, A., Burger, J.A., O'Brien, S., Jain, N.*, et al.* (2014). Stimulation of the B-cell receptor activates the JAK2/STAT3 signaling pathway in chronic lymphocytic leukemia cells. Blood *123*, 3797-3802.

Ruiz, A., Pauls, E., Badia, R., Torres-Torronteras, J., Riveira-Munoz, E., Clotet, B., Marti, R., Ballana, E., and Este, J.A. (2015). Cyclin D3-dependent control of the dNTP pool and HIV-1 replication in human macrophages. Cell Cycle *14*, 1657-1665.

Ryoo, J., Choi, J., Oh, C., Kim, S., Seo, M., Kim, S.Y., Seo, D., Kim, J., White, T.E., Brandariz-Nunez, A.*, et al.* (2014). The ribonuclease activity of SAMHD1 is required for HIV-1 restriction. Nature medicine *20*, 936-941.

Salviati, L., Sacconi, S., Mancuso, M., Otaegui, D., Camano, P., Marina, A., Rabinowitz, S., Shiffman, R., Thompson, K., Wilson, C.M.*, et al.* (2002). Mitochondrial DNA depletion and dGK gene mutations. Annals of neurology *52*, 311-317.

Schaller, T., Pollpeter, D., Apolonia, L., Goujon, C., and Malim, M.H. (2014). Nuclear import of SAMHD1 is mediated by a classical karyopherin alpha/beta1 dependent pathway and confers sensitivity to VpxMAC induced ubiquitination and proteasomal degradation. Retrovirology *11*, 29.

Schneider, C., Oellerich, T., Baldauf, H.M., Schwarz, S.M., Thomas, D., Flick, R., Bohnenberger, H., Kaderali, L., Stegmann, L., Cremer, A.*, et al.* (2016). SAMHD1 is a biomarker for cytarabine response and a therapeutic target in acute myeloid leukemia. Nature medicine.

Schott, K., Fuchs, N.V., Derua, R., Mahboubi, B., Schnellbacher, E., Seifried, J., Tondera, C., Schmitz, H., Shepard, C., Brandariz-Nunez, A.*, et al.* (2018). Dephosphorylation of the HIV-1 restriction factor SAMHD1 is mediated by PP2A-B55alpha holoenzymes during mitotic exit. Nat Commun *9*, 2227.

Schuh, A., Becq, J., Humphray, S., Alexa, A., Burns, A., and Clifford, R. (2012). Monitoring chronic lymphocytic leukemia progression by whole genome sequencing reveals heterogeneous clonal evolution patterns. Blood *120*.

Schwartzberg, L., Kim, E.S., Liu, D., and Schrag, D. (2017). Precision Oncology: Who, How, What, When, and When Not? American Society of Clinical Oncology educational book American Society of Clinical Oncology Meeting *37*, 160-169.

Seamon, K.J., Sun, Z., Shlyakhtenko, L.S., Lyubchenko, Y.L., and Stivers, J.T. (2015). SAMHD1 is a single-stranded nucleic acid binding protein with no active site-associated nuclease activity. Nucleic Acids Res *43*, 6486-6499.

Shah, A., and Mangaonkar, A. (2015). Idelalisib: A Novel PI3Kδ Inhibitor for Chronic Lymphocytic Leukemia. Annals of Pharmacotherapy *49*, 1162-1170.

Shalini, S., Dorstyn, L., Dawar, S., and Kumar, S. (2015). Old, new and emerging functions of caspases. Cell death and differentiation *22*, 526-539.

Shan, B., Pan, H., Najafov, A., and Yuan, J. (2018). Necroptosis in development and diseases. Genes & Development *32*, 327-340.

Sheng, Z., Oka, S., Tsuchimoto, D., Abolhassani, N., Nomaru, H., Sakumi, K., Yamada, H., and Nakabeppu, Y. (2012). 8-Oxoguanine causes neurodegeneration during MUTYH-mediated DNA base excision repair. J Clin Invest *122*, 4344-4361.

Shi, J., Zhao, Y., Wang, K., Shi, X., Wang, Y., Huang, H., Zhuang, Y., Cai, T., Wang, F., and Shao, F. (2015). Cleavage of GSDMD by inflammatory caspases determines pyroptotic cell death. Nature *526*, 660-665.

Shibata, T., Ohto, U., Nomura, S., Kibata, K., Motoi, Y., Zhang, Y., Murakami, Y., Fukui, R., Ishimoto, T., Sano, S.*, et al.* (2015). Guanosine and its modified derivatives are endogenous ligands for TLR7. International immunology.

Shimizu, S., Kanaseki, T., Mizushima, N., Mizuta, T., Arakawa-Kobayashi, S., Thompson, C.B., and Tsujimoto, Y. (2004). Role of Bcl-2 family proteins in a non-apoptotic programmed cell death dependent on autophagy genes. Nat Cell Biol *6*, 1221-1228.

Shimizu, S., Konishi, A., Nishida, Y., Mizuta, T., Nishina, H., Yamamoto, A., and Tsujimoto, Y. (2010). Involvement of JNK in the regulation of autophagic cell death. Oncogene *29*, 2070-2082.

Shimizu, S., Yoshida, T., Tsujioka, M., and Arakawa, S. (2014). Autophagic cell death and cancer. International journal of molecular sciences *15*, 3145-3153.

Shukla, A., Shukla, V., and Joshi, S.S. (2018). Regulation of MAPK signaling and implications in chronic lymphocytic leukemia. Leuk Lymphoma *59*, 1565-1573.

Sidi, Y., Gelvan, I., Brosh, S., Pinkhas, J., and Sperling, O. (1989). Guanine Nucleotide Metabolism in Red Blood Cells: The Metabolic Basis for GTP Depletion in HGPRT and PNP Deficiency. In Purine and Pyrimidine Metabolism in Man VI: Part A: Clinical and Molecular Biology, K. Mikanagi, K. Nishioka, and W.N. Kelley, eds. (Boston, MA: Springer US), pp. 67-71.

Simmonds, H.A., Fairbanks, L.D., Morris, G.S., Morgan, G., Watson, A.R., Timms, P., and Singh, B. (1987). Central nervous system dysfunction and erythrocyte guanosine triphosphate depletion in purine nucleoside phosphorylase deficiency. Archives of Disease in Childhood *62*, 385.

Simmonds, H.A., Watson, A.R., Webster, D.R., Sahota, A., and Perrett, D. (1982). GTP depletion and other erythrocyte abnormalities in inherited pnp deficiency. Biochemical Pharmacology *31*, 941-946.

Snyder, F.F., Jenuth, J.P., Dilay, J.E., Fung, E., Lightfoot, T., and Mably, E.R. (1994). Secondary loss of deoxyguanosine kinase activity in purine nucleoside phosphorylase deficient mice. Biochimica et Biophysica Acta (BBA) - Molecular Basis of Disease *1227*, 33-40.

Spinazzola, A., Invernizzi, F., Carrara, F., Lamantea, E., Donati, A., Dirocco, M., Giordano, I., Meznaric-Petrusa, M., Baruffini, E., Ferrero, I.*, et al.* (2009). Clinical and molecular features of mitochondrial DNA depletion syndromes. Journal of inherited metabolic disease *32*, 143-158.

St Gelais, C., Silva, S., Amie, S.M., Coleman, C.M., Hoy, H., and Hollenbaugh, J.A. (2012). SAMHD1 restricts HIV-1 infection in dendritic cells (DCs) by dNTP depletion, but its expression in DCs and primary CD4+ T-lymphocytes cannot be upregulated by interferons. Retrovirology *9*.

Stein, H., and Hausen, P. (1969). Enzyme from calf thymus degrading the RNA moiety of DNA-RNA Hybrids: effect on DNA-dependent RNA polymerase. Science (New York, NY) *166*, 393-395.

Stetson, D.B., Ko, J.S., Heidmann, T., and Medzhitov, R. (2008). Trex1 prevents cell-intrinsic initiation of autoimmunity. Cell *134*, 587-598.

Sun, L., Wang, H., Wang, Z., He, S., Chen, S., Liao, D., Wang, L., Yan, J., Liu, W., Lei, X.*, et al.* (2012). Mixed lineage kinase domain-like protein mediates necrosis signaling downstream of RIP3 kinase. Cell *148*, 213-227.

Sze, A., Belgnaoui, S.M., Olagnier, D., Lin, R., Hiscott, J., and van Grevenynghe, J. (2013). Host restriction factor SAMHD1 limits human T cell leukemia virus type 1 infection of monocytes via STING-mediated apoptosis. Cell host & microbe *14*, 422-434.

Szmulewicz, M.N., Novick, G.E., and Herrera, R.J. (1998). Effects of Alu insertions on gene function. Electrophoresis *19*, 1260-1264.

Tait, S.W., and Green, D.R. (2008). Caspase-independent cell death: leaving the set without the final cut. Oncogene *27*, 6452-6461.

Tait, S.W., and Green, D.R. (2010). Mitochondria and cell death: outer membrane permeabilization and beyond. Nat Rev Mol Cell Biol *11*, 621-632.

Taylor, R.C., Cullen, S.P., and Martin, S.J. (2008). Apoptosis: controlled demolition at the cellular level. Nat Rev Mol Cell Biol *9*, 231-241.

Thiele, H., du Moulin, M., Barczyk, K., George, C., Schwindt, W., Nurnberg, G., Frosch, M., Kurlemann, G., Roth, J., Nurnberg, P.*, et al.* (2010). Cerebral arterial stenoses and stroke: novel features of Aicardi-Goutieres syndrome caused by the Arg164X mutation in SAMHD1 are associated with altered cytokine expression. Hum Mutat *31*, E1836-1850.

Thientosapol, E.S., Bosnjak, D., Durack, T., Stevanovski, I., van Geldermalsen, M., Holst, J., Jahan, Z., Shepard, C., Weninger, W., Kim, B.*, et al.* (2018). SAMHD1 enhances immunoglobulin hypermutation by promoting transversion mutation. Proc Natl Acad Sci U S A.

Thomas, C.A., Tejwani, L., Trujillo, C.A., Negraes, P.D., Herai, R.H., Mesci, P., Macia, A., Crow, Y.J., and Muotri, A.R. (2017). Modeling of TREX1-Dependent Autoimmune Disease using Human Stem Cells Highlights L1 Accumulation as a Source of Neuroinflammation. Cell Stem Cell *21*, 319-331 e318.

Tijsterman, M., and Plasterk, R.H.A. (2004). Dicers at RISC: The Mechanism of RNAi. Cell *117*, 1-3.

Ting, A.T., and Bertrand, M.J.M. (2016). More to Life than NF-κB in TNFR1 Signaling. Trends in Immunology *37*, 535-545.

Tosar, J.P., Cayota, A., Eitan, E., Halushka, M.K., and Witwer, K.W. (2017). Ribonucleic artefacts: are some extracellular RNA discoveries driven by cell culture medium components? Journal of Extracellular Vesicles *6*, 1272832.

Toy, G., Austin, W.R., Liao, H.I., Cheng, D., Singh, A., Campbell, D.O., Ishikawa, T.O., Lehmann, L.W., Satyamurthy, N., Phelps, M.E.*, et al.* (2010). Requirement for deoxycytidine kinase in T and B lymphocyte development. Proc Natl Acad Sci U S A *107*, 5551-5556.

Tramentozzi, E., Ferraro, P., Hossain, M., Stillman, B., Bianchi, V., and Pontarin, G. (2018). The dNTP triphosphohydrolase activity of SAMHD1 persists during S-phase when the enzyme is phosphorylated at T592. Cell Cycle, 1-13.

Tsuzuki, H., Tani, T., Ueyama, H., and Kodama, M. (2001). Lipopolysaccharide: neutralization by polymyxin B shuts down the signaling pathway of nuclear factor kappaB in peripheral blood mononuclear cells, even during activation. J Surg Res *100*, 127-134.

Unal, O., Hismi, B., Kilic, M., Gulsen, H.H., Coskun, T., Sivri, S.H., Dursun, A., Yuce, A., and Tokatli, A. (2017). Deoxyguanosine kinase deficiency: a report of four patients. Journal of pediatric endocrinology & metabolism : JPEM *30*, 697-702.

Van Der Maaten, L.J.P.H., G.E (2008). Visualizing Data Using t-SNE. Journal of Machine Learning Research, 2579–2605.

Vaux, D.L., Cory, S., and Adams, J.M. (1988). Bcl-2 gene promotes haemopoietic cell survival and cooperates with c-myc to immortalize pre-B cells. Nature *335*, 440.

Vorontsov, II, Minasov, G., Kiryukhina, O., Brunzelle, J.S., Shuvalova, L., and Anderson, W.F. (2011). Characterization of the deoxynucleotide triphosphate triphosphohydrolase (dNTPase) activity of the EF1143 protein from Enterococcus faecalis and crystal structure of the activator-substrate complex. The Journal of biological chemistry *286*, 33158-33166.

Vorontsov, II, Wu, Y., DeLucia, M., Minasov, G., Mehrens, J., Shuvalova, L., Anderson, W.F., and Ahn, J. (2014). Mechanisms of allosteric activation and inhibition of the deoxyribonucleoside triphosphate triphosphohydrolase from Enterococcus faecalis. The Journal of biological chemistry *289*, 2815-2824.

Vozza, A., Blanco, E., Palmieri, L., and Palmieri, F. (2004). Identification of the mitochondrial GTP/GDP transporter in Saccharomyces cerevisiae. The Journal of biological chemistry *279*, 20850-20857.

Wahlfors, J., Hiltunen, H., Heinonen, K., Hamalainen, E., Alhonen, L., and Janne, J. (1992). Genomic hypomethylation in human chronic lymphocytic leukemia. Blood *80*, 2074.

Wang, F., St Gelais, C., de Silva, S., Zhang, H., Geng, Y., Shepard, C., Kim, B., Yount, J.S., and Wu, L. (2015). Phosphorylation of mouse SAMHD1 regulates its restriction of human immunodeficiency virus type 1 infection, but not murine leukemia virus infection. Virology *487*, 273-284.

Wang, L., Limongelli, A., Vila, M.R., Carrara, F., Zeviani, M., and Eriksson, S. (2005). Molecular insight into mitochondrial DNA depletion syndrome in two patients with novel mutations in the deoxyguanosine kinase and thymidine kinase 2 genes. Molecular Genetics and Metabolism *84*, 75-82.

Wang, R., and Brattain, M.G. (2007). The maximal size of protein to diffuse through the nuclear pore is larger than 60 kDa. FEBS Letters *581*, 3164-3170.

Watson, A.R., Evans, D.I., Marsden, H.B., Miller, V., and Rogers, P.A. (1981). Purine nucleoside phosphorylase deficiency associated with a fatal lymphoproliferative disorder. Archives of Disease in Childhood *56*, 563.

Wheeler, L.J., Rajagopal, I., and Mathews, C.K. (2005). Stimulation of mutagenesis by proportional deoxyribonucleoside triphosphate accumulation in Escherichia coli. DNA Repair *4*, 1450-1456.

White, T.E., Brandariz-Nunez, A., Martinez-Lopez, A., Knowlton, C., Lenzi, G., Kim, B., Ivanov, D., and Diaz-Griffero, F. (2017). A SAMHD1 mutation associated with Aicardi-Goutieres Syndrome uncouples the ability of SAMHD1 to restrict HIV-1 from its ability to downmodulate type I interferon in humans. Hum Mutat.

White, T.E., Brandariz-Nunez, A., Valle-Casuso, J.C., Amie, S., Nguyen, L.A., and Kim, B. (2013). The retroviral restriction ability of SAMHD1, but not its deoxynucleotide triphosphohydrolase activity, is regulated by phosphorylation. Cell host & microbe *13*.

Wittmann, S., Behrendt, R., Eissmann, K., Volkmann, B., Thomas, D., Ebert, T., Cribier, A., Benkirane, M., Hornung, V., Bouzas, N.F.*, et al.* (2015). Phosphorylation of murine SAMHD1 regulates its antiretroviral activity. Retrovirology *12*, 103.

Wu, Y.T., Tan, H.L., Huang, Q., Sun, X.J., Zhu, X., and Shen, H.M. (2011). zVAD-induced necroptosis in L929 cells depends on autocrine production of TNF[alpha] mediated by the PKC-MAPKs-AP-1 pathway. Cell death and differentiation *18*, 26-37.

Yan, J., Kaur, S., DeLucia, M., Hao, C., Mehrens, J., Wang, C., Golczak, M., Palczewski, K., Gronenborn, A.M., Ahn, J.*, et al.* (2013). Tetramerization of SAMHD1 Is Required for Biological Activity and Inhibition of HIV Infection. The Journal of biological chemistry *288*, 10406-10417.

Yang, C.A., Huang, H.Y., Chang, Y.S., Lin, C.L., Lai, I.L., and Chang, J.G. (2017). DNA-Sensing and Nuclease Gene Expressions as Markers for Colorectal Cancer Progression. Oncology *92*, 115-124.

Yoneyama, M., and Fujita, T. (2009). RNA recognition and signal transduction by RIG-I-like receptors. Immunol Rev *227*, 54-65.

Zhang, Z., Ohto, U., Shibata, T., Krayukhina, E., Taoka, M., Yamauchi, Y., Tanji, H., Isobe, T., Uchiyama, S., Miyake, K.*, et al.* (2016). Structural Analysis Reveals that Toll-like Receptor 7 Is a Dual Receptor for Guanosine and Single-Stranded RNA. Immunity *45*, 737-748.

Zhao, K., Du, J., Han, X., Goodier, J.L., Li, P., and Zhou, X. (2013). Modulation of LINE-1 and Alu/SVA retrotransposition by Aicardi-Goutieres syndrome-related SAMHD1. Cell reports *4*.

Zhao, K., Du, J., Peng, Y., Li, P., Wang, S., Wang, Y., Hou, J., Kang, J., Zheng, W., Hua, S.*, et al.* (2018). LINE1 contributes to autoimmunity through both RIG-I- and MDA5-mediated RNA sensing pathways. J Autoimmun *90*, 105-115.

Zhou, B., Su, L., Hu, S., Hu, W., Yip, M.L., Wu, J., Gaur, S., Smith, D.L., Yuan, Y.C., Synold, T.W.*, et al.* (2013a). A small-molecule blocking ribonucleotide reductase holoenzyme formation inhibits cancer cell growth and overcomes drug resistance. Cancer Res *73*, 6484-6493.

Zhou, Y., Guo, M., Wang, X., Li, J., Wang, Y., Ye, L., Dai, M., Zhou, L., Persidsky, Y., and Ho, W. (2013b). TLR3 activation efficiency by high or low molecular mass poly I:C. Innate Immun *19*, 184-192.

Zhu, K.W., Chen, P., Zhang, D.Y., Yan, H., Liu, H., Cen, L.N., Liu, Y.L., Cao, S., Zhou, G., Zeng, H.*, et al.* (2018). Association of genetic polymorphisms in genes involved in Ara-C and dNTP metabolism pathway with chemosensitivity and prognosis of adult acute myeloid leukemia (AML). J Transl Med *16*, 90.

Zimanyi, C.M., Chen, P.Y.-T., Kang, G., Funk, M.A., and Drennan, C.L. (2016). Molecular basis for allosteric specificity regulation in class Ia ribonucleotide reductase from Escherichia coli. eLife *5*, e07141.